

**RYDBERG SPECTROSCOPY OF
BARIUM MONOFLUORIDE**

by

Zygmunt J. Jakubek

S.M., The Jagiellonian University at Cracow, Poland (1982)

Submitted to the Department of Chemistry
in Partial Fulfillment of the Requirements
for the Degree of

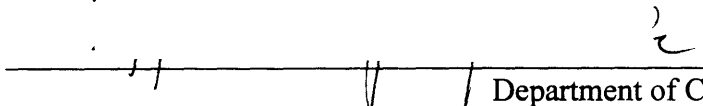
DOCTOR OF PHILOSOPHY IN CHEMISTRY


at the

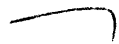
MASSACHUSETTS INSTITUTE OF TECHNOLOGY

February 1995

© Massachusetts Institute of Technology 1995
All rights reserved

Signature of Author  Department of Chemistry
February 3, 1995

Certified by  Robert W. Field
Thesis Supervisor

Accepted by  Dietmar Seyferth
Chairman, Departmental Committee on Graduate Students
Science

RECEIVED

FEB 04 1995

This doctoral thesis has been examined by
a Committee of the Department of Chemistry
as follows:

Professor Keith A. Nelson _____
Chairman

Professor Robert W. Field _____
Thesis Supervisor

Professor Mounji Bawendi _____

Rydberg Spectroscopy of Barium Monofluoride

by
Zygmunt J. Jakubek

Submitted to the Department of Chemistry
on February 3, 1995 in partial fulfillment of the requirements
for the degree of Doctor of Philosophy in Chemistry

Abstract

The BaF molecule, the subject of this work, possesses several exceptional properties, which make it an extremely useful tool in the quest to understand a Rydberg electron \leftrightarrow molecular ion-core energy and angular momentum exchange. The BaF molecule, like other alkaline earth monohalides, has a very simple zero-order electronic structure: two closed shell atomic ions, Ba^{2+} and F^- , and one Rydberg electron. Due to the doubly closed shell molecular ion-core, the entire electronic structure of BaF can be derived from the interaction of the single Rydberg electron with the molecular core. As a result, all observed electronic states of the BaF molecule, including the ground state, $X^2\Sigma^+$, are members of one of the 10 core-penetrating Rydberg series or one of the infinite number of core-nonpenetrating Rydberg series. The conceptual simplicity of the zero-order electronic structure is accompanied by the great complexity of interchannel interactions. The different $l\lambda$ channels are mixed by an l -uncoupling interaction, electrostatic/core-penetration interactions, and a spin-orbit interaction. The l -uncoupling interaction has been studied in the past by several authors and is well understood. The electrostatic/penetration l -mixing interactions have also been studied previously. However, in the BaF molecule, these interactions are several hundred times stronger than in a typical diatomic molecule for which Rydberg structure has been systematically investigated. In addition, in the BaF molecule, spin-orbit interactions cannot be neglected even for high- n^* Rydberg states. The BaF molecule possesses also an extremely rare between diatomic molecules property, its dissociation limit is much higher than the ionization potential.

In order to thoroughly characterize the electronic structure of the BaF molecule 3 types of experiments were performed: (1) fluorescence detected optical-optical double resonance spectroscopy with the $C^2\Pi_{3/2}$ intermediate state (high- n^* Rydberg states), (2) fluorescence-detected optical-optical double resonance spectroscopy with the $B^2\Sigma^+$ intermediate state (low- n^* Rydberg states), and (3) ionization-detected optical-optical double resonance spectroscopy with the $C^2\Pi_{3/2}$ intermediate state ($v=1$ autoionizing Rydberg states). Several thousand spectral lines, belonging to more than a hundred new electronic states have been recorded, measured, and assigned. All of the observed Rydberg states have been organized into ten core-penetrating Rydberg series (four $^2\Sigma^+$, three $^2\Pi$, two $^2\Delta$, and one $^2\Phi$) and two (incomplete) series of nonpenetrating complexes (g - and h -complexes). Most of the states have been fitted to an effective Hamiltonian matrix model and molecular constants are reported. The formation of a series of

s-p-d-f-g-h supercomplexes has been discussed. Different models for the supercomplexes have been analyzed. Autoionization rates, quantum defects, and the derivative of the quantum defect with respect to internuclear distance have been discussed. Several programs for data analysis and computer simulations have been developed.

Thesis Supervisor: Dr. Robert W. Field
Title: Professor of Chemistry

Acknowledgments

I want to acknowledge here many people for making my dream come true. My dream came to life many years ago when I watched, “Love story”, the great movie by Arthur Hiller. The dream was to go to school in Cambridge, and it is really not important right now, that, at that time, I wanted to study in, what they call it at MIT, “the small liberal art college up the river from MIT”.

Bob Field has been the great teacher and friend, genuinely concerned with the progress of my research and the development of my career. His help in my struggles with multiple administrative problems cannot be forgotten. I learned from him not only how to understand molecules, but also how to be enthusiastic about them. His eternal optimism and enthusiasm were always (and will be in the future) very inspiring for me. I will always be grateful to him . Thank you Bob!

Jim Murphy introduced me to the world of lasers. Our endless conversations about Rydberg states, which we had even at such awkward places like a casino at Reno, Nevada, greatly influenced my research. Jim and Gail will always be remembered as great friends.

The rest of our Rydberg group, Nicole Harris and Chris Gittins, were very inspiring competitors and collaborators. I will also remember Nicole, a wonderful friend, as my tireless English tutor. Chris earned his place in my (and my family) memory for selling us his very old car, but still running best at speeds over 75 mph. Thanks to Chris and his venerable Toyota, we visited every interesting place from Montreal to Virginia Beach, including Court Rooms (speeding) in three different states.

I want also thank you other members of the Field group, Mike McCarthy, Foss Hill, Jody Klaassen, Jon Bloch, Jon O’Brien and Stephani Solina, without whom the group would not be the same and my stay at MIT would not have been so enjoyable.

Ma Hui, my host in Beijing, is responsible not only for success of our experiment, but also for the wonderful time I had in China. It was a great pleasure to work with him. He is an exceptional collaborator and a good friend.

I cannot forget my polish Mentors, Professor Marek Rytel and Professor Ryszard Kepa. They introduced me to the art of spectroscopy and their quarter-of-the-century-old collaboration with Bob Field made my way to MIT easier.

Dr. Joëlle Rostas, for a very inspirational discussion we had almost 10 years ago, deserves a special thank you. Joëlle also convinced Dr. Hélène Lefebvre-Brion to give me her last (as I recently learned) copy of The Book, one of the most appreciated gifts in my life. I did not know at that time, that this gift, the book on “Perturbations in the Spectra of Diatomic Molecules”, which would have cost more than 3 months of my salary, and which I could not afford to buy at that time, would lead me from Dr. Hélène Lefebvre-Brion, one co-author, to Bob Field, the other co-author.

I will miss all our polish friends in Greater Boston, who helped me and my family fight “culture shock” and made our lives more enjoyable. Special thanks are for Zosia and Janusz Walczak for their friendship, help, and guidance, especially during my first year in Boston.

Finally and most importantly, I thank my family. My parents, Kazimiera and Aleksander Jakubek, have always loved, supported, and encouraged me. My daughter Ania and my wife Beata, to whom I dedicate this thesis, have been for many years my real treasure, my best friends, and my biggest supporters. Without their understanding and encouragement, their enthusiasm and energy, and their optimism this thesis could not have been finished.

To Ania and Beata

Table of Contents.

ABSTRACT	5
ACKNOWLEDGMENTS	7
TABLE OF CONTENTS.	11
LIST OF FIGURES.	14
LIST OF TABLES.	17
1. INTRODUCTION.	19
2. EXPERIMENTS.	22
2.1 FLUORESCENCE - DETECTED OPTICAL - OPTICAL DOUBLE RESONANCE SPECTROSCOPY.	22
2.2 IONIZATION-DETECTED OPTICAL - OPTICAL DOUBLE RESONANCE SPECTROSCOPY.	27
2.3 INTERMEDIATE STATES: $B^2\Sigma^+$ AND $C^2\Pi$.	31
3. SPECTRA AND THEIR ASSIGNMENTS.	35
3.1 TERM VALUE MATCHING.	35
3.2 ISOTOPE EFFECT.	35
3.3 PATTERNS IN SPECTRA.	37
3.4 RYDBERG SERIES.	39
4. SINGLE STATE AND ISOLATED SUPERCOMPLEX HAMILTONIANS.	41
4.1 HAMILTONIAN FOR A ONE-ELECTRON MOLECULE.	41
4.2 NON-SYMMETRIZED HUND'S CASE (A) BASIS.	43
4.3 SYMMETRIZED HUND'S CASE (A) BASIS.	44
4.4 ISOLATED STATE MATRIX ELEMENTS IN HUND'S CASE (A) BASIS.	45
4.5 MATRIX ELEMENTS IN THE HUND'S CASE (B) BASIS.	46
4.6 MODELS FOR CORE-NONPENETRATING STATES OF DIATOMIC MOLECULES.	51
4.6.1 <i>Long-range model in spherical coordinates.</i>	51
4.6.2 <i>Core-penetration effects.</i>	54
4.6.3 <i>Watson's model for dipolar diatomic molecules.</i>	56
4.6.4 <i>Long-range model in prolate spheroidal coordinate system.</i>	59

5. COMPUTER PROGRAMS.	64
5.1 IMPLEMENTATION OF HELLMANN-FEYNMAN THEOREM IN LSQ FITTER.	64
5.2 ELECTRONIC ENERGY OF NONPENETRATING STATES IN PROLATE SPHEROIDAL COORDINATES.	66
5.3 ELECTRONIC ENERGY OF NONPENETRATING STATES IN SPHERICAL COORDINATES.	67
6. SINGLE STATE FITS.	69
6.1 EXPERIMENTAL DATA WITH THE $B^2\Sigma^+$ STATE AS AN INTERMEDIATE.	69
6.1.1 $G^2\Sigma^+$ and $H^2\Sigma^+$ states.	72
6.1.2 New $^2\Pi$ and $^2\Delta$ states.	73
6.1.3 New $^2\Sigma^+$ states.	75
6.2 FLUORESCENCE DETECTED SPECTRA RECORDED VIA THE $C^2\Pi_{3/2}$ INTERMEDIATE STATE.	77
6.2.1 Core-penetrating $^2\Sigma^+$ Rydberg series.	77
6.2.2 Core-penetrating $^2\Pi$ Rydberg series.	84
6.2.3 Core-penetrating $^2\Delta$ Rydberg series.	86
6.2.4 Core-penetrating $^2\Phi$ Rydberg series.	90
7. SUPERCOMPLEXES.	92
7.1 MOLECULAR CONSTANT SCALING LAWS AND SUPERCOMPLEX FORMATION.	92
7.2 CORE-NONPENETRATING COMPLEXES.	105
7.3 ASSIGNMENT OF CORE-NONPENETRATING PERTURBERS.	109
8. IONIZATION DETECTED SPECTRA RECORDED VIA THE $C^2\Pi_{3/2}$ INTERMEDIATE STATE.	113
8.1 $v=1$ $0.86^2\Phi$, $0.94^2\Delta$ AND $0.88^2\Sigma^+$ SERIES.	113
8.2 AUTOIONIZATION RATES.	116
9. APPENDIX A.	120
9.1 ROTATIONAL TERM VALUES FOR THE $v=0$ $B^2\Sigma^+$ STATE.	121
9.2 ROTATIONAL TERM VALUES FOR THE $v=0$ $C^2\Pi_{3/2}$ STATE.	122
10. APPENDIX B. LISTING OF COMPUTER PROGRAMS.	123
10.1 SUBROUTINE LEVEL USED WITH LSQ FITTER.	123
10.2 TOCENTER PROGRAM FOR SOLUTION OF ONE-ELECTRON TWO-CENTER PROBLEM.	127
10.3 PROGRAM BAFSPEC FOR ELECTRONIC ENERGIES OF CORE-NONPENETRATING STATES.	132
10.4 PROGRAM RADIAL FOR VARIOUS RADIAL INTEGRALS IN HYDROGENIC PROBLEM.	140
11. APPENDIX C.	146

12. APPENDIX D.	151
12.1 FLUORESCENCE DETECTED OODR VIA THE $B^2\Sigma^+$ INTERMEDIATE STATE: TRANSITION FREQUENCIES FOR THE ^{138}BAF MOLECULE.	151
12.2 FLUORESCENCE DETECTED OODR VIA THE $B^2\Sigma^+$ INTERMEDIATE STATE: TRANSITION FREQUENCIES FOR THE ^{137}BAF , ^{136}BAF , AND ^{135}BAF MOLECULES.	161
12.3 FLUORESCENCE DETECTED OODR VIA THE $C^2\Pi_{3/2}$ INTERMEDIATE STATE: TERM VALUES FOR THE $0.88\ ^2\Sigma^+$ RYDBERG SERIES.	164
13. APPENDIX E: LIST OF PROGRAM AND DATA FILES.	178

List of Figures.

- Figure 1: Fluorescence-Detected Optical Optical Double Resonance of BaF. Only selected states are drawn above 30000 cm^{-1} . Two schemes of excitation, via $B^2\Sigma^+$ and $C^2\Pi_{3/2}$ as the intermediate states, are shown. 23
- Figure 2: Fluorescence-Detected OODR - Experimental Setup 24
- Figure 3: Organized gas flow in the high temperature oven. 26
- Figure 4: High temperature molecular beam source used in ionization-detected, mass-selected optical-optical double resonance experiments on the BaF molecule. 30
- Figure 5: Fragment of the R_{2f} branch (\downarrow) of the $(0,0) C^2\Pi_{3/2}-X^2\Sigma^+$ band. Lines with $J'' < 5.5$ are obstructed by the $(1,1) C^2\Pi_{3/2}-X^2\Sigma^+$ transition bandhead. Unmarked lines belong to the $(1,1)$ and $(2,2) C^2\Pi_{3/2}-X^2\Sigma^+$ bands. 31
- Figure 6: Level diagram illustrating how different probe transitions lead to a common Rydberg level. 35
- Figure 7: Isotope structure of the $R(31.5) (1,0) G^2\Sigma^+ - B^2\Sigma^+$ line. 36
- Figure 8: Typical spectral patterns for $^2\Sigma^+$, and case(a) $^2\Pi$ and $^2\Delta$ states. The $^2\Sigma^+$ state shown here has unusually large splitting between PQ and P lines. Most unmarked lines belong to other isotopomers. The spectrum was recorded via the $J=8.5f v=0$ $C^2\Pi_{3/2}$ intermediate level. 39
- Figure 9: Simple model of BaF^+ and definition of the spheroidal coordinate system. 59
- Figure 10: Spectrum in the $31950-32400 \text{ cm}^{-1}$ region obtained via the $B^2\Sigma^+$ state as an intermediate. Upper trace: $C^2\Pi - X^2\Sigma^+$ fluorescence detected; lower trace: direct fluorescence from Rydberg states down to the ground state is detected. 70
- Figure 11: $n^* \bmod 1$ vs n^* plot for $0.88 \ ^2\Sigma^+$ series. (\times 's mark deperturbed positions of the states, see text). 79
- Figure 12: Reduced term value plot for the $7.08 \ ^2\Sigma^+$ state; solid circles - e levels, open diamonds - f levels. 82
- Figure 13: Reduced term value (in cm^{-1}) plotted vs $J(J+1)$ for the $8.24^2\Sigma^+$ and $8.23^2\Delta$ states. (solid circles for e -symmetry, open circles for f -symmetry levels.) 84

- Figure 14: $n^* \bmod 1$ vs n^* plot for $0.94^2\Delta$ series. (Error bars present if greater than the radius of the circle; \times denotes deperturbed values of $n^* \bmod 1$ as discussed in the text). 89
- Figure 15: n^* -variation of the effective rotational constants for the four $^2\Sigma^+$ series. 97
- Figure 16: $n^* \bmod 1$ vs n^* plot for all known core-penetrating electronic Rydberg states of BaF. 100
- Figure 17: n^* -variation of the effective spin-rotation constants for the four $^2\Sigma^+$ series. Error bars denote 3σ uncertainties (when larger than marker size). (\times denotes γ value obtained for the $7.08^2\Sigma^+$ state using the same model as for the other three members of the $0.08^2\Sigma^+$ series, i.e. $\gamma_D \equiv 0$). 102
- Figure 18: Plot of $(n^* - \text{nearest integer})$ vs n^* , illustrating the concept of supercomplexes. *All* states interact and the interactions within each supercomplex are dominant over interactions between neighboring supercomplexes. In addition, many series of core-nonpenetrating states are located near integer- n^* , in the region of $(-0.15, +0.15)$, and forming a spectroscopic black hole. 103
- Figure 19: $A^*(n^*)^3$ vs n^* plot for the $0.23^2\Delta$ and $0.94^2\Delta$ series. The entry for the $A'^2\Delta$ state, $A^*(n^*)^3 = 1619 \text{ cm}^{-1}$ was not included in either of the plots. Error bars denote 3σ uncertainties. 105
- Figure 20: Reduced term value vs $N(N+1)$ plot for the $10.86^2\Phi$, $10.88^2\Sigma^+$, and $10.94^2\Delta$ states, showing multiple perturbations by core-nonpenetrating states. Solid (open) circles denote levels of $+(-)$ Kronig symmetry. 107
- Figure 21: Reduced term value vs $J(J+1)$ plot for the e -levels of the $10.94^2\Delta$, $10.88^2\Sigma^+$, and $10.86^2\Phi$ states, illustrating core-penetrating~core-nonpenetrating perturbations. 108
- Figure 22: Reduced term value vs $N(N+1)$ plot for the $11.86^2\Phi$, $11.88^2\Sigma^+$, and $11.94^2\Delta$ states, showing multiple perturbations by core-nonpenetrating states. Solid (open) circles denote levels of $+(-)$ Kronig symmetry. 111
- Figure 23: Perturbations between $v=1$ $0.86^2\Phi$ series and core-nonpenetrating states. Open (solid) circles are for $+(-)$ Kronig symmetry states. 114

Figure 24: Reduced term value plot of the $v=1$ $0.88^2\Sigma^+$ and $0.94^2\Delta$ series. Solid(open) circles are for $-(+)$ Kronig symmetry states. 115

Figure 25: Autoionization broadened P(11.5) and $^PQ(11.5)$ $v=1$ $15.88^2\Sigma^+$ - $v=0$ $C^2\Pi_{3/2}$ lines. Solid circles denote experimental points. Solid line shows the best fit of the experimental data to Lorentzian lineshapes. Broken lines show individual Lorentzian profiles of P and PQ lines. 117

Figure 26: Evolution of the linewidth of the “+” Kronig symmetry branch in the region of the $v=1$ $15.88^2\Sigma^+ \sim v=1$ $15.94^2\Delta^+$ perturbation. (compare to Figure 24, bottom panel, lowest term) 119

List of Tables.

Table 1: The lowest multipole moments of BaF^+ (2-point charge model) in the center-of-mass coordinate system.	53
Table 2: Molecular constants for the $\text{B}^2\Sigma^+$ state (in cm^{-1}) (see text).	71
Table 3: Molecular constants for the $v=0$ $\text{H}^2\Sigma^+$ state (cm^{-1}).	72
Table 4: Effective molecular constants for the $\text{G}^2\Sigma^+$ state (in cm^{-1}).	73
Table 5: Molecular constants for the $v=0$ $\text{J}^2\Pi$ and $v=1$ $3.94^2\Delta$ states.	75
Table 6: Molecular constants for the 32166 $^2\Sigma^+$ state (in cm^{-1}).	76
Table 7: Molecular constants for the 32110 $^2\Sigma^+$ state (in cm^{-1}).	76
Table 8: Fit results for 32166 $^2\Sigma^+$ and 32110 $^2\Sigma^+$ interacting states (in cm^{-1}).	76
Table 9: Effective molecular constant (in cm^{-1}) for the $0.88^2\Sigma^+$ series.	78
Table 10: Effective molecular constant (in cm^{-1}) for the $0.76^2\Sigma^+$ series.	81
Table 11: Effective molecular constants (in cm^{-1}) for the states of the $0.08^2\Sigma^+$ series.	83
Table 12: Effective molecular constants (in cm^{-1}) for the $0.24^2\Sigma^+$ series.	83
Table 13: Effective molecular constants (in cm^{-1}) for the $0.45^2\Pi$ series.	85
Table 14: Effective molecular constants (in cm^{-1}) for the $0.23^2\Delta$ series.	87
Table 15: Effective molecular constants (in cm^{-1}) for the $0.94^2\Delta$ series.	88
Table 16: Effective molecular constants (in cm^{-1}) for $0.86^2\Phi$ series.	91
Table 17: First derivatives of quantum defect with respect to internuclear distance (in \AA^{-1}) calculated using harmonic oscillator model and experimental quantum defects and internuclear distances.	97

1. Introduction.

The spectroscopy of Rydberg states of the hydrogen atom played a crucial role in the birth of quantum mechanics. Even today, the Rydberg spectroscopy of atoms and molecules continues to be an important tool for gaining a deeper understanding of the physical properties of matter. An especially attractive feature of Rydberg spectroscopy is that long and sometimes complicated series of states, called Rydberg series, in atoms and molecules can be related to the electronic structure of the hydrogen atom by a minor modification of the well known Rydberg formula

$$E_{n\lambda} = \text{IP} - \frac{\mathfrak{R}}{(n - \mu_{l\lambda})^2}, \quad n - \mu_{l\lambda} \equiv n^*, \quad (1.1)$$

where IP is the ionization potential of the atom or molecule, \mathfrak{R} is the universal (weakly mass dependent) Rydberg constant, n is the principal quantum number, and $\mu_{l\lambda}$ is a quantum defect, which in addition to an explicit dependence on l and λ can also be a slowly varying function of energy. The quantum defects, $\mu_{l\lambda}$, which are zero for the hydrogen atom, *encode all information needed to describe the electronic structure and dynamics of Rydberg states of any atom or molecule*. For low- l states, in which the Rydberg electron can penetrate inside an atomic or molecular ion-core, **penetrating states**, quantum defects parametrize in a simple way the very complicated interaction of the Rydberg electron with the multi-electron, multi-nucleus ion-core. For high- l states, in which the Rydberg electron is kept outside the ion-core by centrifugal forces, **nonpenetrating states**, the quantum defects contain information about the long-range electrostatic properties of the ion-core as well as dynamic Rydberg electron \leftrightarrow ion core energy and angular momentum exchange processes.

Until recently, Rydberg spectroscopy of molecules could be considered as a simple extension of atomic Rydberg spectroscopy in the sense that the angular momentum quantum number, l , which is generally not conserved in molecules, even at relatively low- n^* could be treated as a nominally conserved quantity. The well characterized molecular l -mixing processes have been generally restricted to strong $s\sigma \sim d\sigma$ and weak $p \sim f$

interactions. Therefore most aspects of the theory developed for atomic Rydberg states were also applicable to molecules.

Rydberg states in the alkaline-earth monohalides, studied for the past 6 years in Professor Field's lab at MIT, introduce completely new challenges. The common feature of all molecules in this group is the very high polarity of the molecular ion-core. For the BaF molecule, which is the subject of this work, the molecular ion-core dipole and quadrupole moments in the center-of-mass coordinate system are especially large. The high polarity of the molecular ion-core induces strong **l**-mixing among the $l < 6$ states. All of these states must be treated together as *s-p-d-f-g-h* **supercomplexes**. Within such a supercomplex, the *s*, *p*, and *d* states are very strongly core-penetrating and they have *core-precursors* (core states with the same *l* value as the Rydberg state), the *f* states are strongly core-penetrating but do not have core-precursors, and the *g* and *h* states can be considered as core-nonpenetrating. In the non-rotating molecule, because of the cylindrical symmetry about the internuclear axis, the angular momentum projection on the internuclear axis, λ , is a conserved quantum number, thus the *s-p-d-f-g-h* supercomplex factors into smaller Λ -blocks. A non-rotating diatomic molecule can be best described in the prolate spheroidal coordinate system. However, once the molecule starts rotating, the spherical coordinate system with its *z* axis defined to be along the rotation axis, which is perpendicular to the internuclear axis of a $^1\Sigma^+$ ion-core, is the coordinate system of choice. The **l**-uncoupling interaction term of the rotational Hamiltonian mixes the different Λ -blocks. For molecules containing atoms from the first few rows of the periodic table, as energy increases, the spin of the Rydberg electron uncouples from the internuclear axis, a new (+/-) Kronig symmetry emerges, and the Λ -mixed supercomplex Hamiltonian factors into (+/-) - symmetry blocks. This is the case for CaF, the other molecule most extensively studied in Field's group. In the BaF molecule, however, the spin-orbit interaction is very strong and spin effects cannot be disregarded. The (+/-) Kronig symmetry factorization is incomplete. Analysis of the complete *s-p-d-f-g-h* supercomplex is required.

In this project, several thousand lines have been recorded and measured. More than one hundred newly observed electronic Rydberg states have been characterized and organized into Rydberg series. *All* 10 core-penetrating series have been completely characterized as well as an extensive but incomplete data on *g* and *h* states and fragmentary data on *i* states has been collected. Many small, local perturbations have been analyzed. The global structure and dynamics (autoionization) of the Rydberg states of the BaF molecule can be understood by analyzing all of the supercomplexes in order from the lowest energy, where they are relatively simple, to higher energy ($n^* > 15$), where they are very complicated.

2. Experiments.

In order to thoroughly characterize the electronic structure of the Rydberg states of barium monofluoride, 3 types of experiments were performed:

1. fluorescence-detected optical-optical double resonance spectroscopy, with the $v=0$ $C^2\Pi_{3/2}$ state as an intermediate
2. fluorescence-detected optical-optical double resonance spectroscopy, with the $v=0$ $B^2\Sigma^+$ state as an intermediate
3. mass-selected, ion-detected, optical-optical double resonance spectroscopy, with the $v=0$ $C^2\Pi_{3/2}$ state as an intermediate.

The first and the second sets of experiments were done in Professor R. W. Field's laboratory at MIT and the third one in Professor D. Y. Chen's laboratory at Tsinghua University, Beijing, P. R. China in collaboration with Dr. Ma Hui in the Fall of 1993.

The double resonance experiments at both MIT and Tsinghua University were preceded by single-laser studies of the $C^2\Pi-X^2\Sigma^+$ and $B^2\Sigma^+-X^2\Sigma^+$ transitions in order to characterize the $v=0$ $C^2\Pi_{3/2}$ and $v=0$ $B^2\Sigma^+$ intermediate states.

2.1 Fluorescence - Detected Optical - Optical Double Resonance Spectroscopy.

A schematic for fluorescence-detected optical-optical double resonance applied to the BaF molecule is presented in Figure 1. For clarity, only selected electronic states above 30000 cm^{-1} are shown. The pump laser (Spectra Physics, PDL-1) selectively populates individual rotational levels of the $v=0$ $C^2\Pi_{3/2}$ or $v=0$ $B^2\Sigma^+$ vibronic states. As the probe laser (Lambda Physik, FL3002E) is scanned, an OODR spectrum is recorded by detecting direct or cascade fluorescence from Rydberg states down to the $X^2\Sigma^+$ ground state. Both dye lasers are pumped by the second or third harmonic of the same Nd:YAG laser (Quanta Ray, DCR-2A, 10 Hz) and operated most of the time with intracavity etalons (pump laser bandwidth $<0.05\text{ cm}^{-1}$, probe laser bandwidth $<0.03\text{ cm}^{-1}$). The energy of laser pulses is kept low enough to avoid power broadening the spectra. For the highest observed Rydberg states the probe laser energy does not exceed $500\text{ }\mu\text{J/pulse}$ and is much

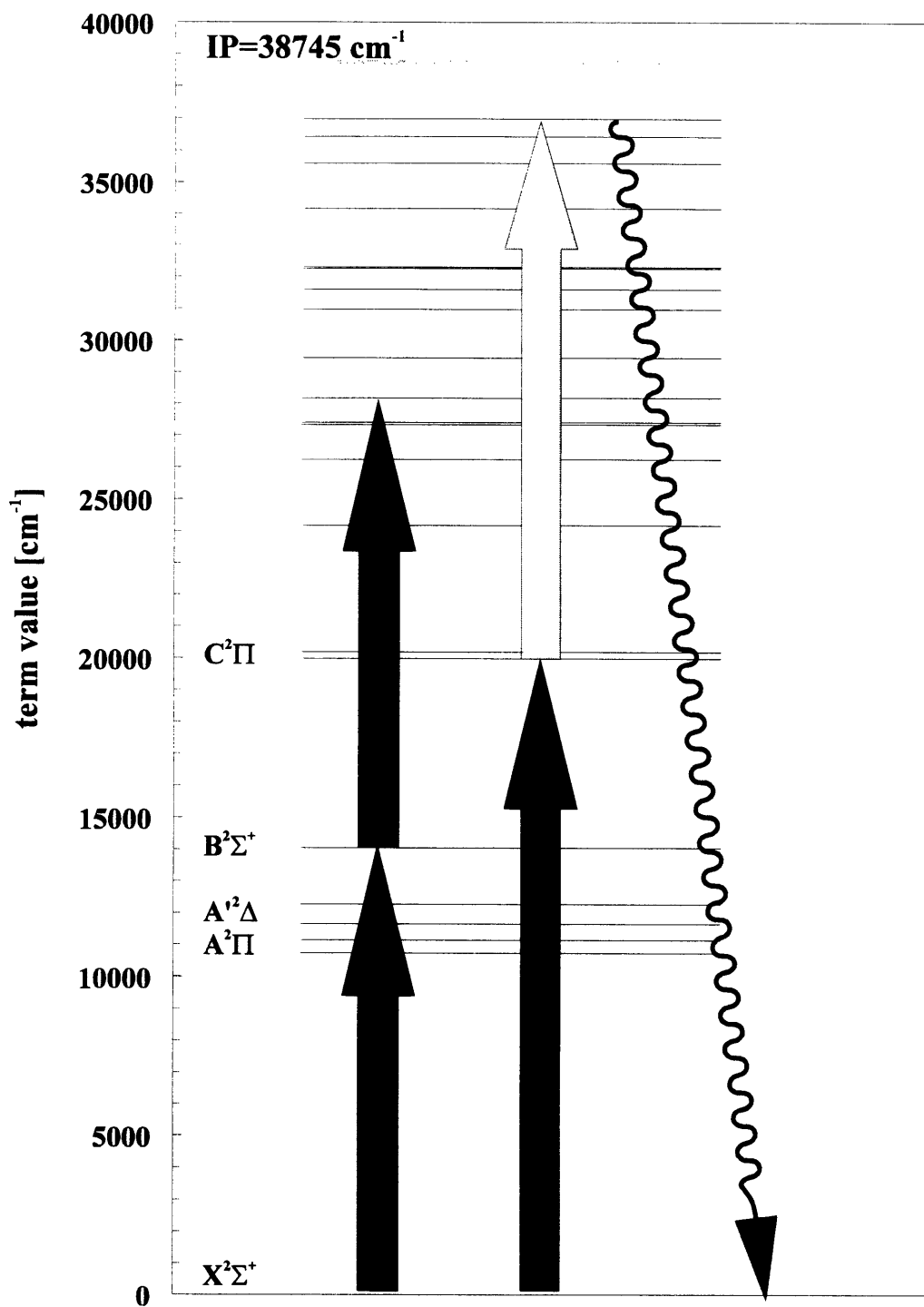


Figure 1: Fluorescence-Detected Optical Optical Double Resonance of BaF. Only selected states are drawn above 30000 cm^{-1} . Two schemes of excitation, via $B^2\Sigma^+$ and $C^2\Pi_{3/2}$ as the intermediate states, are shown.

lower for low and intermediate Rydberg states. Both pump and probe laser beams are expanded and their effective diameter in the reaction region is limited to 1 inch by the size of the input window. The experimental setup for the fluorescence detected OODR experiments is presented in Figure 2.

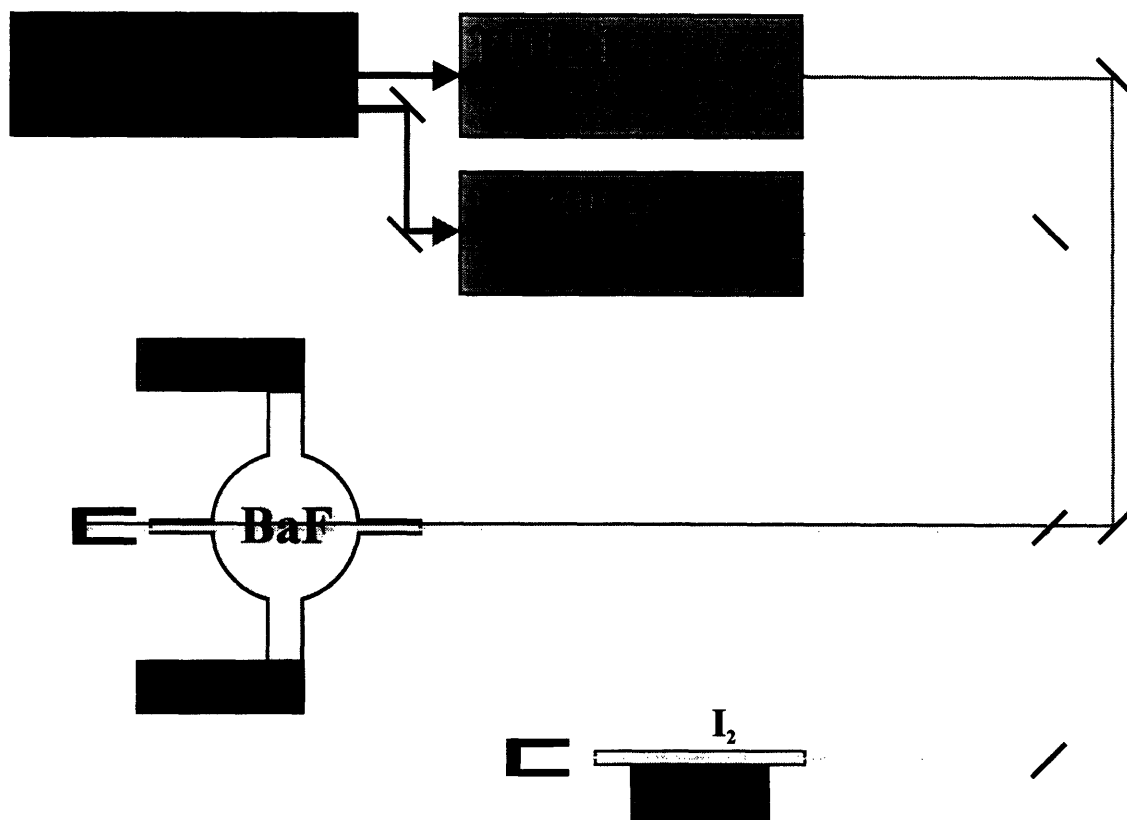


Figure 2: Fluorescence-Detected OODR - Experimental Setup

Both pump electronic transitions used in OODR experiments ($C^2\Pi-X^2\Sigma^+$ and $B^2\Sigma^+-X^2\Sigma^+$) are extremely congested due to the similarity of rotational and vibrational constants in the upper and lower electronic states as well as a very rich isotope structure (5 isotopic species of Ba observable). For this reason, only levels with rotational quantum number $J \geq 6.5$ for f symmetry and $J \geq 14.5$ for e symmetry can be selectively populated in the $v=0$ $C^2\Pi_{3/2}$ intermediate state. The $v=0$ $C^2\Pi_{3/2}$ state is used as an intermediate in OODR experiments on Rydberg states in the region of $4.4 \leq n^* \leq 14.3$. Lower Rydberg states in the region of $3.88 \leq n^* \leq 4.14$ ($31460-32340$ cm^{-1}) are studied via the $v=0$ $B^2\Sigma^+$ intermediate state. Since the Rydberg states in this low energy region are rather widely separated and their structure is well understood (Hund's cases (a) and (b)), it is

convenient to pump R_{11ee} and R_{22ff} bandheads of the (0,0) $B^2\Sigma^+ - X^2\Sigma^+$ transition with the pump laser operated in broadband mode (bandwidth 0.3 cm^{-1}), thus simultaneously populating multiple rotational levels of a selected vibronic state. In this way, most of the levels, both e - and f -symmetry, with rotational quantum numbers in the range of $2.5 \leq J \leq 60.5$ in the $v=0 B^2\Sigma^+$ state are accessed.

Barium monofluoride molecules are produced in a high temperature oven by resistive heating of BaF_2 powder with a small amount of boron powder in a graphite crucible (R. D. Mathis) sitting in a tungsten basket (R. D. Mathis). A single load of BaF_2 ($\sim 30 \text{ g}$) is sufficient for about 6-8 hours of operation. The oven is slowly (~ 30 -40 minutes) heated up and, during normal operation, the power of the heater current do not exceed 255 W (4.4 V and 58 A, 60 Hz AC). The maximum power is applied when the high- n^* ($n^* \approx 13$ -14) states are studied. The transition probabilities for the probe transition and the UV fluorescence are relatively low in that case and a high number density of the BaF molecules is required. The oven is bright yellow in that case. On the other hand, in experiments on the low Rydbergs states ($n^* \approx 4$) the power of the heater current is kept low (the oven is brown red) because the transition probabilities for the probe and UV fluorescence transitions are large and we get good signal-to-noise ratio even with a low number density of the BaF molecules. Flowing argon, at a pressure of about 200 mTorr, carries BaF molecules to the excitation region and cools them rotationally and vibrationally down to approximately 500 K. The translational temperature, as estimated from the linewidths of the pump transition, $\text{FWHM} = 0.05 \text{ cm}^{-1}$, (see Figure 5) using

$$\frac{\Delta\lambda}{\lambda} = \frac{\Delta v}{v} = \sqrt{\frac{8k \ln 2}{c^2} \frac{T}{m}} = 7.162 \cdot 10^{-7} \sqrt{\frac{T(\text{K})}{m(\text{amu})}} \quad (2.1)$$

appears to be lower than 200 K. This is impossible for a high temperature oven system, even assuming thermal equilibrium with the $\sim 300 \text{ K}$ walls of the apparatus. However, this translational temperature can be explained, as follows. The pump laser beam is perpendicular to the axis of the gas (BaF + Ar) flow. The gas flows in a cone defined by diameters of the opening in the oven cover and the pump system inlet (see Figure 3). The

observed in the spectra Doppler broadening is determined by the velocity component,

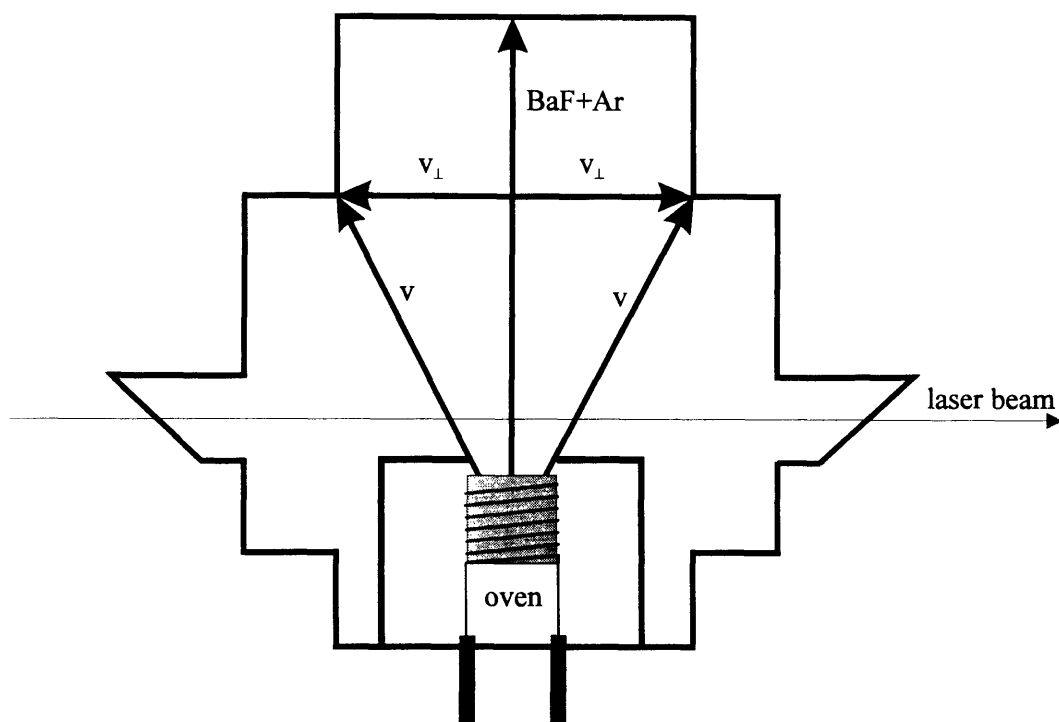


Figure 3: Organized gas flow in the high temperature oven.

$v_{\perp}=222$ m/s at FWHM= 0.05 cm^{-1} , parallel to the laser beam or perpendicular to the axis of the organized gas flow. The velocity is related to the translational temperature by

$$v = \sqrt{\frac{2kT}{m}}, \quad (2.2)$$

where k is Boltzmann constant, T is temperature, and m mass. Assuming that the gas flow is nonturbulent and using simple trigonometry we calculate the average velocity of the gas, $v=700$ m/s and the translational temperature $T_{\text{trans}}=500$ K, which is consistent with our estimate for the rotational and vibrational temperature. Fluorescence from the intermediate state is detected by a photomultiplier tube (Hamamatsu, R928) equipped with a narrow band (5 nm) interference filter centered at 500 nm. UV fluorescence from Rydberg states is detected by a solar blind photomultiplier tube (Hamamatsu, R166) through a solar blind broadband interference filter (Oriol, centered at 290 nm, 65% peak

transmission). In those scans when the $C^2\Pi \rightarrow X^2\Sigma^+$ detection scheme is employed, a narrow band (5 nm) interference filter centered at 500 nm is used instead of the solar blind broadband interference filter. The signal from the PMT is gated and integrated by a boxcar (Stanford Research Systems, SR250) and recorded by a PC AT computer. The format of the data files is described in detail by Ernest Friedman-Hill in his PhD thesis¹. For UV detection, the opening of the gate coincided with the probe laser pulse (no delay) and a typical gate width was 100 ns. For $\Lambda > 1$ high Rydberg states, however, the gate width was set significantly wider, up to 500 ns.* Simultaneously with the Rydberg spectrum, an I_2 fluorescence excitation spectrum is recorded, for absolute frequency calibration (0.01 - 0.02 cm^{-1}). The signal and reference channels are usually averaged over 5-10 laser shots per point. Low resolution scans are carried out with a step size of $\Delta\lambda = 0.002 \text{ nm}$. In high resolution scans, various step sizes in the range of $\Delta\nu = 0.008$ - 0.012 cm^{-1} were used.

2.2 Ionization-Detected Optical - Optical Double Resonance Spectroscopy.

In the ionization-detected experiment the pump laser (Lambda Physik, FL3002EC) selectively populates individual rotational levels, $6.5f \leq J \leq 11.5f$, of the $v=0 \text{ C}^2\Pi_{3/2}$ vibronic state. The probe laser (Lambda Physik, FL3002E) excites Rydberg states in the vicinity ($(IP_0 - 60) \text{ cm}^{-1}$ to $(IP_0 + 420) \text{ cm}^{-1}$) of the $v=0$ ionization limit ($IP_0 = 38745 \text{ cm}^{-1}$).

*Transition moments from a low- l Rydberg state (n^*l) down to the ground state and other low-energy states scale approximately as $(n^*)^{-3/2}$, thus, neglecting the dependence of *Einstein spontaneous emission coefficients* on transition frequency, the radiative lifetime of Rydberg states scales, to the a approximation, as n^{*3} . The radiative lifetime of the $C^2\Pi$ state is $\sim 25 \text{ ns}$ ($n^* = 2.42$). The n^* -scaling rule predicts, for Rydberg states at $n^* = 13$, a radiative lifetime of about $4 \mu\text{s}$. States with $\Lambda > 1$ cannot fluoresce directly to the $X^2\Sigma^+$ ground state. They must first cascade to lower lying $^2\Pi$ and $^2\Sigma^+$ Rydberg states, and these in turn can decay by spontaneous fluorescence to the ground state. States with $\Lambda > 1$ can also acquire some transition moment to the $X^2\Sigma^+$ state from nearby $^2\Sigma^+$ and $^2\Pi$ states via l -mixing processes. For the highest detected $v=0$ Rydberg states at $n^* \approx 14$, UV photons were observed on the oscilloscope at delays up to $\sim 5 \mu\text{s}$ or longer after the double resonance excitation pulses.

Both dye lasers are pumped by the same XeCl laser (Lambda Physik, EMG202MSC, 20 Hz) and are operated with intracavity etalons (bandwidths $<0.05 \text{ cm}^{-1}$).

A BaF molecular beam is produced in a resistively heated high temperature oven. The oven, which I designed and built with Dr. Ma Hui, consists (see Figure 4) of a 3 inch long, 10 mm outside diameter graphite crucible surrounded by tantalum (100 μm) and ceramic (1 mm) tubes. The top of the crucible is closed by a graphite cap with a 0.8 mm hole in the middle. The walls of the graphite crucible are 1 mm thick, except for the top 15 mm, where they are reduced to 0.5 mm thickness. The smaller thickness, thus higher resistance, of the top part of the crucible allows for a higher temperature in this region and prevents the 0.08 mm hole from clogging. The crucible is loaded with barium powder (1.5 g, bottom layer) and barium difluoride (8 g, top layer). The bottom part of the crucible is not shielded (by the tantalum and ceramic tubes) to keep it cooler, since the melting point of barium (998 K) is significantly lower than the melting point of barium difluoride (1553 K). The crucible is isolated from the body of the chamber by boron nitride spacers. Boron nitride spacers also separate the tantalum screen from the crucible. The oven is slowly (~ 40 -60 minutes) heated up and operated at a steady temperature of about 1400 K. The temperature is calculated from the Doppler shift of Ba lines. If the oven is not overheated accidentally, a single load can last for several days of operation. The effusive beam of BaF is excited by counter-propagating pump and probe laser beams. Initially, we tried a setup with the molecular beam perpendicular to the laser beam. However, this scheme failed because of the development in the dye laser beams of longitudinal cavity modes and mode commutations. The problems are attributed to the relatively long ($\sim 28 \text{ ns}$) pump pulse duration of the XeCl laser. The optical length of the oscillator cavity in the Lambda Physik FL3002 laser is $\approx 30 \text{ cm}$. Thus, the 28 ns pulse length allows for ~ 16 round trips of the laser light in the oscillator cavity, which is sufficient to develop well defined longitudinal cavity modes. These longitudinal modes are separated by 0.017 cm^{-1} ($\Delta\nu = 0.5c/l$, where c is the speed of light), thus three of them can oscillate within the laser beam bandwidth of $\sim 0.05 \text{ cm}^{-1}$. Lasing can randomly develop in any of these modes. Since the natural linewidth (Doppler free, in

perpendicular beams configuration) of the $C^2\Pi-X^2\Sigma^+$ transition is only $\sim 0.0012 \text{ cm}^{-1}$, the excitation probability for this transition by one of the commuting longitudinal modes is extremely small. The colinear molecular and laser beams setup eliminated this problem by taking advantage of some Doppler broadening in the molecular beam. The total pressure in the chamber is about $2 \cdot 10^{-6} - 4 \cdot 10^{-6} \text{ Torr}$.

Rydberg states above the $v=0$ ionization limit autoionize and the resulting BaF^+ ions are extracted at about 6 inches above the crucible by an electric field pulse of 250-400 V/cm, switched on 200-250 ns after the probe laser pulse, and kept on for several μs , mass selected ($^{138}\text{BaF}^+$) by a time-of-flight mass spectrometer and detected by a set of microchannel plates (Institute of High Energy Physics, Beijing). Below the $v=0$ ionization limit, BaF^+ ions are produced by field-ionization of the Rydberg states. The time-of-flight for an ion of mass m is given by

$$t = \frac{l}{\sqrt{2ZdE}} \sqrt{m}, \quad (2.3)$$

where l is the distance between the ionization region and the detector (in cm), Z is charge of the ion, d is the distance between electrodes (in cm), and E is the electric field applied between electrodes (V/cm). For $^{138}\text{BaF}^+$ the time-of-flight was 12 μs . The mass resolution, related to the time-of-flight by,

$$\Delta m = 2m \frac{\Delta t}{t}, \quad (2.4)$$

was limited in our experiment to $\Delta m=1 \text{ amu}$ by the minimum gate of the integrator of $\Delta t=38 \text{ ns}$. The mass resolution was sufficient to resolve BaF isotopomers. The signal from the microchannel plates is amplified by a fast amplifier (ORTEC 555), integrated by a gated integrator (homemade, LSAD Laboratory, Tsinghua University), digitized by a charge-digital converter (QDC, Institute of High Energy Physics, Beijing), and recorded by a PC computer. Simultaneously with the BaF^+ ion signal, the I_2 probe laser fluorescence excitation signal is recorded. The ion and reference signals are averaged over 10-20 laser shots per point. Scans are carried out with a step size of $\Delta v \approx 0.01 \text{ cm}^{-1}$.

BaF molecular beam source

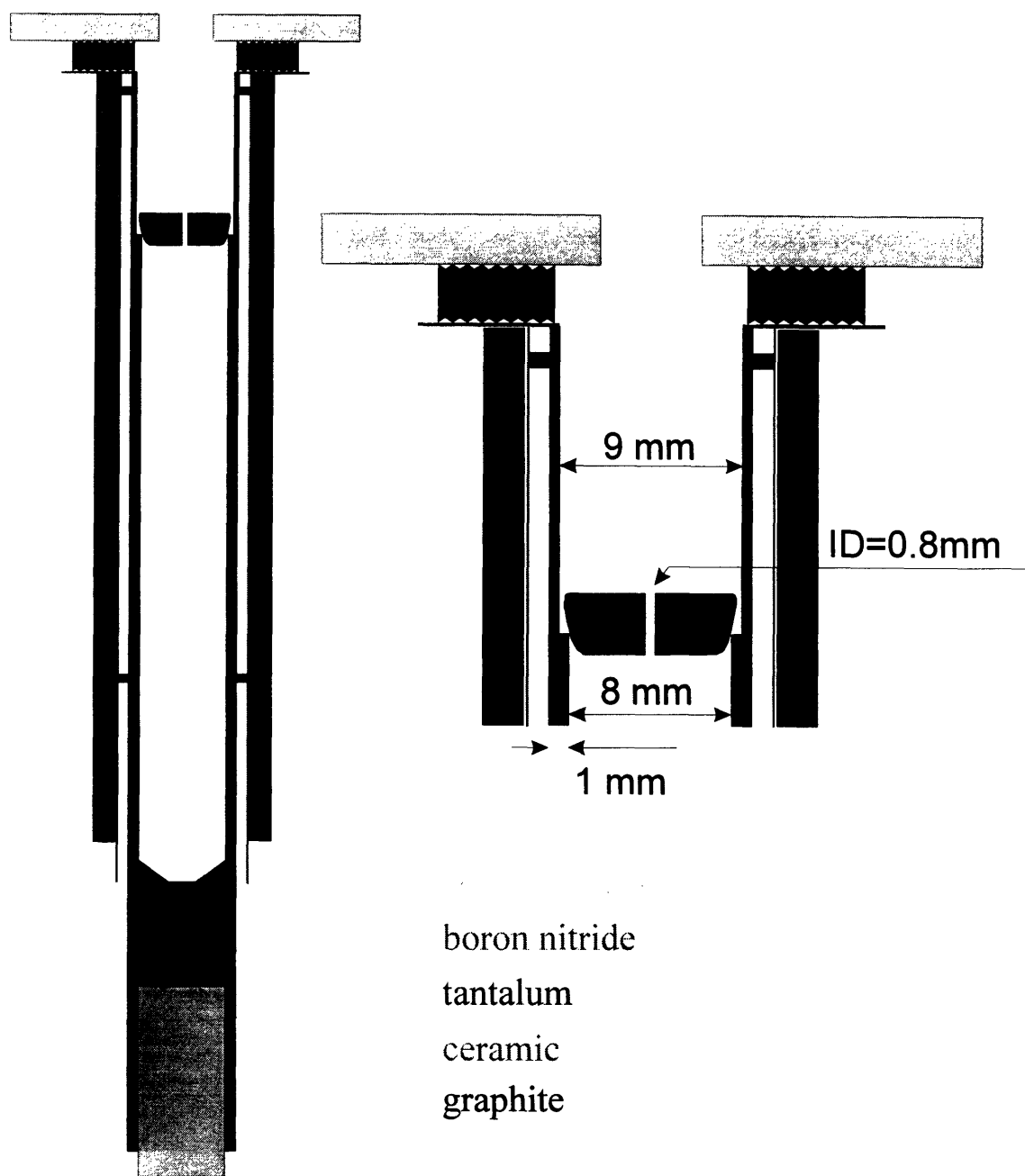


Figure 4: High temperature molecular beam source used in ionization-detected, mass-selected optical-optical double resonance experiments on the BaF molecule.

2.3 Intermediate states: $B^2\Sigma^+$ and $C^2\Pi$.

Prior to this project, the electronic structure of the BaF molecule was studied by several groups. Results of new studies of electronic states below 30000 cm^{-1} , as well as a summary of earlier data on the BaF molecule, were recently published by Effantin and others². They recorded an extensive set of Fourier-transform emission spectra and rotationally analyzed 24 bands in 10 systems with rotational quantum number extending up to $J=130.5$. The resolution of their experimental system was about 0.027 cm^{-1} . The 2 electronic states which we considered as possible intermediates in our OODR studies, $B^2\Sigma^+$ and $C^2\Pi$, were analyzed in detail by them and their effective molecular constants were published. Those constants were used to simulate the spectra of the $B^2\Sigma^+-X^2\Sigma^+$ and $C^2\Pi-X^2\Sigma^+$ transitions. The computed spectra were used to rotationally and vibrationally assign our single-laser experimental spectra. Due to the rather low ionization potential of the BaF molecule and the specific characteristics of the available apparatus, only the $B^2\Sigma^+$ and $C^2\Pi$ states could be chosen as intermediate states for our OODR experiments.

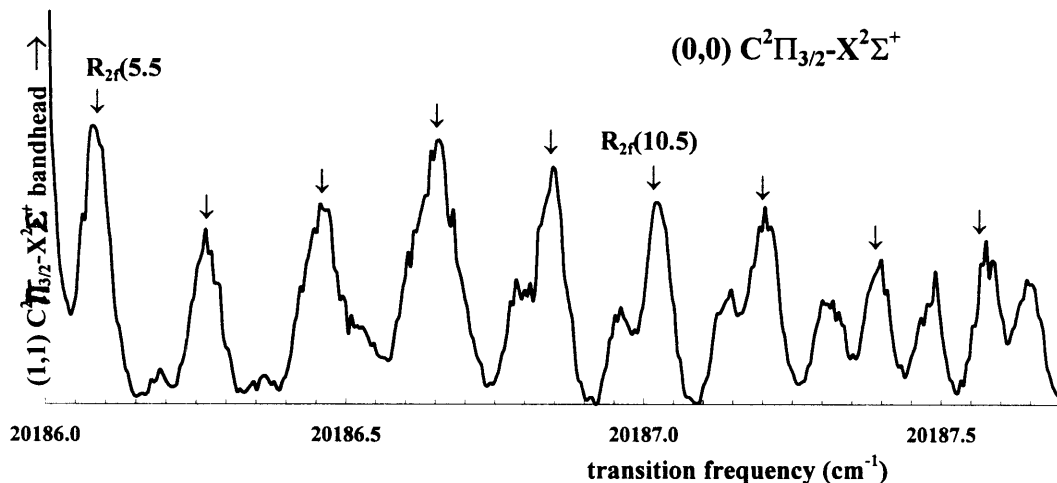


Figure 5: Fragment of the R_{2f} branch (\downarrow) of the $(0,0)$ $C^2\Pi_{3/2}-X^2\Sigma^+$ band. Lines with $J'' < 5.5$ are obstructed by the $(1,1)$ $C^2\Pi_{3/2}-X^2\Sigma^+$ transition bandhead. Unmarked lines belong to the $(1,1)$ and $(2,2)$ $C^2\Pi_{3/2}-X^2\Sigma^+$ bands.

The $C^2\Pi$ state is conveniently located approximately halfway between the ground state and the ionization limit. It was therefore used as an intermediate for roughly 95% of our OODR scans. By pumping in the $(0,0)$ $C^2\Pi-X^2\Sigma^+$ band, we were able to access $J=6.5$ (via

the $R_{2f}(5.5)$ line) as the lowest rotational level of f -symmetry (see Figure 5) and $J=14.5$ (via the ${}^S R_{21ef}(13.5)$ line) as the lowest rotational level of e -symmetry. Lower- J lines were obstructed by very congested bandheads. This initially posed some problems. In order to conclusively assign our double resonance spectra, it became necessary to obtain spectra for several consecutive J -values, in some cases up to at least $J=20.5$ for both e and f symmetries. Later, however, this apparent over-completeness of our data set proved valuable when it became possible to pick out multiple, low- J , core-penetrating \sim core-nonpenetrating perturbations.

¹ Ernest Friedman-Hill, PhD thesis, Massachusetts Institute of Technology, Cambridge, MA, 1992.

² C. Effantin, A. Bernard, J. D'Incan, G. Wannous, J. Vergès, and R. F. Barrow, *Mol. Phys.* **70**(5), 735-745 (1990).

3. Spectra and their assignments.

More than 3000 spectral lines are recorded in the 3 series of experiments. Virtually all of the spectra are calibrated against a simultaneously recorded I₂ fluorescence excitation spectrum.¹ The precision of the calibration (better than 0.01 cm⁻¹) was limited primarily by the resolution element (scanning step size). The few remaining broadband scans are calibrated using the optogalvanic effect in a uranium hollow-cathode lamp.² Spectral measurements and calibration were done using the IBM PLOT program written by Ernest Friedman-Hill and described in detail in his PhD thesis³. Rotational assignments of sometimes very complicated spectra are greatly simplified by a good understanding of the pump transitions and the nature of the OODR technique itself. Vibrational assignment of the fluorescence-detected data is greatly simplified by the Ba isotope effect. Finally, systematic observation of a repeated pattern of electronic states over a range of several units of the principal quantum number followed by an examination of the effective molecular constants of these states allows for an unambiguous grouping of Rydberg states into Rydberg series.

3.1 Term value matching.

By exciting a selected, well understood, rotation-vibration transition with the pump laser, the quantum numbers and symmetry of each intermediate level are well known *a priori*. The symmetry/rotational assignment of each Rydberg level can be summarized as follows. A one-photon probe transition allows only for a $\Delta J=0, \pm 1$ change of the rotational quantum number. The *ef* symmetry of the upper level reached via a P line ($\Delta J=-1$) or an R line ($\Delta J=+1$) is the same as that of the intermediate level; the *ef* symmetry of an upper level reached via a Q line ($\Delta J=0$) is opposite (see Figure 6). Term values for the unknown Rydberg levels are calculated for each scan (probe transition energy + term value of the intermediate state) (see with the total linewidth of 0.06(1) cm⁻¹ and the laser bandwidth of 0.05(1) cm⁻¹, the autoionization broadening is 0.03(3) cm⁻¹. This observation is in agreement with the value of the quantum defect derivative, $<0.08 \text{ \AA}^{-1}$, obtained from intrachannel perturbation.

-
- ¹ S. Gerstenkorn and P. Luc, *Atlas du spectre d'absorption de la molécule d'iode*, CNRS, Paris, 1978.
- ² B. A. Palmer, R. A. Keller, and R. Engleman, Jr., *An Atlas of Uranium Emission Intensities in a Hollow Cathode Discharge.*, LA-8251-MS, Informal Report, Los Alamos Scientific Laboratory, 1980.
- ³ Ernest Friedman-Hill, PhD thesis, Massachusetts Institute of Technology, Cambridge, MA, 1992.

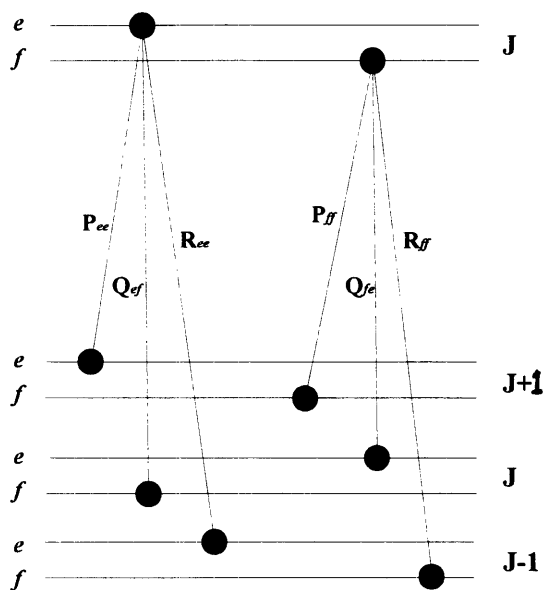


Figure 6: Level diagram illustrating how different probe transitions lead to a common Rydberg level.

Appendix A for the listing of term values of the intermediate $v=0$ $B^2\Sigma^+$ and $v=0$ $C^2\Pi_{3/2}$ state rotational levels). Different scans are compared and Rydberg levels with identical term values are identified. For example, the $P(J+1)$ and $R(J-1)$ lines out of two intermediate levels of the same e/f symmetry terminate in a common Rydberg rotational level. Also $P(J+1)$ and $Q(J)$ lines out of opposite e/f symmetry intermediate levels terminate in a common Rydberg rovibronic level. This is a combination-difference based method of a type that has been known in spectroscopy for many

years.¹ Its combination with OODR is especially powerful. For data obtained via the $B^2\Sigma^+$ intermediate state, when bandheads are pumped, such simple and unambiguous rotational labeling is not present. In that case, second combination differences, $\Delta_2F(J)=F(J+1)-F(J-1)$ are calculated for the intermediate state, branches are picked out and the J numbering of observed probe transitions is varied until the experimental $\Delta_2F(J)=P(J+1)-R(J-1)$ values approximately coincide with the theoretical ones. In order to speed up such an assignment procedure and verify its consistency, rotationally selective pumping is also occasionally applied; $J=4.5$ and $J=55.5$ are simultaneously pumped via a (blended) $R_{22}(3.5)+R_{22}(54.5)$ line. Most of the reported Rydberg term values are calculated via multiple experimental paths. Such redundancy provided an extra protection against calibration or scan errors and incorrect assignments.

3.2 Isotope effect.

Natural barium has 7 appreciably abundant isotopes. Five of these are observed in our fluorescence detected spectra: ^{138}BaF (71.7%), ^{137}BaF (11.3%), ^{136}BaF (7.8%),

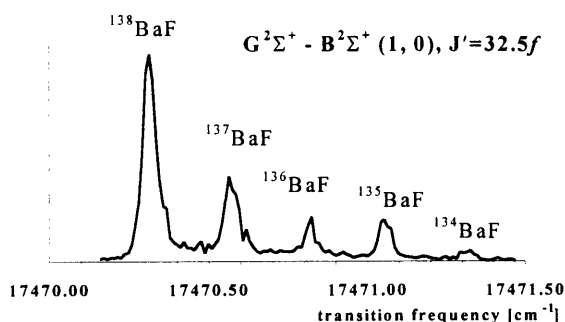


Figure 7: Isotope structure of the R(31.5) (1,0) $G^2\Sigma^+ - B^2\Sigma^+$ line.

the vibrational isotope effect dominates in the range of rotational quantum numbers observed in our experiments. Thus, for assignment purposes, the rotational isotope effect can be neglected. Assuming typical values of vibrational constants for the Rydberg ($'$) and intermediate $C^2\Pi_{3/2}$ states ($''$), $\omega'_e=534\text{ cm}^{-1}$ and $\omega''_e=461\text{ cm}^{-1}$ respectively, and neglecting the rotational contribution, we calculate the isotope shift between the ^{138}BaF and ^{137}BaF lines as 0.02 cm^{-1} for a (0,0) band, 0.25 cm^{-1} for (1,0), and 0.49 cm^{-1} for (2,0) etc. Comparing the calculated intervals against observed spectra makes absolute vibrational assignments in most cases straightforward. One should, however, be aware of large changes of isotope shifts in the spectra of high- n^* states. Some of the isotope shifts we observe are even twice as large as those calculated above.

Such an isotope shift technique is not used for the ionization-detected spectra since only the main ^{138}BaF isotopomer spectrum is recorded. Vibrational assignment in that case is accomplished by comparing the structure of an ion-detected spectrum with the $v=0$ manifold of fluorescence-detected spectra. The appearance (quantum defects, spectral patterns) of same- n^* different- v (vibrational quantum number) supercomplexes are similar as long as the vibrational quantum numbers of the 2 manifolds do not differ significantly. In our case, $n^*\approx 13$ supercomplexes in $v=0$ (fluorescence detection) and $v=1$ (ionization detection) were compared and this enabled us to assign the $v=1$ spectra with confidence.

^{135}BaF (6.6%), ^{134}BaF (2.4%) (see Figure 7). The pump transitions ($\Delta v=0$) are isotopically unselective and the probe transitions terminating on $v>0$ Rydberg states exhibit diagnostically useful isotope splittings. Both rotational and vibrational constants depend on the molecular reduced mass, but, except for $\Delta v=0$ bands,

3.3 Patterns in spectra.

Reappearance of characteristic patterns in Rydberg spectra is often crucial for the correct assignment of a spectrum. A Λ -assignment in the energy region where states belong to case (a) or case (b) can be made based on simple counting of lines. In our experiments with the $C^2\Pi_{3/2}$ intermediate state (which is properly described by the case (a) coupling scheme) we expected to see $^2\Sigma^+$, $^2\Pi$, and $^2\Delta$ Rydberg states. In fact, we observed four $^2\Sigma^+$ series, three $^2\Pi$, two $^2\Delta$, and (unexpectedly, from $n^* \sim 9$ and higher) one $^2\Phi$ series. $^2\Sigma^+$ states appear in the spectrum as a pattern of 3 lines (see Figure 8) with two of them very close to each other and even sometimes overlapping each other, and one standing well apart. The case (a) or intermediate case (a) - case (b) $^2\Pi$ states show two strong lines (P and R) for each spin-orbit component (Figure 8) and, but only for low J, a third very weak Q line approximately in the middle between P and R lines. For case (b) $^2\Pi$ states we see a 4-line pattern, O-, P-, Q-, and R-form lines (with a $^2\Pi_{3/2}$ intermediate state). At low n^* , the P- and R-form lines are usually stronger than O- and Q-form lines. For case (a), or intermediate case (a) - case (b) $^2\Delta$ states we see a 6 line pattern (Figure 8), 3 lines for each spin-orbit component. The middle line (Q) in both triads is significantly stronger than the 2 others. For case (b) $^2\Delta$ states a 4 line pattern is observed. It differs, however, from the $^2\Pi$ case (b) pattern since the 2 middle lines are very strong and the O-form line is weak, or even very weak. $^2\Phi$ states appear in our spectra as case (b) states. They borrow intensity from $^2\Delta$ states so their appearance is very similar to the $^2\Delta$ states. They can, however, be distinguished from $^2\Delta$ states by very small spin-orbit and Λ -doubling splittings. The absolutely conclusive method of the first lines in rotational branches cannot be applied here because the lowest intermediate J is 6.5, thus both $^2\Phi$ and $^2\Delta$ states appear as complete 4-line patterns.

If we go up in energy, the l-uncoupling interaction mixes different Λ states. Relative intensities change and eventually some of the branches completely disappear. The simple patterns described above slowly become more and more complicated. But even in this high- n^* region, certain regularities in the spectrum exist. For a $\Delta l = +1$ (f-complex- $d^2\Pi$) transition, for example, our computer simulation shows that P branches of the high

energy components and R branches of the low energy components of a f -complex are strong. In BaF, l is not a good quantum number. However, since the intermediate state, $C^2\Pi_{3/2}$ is of mixed p and d characters and the states observed at high- n^* have significant f or d characters (especially $^2\Phi$ and $^2\Delta$ states), the above propensity rule is valid to a large extent. Thus, in the $n^*\approx 16$ supercomplex, the Q-form and R-form branches of the $15.86^2\Phi$ and $16.94^2\Delta$ states are very intense while the O-form and P-form branches are weak or even unobserved. At the same time, the O-form and P-form branches of the $16.04^2\Pi$ and $16.24^2\Sigma^+$ states are strong and R-form and Q-form branches are weak. This propensity rule played a very important role in understanding our high- n^* spectra.

If we look at the spectrum systematically from the very low energy region up, we notice that not only do single state patterns appear (although gradually modified) again and again, but also that repeated larger scale structures emerge. By following these “supercomplex” structures and by understanding their evolution as the energy increases, we were able to assign even very complicated spectra in the region where single state patterns have vanished. Supercomplex patterns can also be compared for different (preferably $\Delta v=1$) vibrational quantum number manifolds and apparent structure (patterns of quantum defects) similarities allow one to simply transfer assignments from one manifold to the other.

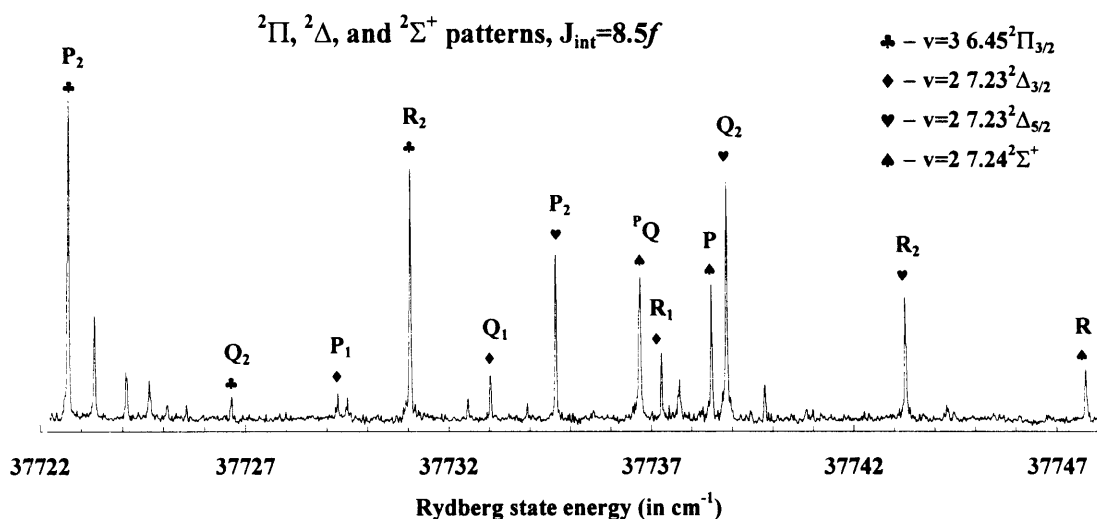


Figure 8: Typical spectral patterns for ${}^2\Sigma^+$, and case(a) ${}^2\Pi$ and ${}^2\Delta$ states. The ${}^2\Sigma^+$ state shown here has unusually large splitting between PQ and P lines. Most unmarked lines belong to other isotopomers. The spectrum was recorded via the $J=8.5f$ $v=0$ $C^2\Pi_{3/2}$ intermediate level.

3.4 Rydberg series.

Rotationally and vibrationally assigned spectra are fitted to an effective Hamiltonian. Effective molecular constants for each electronic state are obtained. Electronic states, both newly observed and previously known, are organized into Rydberg series. Series membership is determined based on the similarity (approximate n^* -independence) of quantum defects, $\mu=(n-n^*) \bmod 1$. Rydberg state electronic energies are described by a modified Rydberg formula

$$E = \text{IP} - \frac{\mathfrak{R}}{(n^*)^2}, \quad (3.1)$$

where IP is the ionization potential, $\text{IP}_{\text{BaF}}=38745(1) \text{ cm}^{-1}$, \mathfrak{R} is the mass-corrected Rydberg constant, $\mathfrak{R}_{\text{BaF}}=109736.93 \text{ cm}^{-1}$, and n^* is the effective (noninteger) principal quantum number. The initially unknown IP is varied until the observed electronic states can be grouped into series (satisfying Eq. 3.1) with quantum defects approximately equal within each series.² As one can see in Figure 16, for $n^*>4.5$, the quantum defects are

approximately constant within each of the 10 observed core-penetrating series. Also, the fine structure constant (spin-orbit, spin-rotation, Λ -doubling) scaling relationships (see Berg *et al.*³) are very useful in the process of arranging Rydberg states into series. Two of the relationships, spin-orbit and spin-rotation n^* -scaling, proved especially useful in this project. The spin-orbit constant is predicted to scale as n^{*-3} , so $A*n^{*3}$ should be approximately constant for a given Rydberg series. Also, the spin-rotation constant (γ) is expected to be constant within a particular $^2\Sigma^+$ Rydberg series.

¹ G. Herzberg, *Molecular Spectra and Molecular Structure. I. Spectra of Diatomic Molecules*. Malabar, Florida: Krieger, 1989.

² Z. J. Jakubek, N. A. Harris, R. W. Field, J. A. Gardner, E. Murad, *Journal of Chemical Physics*, **100** (1), 622-627 (1994).

³ J. M. Berg, J. E. Murphy, N. A. Harris, and R. W. Field, *Phys. Rev A* **48**, 3012 (1993).

4. Single state and isolated supercomplex Hamiltonians.

4.1 Hamiltonian for a one-electron molecule.

The Hamiltonian for a one-electron molecule can be written as

$$\mathbf{H} = \mathbf{H}_0 + \mathbf{H}_r + \mathbf{H}_{fs} + \mathbf{H}_{el}. \quad (4.1)$$

\mathbf{H}_0 is an electronic (diagonal in all quantum numbers) and vibrational Hamiltonian. \mathbf{H}_r is a rotational Hamiltonian. It can be written as (in the molecular-ion-core-center-of-mass coordinate system)

$$\mathbf{H}_r = B(r) \mathbf{R}^2, \quad (4.2)$$

where \mathbf{R} is the operator corresponding to molecular ion-core rotation,

$$\mathbf{R} = \mathbf{J} - \mathbf{s} - \mathbf{l}, \quad (4.3)$$

and \mathbf{J} is the total angular momentum of the molecule, \mathbf{s} is the spin of the Rydberg electron (also the total spin of the molecule), and \mathbf{l} is the orbital angular momentum of the Rydberg electron (and the total orbital angular momentum of the molecule). $B(r)$ is a function of the internuclear distance, r , and depends also on the reduced mass, μ , of the molecule. In spectroscopic units (cm^{-1})

$$B(r) = \frac{h}{800\pi^2 c \mu} \cdot \frac{1}{r^2}$$

($=16.857630/(\mu r^2)$ amu $\text{\AA}^2 \text{cm}^{-1}$). Substituting $\mathbf{R} = \mathbf{R}_x + \mathbf{R}_y$ (since $\mathbf{R}_z = 0$) into Eq. 4.2 we have

$$\begin{aligned} \mathbf{H}_r &= B(r) [(\mathbf{J}_x - \mathbf{s}_x - \mathbf{l}_x)^2 + (\mathbf{J}_y - \mathbf{s}_y - \mathbf{l}_y)^2] \\ &= B(r) [\mathbf{J}_x^2 + \mathbf{s}_x^2 + \mathbf{l}_x^2 - 2\mathbf{J}_x\mathbf{s}_x - 2\mathbf{J}_x\mathbf{l}_x + 2\mathbf{s}_x\mathbf{l}_x + \mathbf{J}_y^2 + \mathbf{s}_y^2 + \mathbf{l}_y^2 - 2\mathbf{J}_y\mathbf{s}_y - 2\mathbf{J}_y\mathbf{l}_y + 2\mathbf{s}_y\mathbf{l}_y] \\ &= B(r) [(\mathbf{J}^2 - \mathbf{J}_z^2) + (\mathbf{s}^2 - \mathbf{s}_z^2) + (\mathbf{l}^2 - \mathbf{l}_z^2) - (\mathbf{J}^+\mathbf{l}^- + \mathbf{J}\mathbf{l}^+) - (\mathbf{J}^+\mathbf{s}^- + \mathbf{J}\mathbf{s}^+) + (\mathbf{s}^+\mathbf{l}^- + \mathbf{s}\mathbf{l}^+)], \end{aligned} \quad (4.4)$$

where

$$\begin{aligned}\mathbf{J}^\pm &= \mathbf{J}_x \pm i\mathbf{J}_y, \\ \mathbf{l}^\pm &= \mathbf{l}_x \pm i\mathbf{l}_y, \\ \mathbf{s}^\pm &= \mathbf{s}_x \pm i\mathbf{s}_y.\end{aligned}\tag{4.5}$$

The \mathbf{H}_{fs} term in Eq. 4.1 is the fine-structure Hamiltonian,

$$\mathbf{H}_{fs} = \mathbf{H}_{so} + \mathbf{H}_{sr},$$

where \mathbf{H}_{so} is the spin-orbit Hamiltonian, given below by a phenomenological expression,

$$\mathbf{H}_{so} = A(r) \mathbf{l} \cdot \mathbf{s} = A(r) [\mathbf{l}_z \mathbf{s}_z + \frac{1}{2}(\mathbf{l}^+ \mathbf{s}^- + \mathbf{l} \mathbf{s}^+)],\tag{4.6}$$

and \mathbf{H}_{sr} is the spin-rotation Hamiltonian,

$$\begin{aligned}\mathbf{H}_{sr} &= \gamma(r) \mathbf{R} \cdot \mathbf{s} = \gamma(r) (\mathbf{J} - \mathbf{s} - \mathbf{l}) \cdot \mathbf{s} \\ &= \gamma(r) [\mathbf{J}_z \mathbf{s}_z - \mathbf{l}_z \mathbf{s}_z - \mathbf{s}^2 + \frac{1}{2}(\mathbf{J}^+ \mathbf{s}^- + \mathbf{J} \mathbf{s}^+) - \frac{1}{2}(\mathbf{l}^+ \mathbf{s}^- + \mathbf{l} \mathbf{s}^+)].\end{aligned}\tag{4.7}$$

The last term in Eq. 4.1, \mathbf{H}_{el} , describes the long-range electrostatic plus core-penetration interaction between the ion-core and the Rydberg electron. Electronic Hamiltonian, \mathbf{H}_{el} , which can be written in a general form as

$$\mathbf{H}_{el} = \sum_{k=0}^{\infty} \sqrt{\frac{4\pi}{2k+1}} \tilde{\mathbf{K}}_{k0}(r_{el}) Y_{k0}(\vartheta, \varphi),\tag{4.8}$$

where $Y_{k0}(\vartheta, \varphi)$ is a spherical harmonic and $\tilde{\mathbf{K}}_{k0}(r_{el})$ is a radial electrostatic/penetration operator, will be extensively discussed in Section 4.6.1.

Substituting (4.4), (4.6), and (4.7) into (4.1) one obtains

$$\mathbf{H} = \mathbf{H}_0 + B(r) [(\mathbf{J}^2 - \mathbf{J}_z^2) + (\mathbf{s}^2 - \mathbf{s}_z^2) + (\mathbf{l}^2 - \mathbf{l}_z^2)] + A(r) \mathbf{l}_z \mathbf{s}_z + \gamma(r) [\mathbf{J}_z \mathbf{s}_z - \mathbf{l}_z \mathbf{s}_z - \mathbf{s}^2]\tag{4.9a}$$

$$- B(r) (\mathbf{J}^+ \mathbf{l} + \mathbf{J} \mathbf{l}^+)\tag{4.9b}$$

$$- [B(r) - \frac{1}{2}\gamma(r)] (\mathbf{J}^+ \mathbf{s}^- + \mathbf{J} \mathbf{s}^+)\tag{4.9c}$$

$$+ [B(r) + \frac{1}{2}A(r) - \frac{1}{2}\gamma(r)] (\mathbf{l}^+ \mathbf{s}^- + \mathbf{l} \mathbf{s}^+)\tag{4.9d}$$

$$+ \mathbf{H}_{el}.\tag{4.9e}$$

4.2 Non-symmetrized Hund's case (a) basis.

As a basis set to evaluate the Hamiltonian we choose Hund's case (a) (non-symmetrized) basis functions,

$$|n^* J \Omega M s \sigma l \lambda; r_{el}; v\rangle = |n^* l \lambda\rangle |s \sigma\rangle |J \Omega M\rangle |v\rangle. \quad (4.10)$$

The separation of the Hund's case (a) basis functions into electronic orbital, electronic spin, rotational, and vibrational parts, as in Eq. 4.10, can be done only for molecules with one or two valence electrons. The diagonal matrix elements of the Hamiltonian (4.9a), in the given basis, are

$$\begin{aligned} E_0 &= \langle n^* J \Omega M s \sigma l \lambda v | \mathbf{H} | n^* J \Omega M s \sigma l \lambda v \rangle \\ &= \langle B(r) \rangle [J(J+1) - \Omega^2 + s(s+1) - \sigma^2 + l(l+1) - \lambda^2] + \langle A(r) \rangle \lambda \sigma + \langle \gamma(r) \rangle (\Omega \sigma - \lambda \sigma - s(s+1)) \end{aligned} \quad (4.11)$$

where*

$$\langle B(r) \rangle = \langle n^* J \Omega M s \sigma l \lambda v | B(r) | n^* J \Omega M s \sigma l \lambda v \rangle = B_{n^* l \lambda, v}(r), \quad (4.12a)$$

$$\langle A(r) \rangle = \langle n^* J \Omega M s \sigma l \lambda v | A(r) | n^* J \Omega M s \sigma l \lambda v \rangle = A_{n^* l \lambda, v}(r), \quad (4.12b)$$

and

$$\langle \gamma(r) \rangle = \langle n^* J \Omega M s \sigma l \lambda v | \gamma(r) | n^* J \Omega M s \sigma l \lambda v \rangle = \gamma_{n^* l \lambda, v}(r). \quad (4.12c)$$

There are also four kinds of off-diagonal matrix elements: **l**-uncoupling (4.9b), **s**-uncoupling (plus off-diagonal spin-rotation) (4.9c), **l-s**-coupling (plus off-diagonal spin-orbit) (4.9d), and electrostatic/penetration (4.9e). The **l**-uncoupling term (4.9b) connects states with $\Delta\lambda = \Delta\Omega = \pm 1$ and $\Delta\sigma = 0$, the **s**-uncoupling term (4.9c) connects states with $\Delta\lambda = 0$ and $\Delta\Omega = \pm 1$, the **l-s**-coupling term (4.9d) connects states with $\Delta\lambda = \pm 1$ and $\Delta\Omega = 0$, and the electrostatic/penetration term connects terms with $\Delta\lambda = 0$, $\Delta\sigma = 0$, $\Delta\Omega = 0$, and $\Delta l \neq 0$. Explicitly evaluating the off-diagonal matrix elements, we get for the **l**-uncoupling term:

* For simplicity we use abbreviated notation for matrix elements. By definition $\langle \mathbf{X} \rangle$ is a matrix element of an operator \mathbf{X} between two state vectors, which are described in the text.

$$\langle \mathbf{B}(\mathbf{r}) (\mathbf{J}^+ \mathbf{I} + \mathbf{J} \mathbf{I}^+) \rangle = \mathbf{B}_{n^* n'' l \lambda \lambda'' ; \nu}(\mathbf{r}) [J(J+1) - \Omega' \Omega'']^{1/2} [l(l+1) - \lambda' \lambda'']^{1/2}; \quad (4.13a)$$

for the s-uncoupling term:

$$\langle [\mathbf{B}(\mathbf{r}) - 1/2\gamma(\mathbf{r})] (\mathbf{J}^+ \mathbf{s}^- + \mathbf{J} \mathbf{s}^+) \rangle = [\mathbf{B}_{n^* l \lambda ; \nu}(\mathbf{r}) - 1/2\gamma_{n^* l \lambda ; \nu}(\mathbf{r})] [J(J+1) - \Omega' \Omega'']^{1/2}; \quad (4.13b)$$

for the l-s-coupling term:

$$\begin{aligned} & \langle [\mathbf{B}(\mathbf{r}) + 1/2\mathbf{A}(\mathbf{r}) - 1/2\gamma] (\mathbf{I}^+ \mathbf{s}^- + \mathbf{I} \mathbf{s}^+) \rangle = \\ & = [\mathbf{B}_{n^* n'' l \lambda \lambda'' ; \nu}(\mathbf{r}) + 1/2\mathbf{A}_{n^* n'' l \lambda \lambda'' ; \nu}(\mathbf{r}) - 1/2\gamma_{n^* n'' l \lambda \lambda'' ; \nu}(\mathbf{r})] [l(l+1) - \lambda' \lambda'']^{1/2}, \end{aligned} \quad (4.13c)$$

and for the electrostatic/penetration term (due to cylindrical symmetry of a molecule $\lambda' = \lambda'' = \lambda$)

$$\left\langle \sum_{k=0}^{\infty} \sqrt{\frac{4\pi}{2k+1}} \tilde{\mathbf{K}}_{k0} \mathbf{Y}_{k0} \right\rangle = \sum_{k=0}^{\infty} \langle n^* l' | \tilde{\mathbf{K}}_{k0} | n'' l'' \rangle (-1)^{\lambda} \sqrt{(2l'+1)(2l''+1)} \begin{pmatrix} l' & k & l'' \\ 0 & 0 & 0 \end{pmatrix} \begin{pmatrix} l' & k & l'' \\ -\lambda & 0 & \lambda \end{pmatrix} \quad (4.13d)$$

4.3 Symmetrized Hund's case (a) basis.

Rovibronic levels are classified as + or - according to their parity. The parity describes the behavior of the total wavefunction of the molecule under the operation of inversion, I , of the *laboratory-fixed* Cartesian coordinates of *all particles*. A rovibronic level is called +, or even, when its total wavefunction is invariant under the operation of space inversion, and -, or odd, when the wavefunction changes sign.¹ In order to define symmetrized wavefunctions we first consider the transformation properties of non-symmetrized wavefunctions under the reflection operation, σ_v . Choosing the phase convention of Condon and Shortley² for a one-electron molecule,

$$\sigma_v | n^* J \Omega M s \sigma l \lambda; r_{el}; \nu \rangle = (-1)^{l+l-\lambda+s-\sigma+J-\Omega} | n^* J -\Omega M s -\sigma l -\lambda; r_{el}; \nu \rangle,$$

or, since $\sigma + \lambda = \Omega$, l is integer, and Ω and s are half-integer,

$$\sigma_v | n^* J \Omega M s \sigma l \lambda; r_{el}; \nu \rangle = (-1)^{J-s} | n^* J -\Omega M s -\sigma l -\lambda; r_{el}; \nu \rangle.$$

Next we can define symmetrized basis functions as

$$|n^* l^{2s+1} \Lambda_{\Omega}; J \Omega M; r_{el}; v \pm \rangle = \frac{1}{\sqrt{2}} \{ |n^* J \Omega s \sigma l \lambda; r_{el}; v \rangle \pm (-1)^{J-s} |n^* J - \Omega s - \sigma l - \lambda; r_{el}; v \rangle \}. \quad (4.14a)$$

The symmetrized basis functions defined in this way alternate between even and odd with J. Using an alternative *e/f* labeling scheme³, *e/f* symmetrized basis functions are described independently of J as

$$|n^* l^{2s+1} \Lambda_{\Omega}; J \Omega M; r_{el}; v (^e f) \rangle = \frac{1}{\sqrt{2}} \{ |n^* J \Omega s \sigma l \lambda; r_{el}; v \rangle \pm |n^* J - \Omega s - \sigma l - \lambda; r_{el}; v \rangle \}, \quad (4.14b)$$

where $\Lambda=|\lambda|$ and $\Omega=|\Omega|$. Thus,

$$\sigma_v |n^* l^{2s+1} \Lambda_{\Omega}; J \Omega M; r_{el}; v (^e f) \rangle = \pm |n^* l^{2s+1} \Lambda_{\Omega}; J \Omega M; r_{el}; v (^e f) \rangle.$$

In the basis set of *e/f* functions, the matrix of the Hamiltonian factors into two blocks, *e* and *f*. For simplicity, the symmetrized basis functions will be written hereafter as

$$|n^* l^{2s+1} \Lambda_{\Omega}; J \Omega; r_{el}; v (^e f) \rangle = |^2 \Lambda_{\Omega} (^e f) \rangle \quad (4.15)$$

and we will remember that they also depend on n^* , l , J , and v .

In the *e/f* symmetrized basis, the matrix elements are the same as those given by Eqs. 4.11 and 4.13a-d (where now $\Lambda \geq 0$ and $\Omega > 0$), *except* for matrix elements involving $^2\Sigma^+$ states, which now depend on the *e/f* label. They are:

$$\langle ^2\Sigma^+ (^e f) | \mathbf{H} | ^2\Sigma^+ (^e f) \rangle = \langle \mathbf{B}(\mathbf{r}) \rangle [(J+1/2)^2 + l(l+1) \mp (J+1/2)] - 1/2 \langle \gamma(\mathbf{r}) \rangle [1 \mp (J+1/2)], \quad (4.16)$$

and

$$\langle ^2\Sigma^+ (^e f) | \mathbf{H} | ^2\Pi_{1/2} (^e f) \rangle = \mp \langle \mathbf{B}(\mathbf{r}) \rangle (J+1/2) [l(l+1)]^{1/2} + \langle [\mathbf{B}(\mathbf{r}) + 1/2 \mathbf{A}(\mathbf{r}) - 1/2 \gamma(\mathbf{r})] \rangle [l(l+1)]^{1/2}. \quad (4.17)$$

4.4 Isolated state matrix elements in Hund's case (a) basis.

When a single, isolated state is being fitted, all of its interactions with other nearby and remote states are taken into account by a Van Vleck transformation⁴. As a result, in

addition to the parameters introduced in the previous section, rotationless energy (T), rotational (B), spin-orbit (A), and spin-rotation (γ) constants, additional *effective* parameters are introduced, a centrifugal distortion contribution to each of the above parameters (except for T), Λ -doubling constants (p, q), centrifugal distortion contributions to Λ -doubling constants, etc.

Matrix elements for the Hamiltonian of an isolated state were calculated by several authors^{5,6,7,8,9}. The matrix elements used in our single state fits are presented below. The upper/lower sign is for *e/f* levels and $x \equiv J + 1/2$.

$$\langle {}^2\Sigma^+ | \mathbf{H}^2 | \Sigma^+ \rangle = T_\Sigma + B_\Sigma x(x \mp 1) - D_\Sigma x^2(x \mp 1)^2 - \frac{1}{2}\gamma_\Sigma(1 \mp x) - \frac{1}{2}\gamma_{D\Sigma}(1 \mp x)J(J+1), \quad (4.18)$$

$$\langle {}^2\Pi_{1/2} | \mathbf{H}^2 | \Pi_{1/2} \rangle = T_\Pi - \frac{1}{2}A_\Pi + B_\Pi x^2 - D_\Pi(x^4 + x^2 + 1) - A_{D\Pi}x^2 + \frac{1}{2}p_\Pi(1 \mp x) + \frac{1}{2}q_\Pi(1 \mp x)^2, \quad (4.19)$$

$$\langle {}^2\Pi_{3/2} | \mathbf{H}^2 | \Pi_{3/2} \rangle = T_\Pi + \frac{1}{2}A_\Pi + B_\Pi(x^2 - 2) - D_\Pi(x^4 - 3x^2 + 3) - A_{D\Pi}(x^2 - 2) + \frac{1}{2}q_\Pi(x^2 - 1)^2, \quad (4.20)$$

$$\langle {}^2\Pi_{1/2} | \mathbf{H}^2 | \Pi_{3/2} \rangle = -B_\Pi(x^2 - 1)^{1/2} + 2D_\Pi(x^2 - 1)^{3/2} - \frac{1}{4}p_\Pi(x^2 - 1)^{1/2} - \frac{1}{2}q_\Pi(1 \mp x)(x^2 - 1)^{1/2}, \quad (4.21)$$

$$\langle {}^2\Delta_{3/2} | \mathbf{H}^2 | \Delta_{3/2} \rangle = T_\Delta - A_\Delta + B_\Delta(x^2 - 2) - D_\Delta x^2(x^2 - 3) - A_{D\Delta}(x^2 - 2) \pm \frac{1}{2}p_\Delta(x^2 - 1)x \pm 2q_\Delta(x^2 - 1)x, \quad (4.22)$$

$$\langle {}^2\Delta_{5/2} | \mathbf{H}^2 | \Delta_{5/2} \rangle = T_\Delta + A_\Delta + B_\Delta(x^2 - 6) - D_\Delta(x^4 - 11x^2 + 32) - A_{D\Delta}(x^2 - 6), \quad (4.23)$$

$$\langle {}^2\Delta_{3/2} | \mathbf{H}^2 | \Delta_{5/2} \rangle = -B_\Delta(x^2 - 4)^{1/2} + 2D_\Delta(x^2 - 4)^{3/2} \pm \frac{1}{2}q_\Delta(x^2 - 1)x(x^2 - 4)^{1/2}, \quad (4.24)$$

$$\langle {}^2\Phi_{5/2} | \mathbf{H}^2 | \Phi_{5/2} \rangle = T_\Phi - \frac{3}{2}A_\Phi + B_\Phi(x^2 - 6) - D_\Phi(x^4 - 11x^2 + 27), \quad (4.25)$$

$$\langle {}^2\Phi_{7/2} | \mathbf{H}^2 | \Phi_{7/2} \rangle = T_\Phi + \frac{3}{2}A_\Phi + B_\Phi(x^2 - 12) - D_\Phi(x^4 - 23x^2 + 135), \quad (4.26)$$

$$\langle {}^2\Phi_{5/2} | \mathbf{H}^2 | \Phi_{7/2} \rangle = -B_\Phi(x^2 - 9)^{1/2} + 2D_\Phi(x^2 - 9)^{3/2}. \quad (4.27)$$

The matrix elements 4.18 - 4.27 differ from those developed in Sections 4.2 and 4.3 by inclusion of the $B[l(l+1) - \lambda^2]$ term into the T_Λ constant. Such a change is dictated by the fact that l is not a good quantum number in a molecule and, in a single state fit, must be treated as an adjustable parameter.

4.5 Matrix elements in the Hund's case (b) basis.

With increasing n^* , the spin of a Rydberg electron gradually uncouples from the internuclear axis and core-penetrating states can be well described by the Hund's case (b) coupling scheme. The total angular momentum without spin, $N = J - s$, is conserved in such a case and N is a good quantum number. In the BaF molecule, unlike most others for

which Rydberg states have been studied, the spin-orbit interaction is very strong and spin effects do not disappear, even at n^* as high as 10. For example, the spin-orbit constant for the $9.23^2\Delta$ state, as fitted from the spectra, is $A=1.229(24) \text{ cm}^{-1}$ (see Table 14). In spite of this, it is very advantageous to perform an initial supercomplex analysis in the case (b) basis because, due to an extra symmetry, the size of matrices can be significantly reduced. For example, the size of the isolated $s\sim p\sim d\sim f\sim g\sim h$ supercomplex matrix in the case (a) basis is 36 for both e - and f -symmetry levels. In the case (b) basis, however, the matrix factors into 2 smaller ones, one of the size of 15 for “-” Kronig symmetry levels and the other of size 21 for “+” symmetry levels. The “+/-” Kronig symmetry of states is related to the behavior of the electronic wavefunction (without the spin part) under reflection in a plane containing the internuclear axis. If the wavefunction does not change, a state is classified as “+”, and if the wavefunction changes sign a state is called “-”. For one-electron molecule, $^2\Sigma$ states are always of “+” symmetry, and this Kronig symmetry is denoted by a “+” superscript. Higher- Λ states can be of both “+” or “-” symmetry. A practical method of verifying the Kronig symmetry of a particular level of a $\Lambda>0$ state is to compare its J , N , parity and (e/f) labels with levels of a $^2\Sigma^+$ state. If a $\Lambda>0$ level exists with the same (J , N , parity (e/f)) set as for a $^2\Sigma^+$ state, the level of the $\Lambda>0$ state belongs to the “+” symmetry component, Λ^+ , otherwise to the “-” symmetry component, Λ^- . Let us consider two levels of the $C^2\Pi_{3/2}$ states used in our experiments as intermediates: $J=6.5f$ and $J=14.5e$. The $J=6.5f$ level is characterized by the following set of quantum numbers ($J=6.5$, $N=7$, parity -, f label). A level described by the same set of quantum numbers also exists for the $^2\Sigma^+$ state, thus the $J=6.5f$ level of the $C^2\Pi_{3/2}$ state has “+” Kronig symmetry. The $J=14.5e$ level is characterized by ($J=14.5$, $N=15$, parity +, e label) and an analogous level does not exist for a $^2\Sigma^+$ state, thus it has “-” Kronig symmetry. It is also very useful to remember the related rotational selection rules: P- and R-form lines connect levels with the same Kronig symmetry, while O- and Q-form lines connect those of opposite symmetry.

Substituting $\mathbf{N}=\mathbf{J}-\mathbf{l}$ in Eq. 4.3, the rotational Hamiltonian can be written as

$$\mathbf{H}_{\text{rot}} = B(\mathbf{r}) (\mathbf{N} - \mathbf{l}) = B(\mathbf{r}) [(\mathbf{N}^2 - \mathbf{N}_z^2) + (\mathbf{l}^2 - \mathbf{l}_z^2) - (\mathbf{N}^+\mathbf{l} + \mathbf{N}\mathbf{l}^+)]. \quad (4.28)$$

The symmetrized case(b) basis functions are defined for $\Lambda > 0$ as

$$|\Lambda J N \Lambda \pm \rangle = 2^{-1/2} (|\Lambda J N \Lambda \rangle \pm |-\Lambda J N -\Lambda \rangle) \quad (4.29)$$

and for $\Lambda = 0$

$$|0 J N 0 \rangle. \quad (4.30)$$

The diagonal matrix elements of the rotational Hamiltonian can be calculated as

$$\langle \Lambda J N \Lambda | \mathbf{H} | \Lambda J N \Lambda \rangle = \langle B(r) \rangle [N(N+1) + l(l+1) - 2\Lambda^2] \quad (4.31)$$

and the off-diagonal matrix elements as

$$\langle \Lambda J N \Lambda | \mathbf{H} | \Lambda+1 J N \Lambda+1 \rangle = \langle B(r) \rangle \sqrt{\frac{2}{2 - \delta_{\Lambda 0}}} \sqrt{N(N+1) - \Lambda(\Lambda+1)} \sqrt{l(l+1) - \Lambda(\Lambda+1)}. \quad (4.32)$$

When spin-orbit interaction cannot be neglected, as in the case of the BaF molecule, the spin-orbit Hamiltonian has to be added to the total Hamiltonian of the molecule. The spin-orbit interaction can mix the “+” and “-” Kronig symmetries, thus the isolated *s-p-d-f-g-h* supercomplex matrix is again of the size of 36. However, since spin-orbit splittings in the BaF molecule are smaller than electronic splittings (Hund’s case (a) rather than Hund’s case (c) at low- n^*) the matrix can be written as “almost” block-diagonal in the Kronig symmetry. As N increases, the off-block-diagonal matrix elements become less and less important and at some N , which, for a particular molecule, depends on experimental precision, can be neglected. Like before, the spin-orbit Hamiltonian is given by (see Eq. 4.6)

$$\mathbf{H}_{so} = A(r) \mathbf{l} \cdot \mathbf{s} = A(r) L_z s_z + \frac{1}{2} A(r) (\mathbf{l}^+ \mathbf{s}^- + \mathbf{l} \mathbf{s}^+), \quad (4.33)$$

where the first term is diagonal in Λ and the second term produces matrix elements off-diagonal in Λ . Now, when spin-orbit interaction is included in the total Hamiltonian, N is not a rigorously good quantum number anymore. The both terms of the spin-orbit

Hamiltonian (Eq. 4.33) can produce matrix elements both diagonal and off-diagonal in N (but diagonal in J).

The first term, $A(r)\mathbf{l}_z\mathbf{s}_z$, which is diagonal in Λ ($\Lambda=\lambda$), can be rewritten as

$$A(r)\mathbf{l}_z\mathbf{s}_z = A(r)\Lambda s = A(r)\Lambda_{\parallel}s + A(r)\Lambda_{\perp}s, \quad (4.34)$$

where Λ is the component of the angular momentum of the Rydberg electron (and total angular momentum of the molecule) along the internuclear axis and Λ_{\parallel} and Λ_{\perp} are components of Λ , parallel and perpendicular to the \mathbf{N} vector, respectively. The first term of Eq. 4.34 produces matrix elements diagonal in the N quantum number and the second term off-diagonal. The matrix elements of the spin-orbit Hamiltonian in Hund's case (b) have been discussed by Kovacs¹⁰ and matrix elements for some special cases have been given. The spin-orbit matrix elements diagonal in Λ can be calculated as

$$\langle \Lambda J N \Lambda | \mathbf{H} | \Lambda J N \Lambda \rangle = \langle A(r) \rangle \Lambda^2 \frac{J(J+1) - N(N+1) - S(S+1)}{2N(N+1)}, \quad (4.35)$$

and

$$\begin{aligned} \langle \Lambda J N \Lambda | \mathbf{H} | \Lambda J N+1 \Lambda \rangle &= \\ &= \langle A(r) \rangle \Lambda \frac{\sqrt{[(N+1)^2 - \Lambda^2][(J+N+1)(J+N+2) - S(S+1)][S(S+1) - (J-N)(J-N-1)]}}{2(N+1)\sqrt{(2N+1)(2N+3)}}. \end{aligned} \quad (4.36)$$

The matrix elements off-diagonal in Λ are

$$\begin{aligned} \langle \Lambda J N \Lambda | \mathbf{H} | \Lambda+1 J N \Lambda+1 \rangle &= \\ &= \langle A(r) \rangle \sqrt{\frac{2}{2-\delta_{\Lambda 0}}} \sqrt{l(l+1) - \Lambda(\Lambda+1)} \sqrt{(N-\Lambda)(N+\Lambda+1)} \frac{N(N+1) + S(S+1) - J(J+1)}{4N(N+1)}, \end{aligned} \quad (4.37)$$

and

$$\begin{aligned} \langle l \Lambda J N \Lambda | \mathbf{H} | l \Lambda + 1 J N + 1 \Lambda + 1 \rangle &= \sqrt{\frac{2}{2 - \delta_{\Lambda 0}}} \sqrt{l(l+1) - \Lambda(\Lambda+1)} \times \\ &\times \sqrt{\frac{[(J+N+1)(J+N+2) - S(S+1)][S(S+1) - (J-N)(J-N-1)](N+\Lambda+1)(N+\Lambda+2)}{16(N+1)^2(2N+1)(2N+3)}}. \end{aligned} \quad (4.38)$$

It was previously mentioned that in the BaF molecule the spin-orbit splittings are nonnegligible even at high- n^* Rydberg states. Below, we will estimate the N value, at which the spin-orbit effects can be neglected at given experimental precision (0.01 cm^{-1}). Let us first consider the spin-orbit matrix element diagonal in N and Λ (Eq. 4.35). Substituting $J=N+\frac{1}{2}$ into Eq. 4.35 we get

$$\langle l \Lambda J N \Lambda | \mathbf{H} | l \Lambda J N \Lambda \rangle = \langle A(r) \rangle \Lambda^2 \frac{1}{2(N+1)}. \quad (4.39)$$

In the particular case of the $9.23^2\Delta$ state, $A=1.229 \text{ cm}^{-1}$ and $\Lambda=2$, assuming experimental precision equal 0.01 cm^{-1} we estimate that the spin-orbit matrix element given by Eq. 4.39 can be neglected for $N>245$, thus well beyond our experimental range of N . We can also consider the off-diagonal in N matrix element (Eq. 4.36) and estimate the N value at which term value shifts due to this matrix elements are smaller than experimental precision. Substituting $J=N+\frac{1}{2}$ into Eq. 4.36 we get

$$H_{so} = \langle l \Lambda J N \Lambda | \mathbf{H} | l \Lambda J N + 1 \Lambda \rangle = \frac{\sqrt{2}}{4} \langle A(r) \rangle \Lambda \frac{\sqrt{(N+1)^2 - 4}}{N+1}. \quad (4.40)$$

The splitting between rotational terms with the same value of J quantum number and N different by 1 can be calculated as

$$\Delta E = T(N+1) - T(N) = 2B(N+1). \quad (4.41)$$

Using Eqs. 4.40 and 4.41 we can calculate the energy shifts due to the off-diagonal spin-orbit matrix element as

$$\Delta = \frac{\Delta E}{2} - \sqrt{\left(\frac{\Delta E}{2}\right)^2 + |H_{so}|^2}. \quad (4.42)$$

Substituting Eqs. 4.40 and 4.41 into 4.42 we calculate that at $N=160$ the energy shifts due to the off-diagonal spin-orbit matrix element can be neglected at experimental precision 0.01 cm^{-1} .

The above analysis clearly shows that, in the BaF molecule, the spin-orbit effects are nonnegligible even at $n^*\approx 9-10$. The effects at intermediate and high- n^* are, however, small enough that Hund case (b) basis function can be used to evaluate matrix elements of the Hamiltonian.

4.6 Models for core-nonpenetrating states of diatomic molecules.

4.6.1 Long-range model in spherical coordinates.

In Section 4.1 we introduced the electrostatic/penetration Hamiltonian, \mathbf{H}_{el} , describing the interaction of a Rydberg electron with the molecular ion-core. Models utilizing this kind of Hamiltonian, so called long-range models, have been successfully applied in the analysis of core-nonpenetrating states first, by Jungen and Miescher¹¹, for f -complexes of the NO molecule and later by others¹² to various molecules. The model is based on the assumption that the charge distribution of a molecular ion-core does not differ appreciably from spherical, thus l -mixing interactions due to core nonsphericity can be treated in a perturbative way. The model treats a Rydberg electron-molecular core interaction as an electrostatic interaction. Such an assumption is well justified for core-nonpenetrating states, for which there is no spatial overlap between the orbitals of a Rydberg electron and those of the core electrons. Further, we will attempt to modify the \mathbf{H}_{el} model so it could also be used with weakly-penetrating states.

We assume now, that a Rydberg electron interacts electrostatically with a molecular core, for which the charge distribution is $\rho(\mathbf{r})$, and we allow for core-penetration. The electrostatic/penetration Hamiltonian, \mathbf{H}_{el} , can, thus be defined as

$$\mathbf{H}_{el} = \int_0^{\infty} \rho(\mathbf{r}) \frac{1}{|\mathbf{r}_{el} - \mathbf{r}|} d^3\mathbf{r}. \quad (4.43)$$

Using the well known expansion

$$\frac{1}{|\mathbf{r}_{el} - \mathbf{r}|} = \sum_{k=0}^{\infty} \frac{4\pi}{2k+1} \frac{r_{<}^k}{r_{>}^{k+1}} \sum_{m=-k}^k Y_{km}^*(\hat{\mathbf{r}}) Y_{km}(\hat{\mathbf{r}}_{el}), \quad (4.44)$$

where $r_{<}$ and $r_{>}$ are the smaller and larger of r and r_{el} , and making the assumption that outside the molecular core* ($r > r_{core}$) the core charge distribution, $\rho(\mathbf{r})$, is zero, \mathbf{H}_{el} can be rewritten as

$$\mathbf{H}_{el} = \sum_{k=0}^{\infty} \frac{4\pi}{2k+1} Y_{k0}(\hat{\mathbf{r}}_{el}) \left(\int_0^{r_{core}} \rho(\mathbf{r}) \frac{r_{<}^k}{r_{>}^{k+1}} Y_{k0}(\hat{\mathbf{r}}) d^3\mathbf{r} \right). \quad (4.45)$$

In the above expression, the summation over m collapsed due to the cylindrical symmetry of the molecule. Substituting r and r_{el} for $r_{<}$ and $r_{>}$ and considering 2 possible cases, the Eq. () takes the form

$$\mathbf{H}_{el} = \sum_{k=0}^{\infty} \sqrt{\frac{4\pi}{2k+1}} Y_{k0}(\hat{\mathbf{r}}_{el}) \tilde{\mathbf{K}}_{k0}(r_{el}) \quad (4.46)$$

where

$$\tilde{\mathbf{K}}_{k0}(r_{el}) = \sqrt{\frac{4\pi}{2k+1}} \left(\int_0^{\min(r_{el}, r_{core})} \rho(\mathbf{r}) r^k Y_{k0}(\hat{\mathbf{r}}) d^3\mathbf{r} \cdot \frac{1}{r_{el}^{k+1}} + \int_{\min(r_{el}, r_{core})}^{r_{core}} \rho(\mathbf{r}) \frac{1}{r^{k+1}} Y_{k0}(\hat{\mathbf{r}}) d^3\mathbf{r} \cdot r_{el}^k \right). \quad (4.47)$$

For core-nonpenetrating states $\min(r_{el}, r_{core}) = r_{core}$, thus the second term in the sum above is zero. Recognizing the first integral as a familiar expression for a 2^k -pole electrostatic moment, electrostatic/penetration Hamiltonian, \mathbf{H}_{el} , for core-nonpenetrating states is

$$\mathbf{H}_{el}^{nonpen.} = \sum_{k=0}^{\infty} \sqrt{\frac{4\pi}{2k+1}} Y_{k0}(\hat{\mathbf{r}}_{el}) \tilde{\mathbf{Q}}_{k0} \frac{1}{r_{el}^{k+1}}, \quad (4.48)$$

where the multipole moments are defined as

* There is no strict definition of r_{core} . For the purpose of a multipole expansion in the BaF^+ center-of-mass coordinate system, r_{core} can be taken as the sum of the ionic radius of Ba^{2+} and twice the ionic radius of F^- , $r_{core} = r_{\text{Ba}^{2+}} + 2 \cdot r_{\text{F}^-} \approx 4 \text{ \AA}$ (in BaF , the center-of-mass is located about $0.12r_e$ from Ba^{2+} , so one can almost say that the F^- ion rotates around the Ba^{2+} ion).

$$\tilde{Q}_{k0} = \sqrt{\frac{4\pi}{2k+1}} \int_0^{r_{\text{core}}} \rho(\mathbf{r}) r^k Y_{k0}^*(\hat{\mathbf{r}}) d^3\mathbf{r}. \quad (4.49)$$

The long-range models utilize spherical harmonics and hydrogenic radial wavefunctions (or hydrogenic wavefunction modified for non-integer n^*) to evaluate corrections to the hydrogenic energies due to the multipole moments and polarizabilities of the molecular core. Calculations are done in a spherical coordinate system with the origin located at the center-of-mass of the molecule. An attempt to apply this kind of model to highly polar diatomic molecules like BaF must fail. The strong asymmetry of the charge distribution of the molecular ion-core leads, in the center-of-mass coordinate system, to a slowly converging multipole expansion with very large dipole, quadrupole and higher electric multipole moments. Assuming, for simplicity, a 2-point charge model for the BaF^+ ion-core (+2 charge on the Ba^{2+} closed shell ion and -1 charge on the F^- closed shell ion), one can calculate BaF^+ multipole moments in the center-of-mass coordinate system (Table 1). The values are extremely large, significantly larger than for any molecule for which this kind of model has been previously applied.

Table 1: The lowest multipole moments of BaF^+ (2-point charge model) in the center-of-mass coordinate system.

l		2^l -moment [au]
1	dipole	-4.41
2	quadrupole	-11.48
3	octupole	-41.45
4	hexadecapole	-142.34

To see the scale of the problem one can compare the BaF^+ quadrupole moment of -11.48 au to the almost 20 times smaller quadrupole moment of the NO^+ ion (0.59(5) au)¹¹. But it is primarily the dipole moment of -4.41 au or 11.2 D which makes the multipole model (with the multipole expansion in the center-of-mass coordinate system) inapplicable for the BaF molecule. Inapplicability is related to the fact that off-diagonal matrix elements of the long-range interaction calculated in the spherical basis

are comparable or, in some cases, even larger than the spacing of the Λ -states. We illustrate this by calculating diagonal and off-diagonal long-range interaction matrix elements for the $^2\Phi$ states of the $n^*=11$ supercomplex with l quantum number in the range of 3-6, in a spherical coordinate system, using modified hydrogenic wavefunctions and multipole moments from the 2-point charge model. The results are presented below.

	$f^2\Phi$	$g^2\Phi$	$h^2\Phi$	$i^2\Phi$
$f^2\Phi$	-14.8	5.08	0.06	
$g^2\Phi$	5.08	-8.58	1.35	0.02
$h^2\Phi$	0.06	1.35	-2.8	0.04
$i^2\Phi$		0.02	0.04	-2.4

Note: The term value of 37838.08 cm^{-1} is subtracted from the diagonal matrix elements.

In the calculation we used a quantum defect of 0.86 for the f , 0.02 for the g , and 0.0 for the h and i states. For the $f^2\Phi \sim g^2\Phi$ and $g^2\Phi \sim h^2\Phi$ interactions, the $\Delta l=1$ matrix elements are especially large. A similar calculation can be done for lower- Λ states, for which the off-diagonal matrix elements are even more significant.

4.6.2 Core-penetration effects.

Continuing the evaluation of the electrostatic/penetration Hamiltonian, we will discuss some of the core-penetration effects. Reorganizing the first integral in the expression for $\tilde{K}_{k0}(r_{el})$, Eq. (), as follows

$$\tilde{K}_{k0}(r_{el}) = \sqrt{\frac{4\pi}{2k+1}} \left(\int_0^{r_{core}} \rho(\mathbf{r}) r^k Y_{k0}^*(\hat{\mathbf{r}}) d^3\mathbf{r} \cdot \frac{1}{r_{el}^{k+1}} - \int_{\min(r_{el}, r_{core})}^{r_{core}} \rho(\mathbf{r}) r^k Y_{k0}^*(\hat{\mathbf{r}}) d^3\mathbf{r} \cdot \frac{1}{r_{el}^{k+1}} + \int_{\min(r_{el}, r_{core})}^{r_{core}} \rho(\mathbf{r}) \frac{1}{r^{k+1}} Y_{k0}^*(\hat{\mathbf{r}}) d^3\mathbf{r} \cdot r_{el}^k \right), \quad (4.50)$$

and combining the second and the third integrals

$$\tilde{\mathbf{K}}_{k0}(r_{el}) = \sqrt{\frac{4\pi}{2k+1}} \left(\frac{1}{r_{el}^{k+1}} \int_0^{r_{core}} \rho(\mathbf{r}) r^k Y_{k0}^*(\hat{\mathbf{r}}) d^3\mathbf{r} + \int_{\min(r_{el}, r_{core})}^{r_{core}} \rho(\mathbf{r}) \left(\frac{r_{el}^k}{r^{k+1}} - \frac{r^k}{r_{el}^{k+1}} \right) Y_{k0}^*(\hat{\mathbf{r}}) d^3\mathbf{r} \right) \quad (4.51)$$

we can write $\tilde{\mathbf{K}}_{k0}(r_{el})$ as a sum of 2 terms

$$\tilde{\mathbf{K}}_{k0}(r_{el}) = \frac{1}{r_{el}^{k+1}} \tilde{\mathbf{Q}}_{k0} + \tilde{\mathbf{W}}_{k0}(r_{el}), \quad (4.52)$$

where

$$\tilde{\mathbf{W}}_{k0}(r_{el}) = \sqrt{\frac{4\pi}{2k+1}} \int_{\min(r_{el}, r_{core})}^{r_{core}} \rho(\mathbf{r}) \left(\frac{r_{el}^k}{r^{k+1}} - \frac{r^k}{r_{el}^{k+1}} \right) Y_{k0}^*(\hat{\mathbf{r}}) d^3\mathbf{r} \quad (4.53)$$

is the penetration operator (functional).

The penetration operator just derived, Eq. (4.53), describes, however, only one kind of penetration effect: increase of the effective charge of the molecular core for $r_{el} < r_{core}$. In the general case of a penetration interaction of a Rydberg electron with a molecular core, two additional effects must be taken into account: exchange interaction between Rydberg and molecular core electrons and the possible nonorthogonality of the Rydberg and core electron wavefunctions. These effects, together with the Coulomb interaction considered above, are treated by pseudopotential theory¹³. The core pseudopotential, U^{core} , consists of a local Coulomb potential (considered in \mathbf{H}_{el}), and nonlocal parts, the exchange and the orthogonalization terms. The exchange interaction and the additional Coulomb attraction are of the same order of magnitude¹⁴ and both lower the energy, thus also n^* . The orthogonalization term, which ensures orthogonality between the Rydberg and core electron orbitals, can be described by the Phillips-Kleinman term as

$$V_{\lambda}^{PK} = \sum_i (E_{n^*\lambda} - E_{i,\lambda}) |\lambda; i\rangle \langle \lambda; i|. \quad (4.54)$$

The Phillips-Kleinman term is always repulsive, since the energy of the Rydberg state, $E_{n^*\lambda}$, is greater than the energy of the core electrons, $E_{i,\lambda}$. We can also see, that this term

is zero for Rydberg orbitals which have no core precursor^{*15} (f and higher- l states in the BaF molecule). The exchange and extra Coulomb attraction terms disappear only for nonpenetrating states.

For the heteronuclear molecules with the large asymmetry of core charge distribution, like in the alkaline earth monohalides, the effective (pseudo)potential in the case of core-penetrating states is highly nonlocal. The electrostatic/penetration Hamiltonian, \mathbf{H}_{el} , described above does not contain a nonlocal part, thus, when applied to weakly penetrating states it does not properly treat exchange corrections. We can modify it assuming a more general, nonlocal form of the penetration operator, to get

$$\mathbf{H}'_{el} = \sum_{k=0}^{\infty} \sqrt{\frac{4\pi}{2k+1}} \tilde{\mathbf{K}}'_{k0}. \quad (4.55)$$

The core penetration operator is defined now as the difference between the Rydberg electron ~ molecular core interaction operator (electrostatic/penetration operator) and the long-range interaction operator between the Rydberg electron and the molecular core treated as a structureless object with electric multipole moments equal to those of the real core

$$\tilde{\mathbf{W}}'_{k0}(\mathbf{r}_{el}) = \tilde{\mathbf{K}}'_{k0}(\mathbf{r}_{el}) - Y_{k0}(\hat{\mathbf{r}}_{el}) \frac{1}{r_{el}^{k+1}} \tilde{\mathbf{Q}}_{k0}. \quad (4.56)$$

Penetration effects and their relevance to the BaF molecule will be further discussed later.

4.6.3 Watson's model for dipolar diatomic molecules.

Watson¹⁶, who recognized the importance of the effects of a large molecular core dipole moment on Rydberg structure, considered a simple model of a hydrogen atom with a

* Core precursors of the Rydberg orbitals are defined as occupied core orbitals with the same value of l . In the case of alkaline earth monohalides these are core orbitals of the alkaline earth atomic ion. For most of the molecules core penetrating Rydberg orbitals also have core precursors. In the BaF molecule, however, f states are core penetrating, but f orbitals (for example $f^2\Phi$) have no core precursors. Similarly, core penetrating d states in the CaF molecule have no core precursors.

point dipole moment. He pointed out that, in long-range models, a dipole moment term is often omitted because first-order energetic effects of a dipole moment are zero. However, its first-order effects on wavefunctions can be very significant, and in this way affecting energetic structure, intensities and other molecular properties. Even if Watson's model is strictly correct in the limit of a small dipole moment it provides a lot of insight into effects of a core dipole on the properties of Rydberg states.

Let us consider a zero-order wavefunction as

$$|n l \lambda\rangle_0 = |n l\rangle |l \lambda\rangle.$$

The correction to the zero-order wavefunction due to the core dipole moment, according to Watson, is

$$|n l \lambda\rangle_1 = |n l\rangle \sum_{l'=l\pm 1} C_{ll'\lambda} |l' \lambda\rangle,$$

where

$$C_{l+1,l,\lambda} = -C_{l,l+1,\lambda} = \frac{Q_{10}}{(l+1)} \sqrt{\frac{(l+1)^2 - \lambda^2}{(2l+1)(2l+3)}}. \quad (4.57)$$

Thus, the core dipole moment, Q_{10} , mixes the angular part of the $n l \lambda$ wavefunction with wavefunctions of $l \pm 1$ states leaving the radial part unchanged. Using the corrected wavefunctions, the second-order correction to the Rydberg state energy (in cm^{-1}) can be calculated as

$$E_{n l \lambda}^{(2)} = Q_{10}^2 \frac{4\Re [l(l+1) - 3\lambda^2]}{(n^*)^3 (2l+3)(2l+1)(2l-1)l(l+1)}. \quad (4.58)$$

Watson also noticed that the second-order energy corrections due to the core dipole moment equal Q_{10} , are the same as the first-order corrections due to the core quadrupole moment equal $Q_{20} = -(Q_{10})^2$. Now, it is straightforward to generalize the Eq. (4.58) for the case when the molecular core also possesses a quadrupole moment, Q_{20} . The generalized energy correction is now

$$E_{n\lambda}^{(2)} = (Q_{10}^2 - Q_{20}) \cdot \frac{4\Re [l(l+1) - 3\lambda^2]}{(n^*)^3 (2l+3)(2l+1)(2l-1)l(l+1)}. \quad (4.59)$$

The Λ -splitting is, thus, determined by $(Q_{10}^2 - Q_{20})$, which for the BaF molecule ($Q_{20} < 0$) is extremely large (30.9 au). For high- n^* states, by comparing the energy corrections, Eq. (4.59), with the term linear in μ in an expansion of the Rydberg formula near integer- n^* ($\mu_{n\lambda}=0$), we can obtain quantum defect corrections, $\mu_{n\lambda}$, as

$$\mu_{n\lambda} = -(Q_{10}^2 - Q_{20}) \cdot \frac{2[l(l+1) - 3\lambda^2]}{(2l+3)(2l+1)(2l-1)l(l+1)}. \quad (4.60)$$

Watson also discussed the dependence of the dipole and quadrupole moments on the choice of the coordinate system. Since the total charge of the molecular ion-core is nonzero ($Z=1$), the values of all multipole moments, except for the monopole, depend on the choice of coordinate system. Let us consider two coordinate systems separated by Δz , with the dipole and quadrupole moments defined as (Q_{10}, Q_{20}) and (Q'_{10}, Q'_{20}) , respectively. The following relations describe the effect of the change of origin of the coordinate system

$$Q'_{10} = Q_{10} - \Delta z \quad (4.61)$$

and

$$Q'_{20} = Q_{20} - 2Q_{10}\Delta z + (\Delta z)^2. \quad (4.62)$$

These origin dependences of Q_{10} , and Q_{20} led Watson to the idea of an isotope effect induced by the origin dependence of the core dipole moment. This conclusion is, however, incorrect. We can guess that the reason for arriving at the wrong conclusion is that he considered only dipole corrections to the energy. If both dipole and quadrupole corrections are considered together, as in Eq 4.59, we can verify that even if dipole and quadrupole moments depend separately on the choice of origin, the value of $(Q_{10}^2 - Q_{20})$ is invariant with respect to the change of coordinate system. Assuming so, we substitute Eqs. 4.61 and 4.62 into $(Q_{10}^2 - Q_{20})$ obtaining

$$(Q'_{10}{}^2 - Q'_{20}) = (Q_{10} - \Delta z)^2 - (Q_{20} - 2Q_{10}\Delta z + (\Delta z)^2) = (Q_{10}^2 - Q_{20}), \quad (4.63)$$

which proves that there is no dipole (or quadrupole) related isotope effect. It also means that the energy of a molecular state cannot depend on the choice of coordinate system.

4.6.4 Long-range model in prolate spheroidal coordinate system.

The long-range kind of model can be applied to polar molecules by using the prolate spheroidal coordinate system, which is more natural for such systems. Such a coordinate system has been applied in the past to a variety of one-electron, two-center problems. Recently, Harris and Jungen¹⁷ used it in their multichannel quantum defect theory calculations of the electronic structure of the CaF molecule. Hadinger and others¹⁸ reviewed various methods used to solve the Schrödinger equation and proposed an efficient computational technique to obtain simultaneously eigenvalues and eigenfunctions of the one-electron two-center problem.

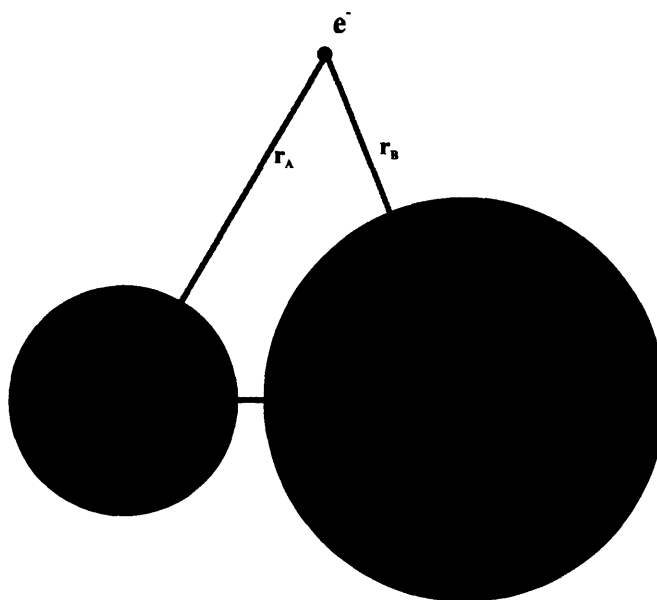


Figure 9: Simple model of BaF^+ and definition of the spheroidal coordinate system.

The prolate spheroidal coordinates (ξ, η, φ) are defined (see Figure 9) in terms of distances from two foci, A and B, and the separation of foci, R, as

$$\begin{aligned}
\xi &= (r_A + r_B)/R & 1 \leq \xi < \infty \\
\eta &= (r_A - r_B)/R & -1 \leq \eta \leq 1 \\
\varphi & & 0 \leq \varphi \leq 2\pi.
\end{aligned} \tag{4.64}$$

The BaF^+ molecular ion-core can be well described as two closed shell atomic ions, Ba^{2+} and F^- . The 2 foci, A and B, of the spheroidal coordinate system are chosen at the Ba and F nuclei, respectively. The charge distribution of the molecular ion-core is represented by $\rho_A(\mathbf{r}'_A)$ and $\rho_B(\mathbf{r}'_B)$. The electrostatic interactions in the 3 particle system are given as

$$V = \int \frac{\rho(\mathbf{r}'_A)}{|\mathbf{r}_A - \mathbf{r}'_A|} d^3 r'_A + \int \frac{\rho(\mathbf{r}'_B)}{|\mathbf{r}_B - \mathbf{r}'_B|} d^3 r'_B + \iint \frac{\rho(\mathbf{r}'_A)\rho(\mathbf{r}'_B)}{|\mathbf{r}'_A - \mathbf{r}'_B - \mathbf{R}|} d^3 r'_A d^3 r'_B. \tag{4.65}$$

The third term, in a *frozen core approximation*, for core-nonpenetrating states, can be assumed to be independent of electronic state, thus can be included in the total energy. The Rydberg electron in the core-nonpenetrating state can change charge distribution in the core by inducing core polarization. The molecular ion-core is composed of two closed shell atomic ions, so the Rydberg electron induced core polarization is expected to be negligible in a zero order approximation. The energetic effects due to the third term can, thus, be treated in a perturbative way later. Now, we can concentrate on V_0 defined as the sum of the first and second terms. Using a multipole expansion for the charge distributions $\rho_A(\mathbf{r}_A)$ and $\rho_B(\mathbf{r}_B)$ in spherical coordinate systems centered on A and B, respectively, the V_0 term can be expressed as

$$V_0 = \sum_{l_A=0} \sum_{m_A=-l_A}^{l_A} \frac{4\pi}{2l_A+1} (Q_A)_{l_A m_A} \frac{Y_{l_A m_A}(\theta_A, \varphi_A)}{r_A^{l_A+1}} + \sum_{l_B=0} \sum_{m_B=-l_B}^{l_B} \frac{4\pi}{2l_B+1} (Q_B)_{l_B m_B} \frac{Y_{l_B m_B}(\theta_B, \varphi_B)}{r_B^{l_B+1}}, \tag{4.66}$$

where

$$(Q_A)_{l_A m_A} = \int Y_{l_A m_A}^* r_A^{l_A} \rho(r'_A) d^3 r'_A, \tag{4.67}$$

and

$$(Q_B)_{l_B m_B} = \int Y_{l_B m_B}^* r_B^{l_B} \rho(r'_B) d^3 r'_B. \tag{4.68}$$

Writing the monopole terms explicitly, the potential V_0 can be expressed as a sum of a Coulomb two-center potential, V_C , and a perturbation potential, V_{pert} . Now, we have

$$V_C = \frac{Z_A}{r_A} + \frac{Z_B}{r_B}, \quad (4.69)$$

and

$$V_{\text{pert}} = \sum_{l_A=1} \frac{4\pi}{2l_A+1} (Q_A)_{l_A 0} \frac{Y_{l_A m}(\theta_A, \varphi_A)}{r_A^{l_A+1}} + \sum_{l_B=1} \frac{4\pi}{2l_B+1} (Q_B)_{l_B 0} \frac{Y_{l_B m}(\theta_B, \varphi_B)}{r_B^{l_B+1}}, \quad (4.70)$$

where the summation over m collapses due to the cylindrical symmetry of the problem and the summation over l now starts from 1. The Schrödinger equation with the zero-order Hamiltonian including the Coulomb two-center potential, V_C , is separable in the spheroidal coordinate system and can be solved iteratively using, for example, the method described by Hadinger and others¹⁸. (See Section 5.2 for the description of the computer program and Appendix B for source code listing). Solution of the two-center Coulomb problem produces 3 eigenvalues: total energy, E , spheroidal separation constant (a function of angular momentum), A , and the projection of the electron angular momentum on the z axis, λ , as well as an eigenfunction, Ψ , expressed as a product

$$\Psi = M(\eta, \varphi) \Lambda(\xi), \quad (4.71)$$

where

$$M(\eta, \varphi) = e^{i\lambda\varphi} e^{-p\eta} \sum_{k=\lambda} a_k P_k^\lambda(\eta) \quad (4.72)$$

and

$$\Lambda(\xi) = (\xi^2 - 1)^{\lambda/2} e^{-p(\xi-1)} \sum_{k=0} C_k L_{\lambda+k}^\lambda(2p(\xi-1)). \quad (4.73)$$

The “angular” functions, $M(\eta, \varphi)$, are expressed in terms of Legendre polynomials, $P_k^\lambda(\eta)$, and the “radial” functions, $\Lambda(\xi)$, are expressed in terms of Laguerre polynomials $L_{\lambda+k}^\lambda(2p(\xi-1))$. The parameter p is a function of energy and internuclear distance, R , and is defined as

$$p = \frac{1}{2}R(2(IP - E))^{1/2}. \quad (4.74)$$

Once we calculate two-center energies and wavefunctions we can calculate corrections to the energies due to the higher multipole moments, which are localized on the 2 atomic ions, Ba^{2+} and F^- . The lowest-order corrections come from the dipole and quadrupole moments of the Ba^{2+} and F^- ions. One may notice at this point that these multipole moments of atomic ions, expressed in spherical coordinate systems centered on their respective nuclei, are much smaller than the total multipole moments of the molecule expressed in the center-of-mass coordinate system. They, however, still can be quite large as either ion is subjected to the very large electric field of its counter-ion. As a result, off-diagonal long-range interaction matrix elements should now be much smaller than the energy separations between zero-order states and a perturbative treatment of these electrostatic interactions should be justified.

The dipole corrections (see Section 4.2 for a general expression for multipole corrections in spherical coordinate system) to the two-center Coulomb energies are

$$\left\langle \Psi' \left| (Q_A)_{10} \frac{\cos\theta_A}{r_A^2} + (Q_B)_{10} \frac{\cos\theta_B}{r_B^2} \right| \Psi'' \right\rangle, \quad (4.75)$$

or, expressed in spheroidal coordinates, where

$$r_A = \frac{1}{2}R(\xi + \eta) \quad \text{and} \quad r_B = \frac{1}{2}R(\xi - \eta), \quad (4.76)$$

and

$$\cos\theta_A = \frac{-1 - \xi\eta}{\xi + \eta} \quad \text{and} \quad \cos\theta_B = \frac{1 - \xi\eta}{\xi - \eta}, \quad (4.77)$$

they take the form

$$-\frac{4}{R} \left\langle \Psi' \left| (Q_A)_{10} \frac{1 + \xi\eta}{(\xi + \eta)^3} + (Q_B)_{10} \frac{1 - \xi\eta}{(\xi - \eta)^3} \right| \Psi'' \right\rangle. \quad (4.78)$$

¹ J. T. Hougen, *The Calculation of Rotational Energy Levels and Rotational Line Intensities in Diatomic Molecules.*, Nat. Bur. Stand. (U.S.), Monogr. 115, 1970.

-
- ² E. U. Condon and G. H. Shortley, *The Theory of Atomic Spectra* (Cambridge University Press), Cambridge, U. K., 1951.
- ³ J. M. Brown, J. T. Hougen, K.-P. Huber, J. W. C. Johns, I. Kopp, H. Lefebvre-Brion, A. J. Merer, D. A. Ramsay, J. Rostas, and R. N. Zare, *J. Mol. Spectrosc.* **55**, 500 (1975).
- ⁴ Hélène Lefebvre-Brion and Robert W. Field, *Perturbations in the Spectra of Diatomic Molecules*, Academic Press (1986).
- ⁵ J. M. Brown, E. A. Colbourn, J. K. G. Watson, and F. D. Wayne, *J. Mol. Spectrosc.* **74**, 294-318 (1979).
- ⁶ C. Amiot, J.-P. Maillard, and J. Chauville, *J. Mol. Spectrosc.* **87**, 196-218 (1981).
- ⁷ J. A. Coxon, *J. Mol. Spectrosc.* **58**, 1-28 (1975).
- ⁸ A. J. Kotlar, R. W. Field, J. I. Steinfeld, and J. A. Coxon, *J. Mol. Spectrosc.* **80**, 86-108 (1980).
- ⁹ S. F. Rice, W. J. Childs, and R. W. Field, *J. Mol. Spectrosc.* **133**, 22-35 (1989).
- ¹⁰ I. Kovacs, *Rotational Structure in the Spectra of Diatomic Molecules.*, Akademiai Kiado, Budapest (1969).
- ¹¹ Ch. Jungen and E. Miescher, *Can. J. Phys.* **47**, 1769-1787 (1969).
- ¹² E. E. Eyler and F. M. Pipkin, *Phys. Rev. A*, **27** (5), 2462-2478 (1983).
- ¹³ R. N. Dixon, I. L. Robertson, *The Use of Pseudopotentials in Molecular Calculations in Adv. Theor. Chem.* , 100-134 ().
- ¹⁴ C. A. Coulson, J. G. Stamper, *Mol. Phys.* **6**, 609 (1963).
- ¹⁵ R. S. Mulliken, *J. Am. Chem. Soc.* **86**, 3183 (1964).
- ¹⁶ J. K. G. Watson, *Mol. Phys.* **81** (2), 277-289 (1994).
- ¹⁷ N. A. Harris and Ch. Jungen, *Phys. Rev. Lett.* **70** (17), 2549-2552 (1993).
- ¹⁸ G. Hadinger, M. Aubert-Frécon, and G. Hadinger, *J. Phys. B: At. Mol. Opt. Phys.* **22**, 697-712 (1989).

5. Computer programs.

5.1 Implementation of Hellmann-Feynman theorem in LSQ fitter.

In any experimental work, a least-squares optimization routine, used to fit a parametrized model to experimental data, is usually of major importance. Field's group fitter, LSQ, has been used in the group for 21 years. Several improvements have been made in the past. Now it is time for a major update. We made two kinds of important changes. First of all, the Hellmann-Feynman theorem¹ has been applied to calculate derivatives with respect to fitted parameters, replacing the traditional method of finite differences. Second, several parts of the LSQ fitter have been rewritten in order to speed up execution, make the program more user-friendly, and update it to modern technology. The full description of the program may be found in the PhD thesis of Ernest Friedman-Hill². Below, we will only comment on changes we made to the program.

The most common method of calculating derivatives in any nonlinear optimization problem is by approximating them as ratios of finite differences. Each fitted parameter is varied sequentially and the change of the dependent variable is calculated. This method requires $p+1$ numerical matrix diagonalizations, where p is the number of optimized parameters. Numerical matrix diagonalizations are usually the most time-consuming parts of any optimization program and their cost is, in the most general case, proportional to n^3 , where n is a size of a matrix. When a model involves many adjustable parameters and large dimension matrices must be numerically diagonalized, the fitter execution time may be unacceptably long. In a specific, but also a typical and very common case in the field of molecular spectroscopy, when a model can be written in a pseudolinear form, the Hellmann-Feynman theorem can be applied to significantly speed up LSQ fitter execution time. Then, for a p -parameter model, only a single (instead of $p+1$) numerical matrix diagonalization is required to compute a full set of derivatives.

The model is considered pseudolinear if it is possible to write a total Hamiltonian as

$$\mathbf{H} = \sum_{m=1}^p X_m \mathbf{H}_m = \sum_{m=1}^p X_m \frac{\partial \mathbf{H}}{\partial X_m}, \quad (5.1)$$

where X_m are fitted parameters and \mathbf{H}_m are matrices. With the total Hamiltonian given by Eq. 5.1, one can take advantage of the Hellmann-Feynman theorem

$$\left(\mathbf{U}^\dagger \frac{\partial \mathbf{H}}{\partial X_k} \mathbf{U} \right)_{ii} = \frac{\partial E_i}{\partial X_k}, \quad (5.2)$$

where E_i are eigenvalues of the total Hamiltonian, \mathbf{H} , and \mathbf{U} is a unitary matrix that diagonalizes \mathbf{H} . Many commercial data analysis packages utilize the Hellmann-Feynman theorem. However, they usually require that analytical forms of the $\partial \mathbf{H} / \partial X_m$ derivatives be supplied.

Field's group fitter is composed of 2 parts: the main, universal part, LSQ, and the model part, MATRIX. The latter must be written by a user for a particular problem. Requiring analytical expressions for the derivatives would substantially increase the programming work each time a new problem is to be solved, which is precisely what we wanted to avoid. Luckily, there is a simple method of calculating the derivatives, $\partial \mathbf{H} / \partial X_m$, even if analytical expressions have not been supplied. One can easily notice that when we set $X_{m \neq k} = 0$ and $X_k = 1$ in Eq. 5.1 and evaluate the matrix of the total Hamiltonian (using subroutine MATRIX) we actually obtain $\mathbf{H}_m = \partial \mathbf{H} / \partial X_m$. Having calculated the matrices, obtaining $\partial E / \partial X_m$ derivatives from the Hellmann-Feynman theorem (Eq. 5.2) is straightforward. To implement the Hellmann-Feynman theorem, the subroutine LEVEL (in LSQ) has been completely rewritten. However, its outside appearance (parameters, common blocks etc.) is unchanged.

Summarizing, the procedure of obtaining the $\partial E_i / \partial X_k$ derivatives is as follows. With initial values of parameters, X_m , the full matrix of the total Hamiltonian is evaluated and numerically diagonalized. The unitary matrix \mathbf{U} is obtained. Now, every fitted parameter, in turn, is set to 1, while all others are set to 0, and the set of $\partial \mathbf{H} / \partial X_m$ matrices is calculated. Finally, the $\partial \mathbf{H} / \partial X_m$ matrices are transformed using the already known unitary matrices \mathbf{U} (Eq. 5.2). Thus, for every fitted parameter a numerical matrix diagonalization

is replaced by two matrix multiplications (Eq. 5.2). In test runs, the optimized fitter with a 5-parameter model and a 3×3 Hamiltonian matrix ran more than 50% faster. We have not, however, performed formal tests using problems with larger sets of parameters and larger matrix sizes for which time savings are expected to increase dramatically.

The LSQ fitter was originally written more than 30 years ago when computers were slow and little RAM memory was available. To overcome the shortage of memory some of the intermediate results had to be temporarily stored on tapes or disks. In modern times, when desktop computers are routinely equipped with 8MB (or more) of RAM memory, temporary storage of intermediate results is in most spectroscopic applications, unnecessary. Accordingly, all of the fragments of LSQ dealing with intermediate data storage have been rewritten. Whenever possible, algorithms have been changed to avoid the use of temporary storage, otherwise matrices have been enlarged or new ones added to accommodate intermediate data.

Another obsolete part of LSQ was character-based plotting of $y_{\text{exp}} - y_{\text{cal}}$ (subroutine PLOT). This option has been eliminated. The empty subroutine PLOT has been, however retained for future applications. (In the present project, the fitter has been compiled for use under Microsoft Windows 3.1 and all graphic data presentation has been handled by Microsoft Excel 5.0.)

All of these programming changes have been described in the LSQ header and extensively commented in the program body. The alterations have not changed the structure of input and output files, except for replacing NUC (nuclear spin) in real*8 format by J_{min} (minimum (or minimum - 0.5) rotational quantum number) in integer*4 format.

5.2 Electronic energy of nonpenetrating states in prolate spheroidal coordinates.

The TOCENTER program calculates electronic energies of core-nonpenetrating states for the one-electron, two-center problem. The program code is based on an algorithm described by Hadinger *et al.*³. It handles input data interactively. The following quantities must be supplied: total charges on center A and center B in a.u.; ionization potential in

cm^{-1} ; lowest n^* , l , and λ to be calculated; highest n^* , l , and λ to be calculated; and intercenter (internuclear) distance in a.u. The following quantities are printed out in order for each calculated state in the output file, TOCENTER.OUT: l and λ ; maximum number of expansion terms of wavefunctions (radial and angular), K_{max} , A , and p parameters; calculated energy (in cm^{-1}) and n^* ; and expansion coefficients listed in three columns, k , a_k/a_0 , and C_k/C_0 . The second output file, TOEXCEL.DAT, prepares results for graphic presentation (by Microsoft Excel in the present case). Four quantities, l , λ , A , and p , are printed in space-separated columns in ASCII format.

For the radial solution of the problem, we used the Hylleraas' functions. They are not orthogonal, however, their advantage compared to others is that they lead to three-term (instead of five-term for others) recurrence relationships. For the angular solution, the Baber and Hassé's functions have been used. They also lead to three-term recurrence relationships. A three-term recurrence relationship, arising from a second-order differential equation, results in two solutions, dominant and subdominant. Only the dominant one, which leads to a divergent wavefunction, can be calculated via forward method. The subdominant solution, which leads to a convergent wavefunction, must be calculated using the backward method. Using Killingbeck's method and Miller's algorithm (see Ref. 3 for detailed description), one can obtain both eigenvalues, A , the angular momentum parameter, and p , the energy parameter, and also convergent eigenfunctions. Both A and p parameters are varied until the pair $(A_{n\lambda}, p_{n\lambda})$ is found, for which: (1) radial and angular functions, satisfying radial and angular Schrödinger equations in prolate spheroidal coordinate systems, converge, (2) the convergence is stable with respect to small variations of A and p , and (3) required precision of A and p is achieved.

5.3 Electronic energy of nonpenetrating states in spherical coordinates.

Electronic energies of nonpenetrating states are calculated in spherical coordinate system using multipole moments supplied, or calculated from 2-point-charge model and hydrogenic wavefunctions modified for non-integer n^* and l . Such a modification of

hydrogenic wavefunctions is necessary in order to deal with weakly penetrating states or large electrostatic splittings. The hydrogenic wavefunction for states with non-zero quantum defects are expressed in terms of hypergeometric functions and calculated using recurrence formulas.

Two programs using hydrogenic wavefunctions have been written, RADIAL, which calculates radial matrix elements of r to any power and BAFSPEC, which calculates energies and electrostatic interaction matrix elements for core-nonpenetrating states in BaF (or any other polar molecule).

¹ Hélène Lefebvre-Brion and Robert W. Field, *Perturbations in the Spectra of Diatomic Molecules*, Academic Press (1986) (and references therein).

² Ernest Friedman-Hill, PhD thesis, Massachusetts Institute of Technology, Cambridge, MA, 1992.

³ G. Hadinger, M. Aubert-Frécon, and G. Hadinger, *J. Phys. B: At. Mol. Opt. Phys.* **22**, 697-712 (1989).

6. Single state fits.

Multidigit molecular constants were certainly not the primary goal of this project. However, as a first step in the assembly and analysis of this global data set for BaF we performed, whenever possible, very careful single, or isolated state fits. This should be considered as one of the necessary steps in the process of assigning or verifying the assignment of spectra. These fits also provided a basis for locating weak perturbations which contain information critical to the ultimate big picture. The expected n^* -scaling of molecular constants and (the expected n^* -independence of the quantum defects) helped us to organize the observed states into Rydberg series.

6.1 Experimental data with the $B^2\Sigma^+$ state as an intermediate.

The information about states in the region $31460 - 32400 \text{ cm}^{-1}$ ($3.88 < n^* < 4.16$) was necessary for us to connect the higher energy regions of Rydberg series unambiguously down to their *valence terminus* states. The relatively large changes in $n^* \bmod 1$ that occur near the terminus tell us about the n^* -invariant inner part of the Rydberg orbital which dominates the e^- /nuclear energy and angular momentum exchange. Our initial attempt to include previously observed states^{1,2} into Rydberg series revealed that some of those states could possibly be misassigned in literature. We actually verified that the $G^2\Sigma^+$ state, previously reported by Singh and Mohan¹, had been incorrectly assigned vibrationally. The $I^2\Sigma^+$ state, which Singh and Mohan observed at low resolution, was absent from our spectra and we suspect belongs to a species other than BaF.

For (0,0) bands, our 0.01 cm^{-1} resolution is not sufficient to fully resolve isotope structure. The lighter isotopomer transitions are observed as a tail at the high energy side of the main isotopomer line. For $\Delta v \neq 0$ bands, isotope structure (up to 5 Ba isotopes) is easily observed. We rotationally analyzed, however, transitions of at most 2 isotopomers for each band, with the exception of the (1, 0) $G^2\Sigma^+ - B^2\Sigma^+$ band, for which four isotopomer transitions were analyzed.

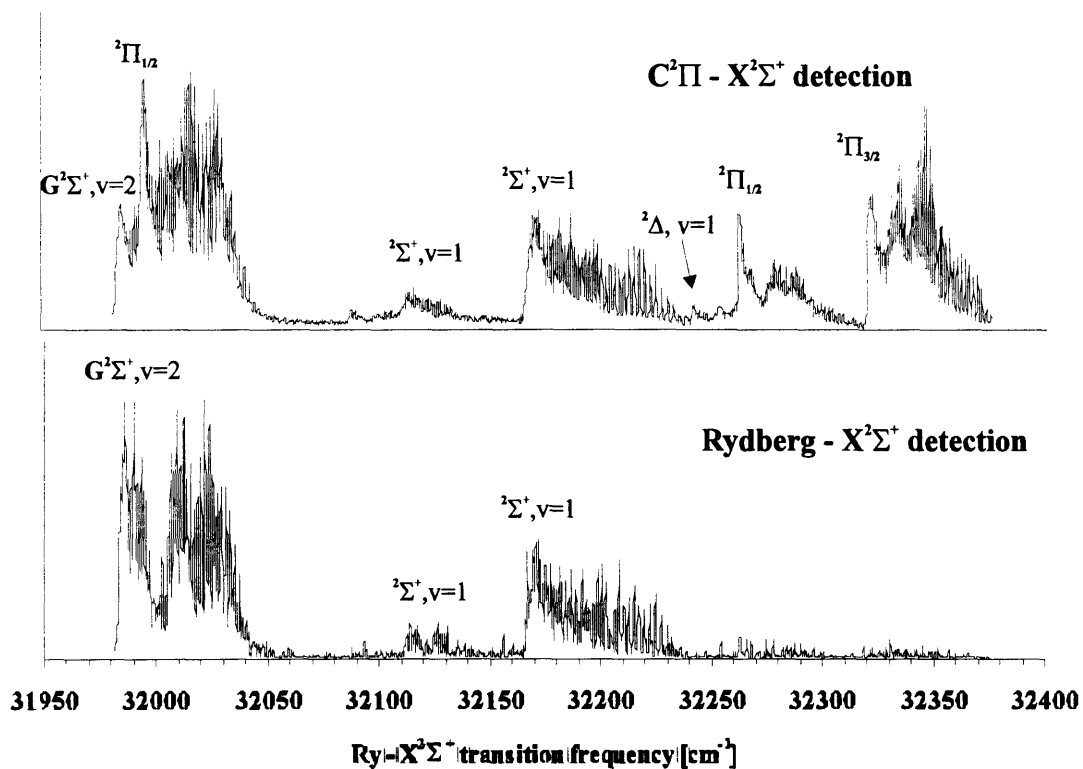


Figure 10: Spectrum in the 31950-32400 cm^{-1} region obtained via the $\text{B}^2\Sigma^+$ state as an intermediate. Upper trace: $\text{C}^2\Pi - \text{X}^2\Sigma^+$ fluorescence detected; lower trace: direct fluorescence from Rydberg states down to the ground state is detected.

In Figure 10, examples of low resolution scans of the same energy region are shown. The lower trace shows the spectrum recorded by detecting direct UV fluorescence from Rydberg states down to the ground state. The upper trace presents the spectrum obtained by monitoring cascade fluorescence ($\lambda \approx 500 \text{ nm}$) from the $\text{C}^2\Pi$ state down to the ground state. The spectrum in the upper trace is significantly more complex. After an excitation by the pump and probe laser pulses, Rydberg states fluoresce to lower lying states. The probability of spontaneous emission is given³ by the Einstein coefficient

$$A_{ij} = |\mu_{ij}|^2 [16\pi^3 / (3h\epsilon_0)] = 3.137 \cdot 10^{-7} |\mu_{ij}|^2 \nu_{ij}^3 [\text{s}^{-1}]. \quad (6.1)$$

The ν_{ij}^3 factor would suggest that fluorescence down to the ground state should be most efficient. However, the transition dipole moment from a Rydberg state to the ground state, μ_{ij} , may not be favorable. The excitation/deexcitation in such a case is a 3-step

process, $X \rightarrow B \rightarrow Ry \rightarrow X$. In each of these steps a photon carries one unit of angular momentum, so in order to conserve angular momentum: (1) $l_C = l_X \pm 1$, (2) $l_{Ry} = l_C \pm 1 = l_X$, $l_X \pm 2$, and (3) $l_X = l_{Ry} \pm 1 = l_X \pm 1$, $l_X \pm 3$. In an atom (with l being a good quantum number) the total probability of such a 3-step process would be zero. In a molecule, due to l -mixing, the total transition probability is usually not zero, but small. It can be large only for selected, mixed- l states. In the case of a 4-step process, $X \rightarrow B \rightarrow Ry \rightarrow C \rightarrow X$, mixing restrictions are relaxed and many more states can be observed. The 4-step process also increases the probability of observing weakly- or non-penetrating states which overlap with a cascade intermediate state (because of its large n^*) much better than with the relatively compact ground state.

Table 2: Molecular constants for the $B^2\Sigma^+$ state (in cm^{-1}) (see text).

	^{138}BaF (a)	^{138}BaF (b)	^{137}BaF (b)	^{136}BaF (b)	^{135}BaF (b)
B_0	0.20719933 (32)	0.2072181 (23)	0.20740149	0.20758740	0.20777560
$D_0 \cdot 10^6$	0.19055 (18)	0.19861 (19)	0.19901265	0.19937025	0.19973257
γ_0	-0.262941 (22)	-0.262858 (47)	-0.26311715	-0.26335346	-0.26359267
$\gamma_{D_0} \cdot 10^6$	-0.203 (16)	-0.241 (11)	-0.241	-0.241	-0.241

Note: (a) this work, (b) from Ref. 1.

For the main isotopomer (^{138}BaF) data we perform a global fit of all transitions observed via the $B^2\Sigma^+$ state (except for the $K^2\Pi_{1/2} - B^2\Sigma^+$ transition) and the $B^2\Sigma^+$ state molecular constants are treated as adjustable parameters (see Table 2). A simultaneous fit of the $B^2\Sigma^+$ and Rydberg $^2\Sigma^+$ state molecular constants, despite strong correlations between fit parameters, is possible due to inclusion in the fit of correlation-breaking transitions to $^2\Pi$ and $^2\Delta$ Rydberg states. For other isotopomers, the $B^2\Sigma^+$ state molecular constants are held fixed in our fits. Their values are calculated from the molecular constants of the ^{138}BaF $B^2\Sigma^+$ state¹ using isotope relationships⁴ (see Table 2). The wavenumbers and assignments of all measured lines are shown in Appendix D.

6.1.1 $G^2\Sigma^+$ and $H^2\Sigma^+$ states.

The $G^2\Sigma^+$ and $H^2\Sigma^+$ states were first observed in low resolution by Fowler⁵ in absorption and later by Singh and Mohan² in emission. They observed and vibrationally analyzed several bands of the G - X and H - X systems. Our first attempts to include the G and H states into Rydberg series strongly suggested that one of these states, most likely $G^2\Sigma^+$, might have been incorrectly assigned or calibrated. A similar conclusion could be drawn from our ligand field calculations⁶. The G state's quantum defect could not be fitted into any of the $^2\Sigma^+$ Rydberg series.

In order to resolve this discrepancy we recorded and rotationally analyzed large sets of data for the G - B and H - B systems:

$G^2\Sigma^+ - B^2\Sigma^+$	(0,0)	no isotope structure detected
	(1,0)	^{138}BaF , ^{137}BaF , ^{136}BaF , and ^{135}BaF
	(2,0)	^{138}BaF and ^{137}BaF
$H^2\Sigma^+ - B^2\Sigma^+$	(0,0)	no isotope structure detected.

Table 3: Molecular constants for the $v=0$ $H^2\Sigma^+$ state (cm^{-1}).

^{138}BaF		
$T_{0,0}$	17566.075	(1)
B_0	0.23031590	(85)
$D_0 \cdot 10^6$	0.15407	(41)
$\gamma_0 \cdot 10^2$	-0.4957	(65)
$\gamma_{D_0} \cdot 10^6$	0.790	(39)

The isotope analysis allowed us to conclusively assign vibrational quantum numbers. The molecular constants obtained in our fits are presented in Table 3 for the $H^2\Sigma^+$ state and in Table 4 for the $G^2\Sigma^+$ state. Taking the term value of the $v=0$ $B^2\Sigma^+$ state, $T_{B-X}=14040.163(1)$, from Ref. 1, we calculate the electronic term values for the G and H states, $T_G=30969.714(4) \text{ cm}^{-1}$ and $T_H=31606.237(4) \text{ cm}^{-1}$. All of the term values

presented in this work are calculated with respect to the zero of energy set at the $N=0$ $v=0$ $X^2\Sigma^+$ level.

Table 4: Effective molecular constants for the $G^2\Sigma^+$ state (in cm^{-1}).

$G^2\Sigma^+ - B^2\Sigma^+$	^{138}BaF	^{137}BaF	^{136}BaF	^{135}BaF	
(0, 0) $T_{0,0}$	16929.552 (1)				
	B_0	0.2297413 (13)			
	$D_0 \cdot 10^6$	0.16755 (99)			
	$\gamma_0 \cdot 10^2$	0.9778 (80)			
	$\gamma_{D0} \cdot 10^6$	0.289 (73)			
(1, 0) $T_{1,0}$	17436.742 (1)	17436.937 (7)	17437.187 (12)	17437.379 (22)	
	B_1	0.2289101 (14)	0.229187 (19)	0.229330 (31)	0.229562 (55)
	$D_1 \cdot 10^6$	0.1601 (12)	0.198 (10)	0.180 (20)	0.163 (32)
	$\gamma_1 \cdot 10^2$	0.7237 (81)	0.756 (20)	0.690 (26)	0.814 (54)
	$\gamma_{D1} \cdot 10^6$	-0.056 (82)			
(2, 0) $T_{2,0}$	17944.782 (1)	17945.213 (5)			
	B_2	0.22754565(73)	0.2277235(85)		
	$D_2 \cdot 10^6$	0.14186 (27)	0.1525 (20)		
	$\gamma_2 \cdot 10^2$	0.2386 (58)	0.244 (15)		
	$\gamma_{D2} \cdot 10^6$	0.783 (30)			

6.1.2 New $^2\Pi$ and $^2\Delta$ states.

In addition to the $G^2\Sigma^+$ and $H^2\Sigma^+$ states, in the region of $31460 - 32400 \text{ cm}^{-1}$ ($3.88 < n^* < 4.16$), we observed several new states*, $K^2\Pi_{1/2}(v=0)$, $J^2\Pi(v=0)$, and $3.94^2\Delta(v=1)$ (see Figure 10). Recently, Effantin *et al*⁷ found a group of two $^2\Pi$ states,

* We suggest the following convention for labeling newly observed states and Rydberg series. Each Rydberg series is labeled by the fractional part of the asymptotic value of the effective principal quantum number, n^* . For example, $0.88^2\Sigma^+$ specifies the series of $^2\Sigma^+$ states with $(n^* \bmod 1) \approx 0.88$. If the newly observed state belongs to some Rydberg series, it is labeled by a real number with 2 digits after the decimal point. The fractional part is the Rydberg series label and the integer part is the integer part of the actual n^* i.e. $\text{int}(n^*)$. Those lowest Rydberg states for which the quantum defects are significantly (>0.02) different from the asymptotic quantum defect for the series are labeled by letters.

$E'^2\Pi_{1/2}$ at 27323 cm^{-1} , $E'^2\Pi_{3/2}$ at 27456 cm^{-1} , and $E''^2\Pi_{1/2}$ at 27302 cm^{-1} , in the $n^*\approx 3$ region, which is 1 unit of n^* below the region we have investigated here. The $\Omega=1/2$ assignment for the observed component of the E'' state was based on the absence of a Q branch in the $E'' - A^2\Pi_{1/2}$ transition and the presence of appreciable Λ -doublet splitting, approximately linear in $(J+1/2)$. Effantin *et al*⁸ were, however, unable to locate the $^2\Pi_{3/2}$ component of the E'' state. The problem of the missing $E''^2\Pi_{3/2}$ state is puzzling to us, since at higher energy ($n^*>6$), we observe both Ω components of the $^2\Pi$ states which belong to the same Rydberg series as the E'' state. At $n^*\approx 4$, however, we also observe only the $^2\Pi_{1/2}$ component of the E'' state.

Both the $K^2\Pi_{1/2}$ and $J^2\Pi$ states reveal no isotope structure, thus they are assigned as $v=0$ levels. The $3.94^2\Delta$ state, weak and partially obstructed by the $J^2\Pi$ state, shows an isotope splitting on the order of 0.25 cm^{-1} , which is characteristic for a $v=1$ upper state. The $J^2\Pi$ state is a textbook example of a Hund's case (a) $^2\Pi$ state, and its assignment and fitting presented no problem.

The $3.94^2\Delta$ state is a near case (b) state, but its small spin-orbit splitting is still resolvable. In order to obtain *unbiased* estimates of spin-orbit and Λ -doubling constants, only O- and R-form lines were included in the fit. The P- and Q-form lines are doublets with unresolved splittings and, as one can see in Appendix D, including them in the fit would introduce systematic errors.

The fact that we were able to detect the $3.94^2\Delta$ state in this experiment also requires some explanation. The intermediate state was a $^2\Sigma^+$ state, so a transition to a $^2\Delta$ state would be forbidden by the $\Delta\Lambda=0,\pm 1$ selection rule. However, as we know from the studies of the 5d-complex by Bernard *et al*⁹, the $B^2\Sigma^+$ state has significant $^2\Pi_{1/2}$ character which is acquired by interaction with the $A^2\Pi$ state. This admixture of $^2\Pi$ character into the $B^2\Sigma^+$ state is the primary source of the $3.94^2\Delta - B^2\Sigma^+$ transition intensity. Another possible, although less likely, explanation for some of the intensity of the $3.94^2\Delta - B^2\Sigma^+$ transition is mixing of the $3.94^2\Delta$ state with the $J^2\Pi$ state, which would then be the transition intensity provider for the $3.94^2\Delta - B^2\Sigma^+$ transition. Molecular constants of the $J^2\Pi$ and $3.94^2\Delta$ states are presented in Table 5. The $K^2\Pi_{1/2}$ state has not been fitted yet

since the rotational assignment for the e -symmetry levels is inconclusive due to insufficient experimental data.

Table 5: Molecular constants for the $v=0$ $J^2\Pi$ and $v=1$ $3.94^2\Delta$ states.

	$J^2\Pi, v=0$		$3.94^2\Delta, v=1$	
T	18257.755	(1)	18212.033	(1)
B	0.22952183	(51)	0.2293711	(16)
D*10⁶	0.16249	(39)	0.1636	(13)
A	57.196	(1)	0.651	(13)
A_D*10³	-0.34842	(53)	-0.0974	(16)
p	-0.132248	(47)	$0.117*10^{-5}$	(18)
p_D	$0.6561*10^{-5}$	(39)		
q	$-0.8351*10^{-3}$	(10)	$-0.195*10^{-7}$	(24)
q_D	$0.3562*10^{-7}$	(74)		

6.1.3 New $^2\Sigma^+$ states.

Two $^2\Sigma^+$ states at 32110 cm^{-1} and 32166 cm^{-1} were not initially included in any of the Rydberg series. These states have isotope splittings of 0.17 cm^{-1} and 0.19 cm^{-1} , respectively. Even if the splittings are significantly smaller than predicted for $\Delta v=1$ transitions, both states have initially been assigned to the $v=1$ quantum number. The $32166\text{ }^2\Sigma^+$ state is located 560 cm^{-1} above the $v=0\text{ H}^2\Sigma^+$ state, thus at least $25\text{-}30\text{ cm}^{-1}$ too high in energy to be considered as $v=1\text{ H}^2\Sigma^+$. The $32110\text{ }^2\Sigma^+$ state is separated from the $v=0\text{ H}^2\Sigma^+$ state by about 503.7 cm^{-1} , which is comparable to $\Delta G_{1/2}=507.2\text{ cm}^{-1}$ for the $G^2\Sigma^+$ state. Both states have effective B values (see Table 6 and Table 7) slightly larger than one would expect for the $v=1\text{ H}^2\Sigma^+$ level. The negative value of the D constant for the $32166\text{ }^2\Sigma^+$ state indicates that this state experiences a J-dependent interaction from some lower lying state, but the positive value of the γ constant suggests that the dominant interaction comes from a $^2\Pi_{1/2}$ state at higher energy. However, the value of the γ constant is small and it is impossible to use it to locate a single $^2\Pi_{1/2}$ perturber.

Table 6: Molecular constants for the 32166 $^2\Sigma^+$ state (in cm^{-1}).

	^{138}BaF		^{137}BaF	
$T_{1,0}$	18126.130	(1)	18126.320	(9)
B_1	0.2333893	(17)	0.233614	(28)
$D_1 \cdot 10^6$	-0.1897	(15)	-0.162	(22)
$\gamma_1 \cdot 10^2$	0.800	(10)	0.852	(69)
$\gamma_{D1} \cdot 10^5$	0.572	(11)	0.48	(11)

Table 7: Molecular constants for the 32110 $^2\Sigma^+$ state (in cm^{-1}).

	^{138}BaF	
$T_{1,0}$	18069.746	(1)
B_1	0.2364933	(17)
$D_1 \cdot 10^6$	0.9391	(12)
$\gamma_1 \cdot 10^1$	0.306	(10)
$\gamma_{D1} \cdot 10^5$	-0.2144	(94)

The 32110 $^2\Sigma^+$ state has a very large and positive effective D constant, which suggests that this state experiences a strong interaction from above. This conclusion suggests that these two $^2\Sigma^+$ states interact strongly with each other. Such a possibility was tested in a separate fit for these two states interacting with each other. The B $^2\Sigma^+$ state molecular constants were held fixed at values obtained in an all-state fit (see Table 2).

The off-diagonal (interaction) matrix element, h_{1-2} , was treated as an adjustable parameter. The 2-state fit, as one can see in Table 8, does not solve the problem of peculiar values for the D parameter.

Table 8: Fit results for 32166 $^2\Sigma^+$ and 32110 $^2\Sigma^+$ interacting states (in cm^{-1}).

	32166 $^2\Sigma^+$		32110 $^2\Sigma^+$	
T	18116.086	(2)	18079.782	(2)
B	0.2325525	(25)	0.2373767	(25)
$D \cdot 10^6$	-0.4095	(21)	1.2141	(19)
$\gamma \cdot 10^1$	0.0575	(15)	0.3499	(15)
h_{1-2}	21.570	(2)		

6.2 Fluorescence detected spectra recorded via the $C^2\Pi_{3/2}$ intermediate state.

The largest set of experimental data in this project was obtained by pumping the $C^2\Pi_{3/2} - X^2\Sigma^+(0, 0)$ transition. As was mentioned previously, the $C^2\Pi$ state has been carefully studied by Effantin and coworkers¹. Since the structure of our data set (one spin-orbit component, shorter branches *etc.*) did not allow for more accurate determination of the $C^2\Pi$ state molecular constants, we decided to convert all of the observed Rydberg - $C^2\Pi_{3/2}$ transitions to term values of the upper state using the Effantin *et al.* term values for the $v=0$ $C^2\Pi_{3/2}$ state. Working exclusively with Rydberg state term values proved both more effective and more convenient than working with transition frequencies.

This part of the data set can be divided into two parts. Lower Rydberg states up to $n^*\approx 8.5$ exhibit little l -uncoupling and can be conveniently described by Hund's case (a) or (b). Above $n^*\approx 8.5$, the l -uncoupling interaction becomes more important and the Rydberg states must be treated as members of supercomplexes, even if at low- J most of the states follow the Hund's case (b) coupling scheme. For most of the states observed in the fluorescence-detected experiment with the $C^2\Pi_{3/2}$ intermediate state we performed isolated state fits. The fit results and detailed discussion of the data are presented below.

6.2.1 Core-penetrating $^2\Sigma^+$ Rydberg series.

In the BaF spectrum we identified 4 core-penetrating $^2\Sigma^+$ Rydberg series: $0.88^2\Sigma^+$, $0.76^2\Sigma^+$, $0.24^2\Sigma^+$, and $0.08^2\Sigma^+$. The $0.88^2\Sigma^+$ series is the strongest of them and very well documented up to the highest energies studied here. We observed altogether 11 members of the $0.88^2\Sigma^+$ series. The lowest member of the series is the $D'^2\Sigma^+$ state, previously studied at low resolution by Singh and Mohan² and high resolution (1-0 band) by Barrow *et al.*¹⁰. The second lowest member is the $H^2\Sigma^+$ state, described in Section 6.1.1. Other members of this series, up to $n^*\approx 13.88$, are discussed below. The results of the isolated state fits are presented in Table 9 (molecular constants) and in Appendix D (term values and line assignments).

Table 9: Effective molecular constant (in cm^{-1}) for the $0.88^2\Sigma^+$ series.

	T	B	$\gamma \cdot 10^1$	$\gamma_D \cdot 10^3$
D' $^2\Sigma^+$	26245.0	0.2264		
H $^2\Sigma^+$	31606.238	0.23031590	-0.04957	0.000790
4.88 $^2\Sigma^+$	34163.039 (6)	0.231262 (20)	-0.1230 (68)	
5.88 $^2\Sigma^+$	35575.814 (4)	0.233574 (37)	0.2932 (73)	0.1571 (72)
6.88 $^2\Sigma^+$	36424.552 (2)	0.232245 (21)	-0.2303 (38)	0.0192 (40)
7.88 $^2\Sigma^+$	36976.545 (4)	0.231904 (34)	-0.2817 (66)	0.0197 (67)
8.88 $^2\Sigma^+$	37351.215 (3)	0.232152 (12)	-0.1619 (36)	
9.88 $^2\Sigma^+$	37619.761 (4)	0.234144 (32)	-0.2312 (74)	0.0514 (53)
10.88 $^2\Sigma^+$	37816.745 (2)	0.232307 (9)	-0.1776 (25)	0.0094 (11)
11.88 $^2\Sigma^+$	37967.246 (6)	0.231392 (77)	-0.2090 (140)	
12.88 $^2\Sigma^+$	38083.247 (3)	0.232513 (30)	-0.1748 (59)	0.0236 (59)
13.88 $^2\Sigma^+$	38175.496 (2)	0.232519 (30)	-0.1573 (50)	
v=1 4.88 $^2\Sigma^+$	34689.057(30)	0.230122 (51)	-0.412 (12)	
v=3 4.88 $^2\Sigma^+$	35736.274 (3)	0.229354 (11)	-0.4948 (33)	
v=2 6.88 $^2\Sigma^+$	37488.301(30)	0.231756 (59)	-0.376 (17)	
v=1 7.88 $^2\Sigma^+$	37510.482(30)	0.237086 (144)	-0.486 (27)	

Note: The centrifugal distortion constant is held fixed at $0.16 \cdot 10^{-6} \text{ cm}^{-1}$.

We intended to use the same set of adjustable molecular constants for all members of a given Rydberg series. Most of the states in the $0.88^2\Sigma^+$ series are fitted to the four-effective-parameter model (rotationless term value (T), rotational constant (B), spin-rotation constant (γ), and the centrifugal correction to the spin-rotation constant (γ_D)), with the centrifugal distortion constant, D, held fixed at the value of $0.16 \cdot 10^{-6} \text{ cm}^{-1}$. However, for the $4.88^2\Sigma^+$, $8.88^2\Sigma^+$, $11.88^2\Sigma^+$, and $13.88^2\Sigma^+$ states, the fitted values of the γ_D constant were statistically indistinguishable from zero. Including γ_D in the set of fit parameters did not significantly alter the values of the three other parameters.

Higher members of the $0.88^2\Sigma^+$ series are affected by an extremely weak, *local* perturbation with a core-nonpenetrating state. Other, stronger perturbations, by $v>0$ vibrational levels, are also observed. The effect of the perturbations by members of higher vibrational manifolds can be best seen (Figure 11), in the plot of $(n^* \bmod 1)$ vs n^* for the

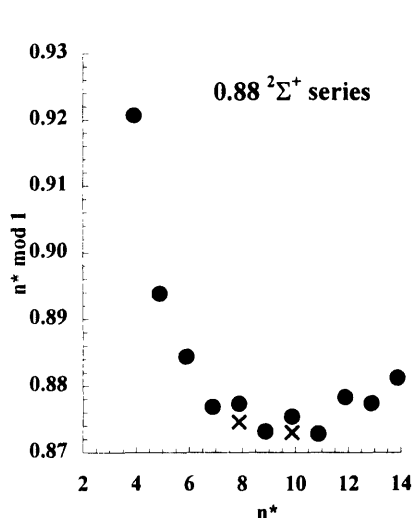


Figure 11: $n^* \bmod 1$ vs n^* plot for $0.88^2\Sigma^+$ series. (x's mark deperturbed positions of the states, see text).

$0.88^2\Sigma^+$ series, as deviations from a smooth curve.

The $v=0$ $7.88^2\Sigma^+$ state at $36976.545(4)$ cm^{-1} interacts with the $v=1$ $6.88^2\Sigma^+$ state at $36958.0(5)$ cm^{-1} . This kind of interaction is called an intrachannel perturbation¹. The observed n^* of the $7.88^2\Sigma^+$ state, 7.8774 , is higher by 0.0027 than the value estimated from the n^* values of adjacent members of this series, which are believed not to be affected by perturbations. Such an n^* shift is equivalent to a $\Delta T=1.23$ cm^{-1} shift of the rotationless energy of the $7.88^2\Sigma^+$ state. If we assume that the $v=1$ $6.88^2\Sigma^+$ state is shifted down in energy (also by 1.23 cm^{-1}) we can calculate $\Delta G_{1/2}=534.6(5)$ cm^{-1} for the $6.88^2\Sigma^+$ state.

Using second-order perturbation theory we can estimate the interaction matrix element from the energy shift and the energy separation of the two interacting states. The interaction matrix element (in cm^{-1} if ΔT , T_1 , and T_2 are in cm^{-1}) is given by $H_{1-2}=(\Delta T*(T_1-T_2))^{1/2}$. For a given $l\Lambda$ Rydberg series, the potential energy curves of all states (at sufficiently high n^*) are very similar and nearly parallel to the potential curve of the molecular-ion. Following Mulliken¹¹, the potential curve for an $n^*l\Lambda$ state can be expressed as

$$U(R) = U^+(R) - \frac{\mathfrak{R}}{(n - \mu(R))^2}. \quad (6.2)$$

Since $\mu(R)$ is a slowly changing function of internuclear distance, R , it can be replaced by a truncated Taylor expansion about the equilibrium internuclear distance of the molecular ion. Keeping only linear term, the potential curve can be approximated as

$$U(R) = U^+(R) - \frac{\mathfrak{R}}{(n^*)^2} - \frac{2\mathfrak{R}}{(n^*)^3} \frac{d\mu}{dR} (R - R_e^+). \quad (6.3)$$

Now, we can calculate an interaction matrix element between 2 wavefunctions of the states (n'^* and n''^*) belonging to the same Rydberg series, but different vibrational manifolds as

$$H_{1-2} = -\frac{2\mathfrak{R}}{(n'^*)^{3/2}(n''^*)^{3/2}} \frac{d\mu}{dR} \langle v' | R - R_e^+ | v'' \rangle. \quad (6.4)$$

In the harmonic approximation, the interaction matrix element takes the form⁴

$$H_{1-2} = -\frac{2\mathfrak{R}}{(n'^*)^{3/2}(n''^*)^{3/2}} 10^{10} \left(\frac{d\mu}{dR} \right)_{R_e} \sqrt{\frac{h}{800\pi^2 mc\omega}} \sqrt{v+1}, \quad (6.5)$$

where \mathfrak{R} is the Rydberg constant (cm^{-1}), h is Planck's constant ($\text{J}\cdot\text{s}$), c is the speed of light (m/s), m is the reduced mass (kg), ω is vibrational frequency (cm^{-1}), μ is a quantum defect, and R is the internuclear distance (\AA), or

$$H_{1-2} = -\frac{901120}{(n'^*)^{3/2}(n''^*)^{3/2}} \left(\frac{d\mu}{dR} \right)_{R_e} \sqrt{\frac{v+1}{m\omega}}, \quad (6.6)$$

where m is in (amu) and all constants are replaced by the numerical factor. In the harmonic approximation the only nonzero matrix elements are for $\Delta v = \pm 1$. Now, combining the 2 equations for the interaction matrix element, we calculate the absolute value of the first derivative of the quantum defect with respect to the internuclear distance as equal to $0.23(1) \text{\AA}^{-1}$.

The $9.88^2\Sigma^+$ state is very strongly perturbed above $J=12.5$, thus in the isolated state fit only lines with $J < 13.5$ were used. One of the perturbers (weak) is a core-nonpenetrating state. This perturbation of the $9.88^2\Sigma^+$ state will be discussed later. The second perturber (strong) is an unidentified state belonging to a $v > 0$ vibrational manifold, possibly $v=2$ $7.08^2\Sigma^+$. The isotope shift of the perturber could not be observed here for vibrational quantum number assignment because of poor S/N ratio. In addition, the $v=0$ $9.88^2\Sigma^+$ state

is perturbed by the $v=1$ $8.08^2\Sigma^+$ state, which is located at slightly lower energy. This interaction is primarily responsible for the deviation of n^* by about 0.0024 observed for $v=0$ $9.88^2\Sigma^+$ state in Figure 11.

The $v=0$ $10.88^2\Sigma^+$ state seems to be free of strong perturbations by higher vibrational levels and the weak perturbation by a core-nonpenetrating state strongly affects only one e ($J=14.5$) and one f ($J=13.5$) level. For the $11.88^2\Sigma^+$ state and higher states of this series, at $J>10.5$ an interaction with the $0.94^2\Delta$ series becomes important, thus only levels with $J<10.5$ are included in single state fits.

In the second $^2\Sigma^+$ series, $0.76^2\Sigma^+$, we observed four new states. The three lowest members of this series are the ground state, $X^2\Sigma^+$, the $D^2\Sigma^+$, and the $G^2\Sigma^+$ states discussed in Section 6.1.1. In addition to these states, we observed $4.76^2\Sigma^+$, $5.76^2\Sigma^+$, $6.76^2\Sigma^+$, and $8.76^2\Sigma^+$. The $4.76^2\Sigma^+$ and $8.76^2\Sigma^+$ states are observed only in their $v=1$ vibrational levels and the $v=0$ term values are calculated assuming $\omega_e=535\text{ cm}^{-1}$ and $\omega_e x_e=2\text{ cm}^{-1}$. The molecular constants of the states in this series are given in Table 10. The centrifugal distortion constant, D , is held fixed in the fits at $0.16\cdot 10^{-6}\text{ cm}^{-1}$. The centrifugal correction to the spin-rotation constant is not included in the fit. The $v=1$ $8.76^2\Sigma^+$ state is perturbed at $N=6$ by another state with very large effective B value, most likely the $v=0$ $11.08^2\Sigma^+$ state, with which it was initially confused¹². The fitted molecular constants, B and γ , clearly show, that the state must be properly labeled as $v=1$ $8.76^2\Sigma^+$.

Table 10: Effective molecular constants (in cm^{-1}) for the $0.76^2\Sigma^+$ series.

	T	B	$\gamma\cdot 10^1$
X $^2\Sigma^+$	0.000	0.2159509 (22)	0.027246 (61)
D $^2\Sigma^+$	24176.608 (1)	0.2274137 (22)	0.07130 (25)
G $^2\Sigma^+$	30969.715 (2)	0.2297413 (13)	0.09778 (80)
4.76 $^2\Sigma^+$	33899. (2)		
5.76 $^2\Sigma^+$	35441.255 (3)	0.231107 (15)	0.1243 (37)
6.76 $^2\Sigma^+$	36347.557 (4)	0.231261 (35)	0.1231 (67)
8.76 $^2\Sigma^+$	37317. (1)		
v=1, 4.76 $^2\Sigma^+$	34434.216 (10)	0.234521 (48)	0.119 (11)

$v=2, 6.76 \text{ } ^2\Sigma^+$	37411.827 (6)	0.229475 (40)	0.3289 (97)
$v=1, 8.76 \text{ } ^2\Sigma^+$	37852.357 (4)	0.231127 (30)	0.1918 (71)

Note: The centrifugal distortion constant is held fixed at $0.16 \cdot 10^{-6} \text{ cm}^{-1}$ for all states except $X^2\Sigma^+$, $D^2\Sigma^+$, and $G^2\Sigma^+$. The italicized term values for the $4.76^2\Sigma^+$ and $8.76^2\Sigma^+$ states are obtained from the term values for the $v=1$ levels using $\Delta G_{1/2}=535 \text{ cm}^{-1}$.

The lowest observed member of the $0.08^2\Sigma^+$ series, the $32110^2\Sigma^+$ state, the valence precursor of which has not yet been observed, is discussed in Section 6.1.3. We observed and analyzed 5 new members of the $0.08^2\Sigma^+$ series. The strangely large values of the B

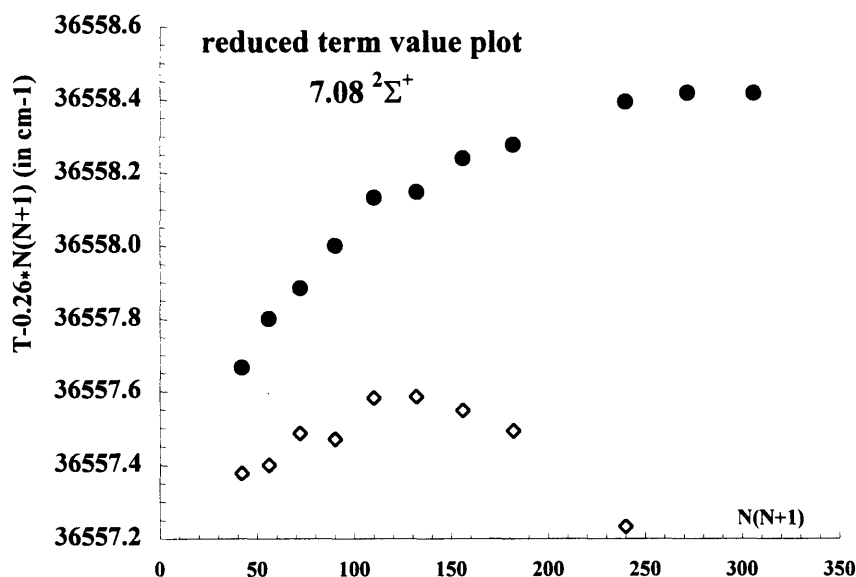


Figure 12: Reduced term value plot for the $7.08^2\Sigma^+$ state; solid circles - e levels, open diamonds - f levels.

and D molecular constants are characteristic features of all members of this series. Since the effective centrifugal distortion constant, D, is very large for this series, D had to be treated as an adjustable parameter in isolated state fits. The reduced term value plot for one of the members of this series, the $7.08^2\Sigma^+$ state, is shown in Figure 12. The effective molecular constants are presented in Table 11. The fitted values for the B and D molecular constants clearly have no mechanical meaning and possible reasons for this will be discussed later. The $v=0$ $10.08^2\Sigma^+$ and the $11.08^2\Sigma^+$ states were only observed as the perturbors of the $v=1$ $8.23^2\Delta$ and $v=1$ $8.76^2\Sigma^+$ states, respectively, and their

rotationless term values were estimated from only few extra lines.

Table 11: Effective molecular constants (in cm^{-1}) for the states of the $0.08^2\Sigma^+$ series.

	T	B	D*10⁴	γ*10¹	γ_D*10³
4.08 $^2\Sigma^+$	32119.568 (17)	0.2397508(23)	0.006037(18)	0.3590 (14)	
5.08 $^2\Sigma^+$	34486.563 (6)	0.246529 (56)	0.0857 (42)	0.449 (12)	
6.08 $^2\Sigma^+$	35774.744 (2)	0.256864 (24)	0.1358 (26)	0.5238 (42)	
7.08 $^2\Sigma^+$	36557.301 (9)	0.266616 (58)	0.1807 (26)	0.336 (16)	0.1671(78)
10.08 $^2\Sigma^+$	<i>37666.1</i> (1)				
11.08 $^2\Sigma^+$	<i>37852.2</i> (5)				
v=1 6.08 $^2\Sigma^+$	36310.013 (3)	0.256607 (32)	0.1856 (37)	0.5923 (55)	
v=1 7.08 $^2\Sigma^+$	37094.651 (4)	0.267325 (44)	0.2773 (49)	0.2679 (78)	0.1313 (94)

Note: The italicized term values were estimated from extra lines at the perturbations $v=0$ $10.08^2\Sigma^+ \sim v=1$ $8.23^2\Delta$ and $v=0$ $11.08^2\Sigma^+ \sim v=1$ $8.76^2\Sigma^+$.

Table 12: Effective molecular constants (in cm^{-1}) for the $0.24^2\Sigma^+$ series.

	T	B	γ	γ_D*10³
B $^2\Sigma^+$	14040.163 (1)	0.2071993 (3)	-0.262941(22)	-0.000203(16)
E $^2\Sigma^+$				
5.24 $^2\Sigma^+$	34747.792 (3)	0.233773 (30)	-0.18528 (62)	0.0685 (55)
6.24 $^2\Sigma^+$	35923.775 (3)	0.236174 (19)	-0.20312 (49)	-0.0272 (25)
7.24 $^2\Sigma^+$	<i>36653.</i> (2)			
8.24 $^2\Sigma^+$	37130.224 (4)	0.242410 (36)	-0.23960 (77)	0.1618 (65)
9.24 $^2\Sigma^+$	37459.844 (3)	0.237742 (33)	-0.11935 (55)	0.6297 (75)
10.24 $^2\Sigma^+$				
v=2 7.24 $^2\Sigma^+$	37720.567 (4)	0.236663 (39)	-0.19734 (70)	-0.0747 (82)

Note: The centrifugal distortion constant is held fixed at $0.16 \cdot 10^{-6} \text{cm}^{-1}$ for all states except for the $B^2\Sigma^+$ and $E^2\Sigma^+$ states. The italicized term value for the $7.24^2\Sigma^+$ state is calculated from the term value for the $v=2$ level, using $\omega_e=539.8 \text{cm}^{-1}$ and $\omega_e x_e=2 \text{cm}^{-1}$.

The fourth core-penetrating $^2\Sigma^+$ series, $0.24^2\Sigma^+$, has the $B^2\Sigma^+$ and $E^2\Sigma^+$ states⁷ as its lowest members. The third state in this series has not been observed so far. In this project we observed 6 new states of the $0.24^2\Sigma^+$ series. The effective molecular constants

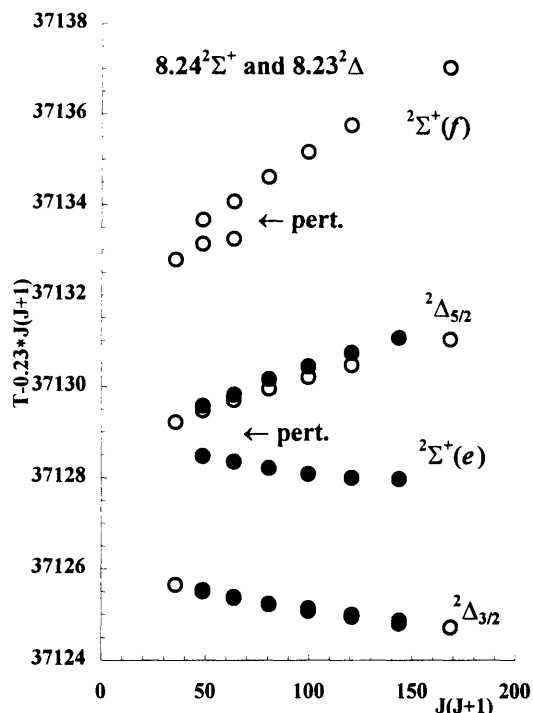


Figure 13: Reduced term value (in cm^{-1}) plotted vs $J(J+1)$ for the $8.24^2\Sigma^+$ and $8.23^2\Delta$ states. (solid circles for e -symmetry, open circles for f -symmetry levels.)

$^2\Sigma^+ \sim ^2\Delta$ perturbation is observed near $n^*=6.24$. It is, however, not so well documented because most of the data were obtained at low resolution (grating scans).

6.2.2 Core-penetrating $^2\Pi$ Rydberg series.

We observed 3 core-penetrating $^2\Pi$ Rydberg series and their single state analysis turned out to be very challenging. One of the series, $0.45^2\Pi$, is very short. We actually found only two new states that belong to this series, the $5.45^2\Pi_{3/2}$ state and the $6.45^2\Pi_{3/2}$ state, both in $v=1$ and $v=3$ vibrational levels. The series has the $C^2\Pi$ state as its lowest member, which is the intermediate state in most of our experiments. The second member of this series is the $F^2\Pi$ state.

obtained in isolated state fits are given in Table 12. The $8.24^2\Sigma^+$ state's f -symmetry component (see Figure 13) is perturbed at $J < 8.5$ by an unidentified state with a very small rotational constant (possibly $v=3$ $5.88^2\Sigma^+$). Thus, lines with $J=6.5$, 7.5 , and 8.5 in f -symmetry were not included in the fit. Also the 4 lowest e -symmetry levels of the $8.24^2\Sigma^+$ state are weakly perturbed by the e -symmetry levels of the $8.23^2\Delta_{3/2}$ state. However level shifts could not be detected in the single state fit of the $8.24^2\Sigma^+$ state. We will see later that those level shifts are actually detectable in a single state fit of the $8.23^2\Delta$ state. The largest observed level shift is $\sim 0.1 \text{ cm}^{-1}$. Thus, the $^2\Sigma^+ \sim ^2\Delta$ perturbation is very weak. A stronger

Table 13: Effective molecular constants (in cm^{-1}) for the $0.45^2\Pi$ series.

	T	B	A	$q \cdot 10^3$
$C^2\Pi$	20086.391 (1)	0.2140080 (23)	197.316(1)	-0.03912(92)
$F^2\Pi$	29471.236 (4)	0.2287458 (25)	57.001(3)	-0.00159(41)
<i>$5.45^2\Pi$</i>	<i>35043.7 (5)</i>			
<i>$6.45^2\Pi$</i>	<i>36103.2 (5)</i>			
$v=1$ <i>$5.45^2\Pi$</i>	35579.797 (4)	0.230441 (40)	[14.3]	0.205 (67)
$v=3$ <i>$5.45^2\Pi$</i>	36639.936 (4)	0.232570 (46)	[14.3]	0.637 (83)
$v=1$ <i>$6.45^2\Pi$</i>	36640.724 (10)	0.237601 (113)	[8.6]	0.64 (17)
$v=3$ <i>$6.45^2\Pi$</i>	37703.819 (19)	0.228934 (23)	[8.6]	3.23 (37)

Note: The centrifugal distortion and the Λ -doubling p parameters were held fixed at $0.16 \cdot 10^{-6} \text{ cm}^{-1}$ and -0.024 cm^{-1} , respectively. The spin-orbit splitting parameter was held fixed at values calculated from its value for the $F^2\Pi$ state using the $A \cdot (n^*)^3$ scaling relationship. The italicized term values (plus ω_e 's) for the $5.45^2\Pi$ and $6.45^2\Pi$ states are calculated from the term values for $v=1$ and $v=3$ levels using $\omega_e x_e = 2 \text{ cm}^{-1}$.

The intermediate $C^2\Pi$ state has a very large spin-orbit splitting, A , compared to the rotational spacing, $2B(J+1)$, and it can be properly described by Hund's case (a). Thus, by pumping rotational levels in the $\Omega=3/2$ component, only $^2\Pi_{3/2}$ Rydberg states can be reached by the probe transition. The transition moment to the $^2\Pi_{1/2}$ states is zero as long as no mixing with $^2\Pi_{3/2}$ occurs. Such mixing for the J -range probed here occurs only if the spin-orbit splitting is less than $4\text{-}5 \text{ cm}^{-1}$. As a result, for low- n^* $^2\Pi$ Rydberg states, only the $\Omega=3/2$ component could be observed. It turns out that the spin-orbit splitting in both $5.45^2\Pi$ and $6.45^2\Pi$ states is still relatively large and we were able to detect only $\Omega=3/2$ components. The fit results presented in Table 13 were obtained with the A constant held fixed at values calculated from the spin-orbit constant of the $F^2\Pi$ state using scaling relationships¹³. Also, the Λ -doubling p parameter, which is predicted to be constant within a Rydberg series, was held fixed in our fits at the value obtained for the $F^2\Pi$ state¹. The fit of the $v=1$ $6.45^2\Pi$ state with the spin-orbit parameter held fixed is very poor. The variance of the fit is 11. The $v=3$ $5.45^2\Pi$ and $v=1$ $6.45^2\Pi$ levels are separated from each other by less than 1 cm^{-1} , thus despite the $\Delta v=2$ difference in vibrational

quantum number they are apparently able to interact strongly. Unfortunately, a two-state fit is impossible in this case. However, we attempted to estimate the effective spin-orbit constants for $v=3$ $5.45^2\Pi$ and $v=1$ $6.45^2\Pi$ in single state fits. By varying the A parameter we obtained significantly better fits for both states. The effective spin-orbit constants are $A_3=21.427(8)$ and $A_1=1.704(42)$ for $v=3$ $5.45^2\Pi$ and $v=1$ $6.45^2\Pi$, respectively. The values are significantly different from ones calculated using scaling relationships (see Table 13). However, their sum $A_1+A_3=23.1\text{ cm}^{-1}$ is very close to the sum (22.9 cm^{-1}) of the spin-orbit parameters (Table 13) predicted using scaling relationships. This agrees with the hypothesis of the strong 2-state interaction of those states. In a 2-state interaction, the energy shifts of both interacting states have equal absolute values and opposite signs. On the other hand, if the spin-orbit separation really were as small as 1.7 cm^{-1} , we should have seen one of the $\Omega=1/2$ components in our spectrum. Despite the strong interaction between the $v=3$ $5.45^2\Pi$ and $v=1$ $6.45^2\Pi$ states, we estimated the $v=0$ level term values for both states without any deperturbation procedure using $\omega_e x_e=2\text{ cm}^{-1}$. The $0.45^2\Pi$ series must be further investigated in order to be completely understood.

The two other $^2\Pi$ Rydberg series, $50.03^2\Pi$ and $0.04^2\Pi$, are even more puzzling. The two lowest states in the $0.04^2\Pi$ series are the $A^2\Pi$ and $E'^2\Pi$ states¹. The third lowest state is the $J^2\Pi$ state described in Section 6.1.2. The lowest member of the $0.03^2\Pi$ series is the $E''^2\Pi$ state¹ and the second one is the $K^2\Pi$ state described in Section 6.1.2. Starting from $n^*\approx 5$, both series follow each other very closely with quantum defects differing by approximately 0.01. Both series will be discussed in detail later as members of supercomplexes.

6.2.3 Core-penetrating $^2\Delta$ Rydberg series.

We have observed two $^2\Delta$ Rydberg series, $0.94^2\Delta$ and $0.23^2\Delta$. The lowest member of the $0.23^2\Delta$ series is the $A'^2\Delta$ state^{1,9}. The second and the third members of the series have not been observed yet. In this work we report on the next 6 higher states. Two of them, $6.23^2\Delta$ and $8.23^2\Delta$ (see Figure 13), were mentioned before as the perturbers of the $6.24^2\Sigma^+$ and $8.24^2\Sigma^+$ states. Since the perturbations are very weak, we decided to neglect them and complete single state fits for the $0.23^2\Delta$ series. The effective molecular

constants are presented in Table 14. The centrifugal distortion constant, D , is held fixed in the fits at $0.16 \cdot 10^{-6} \text{ cm}^{-1}$. Due to multiple perturbations, the assignments and fits of the $v=0$ $7.23^2\Delta$, $9.23^2\Delta$, and $10.23^2\Delta$ states must be verified by additional experimental data.

The $A'^2\Delta$ state is assigned to the $0.23^2\Delta$ series even if its $n^* \bmod 1$, 0.9861, would suggest that it belongs to the $0.94^2\Delta$ series. The main reason for assigning it to the $0.23^2\Delta$ series is its very large scaled spin-orbit splitting, $A \cdot (n^*)^3 \approx 1619$.

Table 14: Effective molecular constants (in cm^{-1}) for the $0.23^2\Delta$ series.

	T	B	A	$A_D \cdot 10^1$	$p \cdot 10^4$	$q \cdot 10^5$
$A'^2\Delta$	10924.289(5)	0.209512 (6)	206.659 (5)	0.00106 (3)		
$5.23^2\Delta$	34725.019(7)	0.245719 (66)	6.487 (8)	0.13658(66)		
$6.23^2\Delta$	35919.281(4)	0.236663 (19)	3.841 (5)	0.04201(19)	0.689 (33)	-0.233 (12)
<i>$7.23^2\Delta$</i>	<i>36650. (2)</i>					
$8.23^2\Delta$	37128.177(3)	0.235859 (27)	1.655 (6)	0.01822(27)	2.508 (82)	-1.134 (41)
$9.23^2\Delta$	37460.89 (1)	0.22260 (14)	1.229(24)		-4.25 (61)	135.7 (35)
$10.23^2\Delta$	37698.04 (2)					
$v=2$ $7.23^2\Delta$	37718.219(4)	0.236997 (41)	2.424 (5)	0.06309(41)	2.02 (14)	-1.415 (96)

Note: The centrifugal distortion constant, D , was held fixed at $0.16 \cdot 10^{-6} \text{ cm}^{-1}$. The italicized term value for the $7.23^2\Delta$ state is calculated from the term value for the $v=2$ level using $\omega_e=540 \text{ cm}^{-1}$ and $\omega_e x_e=2 \text{ cm}^{-1}$.

The *valence terminus* of the second $^2\Delta$ series, $0.94^2\Delta$, has not been observed yet. The second state of this series, $3.94^2\Delta$, is described in Section 6.1.2. States of the $0.94^2\Delta$ series have a very small spin-orbit splitting and, unlike the case of the $0.23^2\Delta$ series, the spin-orbit constant could be fitted for only the few lowest states (see Table 15). Even though the spin-orbit constant is poorly determined, its value is statistically distinct from zero in all cases where it was fitted. The states of the $0.94^2\Delta$ series are strongly perturbed by core-nonpenetrating states. At low- n^* these perturbations occur at high- J and with increasing- n^* move towards lower- J . Starting from $n^*=8.94$, this type of perturbation makes isolated state fits meaningless. Only the lowest rotational levels can be used in the fits. At $n^*=11.94$, interaction with members of the $0.88^2\Sigma^+$ series also becomes important.

Table 15: Effective molecular constants (in cm^{-1}) for the $0.94^2\Delta$ series.

	T	B	A	$A_D \cdot 10^2$	$p \cdot 10^4$	$q \cdot 10^5$
$4.94^2\Delta$	34255. (5)	0.22888 (41)	0.30 (24)			
$5.94^2\Delta$	35634.668 (2)	0.229429 (15)	0.061 (8)		0.196 (45)	
$6.94^2\Delta$	36466.871 (2)	0.224176 (13)	0.603 (25)	-0.4119 (13)	0.056 (36)	-0.144 (12)
$7.94^2\Delta$						
$8.94^2\Delta$	37371.768 (4)	0.224535 (41)	0.032 (17)		0.81 (15)	-1.437 (70)
$9.94^2\Delta$	37634.702 (8)	0.221007 (94)			2.96 (36)	-3.15 (23)
$10.94^2\Delta$	37828.967 (3)	0.217747 (51)		0.0182 (49)	5.85 (23)	-7.11 (12)
$11.94^2\Delta$	37976.43 (2)	0.21593 (22)				-12.29 (57)
$12.94^2\Delta$	38090.6 (1)					
$13.94^2\Delta$	38181.8 (1)					
$v=1$ $6.94^2\Delta$	37001.948 (3)	0.227138 (20)	0.043 (13)		0.393 (49)	-0.290 (18)
$v=1$ $3.94^2\Delta$	32252.196 (2)	0.229371 (2)	0.651 (13)	-0.00974 (16)	0.0117 (18)	-0.00195 (24)

Note: The centrifugal distortion constant, D , is held fixed at $0.16 \cdot 10^{-6} \text{ cm}^{-1}$.

Rotationless term values for the $12.94^2\Delta$ and $13.94^2\Delta$ states were estimated from Figure 14, since, due to strong perturbations, single state fits were impossible in these cases (see text).

The spectrum of the $4.94^2\Delta$ state could not be properly calibrated, because we did not record a reference spectrum in that region. We decided to estimate the absolute wavenumbers using the known offset of the laser calibration. This procedure could introduce an absolute calibration error as large as 5 cm^{-1} . The internal precision is better than 0.06 cm^{-1} . Even if spin-orbit parameters are defined very poorly, it is obvious that, for the $6.94^2\Delta$ state, the spin-orbit splitting is significantly larger than for nearby members of that series (see Table 15). This is most likely due to an interaction with $v=1$ $6.23^2\Delta$ ($A \approx 3.8 \text{ cm}^{-1}$), which is predicted* at 36454 cm^{-1} , only about 12.6 cm^{-1} below the observed term value of the $v=0$ $6.94^2\Delta$ state. From Figure 14 we can estimate the

* We did not look for the $v=1$ $6.23^2\Delta$ state. However, in one of the high resolution scans with the $J=6.5f$ intermediate level, we detected a weak line which could be assigned as a transition to the $J=7.5f$ Rydberg level (R line). The so far unassigned $J=7.5f$ level would be located exactly 14 cm^{-1} below the $J=7.5f$ level of the $v=0$ $6.94^2\Delta$ state, thus 1.4 cm^{-1} higher than the predicted term value for the $v=1$ $6.23^2\Delta$ state.

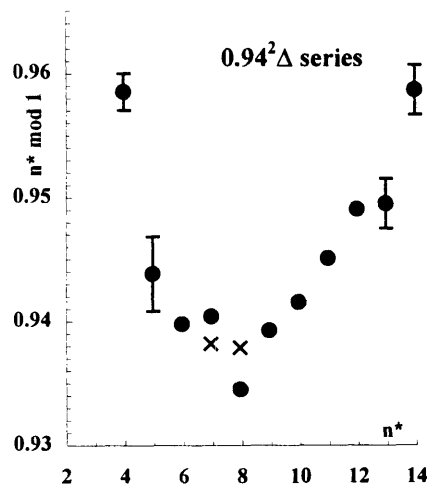


Figure 14: $n^* \bmod 1$ vs n^* plot for $0.94^2\Delta$ series. (Error bars present if greater than the radius of the circle; \times denotes deperturbed values of $n^* \bmod 1$ as discussed in the text).

unperturbed term value of the $v=0$ $6.94^2\Delta$ state at 36465.41 cm^{-1} . Now from the known shift of the $v=0$ $6.94^2\Delta$ state ($\sim 1.41 \text{ cm}^{-1}$) and the energy separation of the unperturbed states ($\sim 11.5 \text{ cm}^{-1}$) we can estimate (see 6.2.1) the strength of the interaction, $\sim 4.27 \text{ cm}^{-1}$, and mixing coefficients, $\alpha=0.950$ and $\beta=-0.313$. The observed $v=0$ $6.94^2\Delta$ state can be represented now as $|6.94^2\Delta\rangle = \alpha|6.94^2\Delta\rangle_0 + \beta|6.23^2\Delta\rangle_0$, where $|6.94^2\Delta\rangle_0$ and $|6.23^2\Delta\rangle_0$ are wavefunctions of the deperturbed states. The spin-orbit interaction of the observed $6.94^2\Delta$ state can, thus, be calculated as

$$A_{\text{obs}} = \langle 6.94^2\Delta | H_{s-o} | 6.94^2\Delta \rangle \quad (6.7)$$

or

$$A_{\text{obs}} = \alpha^2 \langle 6.94^2\Delta | H_{s-o} | 6.94^2\Delta \rangle_0 + \beta^2 \langle 6.23^2\Delta | H_{s-o} | 6.23^2\Delta \rangle_0 + 2\alpha\beta \langle 6.94^2\Delta | H_{s-o} | 6.23^2\Delta \rangle_0 \quad (6.8)$$

The off-diagonal term can be neglected, because of small vibrational overlap between wavefunctions of the $v=0$ $6.94^2\Delta$ and $v=1$ $6.23^2\Delta$ states. The estimate of the spin-orbit interaction, $A=0.04 \text{ cm}^{-1}$, for the unperturbed $v=0$ $6.94^2\Delta$ state is obtained by scaling the spin-orbit interaction of the $5.94^2\Delta$ state. Now, we have

$$A_{\text{obs}} = \alpha^2 * 0.04 + \beta^2 * 3.84 = 0.41 \text{ cm}^{-1} \quad (6.9)$$

The spin-orbit constant estimated here for the $v=0$ $6.94^2\Delta$ state agrees satisfactorily with the fitted value, $0.603(25) \text{ cm}^{-1}$. Thus, we conclude, that the $v=0$ $6.94^2\Delta$ \sim $v=1$ $6.23^2\Delta$ interaction is responsible for the anomaly of the spin-orbit splitting in the $6.94^2\Delta$ state.

The $v=1$ $6.94^2\Delta$ state is perturbed near $J=5.5$ by a state with a very small effective B value, probably a component of a core-nonpenetrating supercomplex. The perturbers,

both e - and f -symmetry levels, are observed between $J=5.5$ and $J=10.5$, but only one level, $J=5.5f$, is detectably shifted by 0.028 cm^{-1} . The core-nonpenetrating perturber is probably the same one that, at higher- J , weakly perturbs the $(v=0) 0.88^2\Sigma^+$ series. It probably also affects other members of $v=0$ and $v=1$ manifolds of the $0.94^2\Delta$ series below $J=5.5f$ and $J=6.5e$, which is the low- J limit of our OODR data, thus we do not observe those perturbations. A perturbation could be observed for the $v=1 6.94^2\Delta$ state because the $v=0 7.94^2\Delta$ state interacts with the $v=1 6.94^2\Delta$ state (intrachannel perturbation) and pushes it slightly to lower energy. The $v=0 7.94^2\Delta$ state is unobservable, even though it is predicted (from Figure 14) to lie near the $v=1 6.94^2\Delta$ state, at 37003.40 cm^{-1} . Since the $v=0 7.94^2\Delta$ and $v=1 6.94^2\Delta$ states interact strongly and are significantly mixed, we included the $v=1 6.94^2\Delta$ state in Figure 14 in place of the unobserved $v=0 7.94^2\Delta$ state. Since we observe only one member of the interacting pair of states, we can only estimate an upper bound limit for the interaction matrix element as $H_{1-2}=1.45 \text{ cm}^{-1}$ (if the first vibrational quantum $\Delta G_{1/2}$ of the $6.94^2\Delta$ state is equal to 536.53 cm^{-1}). The actual interaction matrix element is, however, probably significantly smaller, since $\Delta G_{1/2}$ for the $6.94^2\Delta$ state is expected to be smaller than 535.5 cm^{-1} . Using the upper bound value of the interaction matrix element we can estimate, for the $v=0 7.94^2\Delta$ state, an upper bound on the absolute value of the quantum defect derivative with respect to internuclear distance, as we did in Section 6.2.1 for the $7.88^2\Sigma^+$ state, as equal to 0.08 \AA^{-1} .

6.2.4 Core-penetrating $^2\Phi$ Rydberg series.

The $^2\Phi$ series is observed only above $n^*=9$ where, due to a Λ -mixing l -uncoupling interaction, $^2\Phi$ states borrow transition intensity from $^2\Delta$ states. A direct transition from the intermediate $C^2\Pi$ state to $^2\Phi$ states is forbidden by the $\Delta\Lambda=0,\pm 1$ selection rule. For the sake of completeness, we did single state fits for the four $^2\Phi$ states. However, we used only terms of $^2\Phi^-$ symmetry, because the $^2\Phi^+$ terms are heavily perturbed by core-nonpenetrating states. The centrifugal distortion constant was held fixed at $0.16 \cdot 10^{-6} \text{ cm}^{-1}$ and only the rotationless energy and the rotational constant were fitted.

Table 16: Effective molecular constants (in cm^{-1}) for $0.86^2\Phi$ series.

	T	B
9.86 $^2\Phi$	37614.734 (8)	0.216186 (22)
10.86 $^2\Phi$	37813.818 (4)	0.210987 (26)
11.86 $^2\Phi$	37964.659 (6)	0.205470 (41)
12.86 $^2\Phi$	38081.562 (8)	0.200431 (90)

¹ C. Effantin, A. Bernard, J. D'Incan, G. Wannous, J. Vergès, and R. F. Barrow, *Mol. Phys.* **70**(5), 735-745 (1990).

² J. Singh and H. Mohan, *Indian J. of Pure and Applied Physics* **11**, 918-922 (1973).

³ H el ene Lefebvre-Brion and Robert W. Field, *Perturbations in the Spectra of Diatomic Molecules*, Academic Press (1986).

⁴ G. Herzberg, 1989, *Molecular Spectra and Molecular Structure. I. Spectra of Diatomic Molecules* (Malabar, Florida: Krieger), p. 141-145.

⁵ C. A. Fowler, *Phys. Rev.* **59**, 645 (1941).

⁶ Z. J. Jakubek, (*unpublished*).

⁷ C. Effantin, A. Bernard, J. D'Incan, E. Andrianavalona, and R. F. Barrow, *J. Mol. Spectrosc.* **145**, 456-457 (1991).

⁸ C. Effantin, A. Bernard, J. D'Incan, E. Andrianavalona, and R. F. Barrow, *J. Mol. Spectrosc.* **145**, 456-457 (1991).

⁹ A. Bernard, C. Effantin, J. D'Incan, J. Verg es and R. F. Barrow, *Mol. Phys.*, **70**(5), 747-755 (1990).

¹⁰ R. F. Barrow, M. W. Bastin, and B. Longborough, *Proc. Phys. Soc.* **92**, 518-519 (1967).

¹¹ R. S. Mulliken, *J. Am. Chem. Soc.* **91**, 4615 (1969).

¹² Z. J. Jakubek and R. W. Field, *Phys. Rev. Lett.*, **72** (14), 2167-2170 (1994).

¹³ J. M. Berg, J. E. Murphy, N. A. Harris, and R. W. Field, *Phys. Rev. A*, **48**(4), 3012-3029 (1993).

7. Supercomplexes.

7.1 Molecular constant scaling laws and supercomplex formation.

As mentioned previously, 10 core-penetrating Rydberg series were observed in the BaF molecule. Even if several individual states are missing from this global core-penetrating picture, we believe we have obtained a complete set of experimental data for the core-penetrating Rydberg series, which is sufficient to describe *all* members of *all* 10 core-nonpenetrating series from $n^* \approx 6$ to ∞ . In Figure 16 we show a plot of $n^* \bmod 1$ vs n^* for all 10 series. States belonging to the same Rydberg series are connected by tie lines. The only exception is the $A'^2\Delta$ state which, for clarity, is not shown connected with the other members of the $0.23^2\Delta$ series. Membership in each series is based on the similarity of quantum defects and the proper scaling behavior of the molecular constants. Apart from irregular deviations caused by perturbations of the $v=0$ states by states from higher vibrational manifolds, the $n^* \bmod 1$ quantities are expected to be constant within each Rydberg series.

Before we further discuss properties of the Rydberg series, we will briefly review the basic scaling properties of some of the molecular constants and the possible reasons for departures from the predicted behavior (see also Berg *et al.*¹³ and Murphy¹). A molecule in a Rydberg state can be regarded as a charged molecular-ion-core with an electron attached to, but spending most of the time far from the core. Thus, the vibrational, ω_e , and rotational, B , constants of the Rydberg state should be equal to those of the ion-core, ω_e^+ and B^+ , respectively. This should be strictly true for core-nonpenetrating states. In the case of core-penetrating states, the Rydberg electron periodically enters the ion-core and significantly changes the core structure, thus also the vibrational and rotational constants.

For highly polar diatomic molecules like BaF and other alkaline earth monohalides, the effect of core-penetration by a Rydberg electron on the vibrational and rotational constants can be described by a simple model. Let the molecular core be represented by two point charges, $+2$ and -1 , at an internuclear separation of r_e . We also assume that the

Rydberg electron avoids the negative ligand (F^-) and approaches the positive alkaline earth ion (Ba^{2+}), thereby lowering the effective charge seen by the ligand by Δq . Δq can be written as

$$\Delta q = \text{const}' \cdot \int_0^{r_{\text{core}}} |\Psi|^2 dr = \text{const} \cdot \frac{1}{n^{*3}}, \quad (7.1)$$

where Ψ is the Rydberg electronic wavefunction, the innermost lobe amplitude of which scales as $(n^*)^{-3/2}$. The penetration of the Rydberg electron into the core leads to an extra $Ba \leftrightarrow F$ repulsive electrostatic interaction. This in turn leads to the internuclear distance increases and the rotational and vibrational constants decrease relative to those of the molecular ion. However, since the extra interaction (shielding) goes to zero as $(n^*)^{-3}$, even for intermediate- n^* Rydberg states, the vibrational and rotational constants should be close to those of molecular ion.

In the discussion above we assumed that the extra negative charge of the penetrating Rydberg electron is localized on the Ba^{2+} ion. If, however, there are 2 states of the same symmetry and similar energy, for example two ${}^2\Sigma^+$ states, they will interact and form a pair of complementarily polarized states, one of them polarized away from ligand (normal polarization), but the other towards the ligand (reverse polarization). An electron in the reverse-polarized orbital experiences a stronger repulsive interaction with the F^- ligand than an electron in the normally polarized one. Thus, *reverse polarized states can be recognized by atypically large $n^* \bmod 1$ and small vibrational and rotational constants at low n^* -values*. As the shielding goes to zero with $(n^*)^{-3}$, both normal and reverse polarization effects on the molecular constants also disappear.

The n^* -dependence of the core-penetration effects can be also derived in a more formal way using a simple harmonic oscillator model introduced by Mulliken¹¹ (see also Herzberg and Jungen²). The potential curve of a Rydberg state can be related to the potential curve of the molecular-ion core by

$$U(R) = U^+(R) - \frac{\mathfrak{R}}{(n - \mu(R))^2}. \quad (7.2)$$

The potentials can be approximated by harmonic oscillators (good approximation for the lowest vibrational level) as

$$U(R) = U(R_e) + f(R - R_e)^2 + \dots \quad (7.3)$$

and

$$U^+(R) = IP + f^+(R - R_e^+)^2 + \dots \quad (7.4)$$

Using Eqs. 7.3 and 7.4 and expanding $\mu(R)$ in a Taylor series, Eq. 7.2 takes the form

$$U(R) = U(R_e) + f(R - R_e)^2 = f^+(R - R_e^+)^2 + IP - \frac{\mathfrak{R}}{(n^*)^2} - \frac{2\mathfrak{R}}{(n^*)^3} \frac{d\mu}{dR} (R - R_e^+). \quad (7.5)$$

Differentiating Eq. 7.5 we obtain an equilibrium internuclear distance for the Rydberg state,

$$R_e = R_e^+ + \frac{\mathfrak{R}}{f^+} \frac{1}{(n^*)^3} \frac{d\mu}{dR}. \quad (7.6)$$

Substituting f^+ by

$$f^+ = \frac{2\pi^2 c \mu}{10^{18} h} \cdot m \omega_e^{+2} = 1.4830 \cdot 10^{-2} \cdot m \omega_e^{+2}, \quad (7.7)$$

where μ is a reduced mass in atomic mass units, ω_e^+ is in cm^{-1} and f^+ is in $\text{cm}^{-1}/\text{\AA}^2$, Eq. 7.6 can be written as

$$R_e = R_e^+ + 67.431 \cdot \frac{\mathfrak{R}}{m \omega_e^{+2}} \frac{1}{(n^*)^3} \frac{d\mu}{dR}. \quad (7.8)$$

Substituting Eq. 7.8 into 7.5, one obtains a corrected expression for the energy of the Rydberg state

$$U(R_e) = IP - \frac{\mathfrak{R}}{(n^*)^2} - 67.431 \cdot \frac{\mathfrak{R}^2}{m \omega_e^{+2}} \frac{1}{(n^*)^6} \left(\frac{d\mu}{dR} \right)^2. \quad (7.9)$$

The new term in Eq. 7.9 dependent on $(n^*)^{-6}$ lowers the energy, thus also n^* , at low n^* . The $(n^*)^{-6}$ dependence of the energy term is equivalent to an $(n^*)^{-3}$ dependence of the extra term in $n^*(R)$ or $\mu(R)$. One should notice that the extra term in Eq. 7.9 is always negative, thus the harmonic oscillator model cannot account for the reverse polarization

induced increase of the energy (and n^*) at low n^* . From Eq. 6.16, we conclude that the equilibrium internuclear distance for the Rydberg state is larger or smaller than the molecular-ion core equilibrium internuclear distance when the quantum defect derivative is, respectively positive (antibonding contribution from the Rydberg electron) or negative (bonding contribution from the Rydberg electron). The harmonic oscillator model also predicts an $(n^*)^{-3}$ -dependent correction to the vibrational frequency of the Rydberg state. For this, however, a term proportional to $(R-R_e^+)^2$ must be included in the quantum defect expansion. The corrected Rydberg state force constant will be

$$f = f^+ - \frac{\mathfrak{R}}{(n^*)^3} \frac{d^2\mu}{dR^2}. \quad (7.10)$$

Inclusion of the term proportional to $(R-R_e^+)^2$ in the quantum defect expansion leads to slightly modified forms for Eqs. 7.6, 7.8, and 7.9. We can obtain the modified forms of those equations when ω_e^+ is replaced by the corrected ω_e calculated from Eq. 7.10. Using Eq. 7.7 we can estimate, from Eq. 7.10, a change of the Rydberg state vibrational frequency as

$$\omega_e = \omega_e^+ - 33.715 \cdot \frac{\mathfrak{R}}{m\omega_e^+} \cdot \frac{1}{(n^*)^3} \cdot \frac{d^2\mu}{dR^2}. \quad (7.11)$$

The quantum defect derivatives appear in the equations above as known values on the right side. They can, however, also be calculated from the observed deviations of the rotational constant (internuclear distance), energy (n^*), or vibrational frequency (force constant) at low- n^* . Later, using the thus obtained quantum defect derivatives, other molecular properties, like autoionization rates, perturbation matrix elements etc., can be calculated. From Eq. 7.6, for example, we can calculate

$$\frac{d\mu}{dR} = 1.4830 \cdot 10^{-2} \cdot \frac{(n^*)^3}{\mathfrak{R}} \cdot m\omega_e^{+2} \cdot (R_e - R_e^+). \quad (7.12)$$

Similarly one can estimate the second derivative of the quantum defect from Eqs. 7.10 and 7.7 as

$$\frac{d^2\mu}{dR^2} = 1.4830 \cdot 10^{-2} \cdot \frac{(n^*)^3}{\mathfrak{R}} m(\omega_e^{+2} - \omega_e^2). \quad (7.13)$$

We see from Eq. 7.12 that, in order for $(d\mu/dR)$ to be independent of n^* , the difference of the equilibrium internuclear distances of the Rydberg state and the ground state of the molecular-ion core, $(R_e - R_e^+)$, must decrease approximately as $(n^*)^{-3}$. Even for moderately high- n^* Rydberg states, an accurate determination of the true $(R_e - R_e^+)$ difference is virtually impossible. The reasons are: insufficient experimental precision, accidental $\Delta v \neq 0$ perturbations, I-uncoupling interactions and others. Thus, we cannot apply the model in the region $(R_e \approx R_e^+)$ where the harmonic approximation works best. Being forced to compromise, we estimated $(d\mu/dR)$ for some of the series using experimental data for their 2 lowest members. The agreement of the two values of $(d\mu/dR)$ for each series can be treated as a test of correctness of the estimation.

For the $0.08^2\Sigma^+$ series I-uncoupling is very strong even for the lowest observed members and we did not attempt to calculate $(d\mu/dR)$. The lowest observed state of the $0.94^2\Delta$ series is $v=1$ $3.94^2\Delta$. From ΔB , we calculated for this state $d\mu/dR=0.81 \text{ \AA}^{-1}$, which is 10 times larger than the upper limit for $|d\mu/dR|$ calculated from the intrachannel perturbation discussed in Section 6.2.3. For the $4.94^2\Delta$ and $5.94^2\Delta$ states we calculated $d\mu/dR=1.8 \text{ \AA}^{-1}$ and 2.8 \AA^{-1} , respectively. The strong variation of the $d\mu/dR$ with n^* for the $0.94^2\Delta$ series indicate that even at n^* as low as 3.94, the I-uncoupling interaction significantly affects the value of the effective rotational constant. A similar conclusion is probably also true for the $0.04^2\Pi$ series (see Table 17), for which the $d\mu/dR$ also strongly depends on n^* . Concluding, we can say that, except for the $0.88^2\Sigma^+$, the $0.76^2\Sigma^+$, the $0.24^2\Sigma^+$, and the $0.45^2\Pi$ series, I-uncoupling interaction cannot be disregarded even at as low- n^* as $n^* \approx 3-4$.

Table 17: First derivatives of quantum defect with respect to internuclear distance (in \AA^{-1}) calculated using harmonic oscillator model and experimental quantum defects and internuclear distances.

	$0.88^2\Sigma^+$	$0.76^2\Sigma^+$	$0.24^2\Sigma^+$	$0.45^2\Pi$	$0.04^2\Pi$
$D'^2\Sigma^+$	0.526	$X^2\Sigma^+$ 0.200	$B^2\Sigma^+$ 0.497	$C^2\Pi$ 0.644	$E'^2\Pi$ 0.548
$H^2\Sigma^+$	0.596	$D^2\Sigma^+$ 0.362	$E^2\Sigma^+$ 0.495	$F^2\Pi$ 0.613	$J^2\Pi$ 0.902

Note: First entry in each column is a state name, the second entry is the absolute value of $(d\mu/dR)$ in \AA^{-1} derived from B values.

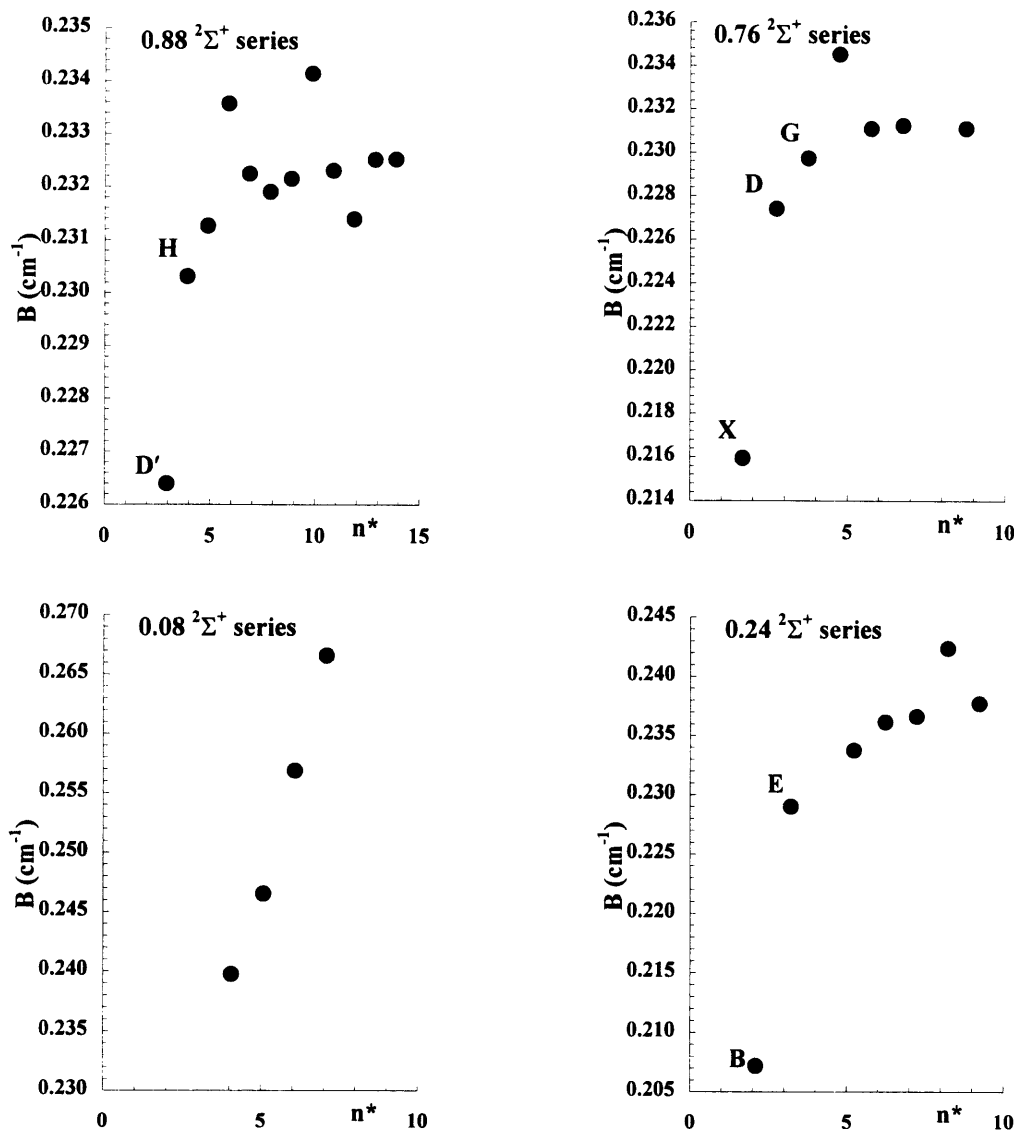


Figure 15: n^* -variation of the effective rotational constants for the four $^2\Sigma^+$ series.

In Figure 16 one can see that the $0.88^2\Sigma^+$ state shows, at low n^* , an unusually large increase of $n^* \bmod 1$ which is typical for a reverse polarized state. In this series, the first vibrational interval, $\Delta G_{1/2}$, is known for the $6.88^2\Sigma^+$ (533.87 cm^{-1}) and $7.88^2\Sigma^+$ (533.94 cm^{-1}) states. These values are smaller than $\Delta G_{1/2}$ for the members of other $^2\Sigma^+$ series, the $6.76^2\Sigma^+$ state (534.14 cm^{-1}) and the $6.08^2\Sigma^+$ state (535.27 cm^{-1}). As a reference we can use $\Delta G_{1/2}=535.08 \text{ cm}^{-1}$ for the $6.94^2\Delta$ state since the Rydberg orbital for $^2\Delta$ states is localized near a plane perpendicular to the internuclear axis and the properties of these $^2\Delta$ states should be only weakly sensitive to the normal/reverse polarization effect. A very strong argument for the reverse polarization of the $0.88^2\Sigma^+$ series comes also from the first derivative of the quantum defect with respect to internuclear distance for the $7.88^2\Sigma^+$ state, as determined in Section 6.2.1. The value of this derivative, $0.23 (1) \text{ \AA}^{-1}$, is much larger than the upperbound estimate of the similar quantity for the $7.94^2\Delta$ state, 0.08 \AA^{-1} , determined in Section 6.2.3. The $0.03^2\Pi$ series is another possible reverse polarized series. The value of $n^* \bmod 1$ of its lowest member, $E''^2\Pi$, is larger than that of the rest of the series by 0.07.

It was mentioned previously that the rotational constant, B , and $n^* \bmod 1$ should have constant values within a Rydberg series, at least for n^* higher than some transitional value. Such an hypothesis seems valid for at least three out of four $^2\Sigma^+$ core-penetrating Rydberg series, as is evident in plots of the effective rotational constant vs n^* in Figure 15. More careful investigation of those plots reveals, however, that the asymptotic values are slightly different for various series; 0.2313 cm^{-1} for the $0.76^2\Sigma^+$, 0.2325 cm^{-1} for the $0.88^2\Sigma^+$, and 0.2377 cm^{-1} for the $0.24^2\Sigma^+$ state. The effective rotational constant for the $0.08^2\Sigma^+$ series is skyrocketing as n^* increases and no asymptotic value can be estimated. The B value of the $0.08^2\Sigma^+$ series illustrates in a dramatic way the fact that the second-order effects neglected (except for centrifugal distortion) in an isolated state approximation become important and contribute significantly to the effective values of fit parameters. The second-order interactions of a $^2\Sigma^+$ state with remote $^2\Sigma^+$ states leads to a J -dependent energy correction which is parametrized by the centrifugal distortion constant.

Let us now consider second-order interactions between a ${}^2\Sigma^+$ state and remote ${}^2\Pi$ states. These states can be connected by the **I**-uncoupling interaction (${}^2\Sigma^+_{1/2} \sim {}^2\Pi_{3/2}$, ${}^2\Sigma^+_{-1/2} \sim {}^2\Pi_{1/2}$, ${}^2\Sigma^+_{-1/2} \sim {}^2\Pi_{-3/2}$, and ${}^2\Sigma^+_{1/2} \sim {}^2\Pi_{-1/2}$) and **I**-s coupling (${}^2\Sigma^+_{1/2} \sim {}^2\Pi_{1/2}$ and ${}^2\Sigma^+_{-1/2} \sim {}^2\Pi_{-1/2}$). We must consider three operators, **H**₄, **H**₇, and **H**₈, : (1) $H_4 = -B(r)[\mathbf{J}^+\Gamma + \mathbf{J}\Gamma^+]$, (2) $H_7 = +B(r)[\Gamma^+s^- + \Gamma s^+]$, and (3) $H_8 = +\frac{1}{2}A(r)[\Gamma^+s^- + \Gamma s^+]$. Evaluating the required matrix elements, we get for the second-order corrections to the molecular constants

$$\Delta^{(2)}E_i = \Delta^{(2)}T_i + \Delta^{(2)}\gamma_i(1 \pm x) + \Delta^{(2)}B_i x(x \pm 1), \quad (7.14)$$

where $x \equiv J+1$ and

$$\Delta^{(2)}T_i = \sum_j c_j \frac{\frac{1}{4}(a_+)_j^2}{E_i - E_j}, \quad (7.15)$$

$$\Delta^{(2)}\gamma_i = -2 \sum_j c_j \frac{(a_+)_j B^+ b_j}{E_i - E_j}, \quad (7.16)$$

$$\Delta^{(2)}B_i = \sum_j c_j \frac{2(B^+ b_j)^2}{E_i - E_j}, \quad (7.17)$$

and $(a_+)_j = A_j(l_j(l_j+1))^{1/2}$ and $b_j = (l_j(l_j+1))^{1/2}$.

It can be shown easily that

$$\frac{1}{E_i - E_j} = \frac{\overline{(n^*)^3}}{4\mathfrak{R}\Delta(n^*)} \quad (7.18)$$

where $\overline{(n^*)}$ is the average- n^* for two interacting states and $\Delta(n^*)$ is the difference between the n^* 's of the interacting states. This approximation is accurate to better than 1-2% for $n^* > 8$. It can also be shown that the spin-orbit parameter is proportional to $(n^*)^{-3}$. This dependence comes from the fact that the spin-orbit operator depends on r^{-3} and the wavefunction amplitude scales near the origin as $(n^*)^{-3/2}$, thus matrix elements of the spin-orbit operator scale as $(n^*_i n^*_j)^{-3/2}$. Using these scaling rules we can estimate n^* -scaling of the second-order parameters.

The $\Delta^{(2)}T$ term, which is J-independent and contributes to the effective rotationless energy, decreases as $(n^*)^{-3}$ and its sign is positive if a dominating interaction comes from a ${}^2\Pi$ state lower in energy than the ${}^2\Sigma^+$ state and is negative otherwise.

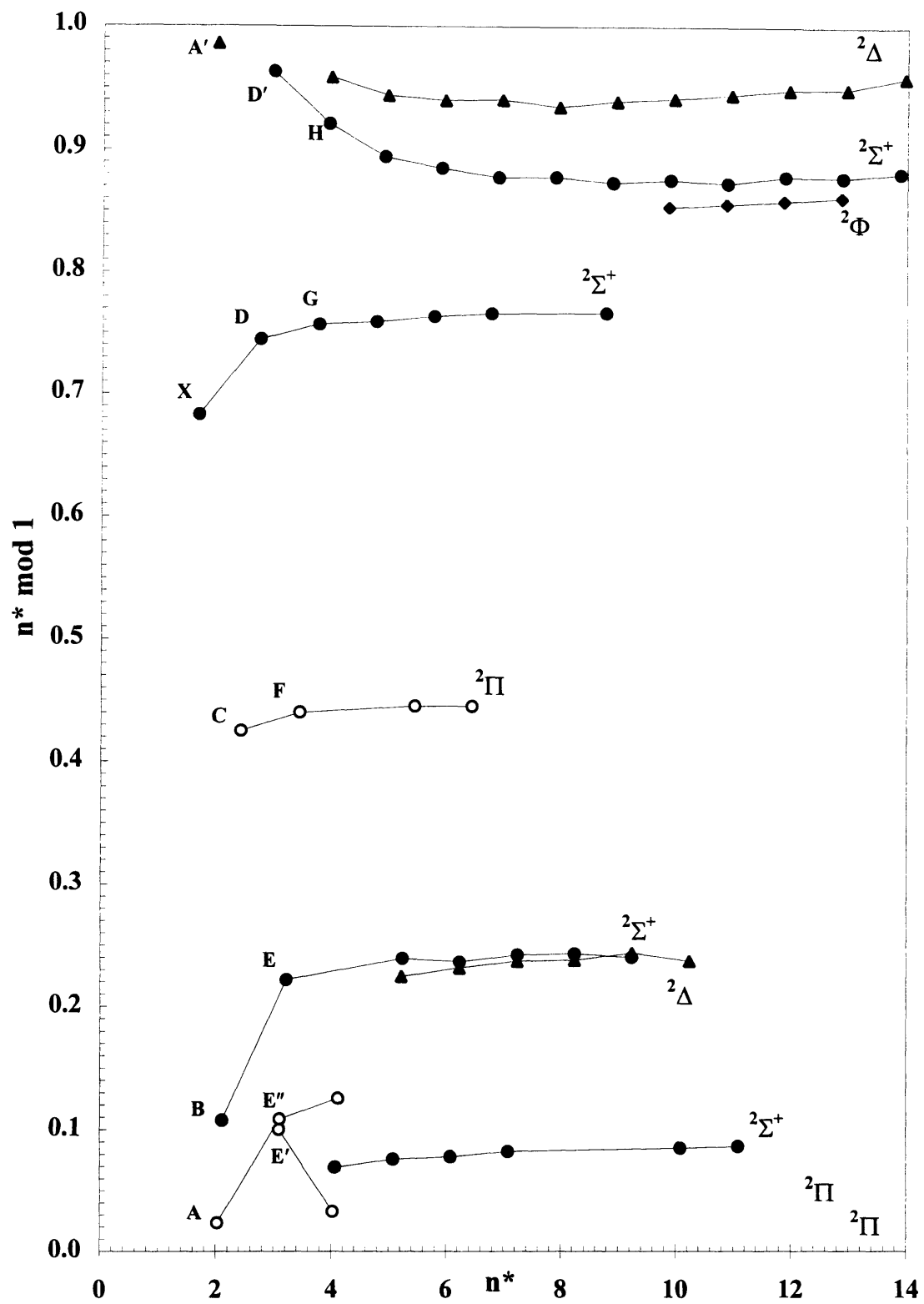


Figure 16: $n^* \bmod 1$ vs n^* plot for all known core-penetrating electronic Rydberg states of BaF.

The n^* -independent $\Delta^{(2)}\gamma$ term contributes to the effective spin-rotation parameter, and contributions are positive for remote ${}^2\Pi$ states located at higher energy than the ${}^2\Sigma^+$ state. The third term, $\Delta^{(2)}B$, has the same J -dependence as the rotational energy and increases with the third power of n^* . Positive contributions come from interactions with ${}^2\Pi$ states below the ${}^2\Sigma^+$ state in question.

The very large positive $\Delta^{(2)}B$ contribution to the B_{eff} constant for the states of the $0.08{}^2\Sigma^+$ series indicates that the $0.08{}^2\Sigma^+$ series interacts dominantly with the nearby $0.03{}^2\Pi$ or $0.04{}^2\Pi$ series at lower energy. The positive value of the spin-rotation constant, γ , on the other hand suggests that the primary interacting ${}^2\Pi$ state should be located at higher energy. This apparent contradiction follows from the fact that we have assumed that the ${}^2\Sigma^+$ state interacts with only a single ${}^2\Pi$ state. Allowing the ${}^2\Sigma^+$ state to interact with two (or more) ${}^2\Pi$ states characterized by different spin-orbit parameters immediately resolves the paradox. One may notice that Eqs. 6.12 and 6.13 are very similar. They differ by one factor in each term of the sum. Replacing $-(a_+)_i$ in 6.12 by (B^+b_i) leads to 6.13. Unlike B^+ , a_+ is different for each ${}^2\Pi$ state interacting with the ${}^2\Sigma^+$ state, thus also the relative magnitudes of respective terms in both sums are different. This may lead to different combinations of signs of $\Delta^{(2)}\gamma$ and $\Delta^{(2)}B$ even if the interacting states considered are the same. For the states of the $0.08{}^2\Sigma^+$ series, the energy interval to the $0.45{}^2\Pi$ state on the higher energy side is about 6 times larger than that to the $0.03{}^2\Pi$ or $0.04{}^2\Pi$ series on the lower energy side. This implies that the $0.08{}^2\Sigma^+$ series interacts primarily with a series at lower energy with a very small spin-orbit splitting.

The three other ${}^2\Sigma^+$ series do not show such dramatic variations of the effective B value with n^* . Taking, for the rotational constant of the ion-core, $B^+=0.234\text{ cm}^{-1}$, we notice that the $\Delta^{(2)}B$ corrections are small and negative for the $0.76{}^2\Sigma^+$ and $0.88{}^2\Sigma^+$ series and positive for the $0.24{}^2\Sigma^+$ series. The positive spin-rotation parameter and the negative $\Delta^{(2)}B$ correction for states of the $0.76{}^2\Sigma^+$ series indicate that this series interacts primarily with states of the $0.03{}^2\Pi$ and $0.04{}^2\Pi$ series at higher energy. The $0.24{}^2\Sigma^+$ series has negative $\Delta^{(2)}\gamma$ and positive $\Delta^{(2)}B$ corrections, therefore it also interacts primarily with the $0.03{}^2\Pi$ and $0.04{}^2\Pi$ series. The negative $\Delta^{(2)}B$ corrections for the states of the $0.88{}^2\Sigma^+$

series show that the $0.03^2\Pi$ and $0.04^2\Pi$ series are also the dominant sources of interaction. However, the negative value of $\Delta^{(2)}\gamma$ indicates that also the $0.45^2\Pi$ series is strongly interacting with the $0.88^2\Sigma^+$ series.

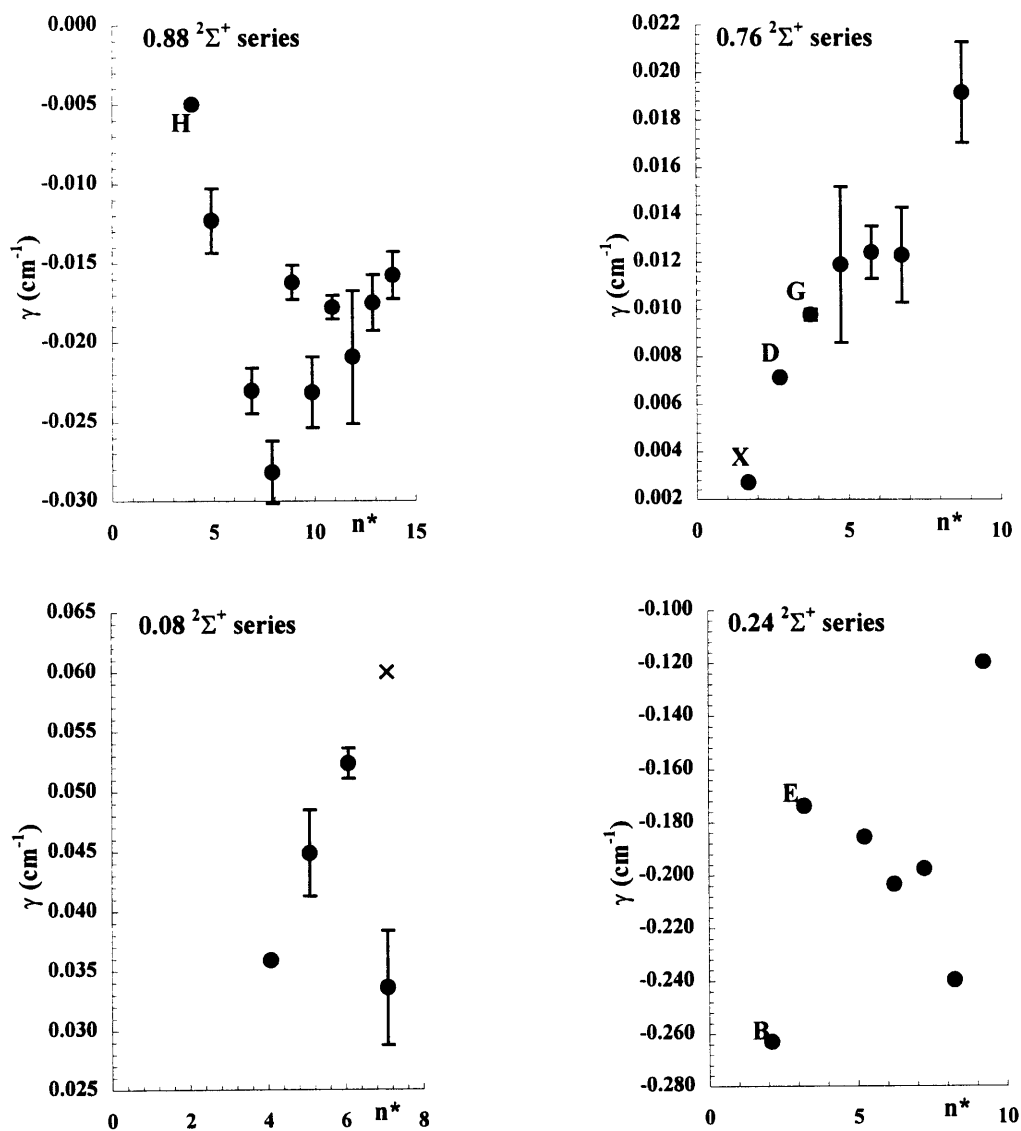


Figure 17: n^* -variation of the effective spin-rotation constants for the four $^2\Sigma^+$ series. Error bars denote 3σ uncertainties (when larger than marker size). (x denotes γ value obtained for the $7.08^2\Sigma^+$ state using the same model as for the other three members of the $0.08^2\Sigma^+$ series, i.e. $\gamma_D \equiv 0$).

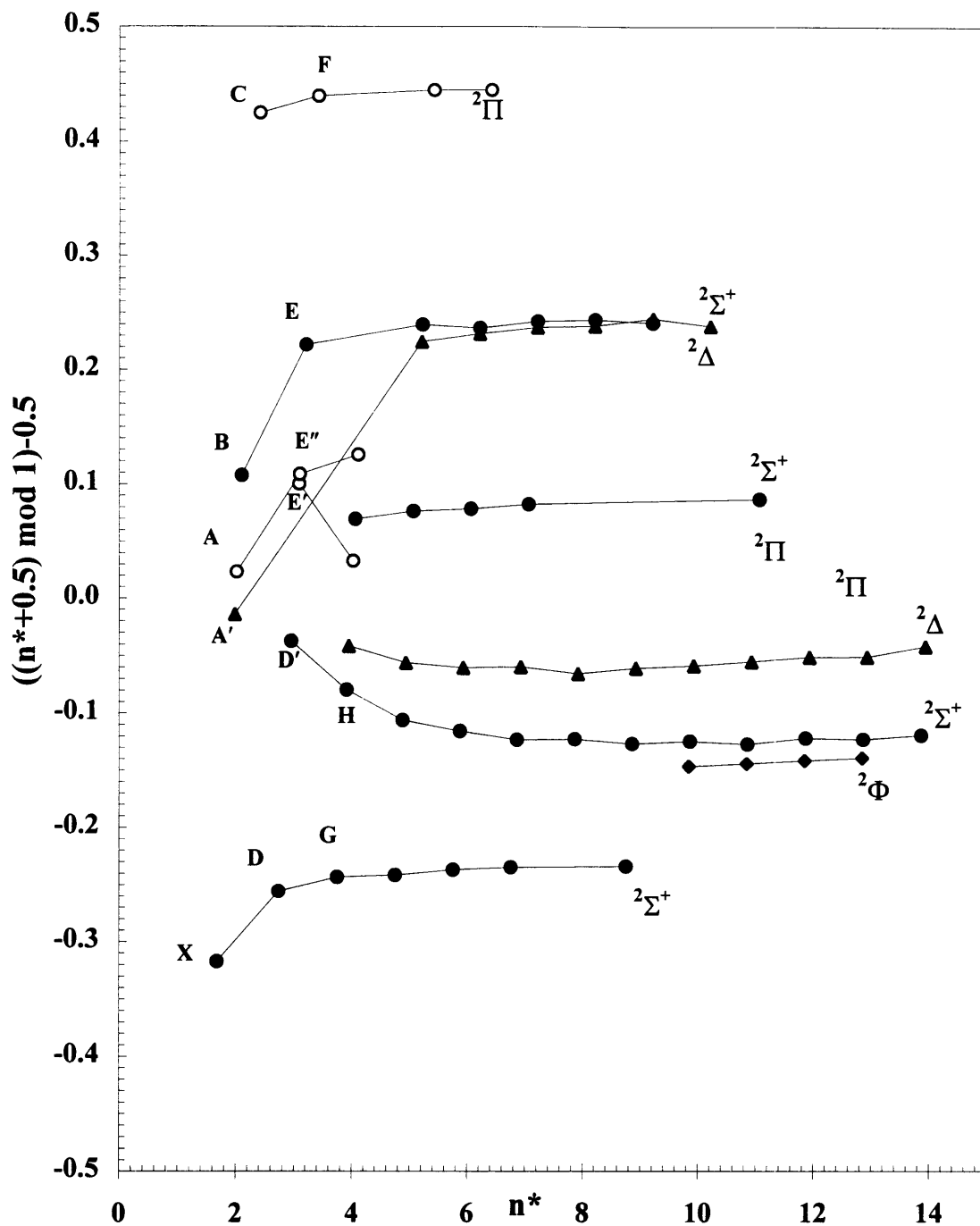


Figure 18: Plot of $(n^* - \text{nearest integer})$ vs n^* , illustrating the concept of supercomplexes. *All* states interact and the interactions within each supercomplex are dominant over interactions between neighboring supercomplexes. In addition, many series of core-nonpenetrating states are located near integer- n^* , in the region of $(-0.15, +0.15)$, and forming a spectroscopic black hole.

This rather informal analysis leads to the concept of “supercomplexes”. We claim that *all* core-penetrating series (and, as we will see in the next Section, also core-nonpenetrating ones) interact and form a series of supercomplexes. Individual supercomplexes are centered around integer n^* 's and the borderline between them can be drawn somewhere between the $0.45^2\Pi$ and $0.76^2\Sigma^+$ states. The individual supercomplexes, of course, interact and the negative sign of $\Delta^{(2)}\gamma$ for the $0.88^2\Sigma^+$ series is a good demonstration of this. However, the positive sign of the q Λ -doubling constant for the $5.45^2\Pi$ and $6.45^2\Pi$ states shows that the $0.45^2\Pi$ series experiences its dominant interaction from $^2\Sigma^+$ series located at lower $n^* \bmod 1$. The concept of supercomplexes in BaF can be well visualized by a plot of $(n^* - \text{nearest integer})$ vs n^* .

It was stated previously that, in the limit of weak (l -uncoupling and l - s coupling) interaction, spin-rotation constants should have an approximately constant value within each Rydberg series. In Figure 17, we see that the spin-rotation parameter for the $0.76^2\Sigma^+$ series apparently approaches an approximately constant value of 0.012 cm^{-1} . The highest- n^* point refers to the $v=1$ $8.76^2\Sigma^+$ state, which is perturbed by the $11.08^2\Sigma^+$ state that has a much larger spin-rotation splitting. The spin-rotation constant for the $0.88^2\Sigma^+$ series, after initial oscillations, for higher n^* seems to be independent of n^* and has a value of -0.017 cm^{-1} . The absolute value of the γ parameter for both $0.08^2\Sigma^+$ and $0.24^2\Sigma^+$ series increases sharply with n^* , showing that the assumption of weak inter-supercomplex interaction is invalid in those cases. The γ -value for the $7.08^2\Sigma^+$ state, if calculated using the same model as for the other members of the series (i.e. $\gamma_D=0$), follows the series trend. The $9.24^2\Sigma^+$ state is strongly perturbed by the $9.23^2\Delta$ state, thus a single state fit is inappropriate.

The n^* -variation of the spin-orbit splitting was examined for the $0.94^2\Delta$ and $0.23^2\Delta$ series. For all states, with the exception of the lowest observed states, the $A^*(n^*)^3$ quantity seems to take constant values for both series. For the $0.23^2\Delta$ series, $A^*(n^*)^3=925 \text{ cm}^{-1}$ and the value is well determined. Due to large relative uncertainties for the spin-orbit splitting parameters, it is more difficult to estimate the value of the $A^*(n^*)^3$ quantity for the $0.94^2\Delta$ series. For reference purposes we can take $A^*(n^*)^3=15 \text{ cm}^{-1}$.

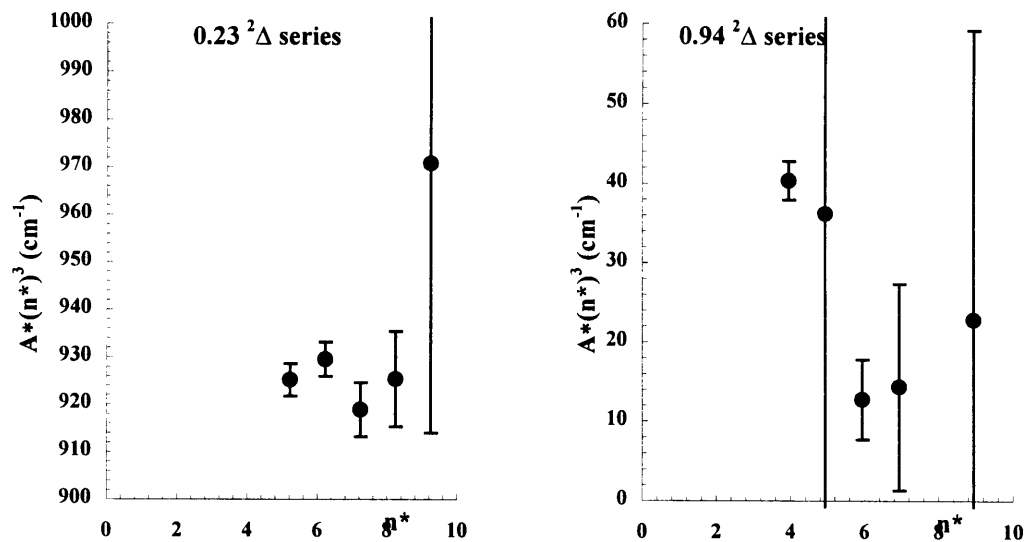


Figure 19: $A^*(n^*)^3$ vs n^* plot for the $0.23^2\Delta$ and $0.94^2\Delta$ series. The entry for the $A'^2\Delta$ state, $A^*(n^*)^3=1619$ cm $^{-1}$ was not included in either of the plots. Error bars denote 3σ uncertainties.

7.2 Core-nonpenetrating complexes.

The most exciting, although unexpected, result of the fluorescence-detected part of the project was the assembly of a large set of data on core-nonpenetrating Rydberg states. In Figure 18 it is evident that the electronic structure of the BaF molecule possesses an interesting feature: the core-penetrating states are clustered near integer- n^* . We also know that, by definition, all core-nonpenetrating states must be even more strongly clustered near integer- n^* . The l -uncoupling effects for the core-nonpenetrating states are expected to be much stronger than for the core-penetrating ones because of the small energy separations between the rotationless Λ -states in the nonpenetrating complexes. Thus, the effective rotational constant for the top and bottom energy components of an n/l nonpenetrating complex are expected to be respectively much larger and smaller than B^+ . Such a situation should inevitably lead to multiple avoided crossings between core-nonpenetrating and core-penetrating states. In the perturbation regions the core-

nonpenetrating states borrow some core-penetrating character, and this makes their excitation and detection possible.

In our fluorescence-detected spectra, we observe multiple core-penetrating ~ core-nonpenetrating perturbations. The easiest to detect are the strong perturbations in the $0.86^2\Phi$ and $0.94^2\Delta$ series. More difficult to identify is a very weak perturbation in the $0.88^2\Sigma^+$ series. We also observe extra states in the region just above integer n^* . Conclusive assignments in that region are not yet possible and more experiments are required.

The systematic perturbations in the $0.94^2\Delta$ series are observed for the $8.94^2\Delta$ and higher series members. In Figure 20, three perturbations are evident in the $10.94^2\Delta$ state, two of them, one strong and one very weak, in the $10.94^2\Delta^+$ (open circles) component and one (weak) in the $10.94^2\Delta^-$ component (solid circles). For the $10.86^2\Phi$ state we observed one strong perturbation in the $10.86^2\Phi^+$ component and two very weak in the $10.86^2\Phi^-$ component. As we go to the higher- n^* members of the $^2\Phi$ series, additional perturbations are observed at high- J . The perturbation in the $0.88^2\Sigma^+$ series is very weak and not very well documented. In the $10.88^2\Sigma^+$ state we observed only 6 extra lines and the biggest level shift is $\sim 0.1 \text{ cm}^{-1}$. Figure 20 shows the plot of reduced term value vs $N(N+1)$. To better illustrate the core-penetrating~core-nonpenetrating perturbations we also present in Figure 21 the reduced term value plot vs $J(J+1)$ for e -symmetry levels. Recall that J , unlike N , is a rigorously good quantum number. Also the total Hamiltonian is strictly block-diagonal for e - and f -symmetry levels.

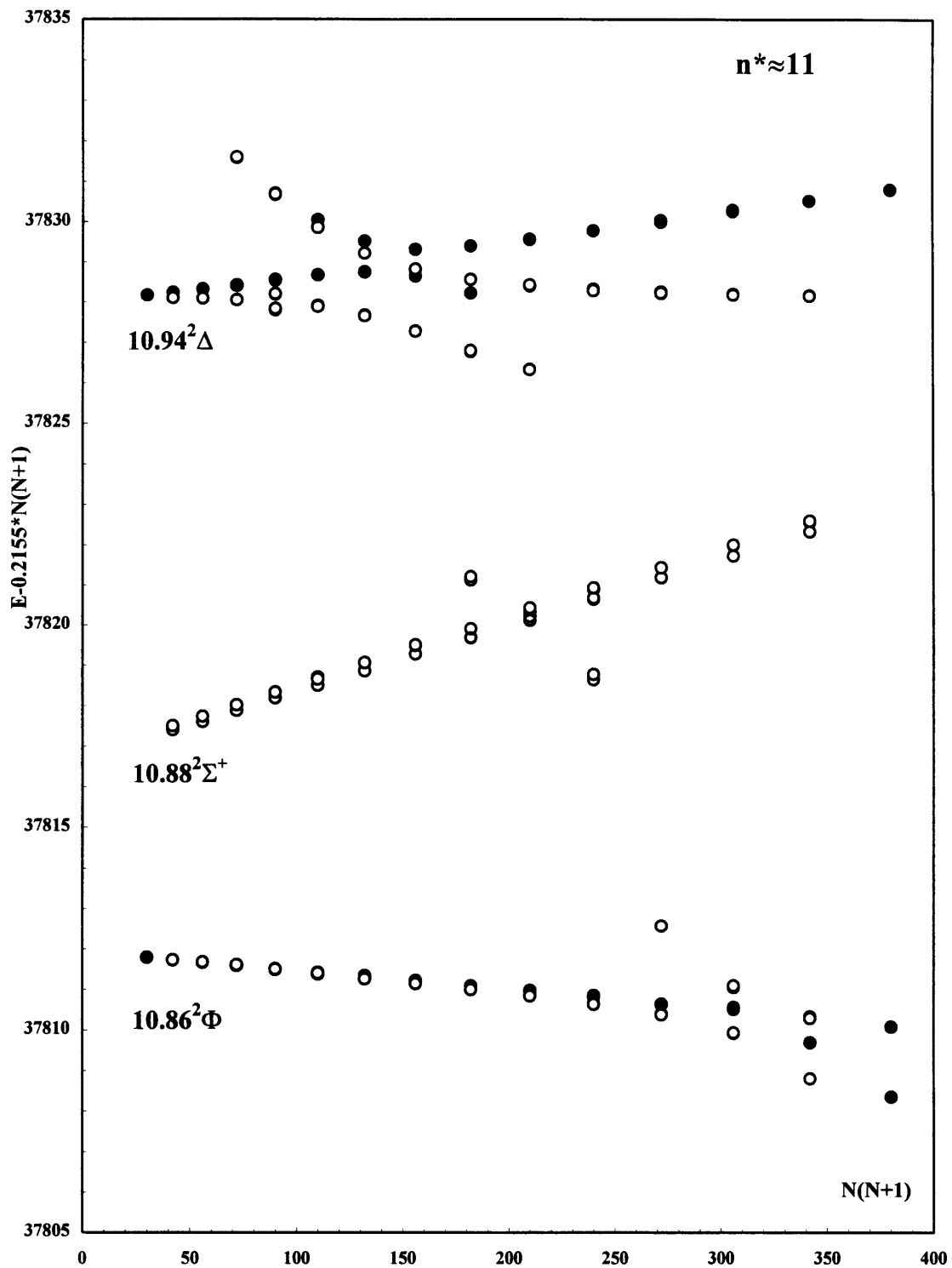


Figure 20: Reduced term value vs $N(N+1)$ plot for the $10.86^2\Phi$, $10.88^2\Sigma^+$, and $10.94^2\Delta$ states, showing multiple perturbations by core-nonpenetrating states. Solid (open) circles denote levels of $+(-)$ Kronig symmetry.

The appearance of the reduced term value plots, as we follow the three Rydberg series, is very similar. Corresponding perturbations appear at high- J for low- n^* states and move towards lower- J with increasing n^* . This systematic shifting of perturbations is explained in the (*not included*). As n^* increases the difference between the core-penetrating state energy and the hydrogenic (integer- n^*) energy (where all of the core-nonpenetrating states originate) decreases approximately as $(n^*)^{-3}$. The separation between different core-penetrating electronic states is much larger than the rotational spacing (Hund's case (a) or (b)) and the I -uncoupling interaction for those states can be neglected. The effective rotational constant does not change (significantly) with n^* . In contrast the core-nonpenetrating states are described well by Hund's case (d). The rotational spacing is large relative to the electronic separation (rotationless Λ -states). The electronic separation is negligible compared to the I -uncoupling interaction.

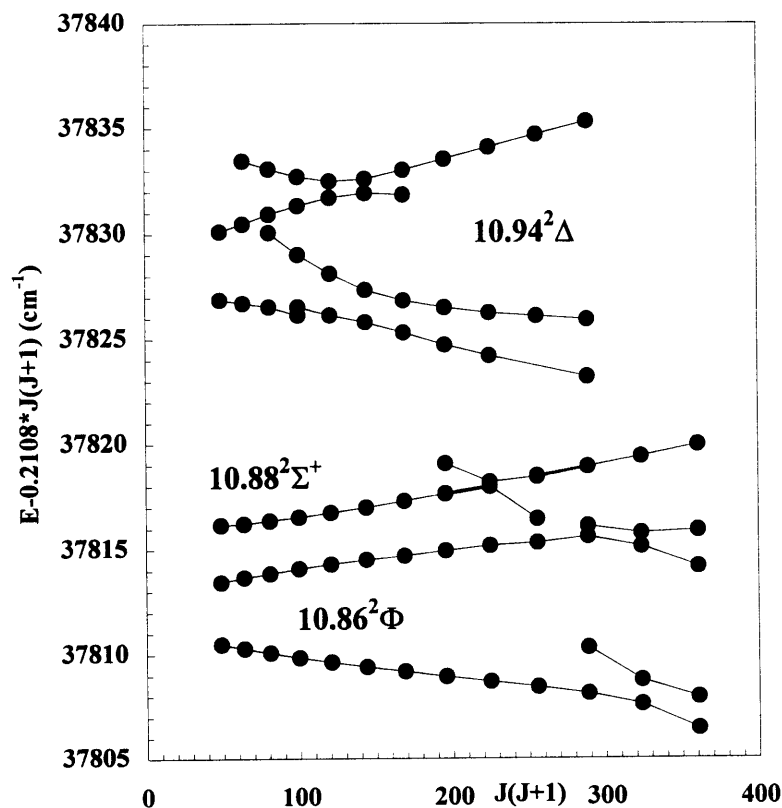


Figure 21: Reduced term value vs $J(J+1)$ plot for the e -levels of the $10.94^2\Delta$, $10.88^2\Sigma^+$, and $10.86^2\Phi$ states, illustrating core-penetrating~core-nonpenetrating perturbations.

The effective rotational constants for the low energy components of the nonpenetrating complexes are very small and do not change (significantly) with n^* . In effect, for increasing consecutive- n^* members of a core-penetrating Rydberg series, the crossings between core-penetrating and core-nonpenetrating terms occur at lower and lower J . Eventually, as n^* increases, multiple level crossings appear simultaneously at very low- J . The l -uncoupling interaction for the core-penetrating states increases and the “slopes” of the core-penetrating states become strongly n^* -dependent. Eventually, at $n^*\approx 14$, this picture of perturbations systematically moving to lower J -values breaks down.

7.3 Assignment of core-nonpenetrating perturbers.

Looking at the $10.86^2\Phi$ state in Figure 20, one may wonder whether there are additional systematic perturbations in that state at lower- N (or J) quantum number. A careful investigation of the reduced term value plot reveals no other systematic level shifts which would suggest such an additional perturbation. Having in mind that this observation is limited by the experimental precision, we can assume that the perturbation in the $10.86^2\Phi^+$ state observed near $N=17$ ($N(N+1)=306$) is caused by the extreme, lowest energy component of the nonpenetrating complexes. To verify such an hypothesis, we calculated the rotationless energies for the nonpenetrating states using the 2-point charge model and the prolate spheroidal coordinate system, as described in Section 4.6. The n^* 's of the $11g$ and $11h$ states are given in the table below.

	$^2\Sigma^+$	$^2\Pi$	$^2\Delta$	$^2\Phi$	$^2\Gamma$	2H
$11g$	11.0934	11.0738	11.0256	10.9589	10.8807	
$11h$	11.0487	11.0432	11.0273	11.0021	10.9690	10.9296

As we can see, *all* of the g and h core-nonpenetrating states are more compact and do not extend down to the $10.86^2\Phi$ state. We also know that the actual splittings between Λ components should be slightly smaller than those predicted in the model because the effective charges on the molecular core atomic-ions are smaller than +2 and larger than -

1, respectively for Ba^{+2} and F^- . Thus, we can rule out the possibility that any components of any nonpenetrating series lie below the ${}^2\Phi$ state.

We can get more information about the perturber of the ${}^2\Phi^+$ state by analyzing the effective rotational constant of each perturber. Assuming that the nonpenetrating perturber is described well by Hund's case (d), its rotational energy can be expressed as

$$T = B^+N^+(N^++1), \quad (7.19)$$

where $N^+=N-\mathcal{L}$ and $\mathcal{L}=-l, \dots, l$. After substitution for N^+ , the rotational energy expression takes the following form

$$T(N) = B^+(N-\mathcal{L})(N-\mathcal{L}+1) = B^+N(N+1) + B^+\mathcal{L}(\mathcal{L}-1) - 2B^+\mathcal{L}N. \quad (7.20)$$

We can now define the "slope" of the perturber (which is related to the effective rotational constant) as

$$\Delta T(N+1/2) = T(N+1) - T(N), \quad (7.21)$$

or

$$\Delta T(N+1/2) = 2B^+(N+1) - 2B^+\mathcal{L}. \quad (7.22)$$

From experimental data for the $10.86{}^2\Phi$ state, we can estimate, for the core-nonpenetrating perturber, $\Delta T(17.5) \approx 6.03 \text{ cm}^{-1}$. Now, with $B^+=0.234 \text{ cm}^{-1}$ we can calculate $\mathcal{L}_{\text{exp}}=5.12$, which indicates that the unknown perturber is the lowest term ($\mathcal{L}=5$) of the h -complex. Similarly, for the perturber of the $10.88{}^2\Sigma^+$ state at $N=14$, we find $\mathcal{L}_{\text{exp}}=4.36$. This value would suggest the $\mathcal{L}=4$ component of either the g - or h -complex as a perturber. The $\mathcal{L}=4$ component of the h -complex has however "-" Kronig symmetry, thus is ruled out as the unknown perturber of this "+" Kronig symmetry penetrating state. Note in Figure 20, that the perturber of the $10.88{}^2\Sigma^+$ state, in order to have the observed curvature, must undergo an avoided crossing with additional nonpenetrating term at N -values near those of the observed perturbation region. A similar analysis can be done for both "+" and "-" symmetry perturbers of the $10.94{}^2\Delta$ state at $N \approx 10-11$. These two perturbers overlap each other at low- N . From the $\Delta T(8.5) \approx 2.98 \text{ cm}^{-1}$ we calculate

$\mathcal{L}_{\text{exp}}=2.62$. The unknown perturbers could, thus, be the $\mathcal{L}=3$ component of the h -complex for the $10.94^2\Delta^+$ state and the $\mathcal{L}=3$ component of the g -complex for the $10.94^2\Delta^-$ state. However, Such an analysis is expected to be much less reliable for the internal components of nonpenetrating complexes.

For the $11.86^2\Phi$ state (as for $10.86^2\Phi$ state) we can observe a second (strong) perturbation at high- N in the $^2\Phi^-$ component. There is also some indication of a second perturbation in the $^2\Phi^+$ component, but the data set is inconclusive in this case.

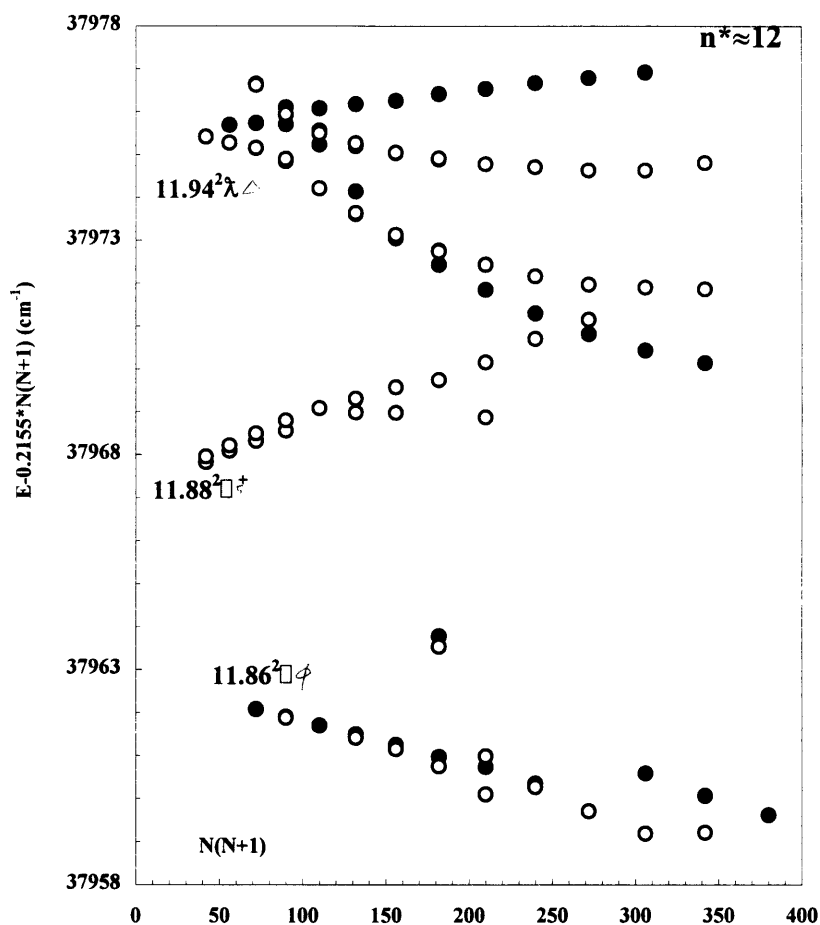


Figure 22: Reduced term value vs $N(N+1)$ plot for the $11.86^2\Phi$, $11.88^2\Sigma^+$, and $11.94^2\Delta$ states, showing multiple perturbations by core-nonpenetrating states. Solid (open) circles denote levels of $+(-)$ Kronig symmetry.

¹J. E. Murphy, *Laser Spectroscopic Studies of Rydberg States in Calcium Monofluoride.*, PhD thesis, Massachusetts Institute of Technology, Cambridge, MA, 1992.

²G. Herzberg and Ch. Jungen, *J. Mol. Spectrosc.*, **41**, 425-486 (1972).

8. Ionization detected spectra via the $C^2\Pi_{3/2}$ intermediate state.

For the states above $n^*\approx 14$, fluorescence to the ground state was so weak that the UV fluorescence detection scheme could no longer be applied. To obtain spectral information for higher- n^* Rydberg states, the ionization-detection technique had to be applied. We observed Rydberg states of the $v=1$ manifold in the range of n^* between 13.5 and 31. Until now, we have analyzed the $n^*\approx 14$, $n^*\approx 15$, and $n^*\approx 16$ supercomplexes; the remaining spectra up to $n^*\approx 32$ remains unanalyzed. Even brief inspection of the ionization-detected spectra makes it clear that, as for high- n^* complexes in the fluorescence detected spectra, members of the $0.76^2\Sigma^+$, $0.45^2\Pi$, and $0.08^2\Sigma^+$ series are missing. This observation suggests that the disappearance of those series from the high- n^* spectra is caused by small transition moments for the probe transition rather than some detection-related problem.

8.1 $v=1$ $0.86^2\Phi$, $0.94^2\Delta$ and $0.88^2\Sigma^+$ series.

The reduced term value plots for the three analyzed $0.86^2\Phi$ states are presented in Figure 23. One can see well developed perturbations in both “+” and “-” Kronig symmetry components. The strong perturbation in the $^2\Phi^+$ component was previously discussed in Section 7.2. In Figure 23 an additional weak perturbation is evident in the “+” symmetry component. This perturbation was not observed in the fluorescence detected spectra. The perturber is very well developed in the $v=1$ $14.86^2\Phi$ and $13.86^2\Phi$ states, but can be also identified in the $15.86^2\Phi$ state. Near the $v=1$ $13.86^2\Phi$ state we can observe the $v=2$ $9.94^2\Delta$ state, which is also perturbed by this new core-nonpenetrating term. With the $v=1$ $13.86^2\Phi$ and $v=2$ $9.94^2\Delta$ states acting as a “background”, we observe 5 extra lines from the core-nonpenetrating perturber. In a manner similar to that discussed in Section 7.2, we estimate $\mathcal{L}_{\text{exp}}=5.3$ for the new perturber. The perturber’s very large “slope” and its very weak interaction with the $^2\Phi$ states indicates that it might be the extreme, low energy component of the i -complex.

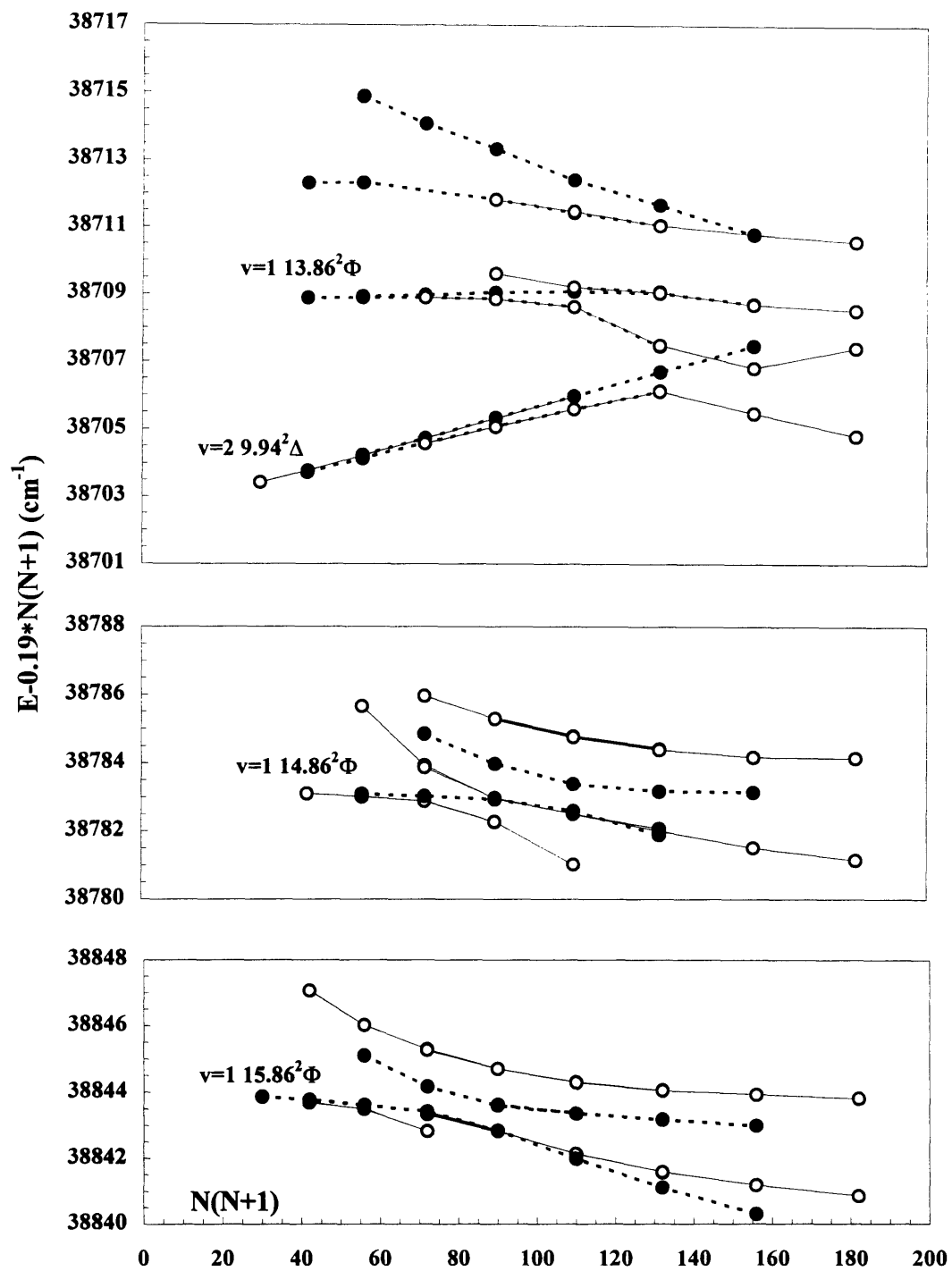


Figure 23: Perturbations between $v=1 \ 0.86^2 \Phi$ series and core-nonpenetrating states. Open (solid) circles are for +(-) Kronig symmetry states.

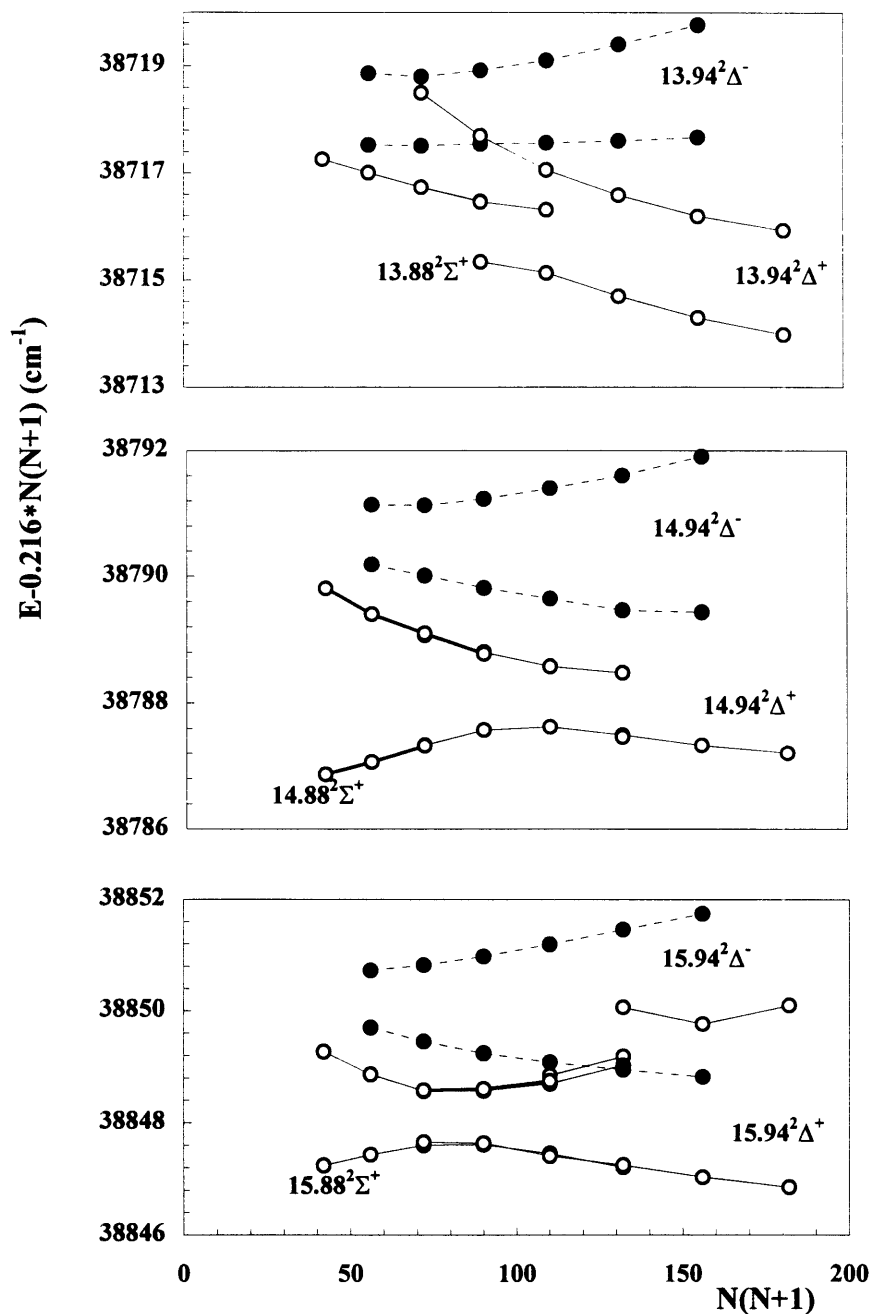


Figure 24: Reduced term value plot of the $v=1$ $0.88^2\Sigma^+$ and $0.94^2\Delta$ series. Solid(open) circles are for $-(+)$ Kronig symmetry states.

The $0.88^2\Sigma^+$ series and the “+” symmetry components of the $0.94^2\Delta$ series perturb each other strongly, as can be seen in the reduced term value plot (Figure 24). A similar interaction was observed in the fluorescence detected spectra ($v=0$ manifold) above

$n^* \approx 11$. Here, the avoided crossings are much better developed, especially for the $15.88^2\Sigma^+ \sim 15.94^2\Delta^+$ interaction.

The terms in Figure 24 are labeled as $^2\Delta^\pm$ or $^2\Sigma^+$, even if they are mixtures of $^2\Delta^\pm$ or $^2\Sigma^+$ and core-nonpenetrating states. Such a labeling system, however, permits us to correlate the observed terms with low- n^* case (a) or case(b) states. It also identifies the source of the transition intensity in mixed character states.

8.2 Autoionization rates.

The widths of most lines observed in the ionization-detected experiment are $\sim 0.07 \text{ cm}^{-1}$, which is comparable to the laser bandwidth. The rather poor S/N ratio makes it very difficult to detect any possible autoionization broadening. We mentioned previously that the series that are unobservable in the ionization-detected spectra are the same ones that disappeared at higher n^* 's in the fluorescence-detected spectra. Their absence is, thus, due to the small transition moment for the pump transition than to strong autoionization broadening. Upon careful examination of the ionization-detected spectra, we realized that the $13.88^2\Sigma^+$ state, which is observed in the fluorescence detected spectra ($v=0$) with intensity comparable to the nearby $13.94^2\Delta$ and $13.86^2\Phi$ states, is (essentially) missing from the spectrum. Only two extra lines were observed near the expected crossing of the $13.88^2\Sigma^+$ state with the $13.94^2\Delta^+$ state (see Figure 24). At higher- n^* , we observe fully developed avoided crossings: $14.88^2\Sigma^+ \sim 14.94^2\Delta^+$ and $15.88^2\Sigma^+ \sim 15.94^2\Delta^+$. The $0.88^2\Sigma^+$ states reveal autoionization broadening and linewidths that can actually be measured in the spectra.

In Figure 25 we present two autoionization broadened lines. The experimental data were fitted to a sum of the Lorentzian profiles. The actual shape of the autoionization + laser bandwidth-broadened line is correctly described by a Voigt profile. However, since the total widths of the lines are much larger than the laser bandwidths, autoionization broadening dominates here and using Lorentzian profiles in the fit does not introduce significant errors. The best fit linewidths (FWHM) are $\Gamma_P = 0.187(13) \text{ cm}^{-1}$ and $\Gamma_Q = 0.176(12) \text{ cm}^{-1}$, respectively for P(11.5) and $^PQ(11.5)$ lines, where uncertainties are

2 standard deviations. The widths of the P(11.5) and ^PQ(11.5) lines are equal within the experimental precision, thus in further analysis we can use the single value $\Gamma=0.18(2) \text{ cm}^{-1}$. The autoionization width is related to the autoionization lifetime as

$$\Gamma(\text{cm}^{-1}) = 5.3 \cdot 10^{-12} / \tau(\text{s}). \quad (8.1)$$

Thus, we estimate the autoionization lifetime of the $v=1 \text{ } 15.88^2 \Sigma^+$ state as $\tau=29(3) \cdot 10^{-12}$ -s.

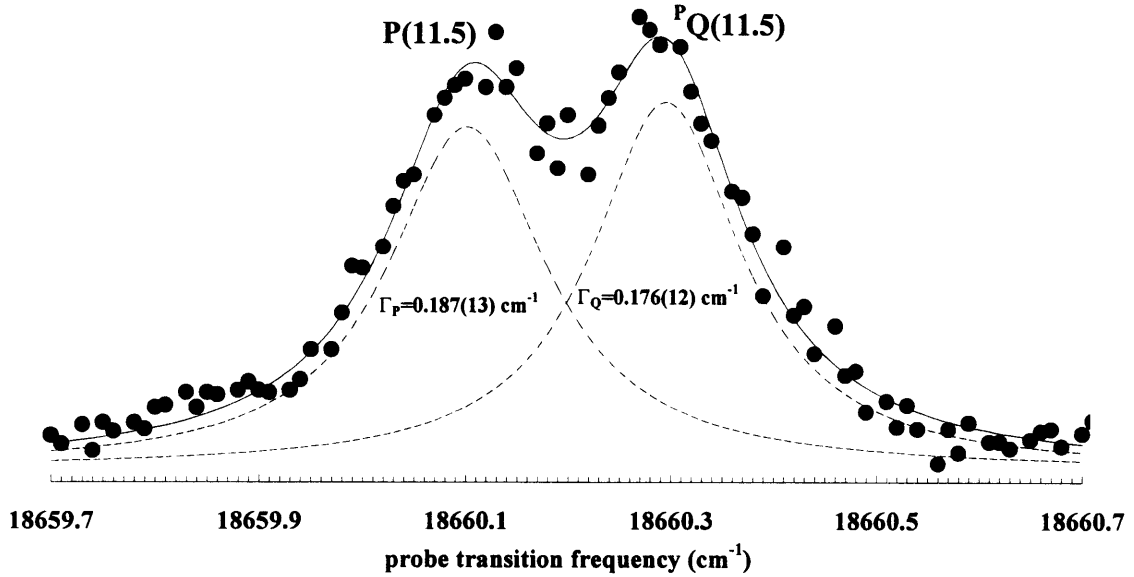


Figure 25: Autoionization broadened P(11.5) and ^PQ(11.5) $v=1 \text{ } 15.88^2 \Sigma^+ - v=0 \text{ } C^2 \Pi_{3/2}$ lines. Solid circles denote experimental points. Solid line shows the best fit of the experimental data to Lorentzian lineshapes. Broken lines show individual Lorentzian profiles of P and ^PQ lines.

In Section 6.2.1 we obtained an expression for the intrachannel perturbation interaction matrix element. Autoionization can also be considered as the intrachannel interaction of a v -th bound vibrational level with the continuum of the $v-1$ manifold. Using Eq. 6.5 and the Golden Rule, we can obtain an expression for the linewidths of autoionizing states^{3,2}

$$\Gamma = 2\pi \frac{2\Re}{(n^*)^3} \left(\frac{d\mu}{dR} \right)^2 \cdot \frac{16.8576}{m\omega_e^+} \cdot (v+1), \quad (8.2)$$

where $(v+1)$ is autoionized into the v -continuum. Using the fitted linewidth of the $v=1$ $15.88^2\Sigma^+$ state, $\Gamma=0.18(2)$ cm^{-1} , and the above expression, we can calculate the quantum defect derivative with respect to internuclear distance, $d\mu/dR = 0.53(3)$ \AA^{-1} . This value is in excellent agreement with the derivatives calculated for the $0.88^2\Sigma^+$ series from the harmonic oscillator model (see Table 17), 0.526 \AA^{-1} and 0.596 \AA^{-1} . It, however, disagrees with the value obtained from the intrachannel perturbation, $v=1$ $6.88^2\Sigma^+ \sim v=0$ $7.88^2\Sigma^+$, $0.23(1)$ \AA^{-1} . This disagreement is very puzzling. The likely explanation is that the $0.88^2\Sigma^+$ series mixes, as n^* increases, with some other Rydberg series with a larger value of the quantum defect derivative, and this broadens $0.88^2\Sigma^+$ states above the first ionization limit. Another possibility would be that the value of the quantum defect derivatives obtained from analysis of the intrachannel perturbation is too small by a factor of 2.5. Such a scenario could be possible if there were another $^2\Sigma^+$ state close to the $v=1$ $6.88^2\Sigma^+$ and $v=0$ $7.88^2\Sigma^+$ states which interacts with them, thus decreasing the energy shift of the $v=0$ $7.88^2\Sigma^+$. Such a state, $v=2$ $6.24^2\Sigma^+$, has been actually predicted to be located ~ 15 cm^{-1} higher in energy than $v=0$ $7.88^2\Sigma^+$. This state was, however, not observed.

The other estimation of the quantum defect derivative from an intrachannel perturbation of the $7.94^2\Delta$ state, $d\mu/dR < 0.08$ \AA^{-1} , seems to be supported by the observed linewidths of the above-ionization-threshold members of the $v=1$ $0.94^2\Delta$ series, in particular the $15.94^2\Delta$ state. The $15.94^2\Delta$ state undergoes a perturbation with the $15.88^2\Sigma^+$ state (see Figure 24, bottom panel). Far from the perturbation region, the $15.94^2\Delta$ state linewidth is smaller than 0.07 cm^{-1} , while in the center of the perturbation, the linewidths of both interacting states are ~ 0.14 cm^{-1} (see Figure 26). When we discussed the linewidths of the $15.88^2\Sigma^+$ state above, no correction was applied to the measured linewidths because the autoionization was by far the dominant line broadening process. In the case of the $15.94^2\Delta$ state, however, with the measured linewidth ~ 0.07 cm^{-1} , the laser bandwidth is the main factor determining the observed linewidths, and autoionization broadening is a smaller contribution. The S/N ratio in this experiment is not good enough to perform a complete deconvolution of line profiles. One can, however, estimate that

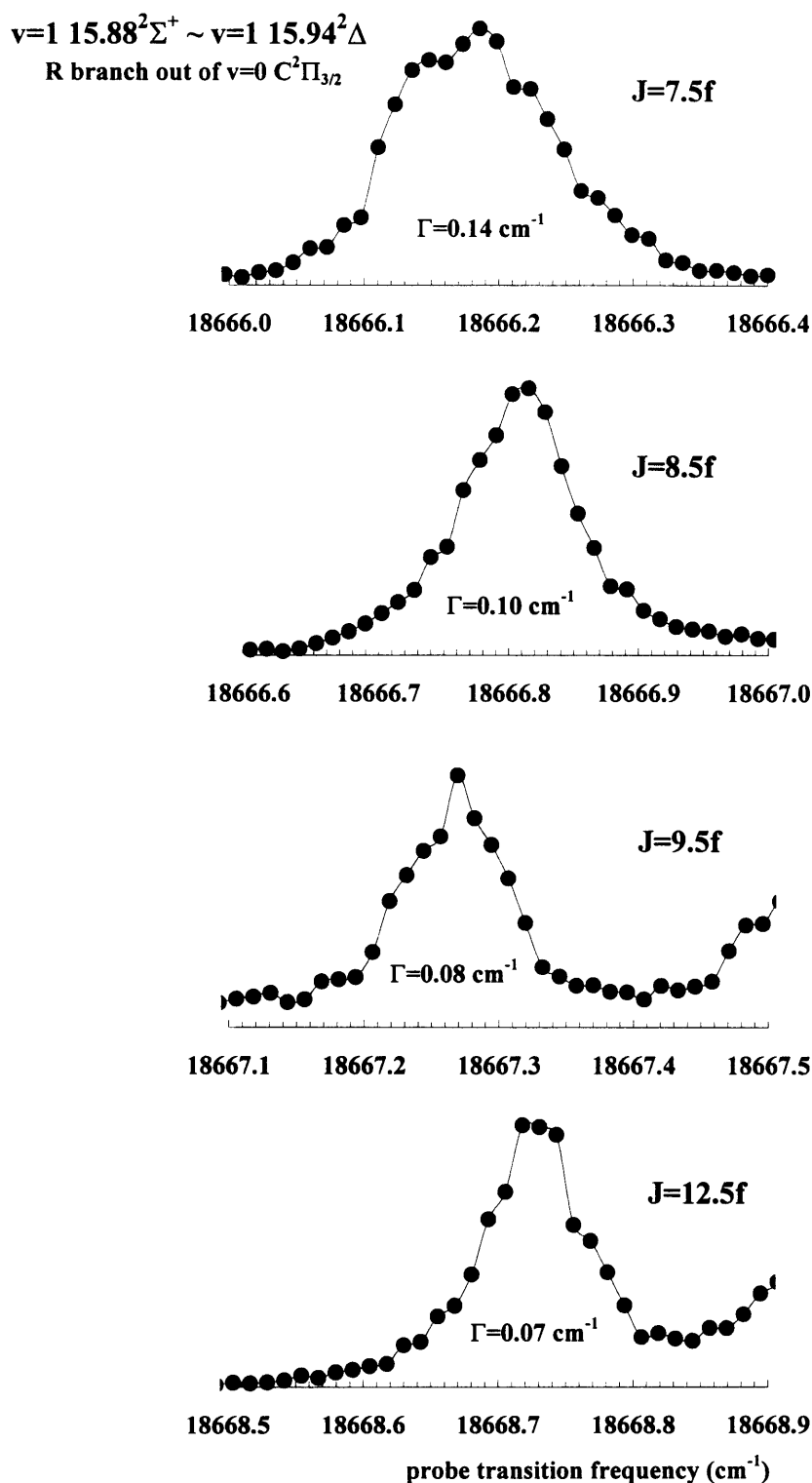


Figure 26: Evolution of the linewidth of the “+” Kronig symmetry branch in the region of the $\nu=1\ 15.88^2\Sigma^+ \sim \nu=1\ 15.94^2\Delta^+$ perturbation. (compare to Figure 24, bottom panel, lowest term)

with the total linewidth of $0.06(1) \text{ cm}^{-1}$ and the laser bandwidth of $0.05(1) \text{ cm}^{-1}$, the autoionization broadening is $0.03(3) \text{ cm}^{-1}$. This observation is in agreement with the value of the quantum defect derivative, $<0.08 \text{ \AA}^{-1}$, obtained from intrachannel perturbation.

9. Appendix A.

9.1 Rotational term values for the $v=0$ $B^2\Sigma^+$ state.

J	T(e)	T(f)	J	T(e)	T(f)
0.5	14040.163	14040.840	31.5	14241.450	14263.105
1.5	14040.446	14041.801	32.5	14254.554	14276.885
2.5	14041.144	14043.175	33.5	14268.070	14291.076
3.5	14042.255	14044.964	34.5	14281.998	14305.679
4.5	14043.782	14047.168	35.5	14296.337	14320.694
5.5	14045.722	14049.786	36.5	14311.088	14336.120
6.5	14048.077	14052.818	37.5	14326.250	14351.957
7.5	14050.847	14056.265	38.5	14341.823	14368.205
8.5	14054.030	14060.125	39.5	14357.807	14384.863
9.5	14057.628	14064.401	40.5	14374.201	14401.932
10.5	14061.640	14069.090	41.5	14391.007	14419.412
11.5	14066.066	14074.193	42.5	14408.222	14437.302
12.5	14070.907	14079.710	43.5	14425.847	14455.601
13.5	14076.161	14085.642	44.5	14443.883	14474.311
14.5	14081.830	14091.987	45.5	14462.328	14493.430
15.5	14087.912	14098.747	46.5	14481.183	14512.958
16.5	14094.408	14105.920	47.5	14500.446	14532.895
17.5	14101.318	14113.506	48.5	14520.119	14553.241
18.5	14108.642	14121.507	49.5	14540.201	14573.996
19.5	14116.379	14129.921	50.5	14560.691	14595.160
20.5	14124.530	14138.748	51.5	14581.589	14616.731
21.5	14133.094	14147.989	52.5	14602.896	14638.710
22.5	14142.072	14157.643	53.5	14624.610	14661.097
23.5	14151.463	14167.710	54.5	14646.732	14683.892
24.5	14161.266	14178.190	55.5	14669.262	14707.093
25.5	14171.483	14189.083	56.5	14692.198	14730.701
26.5	14182.113	14200.389	57.5	14715.541	14754.716
27.5	14193.155	14212.107	58.5	14739.291	14779.138
28.5	14204.610	14224.238	59.5	14763.447	14803.965
29.5	14216.478	14236.782	60.5	14788.009	14829.198
30.5	14228.758	14249.738	61.5	14812.976	14854.837

9.2 Rotational term values for the $v=0$ $C^2\Pi_{3/2}$ state.

J	T(e)	T(f)	J	T(e)	T(f)
1.5	20185.478	20185.478	21.5	20288.459	20288.458
2.5	20186.552	20186.552	22.5	20298.109	20298.107
3.5	20188.054	20188.054	23.5	20308.187	20308.185
4.5	20189.986	20189.986	24.5	20318.693	20318.691
5.5	20192.347	20192.347	25.5	20329.627	20329.625
6.5	20195.137	20195.137	26.5	20340.988	20340.986
7.5	20198.356	20198.356	27.5	20352.777	20352.775
8.5	20202.004	20202.004	28.5	20364.994	20364.992
9.5	20206.081	20206.081	29.5	20377.638	20377.636
10.5	20210.588	20210.588	30.5	20390.710	20390.707
11.5	20215.523	20215.523	31.5	20404.208	20404.205
12.5	20220.888	20220.888	32.5	20418.133	20418.130
13.5	20226.681	20226.681	33.5	20432.486	20432.482
14.5	20232.903	20232.903	34.5	20447.264	20447.260
15.5	20239.554	20239.554	35.5	20462.470	20462.465
16.5	20246.633	20246.633	36.5	20478.101	20478.096
17.5	20254.142	20254.142	37.5	20494.159	20494.154
18.5	20262.078	20262.078	38.5	20510.643	20510.637
19.5	20270.443	20270.443	39.5	20527.553	20527.547
20.5	20279.237	20279.236	40.5	20544.888	20544.882

10. Appendix B. Listing of Computer Programs.

10.1 Subroutine LEVEL used with LSQ fitter.

The Subroutine Level written in FORTRAN 77 is part of the least-squares fitter (LSQ). It has been rewritten in order to utilize the Hellmann-Feynman theorem to calculate energy derivatives with respect to fitted parameters. It can only be used for pseudo-linear problems (see Section 5.1).

```
*****
*                               SUBROUTINE LEVEL                               *
*****
      SUBROUTINE LEVEL (IE, NDATA, IAMAX)
      PARAMETER (NNPAR=40, NNDATA=300, NNHSIZE=56, NNBLOCK=2, NNJMAX=20)
      PARAMETER (NNVEC=2)
      IMPLICIT REAL*8 (A-H, O-Z)
      REAL*4 SNGL
      INTEGER NUMVEC, PRMTRS, IAMAX

C-----
C   (Zygmunt J. Jakubek, May 1994)
C   This subroutine was rewritten
C   to make use of Hellmann-Feynman theorem.
C-----
C EACH EIGENVECTOR IS MADE UP OF A LINEAR COMBINATION OF BASIS VECTORS.
C THE (COEFFICIENT)**2 FOR EACH BASIS VECTOR IS EQUAL TO THE PERCENTAGE
C OF THAT BASIS VECTOR IN THE EIGENVECTOR. NUMVEC IS THE NUMBER OF
C BASIS VECTORS FOR WHICH YOU WANT THAT PERCENTAGE REPORTED. IT IS SET
C AT THE TOP OF THIS PROGRAM AND NOT CHANGED WITHIN THE BODY AS LONG.
C AS IT IS SMALLER THAN THE DIMENSION OF THE HAMILTONIAN
C NOTE ALSO THAT NUMVEC MUST BE <= THE DIMENSIONS OF EACH
C INDEX OF UF ()

      INTEGER UP, UI, UF, SRCH, I, K, KK, B
      DIMENSION GE (NNDATA), NQ (12), NUM (12, NNDATA), NCVAR (NNPAR),
1 GE2 (NNDATA, NNPAR), SLOPES (NNJMAX, NNHSIZE, NNPAR, NNBLOCK), P01 (NNPAR)
      DIMENSION H (NNHSIZE, NNHSIZE), U (NNHSIZE, NNHSIZE), D (NNHSIZE),
1 TERM (NNJMAX, NNHSIZE, NNBLOCK), SLOP (NNHSIZE, NNPAR)
      DIMENSION UI (NNHSIZE), SRCH (NNHSIZE), UF (NNVEC, 2),
1 UP (NNBLOCK, NNJMAX, NNHSIZE, NNVEC, 2)
      DIMENSION P (NNPAR), MAXP (NNBLOCK),
1 EIGVEC (NNBLOCK, 0:100, NNHSIZE, NNHSIZE)
      COMMON/BLK1/ P, GE, NUM
      COMMON/BLK2/ TERM, MAXP, IBK, JMIN, JMAX, PAR
      COMMON/BLK3/ UP
      COMMON/BLK5/ GE2, SLOPES, NCVAR

C MAXP (I) IS DIMENSION OF ITH BLOCK OF HAMILTONIAN.
C TERM (J, rank, IP) ARE TERM ENERGIES. 2ST DIM AGREES WITH MAXP (I),
```

```

C 2ND DIM IS JMAX, 3RD DIM CORRESPONDS TO NUMBER OF BLOCKS (IBK).
C ON LAST PASS, LEVEL IS CALLED ONLY WITH IE=1.NUMVEC = NNVEC
C SEE COMMENTS ABOUT NUMVEC ABOVE
C PRMTRS=2*IAMAX+2!!total # of passes thru LEVEL (B compared to this
C following label 10). IAMAX = # of parameters being fit.
C B=B+1 !! counts # of passes thru LEVEL
C
      M1=JMAX+1

C ----- J loop -----
      DO 10 I=1,M1
      if((i-1).lt.JMIN) goto 10
      X=DBLE(I-1)+PAR
C REMEMBER PAR ADDS IN THE .5 FOR HALF INTEGER J

C ----- block # loop -----
      DO 20 IP=1,IBK
      CALL MATRIX(IP,P,H,X,MAXP) !! compute block #IP
      DO 21 K=1,NNHSIZE
      DO 22 L=1,NNHSIZE
22      U(K,L)=0.D0
21      U(K,K)=1.D0

      M2=MAXP(IP)

      CALL JMEDIAG(H,U,D,M2) !! diagonalize block #IP - return
C eigenvalues (D) and eigenfunctions (U)
C-----
c in the lines below up to 110 slopes are calculated using
C Hellmann-Feynman theorem
      if (ie.eq.1) then
      DO 100 L=1,NNPAR
100     P01(L)=0.0d0
      DO 110 L=1,IAMAX
      NUMB1=NCVAR(L)
      P01(NUMB1)=1.0D0
      CALL MATRIX(IP,P01,H,X,MAXP) !! CALCULATE dh/dP
      DO 120 K=1,M2
      UHU=0.0D0
      DO 130 K1=1,M2
      HUSUM=0.0D0
      DO 140 K2=1,M2
140     HUSUM=HUSUM+H(K1,K2)*U(K2,K)
130     UHU=UHU+U(K1,K)*HUSUM
120     SLOP(K,L)=UHU
110     P01(NUMB1)=0.0D0
      endif

C -----
C SORTING EIGENVALUES, EIGENVECTORS, AND SLOPES
C ESSENTIALLY SUBROUTINE EIGSRT FROM NUMERICAL RECIPES
      DO 1021 II=2,M2
      K1=II-1
      K=K1

```

```

      EL=D(K1)
      DO 1040 K2=II,M2
      IF(D(K2).LE.EL) GO TO 1040
      K=K2
      EL=D(K2)
1040 CONTINUE
      IF(K.EQ.K1) GO TO 1021
      D(K)=D(K1)
      D(K1)=EL
      DO 1010 K2=1,M2
      EL=U(K2,K1)
      U(K2,K1)=U(K2,K)
      U(K2,K)=EL
1010 CONTINUE
      if(ie.eq.1)then
      DO 1020 K2=1,IAMAX
      EL=SLOP(K1,K2)
      SLOP(K1,K2)=SLOP(K,K2)
      SLOP(K,K2)=EL
1020 CONTINUE
      endif
1021 continue

C-----
      DO 23 L=1,M2  !! eigenfunction loop
*      IF (B.NE.PRMTRS) GO TO 26 !! if not on last pass, do not
C          load EIGVEC
      DO 24 K=1,M2  !! basis function loop
*      EIGVEC(IP,X+PAR,K,L)=U(K,L) !!place coefficients in array EIGVEC
*C          (see comments at label 35 for
*C          index meanings)
24      UI(K)=IFIX(100.*SNGL(U(K,L)**2))
      IF (MAXP(IP).LT.NUMVEC) NUMVEC=MAXP(IP)
      CALL MAXSORT(M2,UI,SRCH,NUMVEC,UF)
      DO 25 K=1,NNVEC
      DO 25 KK=1,2
25      UP(IP,I,L,K,KK)=UF(K,KK)
      if(ie.eq.1) then
26      DO 27 K=1,IAMAX
27      SLOPES(I,L,K,IP)=SLOP(L,K)
      endif
23      TERM(I,L,IP)=D(L)
20      CONTINUE  !! to next block
10      CONTINUE  !! to next J

*****
*      IF (B.EQ.PRMTRS) THEN
*      WRITE(10,35)
*35      FORMAT(5X,'EIGENVECTORS FROM LSQ (LEAST SQUARES FITTER
* 1          )',/, 'STORAGE PATTERN: IP=BLOCK #, I=ROT. QUANTUM #',
* 1          /, 'L=EIGENVECTOR # (WITHIN BLOCK IP), K=BASIS',
* 1          /, 'VECTOR # (IN EIGENVECTOR L).',/,
* 1          'DATA MUST BE READ FROM THIS FILE AS IT HAS BEEN',
* 1          /, 'WRITTEN - SEE LEVEL.LIS, LINES *****.',/)

```

```

*      DO 60 IP=1,IBK
*      WRITE(10,90) 'BLOCK #',IP
*90    FORMAT(//,12X,A7,I2,/)
*      DO 65 I=jmin,(M1-1)
*      X=DFLOAT(I-1)+PAR
*      DO 80 L=1,MAXP(IP)
*      WRITE(10,70) X,(EIGVEC(IP,I-1,K,L),K=1,MINO(5,MAXP(IP)))
*      IF (MAXP(IP) .GE. 6) THEN
*      WRITE(10,70) X,(EIGVEC(IP,I-1,K,L),K=6,MAXP(IP))
*      ENDIF
*70    FORMAT(1X,F4.1,6(5X,F6.2))
*85    CONTINUE
*80    CONTINUE
*65    CONTINUE
*60    CONTINUE
*      ENDIF

C SET UP TERM VALUES AND DIFFERENCES TO COMPARE WITH INPUT DATA.
      DO 50 N=1,NDATA
      DO 40 L=1,6
40     NQ(L)=NUM(L,N)
C SECOND STATE TERM VALUE SUBTRACTED FROM FIRST.
      IF(NQ(2).EQ.0) THEN
      TOP=0.0D0
      ELSE
      TOP=TERM(NQ(1)+1,NQ(2),NQ(3))
      if(ie.eq.1)then
      DO 45 L=1,IAMAX
45     GE2(N,L)=SLOPES(NQ(1)+1,NQ(2),L,NQ(3))
      endif
      ENDIF
      IF(NQ(5).EQ.0) THEN
      BOT=0.0D0
      ELSE
      BOT=TERM(NQ(4)+1,NQ(5),NQ(6))
      if(ie.eq.1)then
      DO 47 L=1,IAMAX
47     GE2(N,L)=GE2(N,L)-SLOPES(NQ(4)+1,NQ(5),L,NQ(6))
      endif
      ENDIF
50     GE(N)=TOP-BOT
      RETURN
      END

```

10.2 TOCENTER program for solution of one-electron two-center problem.

```
*****
*   program written by Zygmunt J. Jakubek, November 1994           *
*   tocent calculates one-electron two-center problem: energies,  *
*   generalized angular momentum (A) and orbitals                 *
*   for the method description see:                                *
*       G. Hadinger, M. Aubert-Frecon, and G. Hadinger,          *
*       J. Phys. B: At. Mol. Opt. Phys. 22, 697-712 (1989)      *
*       and references herein                                     *
*                                                                 *
*****

      program tocent

      parameter(maxk=60)
      implicit real*8 (a-h,o-z)
      integer*2 h0,m0,s0,hs0
      dimension F(-1:maxk),DFA(-1:maxk),DFp(-1:maxk),
*             G(-1:maxk),DGA(-1:maxk),DGp(-1:maxk),
*             al(0:maxk),C(0:maxk)
      common /time/ h0,m0,s0,hs0

*   input: ZAIN, ZBIN, ENSTAR, XIP, RABIN (a.u.), l, m,
      print *, 'input ion charges ZA,ZB in [a.u.]'
      read *, ZAIN,ZBIN

      print *, 'input ionization potential in [cm-1]'
      read *, XIP

      print *, 'input initial nstar, l, and lambda'
      read *, ENSTIN,l,m
      print *, 'input final nstar, l, and lambda'
      read *, ENSTFI, lfin, mfin
      print *, 'input internuclear distance in [a.u.]'
      read *, RABIN

      open(10,file='tocenter.out',status='unknown')
      open(11,file='toexcel.dat',status='unknown')

      Ry           = 109737.3177d0 ! Rydberg(infinity) in [cm-1]
      epsdelA      = 1.0d-1       ! accuracy of correction to A [a.u.]
      epsdelp      = 1.0d-4       ! accuracy of correction to p [a.u.]

      epsA         = 1.0d-11      ! accuracy of A [a.u.]
      epsp         = 1.0d-11      ! accuracy of p [a.u.]

      Kstart       = 4            ! iteration starts from K=m+Kstart

      call gettim(h0,m0,s0,hs0)
```

```

do 992 lll=1,lfin
xl = dble(lll)

do 991 mmm=lll,mfin,-1
xm      = dble(mmm)
enstar = xl + 0.5d0

101 do 1 i= -1,maxk
    F(i)  = 0.0d0
    DFA(i) = 0.0d0
    DFp(i) = 0.0d0
    G(i)  = 0.0d0
    DGA(i) = 0.0d0
    DGp(i) = 0.0d0
1    continue
    do 2 i=0,maxk
    al(i) = 0.0d0
    C(i)  = 0.0d0
2    continue

*****
* - calculating initial values for p and A
*****

    pinit = 0.5d0*(ZAin+ZBin)*RABin/enstar

    pm      = -1.0d0
    Ainit   = 0.0d0
    xlx     = xl
    hrobo   = (RABin*(ZAin-ZBin)/2.0d0/pinit)
    do 10 i=1,2
    hlm     = (xlx*xlx-xm*xm)*(hrobo*hrobo-xlx*xlx)/
*           (4.0d0*xlx*xlx-1.0d0)
    if(xl.ne.0.0d0) Ainit = Ainit+pm*hlm/xlx
    xlx=xlx+1.0d0
    pm=-pm
10    continue
    Ainit=2.0d0*pinit*pinit*(Ainit+0.5d0) - xlx*(xlx+1.0d0)

*****
* - starting iterations
*****
* no screening!

    ZA = ZAin
    ZB = ZBin
    RAB = RABin
    R1 = RAB*(ZA-ZB)
    R2 = RAB*(ZA+ZB)

    p = pinit
    A = Ainit
    q = p

```



```

dAold = 0.0d0
dpold = 0.0d0
lastiter = 0
kmax = m + Kstart

30 continue !start of delA iteration until delA changes by < epsdelA

F(kmax) = 1.0d0
F(kmax+1) = 0.0d0
G(kmax) = 1.0d0
G(kmax+1) = 0.0d0
DFA(kmax) = 0.0d0
DFA(kmax+1) = 0.0d0
DFp(kmax) = 0.0d0
DFp(kmax+1) = 0.0d0

do 40 k=kmax,0,-1

xk = dble(k) ! xk = k
xlx = xm + 1.0d0 + xk ! xlx = m+k+1
alfa0 = (xlx-xm)*(xlx+xm)*(R1-2.0d0*q*xlx)*(R1+2.0d0*q*xlx)/
* (4.0d0*xlx*xlx-1.0d0)
alfa1 = A - q*q + (xlx-1.0d0)*xlx
alfa3 = 8.0d0*q*xlx*xlx*(xlx*xlx-xm*xm)/(4.0d0*xlx*xlx-1.0d0)
xk1 = xk+1.0d0 ! xk1 = k+1
gama0 = xk1*(xk1+xm)*(xk1-R2*0.5d0/p)*(xk1+xm-R2*0.5d0/p)
gama1 = A-p*p+R2-(xm+1.0d0)*(p+p+1.0d0-R2*0.5d0/p)-
* 2.0d0*xk*(xk+xm+p+p+1.0d0-R2*0.5d0/p)
gama2 = p+p+(2.0d0*xk+xm+1.0d0)*(2.0d0+R2*0.5d0/p/p)
gama3 = xk1*(xk1+xm)*R2*0.5d0/p/p*(R2/p-2.0d0*xk1-xm)

F(k-1) = -alfa1*F(k) - alfa0*F(k+1)
DFA(k-1) = -alfa1*DFA(k) - alfa0*DFA(k+1) - F(k)
DFp(k-1) = -alfa1*DFp(k) - alfa0*DFp(k+1) +
* (p+p)*F(k) + alfa3*F(k+1)
G(k-1) = -gama1*G(k) - gama0*G(k+1)
DGA(k-1) = -gama1*DGA(k) - gama0*DGA(k+1) - G(k)
DGp(k-1) = -gama1*DGp(k) - gama0*DGp(k+1) +
* gama2*G(k) + gama3*G(k+1)
40 continue

if(lastiter.eq.1) goto 50

del1 = DFA(-1)*DGp(-1) - DGA(-1)*DFp(-1)
delA = (G(-1)*DFp(-1) - F(-1)*DGp(-1))/del1
delp = (F(-1)*DGA(-1) - G(-1)*DFA(-1))/del1

if(abs(delp).lt.(0.01d0*epsp)) delp=0.01d0*epsp
ddelp = abs((dpold-delp)/delp)

if(ddelp.lt.epsdelp) then
if((abs(delA).lt.epsa).and.(abs(delp).lt.epsp)) lastiter=1

```

```

A = A + delA
p = p + delp
q = p
dAold = 0.0d0
dpold = 0.0d0
if(lastiter.ne.1) kmax = m+Kstart ! starting with K=m+Kstart
goto 30
else
dAold = delA
dpold = delp
kmax = kmax + 1
if(kmax.gt.45) then
enstar=enstar+0.001d0
goto 101
endif
goto 30
endif
*****

50  continue

roboal = 1.0d0
roboC  = 1.0d0
al(0)  = F(0)
C(0)   = G(0)

do 60 k=1,kmax
xmk    = dble(m+k)
roboal = roboal*dble(k) * (R1-2.0d0*q*xmk) / (2.0d0*xmk-1.0d0)
roboC  = roboC*dble(k) * (xmk-R2*0.5d0/p)
C(k)   = G(k)*roboC
60  al(k) = F(k)*roboal

call exptime(1,1,1,1)
pause

*****
* calculating wavefunctions
*****

*****
* printing results
*****
energy = XIP - 4.0d0*Ry*p*p/RAB/RAB
xxstar = (ZA+ZB)*RAB/2.0d0/p

write(10,*)
write(10,1001) l1l,mmm
1001 format(1x,'l=',i3,5x,'m=',i3)
print *, 'K=',kmax, ' A=',A, ' p= ',p
write(10,1000) kmax,A,p
1000 format(1x,'K=',i3,5x,'A=',f13.6,4x,'p =',f13.9)
print *, ' ', 'T=',energy, ' n*=',xxstar
write(10,1100) energy,xxstar

```

```

1100 format(1x,10x,'T=',f10.3,7x,'n*=',f16.12)
      write(10,*)
      do 70 k=0,kmax
      write(10,1200) k,al(k)/al(0), C(k)/C(0)
70   write( *,1200) k,al(k)/al(0), C(k)/C(0)
1200 format(1x,i4,2f20.10)
      write(10,*)

      write(11,2000) lll,mmm,A,p
2000 format(1x,i5,4x,i5,4x,f15.8,4x,f15.11)

      enstar = enstar + 0.9d0
103  if(enstar.lt.(enstfi)) goto 101

991  continue
992  continue

      close(10)
      close(11)
      call winexit
      end

      subroutine exptime(h,m,s,hs)
      integer*2 h,m,s,hs,h0,m0,s0,hs0
      common /time/ h0,m0,s0,hs0
      call gettim(h,m,s,hs)
      if (hs.lt.hs0) then
      hs=hs+100
      s=s-1
      endif
      hs=hs-hs0
      if (s.lt.s0) then
      s=s+60
      m=m-1
      endif
      s=s-s0
      if (m.lt.m0) then
      m=m+60
      h=h-1
      endif
      m=m-m0
      if (h.lt.h0) h=h+24
      h=h-h0
      print *, 'time expired from the start of the program'
      print 1000, h,m,s,hs
1000 format(1x,i2.2,':',i2.2,':',i2.2, '.',i2.2)
      return
      end

```

10.3 Program BAFSPEC for electronic energies of core-nonpenetrating states.

Program BAFSPEC is written in FORTRAN. It is used to calculate electronic energies of core-nonpenetrating states in spherical coordinate system with origin in the center-of-mass. Multipole moments can be calculated from the 2-point charge model or supplied by user. The program requires molecule specific data. The current version is set up for the BaF molecule.

```
*****
* program calculates electronic energies of core-nonpenetrating states*
* in spherical coordinate system.                                     *
* multipole moments can be calculated from 2-point charge model or  *
* supplied by user                                                 *
* this version is for the BaF molecule                             *
* for other molecules needs molecule-specific data                 *
*                                                                    *
*                               written by Zygmunt J. Jakubek in January 1993 *
*****
```

```
program bafspec
```

```
real*8 rnl,rnl1,rnl2,rnlrob,r,dr,rmax,z,ylm,hnlm,hnlms,hpart
real*8 dn1,dn2,dl1,dl2,dm1,dm2,qdef1,qdef2,xr,pi,ryd,IP
real*8 radhyp,d9j,sj,tj,gam,hyper11,qmltp
real*8 qml(0:12),radint(0:12)
```

```
pi = 3.141592653589793d0
ryd = 109737.3156841d0
print *, 'IP='
read *, IP
print *, 'n1='
read *, n1
print *, 'l1='
read *, l1
print *, 'quantum defect 1 '
read *, qdef1
print *, 'n2='
read *, n2
print *, 'l2='
read *, l2
print *, 'quantum defect 2 '
read *, qdef2
z=1.0d0
print *, 'rmax(a.u.)='
read *, rmax
print *, 'dr(a.u.)='
read *, dr
open(9,file='radorb.dat')
```

```

open(8, file='bafsp.out')
dn1=dbl(e(n1)-qdef1
dn2=dbl(e(n2)-qdef2
dl1=dbl(e(l1)-qdef1
dl2=dbl(e(l2)-qdef2

l0max=l1+l2
l0min=abs(l1-l2)

do 99 l0=0,12
qml(10)=qmltp(10)
write(8,1099)l0,qml(10)
99 continue
1099 format(1x,i4,f15.4)
write(8,1099)
write(8,1099)

*****
*
* calculate radial integral <n1,l1|r**(-l0+1)|n2,l2>
*
*****

r=0.d0
do 14 l0=0,12
radint(10)=0.0d0
14 continue

10 while (r.le.rmax) do
r=r+dr
rnl1=radhyp(dn1,dl1,z,r)
rnl2=radhyp(dn2,dl2,z,r)
rnlrob=rnl1*rnl2

do 15 l0=l0min,l0max,2
rnl=rnlrob

do 11 i=1,l0+1
rnl=rnl/r
11 continue

radint(10)=radint(10)+rnl
15 continue
end while

do 16 l0=l0min,l0max,2
radint(10)=radint(10)*dr
16 continue

do 250 m1=0,min(l1,l2)
dm1=dbl(e(m1)
dm2=dbl(e(m2)
hnlm=0.0d0
hnlms=0.0d0

```

```

do 200 l0=l0min,l0max,2

*****
*
* calculating angular integral <l1,m1|Yl0m0|l2m2>
*
*****
      x11=real(l1)
      x12=real(l2)
      x10=real(l0)
      xm1=real(m1)
      ylm=-dble(2*(m1-2*int(m1/2))-1)*
*       sqrt((dble(2*l1+1)*(2*l2+1)))*
*       tj(x11,x10,x12,0.0,0.0,0.0)*
*       tj(x11,x10,x12,-xm1,0.0,xm1)

*****
*
* calculating matrix element <n1,l1,m1|Hl0m0|n2,l2,m2>
*
*****
      hpart=2.0d0*ryd*qml(l0)*ylm*radint(l0)
      hnlm=hnlm+hpart
      if (l0.ne.0)hnlms=hnlms+hpart
      write(8,2000) n1,l1,m1,l0,n2,l2,m1,hpart

2000 format(1x,'<',i2,',',i2,',',i2,'| H ',i2,' |',
*          i2,',',i2,',',i2,'> = ',f15.9)

200  continue

      write(8,1099)
      write(*,1099)
      if (l1.eq.l2.and.n1.eq.n2) hnlm=IP-hnlm+ryd/(dn1**2)
      write(8,2100) n1,l1,m1,n2,l2,m1,hnlms
      write(8,2100) n1,l1,m1,n2,l2,m1,hnlm
      write(*,2100) n1,l1,m1,n2,l2,m1,hnlm
      write(8,1099)
      write(8,1099)

250  continue
2100 format(1x,'<',i2,',',i2,',',i2,'| H |',
*          i2,',',i2,',',i2,'> = ',f15.9)

*****
*
* calculating radial orbitals and saving them in file radorb.dat
*
*****
      dr=rmax/3000.0d0
      r=0.0d0
      while (r.le.rmax) do

```

```

r=r+dr
rnl1=radhyp (dn1,dl1,z,r)
rnl2=radhyp (dn2,dl2,z,r)
write (9,1000) r,rnl1,rnl2
end while

close (9)
close (8)
1000 format (1x,f10.5,2x,f15.12,2x,f15.8)

stop
end

real*8 function radhyp(an,al,z,r)
implicit real*8 (a-h,o-z)
pi=3.141592653589793d0
x=2.0d0*z*r/an
coef=sqrt (gamma (an+al+1.0d0) /gamma (an-al) /an/an*z) /
* gamma (2.0d0*al+2.0d0) *exp (-x/2.0d0) *x** (al+1.0d0)
alfa=-an+al+1.0d0
beta=2.0d0*al+2.0d0

rnl=-coef*hyper11 (alfa,beta,x)
radhyp=rnl
return
end

real*8 function hyper11(a,b,x)
implicit real*8 (a-h,o-z)
eps=1.0d-15
t=0.0d0
c=1.0d0
f=1.0d0
while (abs(c) .ge. eps) do
c=c*(a+t) / (b+t) / (t+1.0d0) *x
t=t+1.0d0
f=f+c
end while
hyper11=f
return
end

REAL*8 FUNCTION D9J (X11,X12,X13,X21,X22,X23,X31,X32,X33)
REAL*8 PROD,SJ,DBLE
D9J=0.D0
DELTA=1.0
Y1=ABS (X21-X32)
Y2=ABS (X11-X33)
Y3=ABS (X12-X23)
ZJL=AMAX1 (Y1,Y2,Y3)

```

```

Y1=X21+X32
Y2=X11+X33
Y3=X12+X23
ZJU=AMIN1 (Y1, Y2, Y3)
IF (ZJU.LE.0.) RETURN
ZSAVE=ZJU
ZJU=AMAX1 (ZJU, ZJL)
ZJL=AMIN1 (ZSAVE, ZJL)
IF (IFIX (ZJL) .NE. IFIX (ZJL+0.5)) DELTA=0.5
ZJ=ZJL-DELTA
10 ZJ=ZJ+DELTA
IF (ZJ.GT.ZJU) GO TO 20
PROD=SJ (X11, X21, X31, X32, X33, ZJ)
IF (PROD.EQ.0.D0) GO TO 10
PROD=PROD*SJ (X12, X22, X32, X21, ZJ, X23)
IF (PROD.EQ.0.D0) GO TO 10
PROD=PROD*SJ (X13, X23, X33, ZJ, X11, X12)
IF (PROD.EQ.0.D0) GO TO 10
PROD=DBLE (2.*ZJ+1.) *PROD* (-1.D0)**IFIX (2.*ZJ)
20 D9J=D9J+PROD
IF (ZJ.LT.ZJU) GO TO 10
RETURN
END

```

```

SUBROUTINE TRIAD (A, B, C, DNORM, IERR)
REAL*4 VEC (3)
REAL*8 GAM, DELTA, DNORM
VEC (1) =A+B-C
VEC (2) =A-B+C
VEC (3) =-A+B+C
DO 10 I=1, 3
IF (VEC (I) .LT.0.0.OR. IFIX (VEC (I)) .NE. IFIX (VEC (I) +.5)) GO TO 20
10 CONTINUE
DELTA=GAM (VEC (1) ) +GAM (VEC (2) ) +GAM (VEC (3) ) -GAM (A+B+C+1.)
DNORM=DNORM+0.5D0*DELTA
IERR=0
RETURN
20 DNORM=0.D0
IERR=-1
RETURN
END

```

```

DOUBLE PRECISION FUNCTION SJ (X1, X2, X3, Y1, Y2, Y3)
C=====
C THIS SUBPROGRAM COMPUTES THE VALUES OF 6-J SYMBOLS FOR ANY SET OF
C POSITIVE REAL ARGUMENTS X1, X2, X3, Y1, Y2, AND Y3 USING A MODIFIED
C VERSION OF RACAH'S FORMULA FOR THE W-COEFFICIENT.
C DETAILS ARE GIVEN IN THE REFERENCE "THE 3-J AND 6-J SYMBOLS"
C ROTENBERG, METROPOLIS, BIVINS, AND WOOTEN, JR., MIT PRESS 1959.
C
C FUNCTIONS OR SUBROUTINES REQUIRED: TRIAD, GAM, DEXP
C

```



```

      REAL*8 DNORM,GAM,DELTA,SUM,DEXP
      DIMENSION Z(7)
C
C CHECK FOR AUTOMATIC ZEROES
C VIA TRIANGULAR CONDITIONS
C
C 1. A ZERO VALUE FOR ANY ONE OF THE FOUR TRIADS: (X1,X2,X3),
C (Y1,Y2,X3), (X1,Y2,Y3), AND (Y1,X2,Y3).
C
C 2. A NONINTEGER VALUE FOR ANY ELEMENT OF ANY TRIAD.
C
C THE SUBROUTINE TRIAD(ARG1,ARG2,ARG3, DNORM, IERR)
C RETURNS THE ERROR CODE IERR=-1 IF THE TRIANGULAR
C CONDITIONS ARE NOT SATISFIED (OTHERWISE IERR=0)
      SJ=0.D0
      DNORM=0.0D0
C TEST TRIAD (X1,X2,X3)
      CALL TRIAD(X1,X2,X3, DNORM, IERR)
      IF(IERR.EQ.-1) RETURN
C TEST TRIAD (X1,Y2,Y3)
      CALL TRIAD(X1,Y2,Y3, DNORM, IERR)
      IF(IERR.EQ.-1) RETURN
C TEST TRIAD (Y1,X2,Y3)
      CALL TRIAD(Y1,X2,Y3, DNORM, IERR)
      IF(IERR.EQ.-1) RETURN
C TEST TRIAD (Y1,Y2,X3)
      CALL TRIAD(Y1,Y2,X3, DNORM, IERR)
      IF(IERR.EQ.-1) RETURN
      Z(1)=X1+X2+X3
      Z(2)=X1+Y2+Y3
      Z(3)=Y1+X2+Y3
      Z(4)=Y1+Y2+X3
      Z(5)=X1+X2+Y1+Y2
      Z(6)=X2+X3+Y2+Y3
      Z(7)=X1+X3+Y1+Y3
      IM=MAX1(Z(1),Z(2),Z(3),Z(4))+1
      IN=MIN1(Z(5),Z(6),Z(7))+1
      M=MIN0(IM,IN)
      N=MAX0(IM,IN)
      DO 20 I=M,N
      SUM=0.D0
      ZZ=FLOAT(I-1)
      DO 30 K=1,4
30 SUM=SUM+GAM(ZZ-Z(K))
      DO 40 K=5,7
40 SUM=SUM+GAM(Z(K)-ZZ)
      SJ=SJ+(-1.D0)**(I-1)*DEXP(GAM(ZZ+1.)+DNORM-SUM)
20 CONTINUE
      RETURN
      END

```

```

      DOUBLE PRECISION FUNCTION TJ(X1,X2,XT, XM1, XM2, XMT)
C FUNCTION TO CALCULATE THREE-J SYMBOLS WITH ARGUMENTS J1, J2,

```

```

C J3, M1, M2, M3.
C FUNCTIONS OR SUBROUTINES REQUIRED: GAM,DEXP
  REAL*8 NORM,DEM,DEXP,GAM
  TJ=0.D0
  IF (ABS (XM1) .GT.X1.OR.ABS (XM2) .GT.X2) RETURN
  IF (ABS (XMT) .GT.XT) RETURN
  IF (XM1+XM2+XMT.NE.0.0) RETURN
  IF (X1+X2-XT.LT.0.0) RETURN
  IF (X1-X2+XT.LT.0.0) RETURN
  IF (-X1+X2+XT.LT.0.0) RETURN
  NORM=GAM (X1+X2-XT) +GAM (X1-X2+XT) +GAM (-X1+X2+XT) +GAM (X1+XM1) +
1GAM (X1-XM1) +GAM (X2+XM2) +GAM (X2-XM2) +GAM (XT+XMT) +GAM (XT-XMT) -
2GAM (X1+X2+XT+1.)
  NORM=0.5D0*NORM
  M=MAX1 (X2-XT-XM1, X1-XT+XM2, 0.0) +1
  N=MIN1 (X1+X2-XT, X1-XM1, X2+XM2) +1
  DO 10 I=M,N
  Z=FLOAT (I-1)
  DEM=GAM (Z) +GAM (X1+X2-XT-Z) +GAM (X1-XM1-Z) +GAM (X2+XM2-Z) +
1GAM (XT-X2+XM1+Z) +GAM (XT-X1-XM2+Z)
  L=IFIX (ABS (X1-X2-XMT+Z) )
  TJ=TJ+DEXP (NORM-DEM) * (-1.D0) **L
10  CONTINUE
  RETURN
  END

```

```

  DOUBLE PRECISION FUNCTION GAM(Z)
C COMPUTES THE FUNCTION LOG N! IN DOUBLE PRECISION
  DOUBLE PRECISION DLOG,DFLOAT
  GAM=0.0D0
  M=IFIX (Z)
  IF (M .LT. 2) RETURN
  DO 10 I=2,M
10  GAM=GAM+DLOG (DFLOAT (I) )
  RETURN
  END

```

```

  real*8 function qmltp(l)
  implicit real*8 (a-h,o-z)
  pi=3.141592653589793d0
  a0=.529177086d0
* !!!!!!!!!!!!!!!!!!!!!!!!!!!!!!!!!!!!!
*  molecule specific segment
*
  re=2.080d0
  amet=137.905
  alig=18.9984046
*****
  delz=alig/(amet+alig)
  rmet=delz*re/a0
  rlig=(1.0d0-delz)*re/a0
  emet=2.0d0

```

```

elig=-1.0d0
q=emet*plgndr(1,0,-1.0d0)*rmet**1+elig*plgndr(1,0,1.0d0)*rlig**1
qmltp=q
return
end

real*8 FUNCTION PLGNDR(L,M,X)
implicit real*8 (a-h,o-z)
IF(M.LT.0.OR.M.GT.L.OR.ABS(X).GT.1.)PAUSE 'bad arguments'
PMM=1.d0
IF(M.GT.0) THEN
SOMX2=SQRT((1.d0-X)*(1.d0+X))
FACT=1.d0
DO 11 I=1,M
PMM=-PMM*FACT*SOMX2
FACT=FACT+2.d0
11 CONTINUE
ENDIF
IF(L.EQ.M) THEN
PLGNDR=PMM
ELSE
PMMP1=X*dble(2*M+1)*PMM
IF(L.EQ.M+1) THEN
PLGNDR=PMMP1
ELSE
DO 12 LL=M+2,L
PLL=(X*dble(2*LL-1)*PMMP1-dble(LL+M-1)*PMM)/dble(LL-M)
PMM=PMMP1
PMMP1=PLL
12 CONTINUE
PLGNDR=PLL
ENDIF
ENDIF
RETURN
END

```

10.4 Program RADIAL for various radial integrals in hydrogenic problem.

Program RADIAL written in FORTRAN is used to calculate radial integrals in hydrogenic problem. It allows for nonzero quantum defects and both negative and positive powers of r .

```
*****
*   Zygmunt J. Jakubek - February 1993                               *
*   program calculates various radial integrals for hydrogenic problems *
*****

      program radial

      real*8 rnl,rnl1,rnl2,intrnl,radial,r,dr,rmax,rmin,z,radhyp
      real*8 nfl1,nfl2,lfl1,lfl2,qdef1,qdef2,pi
      common itadd
      pi=3.141592653589793d0
      print *, 'n1='
      read *,nfl1
      print *, 'n2='
      read *,nfl2
      print *, 'l1='
      read *,lfl1
      print *, 'l2='
      read *,lfl2
      z=1.0d0
      print *, 'rmax(a.u.)='
      read *,rmax
      print *, 'rmin(a.u.)='
      read *,rmin
      print *, 'dr(a.u.)='
      read *,dr
      print *, 'exponent of operator'
      read *,k
c     print *, 'bates summing correction'
c     read *,itadd
      open(21,file='radorb.dat')
      open(9,file='matelem.dat')

      r=rmin
      intrnl=0.0d0
      kabs=abs(k)
      if(k) 10,10,20

10    while (r.le.rmax) do
      r=r+dr
      rnl1=radhyp(nfl1,lfl1,z,r)
      rnl2=radhyp(nfl2,lfl2,z,r)
c     rnl1=bates(nfl1,lfl1,r)
c     rnl2=bates(nfl2,lfl2,r)
```

```

        rnl=rnl1*rnl2*dr
        do 11 i=1,kabs
        rnl=rnl/r
11    continue
        intrnl=intrnl+rnl
        write(9,1010)r,10000*intrnl
        end while
        print *,intrnl
        goto 111

20    while (r.le.rmax) do
        r=r+dr
        rnl1=radhyp(nfl1,lf11,z,r)
        rnl2=radhyp(nfl2,lf12,z,r)
c      rnl1=bates(nfl1,lf11,r)
c      rnl2=bates(nfl2,lf12,r)
        rnl=rnl1*rnl2*dr
        do 21 i=1,kabs
        rnl=rnl*r
21    continue
        intrnl=intrnl+rnl
        write(9,1010)r,10000*intrnl
        end while
        print *,intrnl
1010  format(1x,f6.3,2x,f18.11)

111  continue
        dr=(rmax-rmin)/3000.0d0
        r=rmin
        while (r.le.rmax) do
        r=r+dr
        rnl1=radhyp(nfl1,lf11,z,r)
        rnl2=radhyp(nfl2,lf12,z,r)
c      rnl1=bates(nfl1,lf11,r)
c      rnl2=bates(nfl2,lf12,r)
        write(21,1000)r,rnl1,rnl2
        end while
100  continue
        close(9)
        close(21)
1000 format(1x,f10.5,4(2x,f15.12))
        end

real*8 function radhyp(an,al,z,r)
implicit real*8 (a-h,o-z)
pi=3.141592653589793d0
x=2.0d0*z*r/an
coef=sqrt(gamma(an+al+1.0d0)/gamma(an-al)/an/an*z)/
* gamma(2.0d0*al+2.0d0)*exp(-x/2.0d0)*x**(al+1.0d0)
alfa=-an+al+1.0d0
beta=2.0d0*al+2.0d0

rnl=-coef*hyper11(alfa,beta,x)

```

```

radhyp=rnl
return
end

real*8 function radial(n,l,z,r)
c
c r must be given in atomic units
c
real*8 r,rho,temp,rnl,lager,z
rho=2.0d0*z*r/dble(n)
ll1=2*l+1
nl=n-l-1
temp=exp(-rho/2.0d0)*rho**(l+1)*lager(nl,ll1,rho)
rnl=-sqrt(dble(z*factrl(nl))/dble(n*n)/(factrl(n+1)))
**temp
radial=rnl
return
end

real*8 function lager(nl,ll1,rho)

real*8 h,f,mm,g,rho
h=1.d0
f=1.d0
j=1
mm=dble(ll1)

if(nl.eq.0) goto 2

f=1.d0+mm-rho
if(nl.eq.1) goto 2
1 j=j+1
g=f
f=((dble(2*j)+mm-1.0d0-rho)*g-(dble(j)+mm-1.0d0)*h)/dble(j)
h=g
if(j.lt.nl) goto 1
2 lager=f
end

real*8 function radass(n,l,z,r)
real*8 n,l,z,r,rnl,pi

pi=3.141592653589793d0
rnl=sqrt(sqrt(2.0d0/r/r/r)/n/n/n/pi)*cos(sqrt(8.0d0*r)-.25d0*pi)
*   -(l+.5d0)*pi)*r
radass=rnl
return
end

```

```

real*8 FUNCTION FACTRL(N)
real*8 a(33)
DATA NTOP,A(1)/0,1.d0/
IF (N.LT.0) THEN
PAUSE 'negative factorial'
ELSE IF (N.LE.NTOP) THEN
FACTRL=A(N+1)
ELSE IF (N.LE.32) THEN
DO 11 J=NTOP+1,N
A(J+1)=dble(J)*A(J)
11 CONTINUE
NTOP=N
FACTRL=A(N+1)
ELSE
FACTRL=EXP(GAMMA(dble(N+1)))
ENDIF
RETURN
END

real*8 FUNCTION BESSJ(N,X)
implicit real*8 (a-h,o-z)
PARAMETER (IACC=40,BIGNO=1.d10,BIGNI=1.d-10)
IF(N.LT.2)PAUSE 'bad argument N in BESSJ'
TOX=2.d0/X
IF(X.GT.dble(N)) THEN
BJM=BESSJ0(X)
BJ=BESSJ1(X)
DO 11 J=1,N-1
BJP=J*TOX*BJ-BJM
BJM=BJ
BJ=BJP
11 CONTINUE
BESSJ=BJ
ELSE
M=2*((N+INT(SQRT(dble(IACC*N)))))/2)
BESSJ=0.d0
JSUM=0
SUM=0.d0
BJP=0.d0
BJ=1.d0
DO 12 J=M,1,-1
BJM=J*TOX*BJ-BJP
BJP=BJ
BJ=BJM
IF(ABS(BJ).GT.BIGNO) THEN
BJ=BJ*BIGNI
BJP=BJP*BIGNI
BESSJ=BESSJ*BIGNI
SUM=SUM*BIGNI
ENDIF
IF(JSUM.NE.0) SUM=SUM+BJ
JSUM=1-JSUM
IF(J.EQ.N) BESSJ=BJP

```

```

12  CONTINUE
    SUM=2.d0*SUM-BJ
    BESSJ=BESSJ/SUM
    ENDIF
    RETURN
    END

```

```

real*8 FUNCTION BESSJ0(X)
REAL*8 Y,P1,P2,P3,P4,P5,Q1,Q2,Q3,Q4,Q5,R1,R2,R3,R4,R5,R6,
*   S1,S2,S3,S4,S5,S6,x,ax,z,xx
DATA P1,P2,P3,P4,P5/1.D0,-.1098628627D-2,.2734510407D-4,
*   -.2073370639D-5,.2093887211D-6/, Q1,Q2,Q3,Q4,Q5/-.1562499995D-1,
*   .1430488765D-3,-.6911147651D-5,.7621095161D-6,-.934945152D-7/
DATA R1,R2,R3,R4,R5,R6/57568490574.D0,-13362590354.D0,651619640.7D
*0,
*   -11214424.18D0,77392.33017D0,-184.9052456D0/,
*   S1,S2,S3,S4,S5,S6/57568490411.D0,1029532985.D0,
*   9494680.718D0,59272.64853D0,267.8532712D0,1.D0/
IF (ABS(X) .LT. 8.d0) THEN
  Y=X**2
  BESSJ0=(R1+Y*(R2+Y*(R3+Y*(R4+Y*(R5+Y*R6))))
*   / (S1+Y*(S2+Y*(S3+Y*(S4+Y*(S5+Y*S6))))
ELSE
  AX=ABS(X)
  Z=8.d0/AX
  Y=Z**2
  XX=AX-.785398164d0
  BESSJ0=SQRT(.636619772d0/AX)*(COS(XX)*(P1+Y*(P2+Y*(P3+Y*(P4+Y
*   *P5))))-Z*SIN(XX)*(Q1+Y*(Q2+Y*(Q3+Y*(Q4+Y*Q5))))
ENDIF
RETURN
END

```

```

real*8 FUNCTION BESSJ1(X)
REAL*8 Y,P1,P2,P3,P4,P5,Q1,Q2,Q3,Q4,Q5,R1,R2,R3,R4,R5,R6,
*   S1,S2,S3,S4,S5,S6,x,ax,z,xx
DATA R1,R2,R3,R4,R5,R6/72362614232.D0,-7895059235.D0,242396853.1D0
* ,
*   -2972611.439D0,15704.48260D0,-30.16036606D0/,
*   S1,S2,S3,S4,S5,S6/144725228442.D0,2300535178.D0,
*   18583304.74D0,99447.43394D0,376.9991397D0,1.D0/
DATA P1,P2,P3,P4,P5/1.D0,.183105D-2,-.3516396496D-4,.2457520174D-5
* ,
*   -.240337019D-6/, Q1,Q2,Q3,Q4,Q5/.04687499995D0,-.2002690873D-3
* ,
*   .8449199096D-5,-.88228987D-6,.105787412D-6/
IF (ABS(X) .LT. 8.d0) THEN
  Y=X**2
  BESSJ1=X*(R1+Y*(R2+Y*(R3+Y*(R4+Y*(R5+Y*R6))))
*   / (S1+Y*(S2+Y*(S3+Y*(S4+Y*(S5+Y*S6))))
ELSE
  AX=ABS(X)

```



```

Z=8.d0/AX
Y=Z**2
XX=AX-2.356194491d0
BESSJ1=SQRT(.636619772d0/AX)*(COS(XX)*(P1+Y*(P2+Y*(P3+Y*(P4+Y
*      *P5))))-Z*SIN(XX)*(Q1+Y*(Q2+Y*(Q3+Y*(Q4+Y*Q5))))))
*      *SIGN(1.d0,X)
ENDIF
RETURN
END

```

```

real*8 function hyper11(a,b,x)
implicit real*8 (a-h,o-z)
eps=1.0d-15
t=0.0d0
c=1.0d0
f=1.0d0
while(abs(c).ge.eps) do
c=c*(a+t)/(b+t)/(t+1.0d0)*x
t=t+1.0d0
f=f+c
end while
hyper11=f
return
end

```

```

real*8 function bates(xn,xl,xr)
implicit real*8 (a-h,o-z)
common itadd

at=(2.0d0/xn)**(xn)/dsqrt(xn*xn*gamma(xn+xl+1.0d0)*gamma(xn-xl))
bat=at*xr**(xn)
itmax=dint(xn)
do 10 it=1,itmax+itadd
dt=dbl(it)
at=at*xn/2.0d0/dt*(xl*(xl+1.0d0)-(xn-dt)*(xn-dt+1.0d0))
bat1=at*xr**(xn-dt)
bat=bat+bat1
10 continue
bates=bat*dexp(-xr/xn)
return
end

```

11. Appendix C.

In isolated state or isolated supercomplex fits, the matrix of a Hamiltonian is of finite dimension. Interactions between a finite number of states are treated explicitly. All other interactions, between the selected state or states and other remote states must be taken into account in some approximate way¹. Let \mathbf{H} be a matrix of the total Hamiltonian in an infinite basis set composed of 2 classes of basis functions. Class 1 basis functions are the functions related to the given $s\sim p\sim d\sim f\sim g\sim h$ supercomplex states. Class 2 functions are all other higher- l molecular basis functions. The matrix of the Hamiltonian can be written as

$$\mathbf{H} = \begin{pmatrix} \mathbf{H}_1 & \mathbf{H}_{1\sim 2} \\ \mathbf{H}_{2\sim 1} & \mathbf{H}_2 \end{pmatrix}. \quad (\text{C.1})$$

By applying the Van Vleck or contact transformation, the class 1 ~ class 2 matrix elements in the transformed matrix can be minimized. The transformation is defined by

$$\mathbf{T}^\dagger \mathbf{H} \mathbf{T} = \tilde{\mathbf{H}} = \begin{pmatrix} \tilde{\mathbf{H}}_1 & \tilde{\mathbf{H}}_{1\sim 2} \\ \tilde{\mathbf{H}}_{2\sim 1} & \tilde{\mathbf{H}}_2 \end{pmatrix}. \quad (\text{C.2})$$

The matrix \mathbf{T} can be chosen to minimize $\tilde{\mathbf{H}}_{1\sim 2}$ relative to $\mathbf{H}_{1\sim 2}$ without introducing any mixing between class 1 basis functions.

Let

$$\mathbf{H} = \mathbf{H}^0 + \lambda \mathbf{H}' \quad (\text{C.3})$$

and

$$\tilde{\mathbf{H}} = \tilde{\mathbf{H}}^0 + \lambda \tilde{\mathbf{H}}' + \lambda^2 \tilde{\mathbf{H}}'' + \dots, \quad (\text{C.4})$$

where λ is an order-sorting parameter. \mathbf{T} is a unitary matrix and can be expressed as

$$\mathbf{T} = e^{i\lambda \mathbf{S}}, \quad (\text{C.5})$$

where \mathbf{S} is a Hermitian matrix. Using the Baker-Hausdorff lemma

$$e^{-i\lambda \mathbf{S}} \mathbf{H} e^{i\lambda \mathbf{S}} = \mathbf{H} - i\lambda [\mathbf{S}, \mathbf{H}] + (i^2 \lambda^2 / 2!) [\mathbf{S}, [\mathbf{S}, \mathbf{H}]] + \dots + ((-1)^n i^n \lambda^n / n!) [\mathbf{S}, [\mathbf{S}, [\mathbf{S}, \dots [\mathbf{S}, \mathbf{H}] \dots]]] \quad (\text{C.6})$$

we can easily compare terms with the same power of λ .

$$\lambda^0 : \tilde{\mathbf{H}}^0 = \mathbf{H}^0 \quad (\text{C.7a})$$

$$\lambda^1 : \tilde{\mathbf{H}}' = \mathbf{H}' - i[\mathbf{S}, \mathbf{H}^0] \quad (\text{C.7b})$$

$$\lambda^2 : \tilde{\mathbf{H}}'' = -i[\mathbf{S}, \mathbf{H}'] - \frac{1}{2}[\mathbf{S}, [\mathbf{S}, \mathbf{H}^0]] \quad (\text{C.7c})$$

$$\lambda^3 : \tilde{\mathbf{H}}''' = (i/6)[\mathbf{S}, [\mathbf{S}, [\mathbf{S}, \mathbf{H}^0]]] - \frac{1}{2}[\mathbf{S}, [\mathbf{S}, \mathbf{H}']] \quad (\text{C.7d})$$

By choosing

$$S_{ab} = 0 \quad (\text{C.8a})$$

$$S_{\alpha\beta} = 0 \quad (\text{C.8b})$$

and
$$S_{a\alpha} = \frac{iH'_{a\alpha}}{E_a - E_\alpha}, \quad (\text{C.8d})$$

where Roman and Greek indices denote, respectively, class 1 and 2 basis functions, it is possible to make $\tilde{\mathbf{H}}'_{1\sim 2}$ vanish i.e $\tilde{\mathbf{H}}'_{a\alpha} = 0$.

The lowest-order interblock matrix elements of $\tilde{\mathbf{H}}$ occur now in the second-order term, $\tilde{\mathbf{H}}''$, and neglecting it will be a source of smaller error than if $\mathbf{H}_{1\sim 2}$ would be neglected. We can estimate what kind of error will be made by assuming $\tilde{\mathbf{H}}''_{a\alpha} = 0$.

$$\begin{aligned} \tilde{\mathbf{H}}''_{a\alpha} &= i[(\mathbf{H}'\mathbf{S})_{a\alpha} - (\mathbf{S}\mathbf{H}')_{a\alpha}] + (\mathbf{S}\mathbf{H}^0\mathbf{S})_{a\alpha} - \frac{1}{2}[(\mathbf{H}^0\mathbf{S}\mathbf{S})_{a\alpha} + (\mathbf{S}\mathbf{S}\mathbf{H}^0)_{a\alpha}] \\ &= i \sum_b [H'_{ab} S_{b\alpha} - S_{ab} H'_{b\alpha}] + i \sum_\beta [H'_{a\beta} S_{\beta\alpha} - S_{a\beta} H'_{\beta\alpha}] \\ &\quad + \sum_{\beta,\gamma} S_{a\beta} H^0_{\beta\gamma} S_{\gamma\alpha} + \sum_{\beta,c} S_{a\beta} H^0_{\beta c} S_{c\alpha} + \sum_{c,\beta} S_{ac} H^0_{c\beta} S_{\beta\alpha} + \sum_{c,d} S_{ac} H^0_{cd} S_{d\alpha} \\ &\quad - \frac{1}{2}[(\mathbf{H}^0\mathbf{S}\mathbf{S})_{a\alpha} + (\mathbf{S}\mathbf{S}\mathbf{H}^0)_{a\alpha}] \end{aligned} \quad (\text{C.9})$$

By substituting $S_{ab} = 0$, $S_{\alpha\beta} = 0$, $H^0_{ab} = 0$, and $H^0_{\alpha\beta} = 0$, Eq. C.9 simplifies to

$$\tilde{\mathbf{H}}''_{a\alpha} = i \sum_b H'_{ab} S_{b\alpha} - i \sum_\beta S_{a\beta} H'_{\beta\alpha}, \quad (\text{C.10})$$

or substituting Eq. C.8d

$$\tilde{\mathbf{H}}''_{a\alpha} = -\sum_b \frac{H'_{ab} H'_{b\alpha}}{E_b - E_\alpha} + \sum_\beta \frac{H'_{a\beta} H'_{\beta\alpha}}{E_a - E_\beta}. \quad (\text{C.11})$$

Thus, neglect of $\tilde{\mathbf{H}}''_{a\alpha}$ matrix elements will result in a small error if

$$H'_{a\alpha} \ll E_a - E_\alpha.$$

Having transformed the total Hamiltonian, we can calculate effective matrix elements within a selected block, for example the *s-p-d-f-g-h* supercomplex, as

$$\begin{aligned} \tilde{\mathbf{H}}_{ab} &= \tilde{\mathbf{H}}_{ab}^0 + \lambda \tilde{\mathbf{H}}'_{ab} + \lambda^2 \tilde{\mathbf{H}}''_{ab} \\ &= H_{ab}^0 + \lambda H'_{ab} + i\lambda \sum_\alpha (H_{a\alpha}^0 S_{\alpha b} - S_{a\alpha} H_{\alpha b}^0) + \\ &\quad + \lambda^2 i \sum_\alpha (H'_{a\alpha} S_{\alpha b} - S_{a\alpha} H'_{\alpha b}) + \lambda^2 \sum_{\alpha,\beta} S_{a\alpha} H_{\alpha\beta}^0 S_{\beta b} - \lambda^2 \frac{1}{2} \sum_{\alpha,c} (H_{ac}^0 S_{c\alpha} S_{\alpha b} + S_{a\alpha} S_{\alpha c} H_{cb}^0) \\ &= E_a \delta_{ab} + \lambda H'_{ab} - \lambda^2 \sum_\alpha \left(\frac{H'_{a\alpha} H'_{\alpha b}}{E_\alpha - E_b} + \frac{H'_{a\alpha} H'_{\alpha b}}{E_\alpha - E_a} \right) + \\ &\quad - \lambda^2 \sum_\alpha \frac{H'_{a\alpha} H'_{\alpha b} E_\alpha}{(E_a - E_\alpha)(E_\alpha - E_b)} + \lambda^2 \frac{1}{2} \sum_\alpha \frac{H'_{a\alpha} H'_{\alpha b} E_a}{(E_a - E_\alpha)(E_\alpha - E_b)} \\ &\quad + \lambda^2 \frac{1}{2} \sum_\alpha \frac{H'_{a\alpha} H'_{\alpha b} E_b}{(E_a - E_\alpha)(E_\alpha - E_b)} = \\ &= E_a \delta_{ab} + \lambda H'_{ab} + \lambda^2 \frac{1}{2} \sum_\alpha \left(\frac{H'_{a\alpha} H'_{\alpha b}}{E_a - E_\alpha} + \frac{H'_{a\alpha} H'_{\alpha b}}{E_b - E_\alpha} \right), \end{aligned} \quad (\text{C.12})$$

where the first 2 terms can be identified with the matrix elements of the Hamiltonian defined in Eqs. 4.9, and the third term is the contact transformation correction to the Hamiltonian. The correction terms can be written for simplicity as

$$\Delta E_{ab} = \sum_\alpha H'_{a\alpha} H'_{\alpha b} f(E_a, E_b, E_\alpha), \quad (\text{C.13})$$

where

$$f(E_a, E_b, E_\alpha) = \frac{\frac{1}{2}(E_a + E_b) - E_\alpha}{(E_a - E_\alpha)(E_b - E_\alpha)} \equiv f_{ab\alpha}. \quad (\text{C.14})$$

The \mathbf{H}' part of the exact Hamiltonian will be chosen as $\mathbf{H}_{\text{tot}} - \mathbf{H}_0$, thus

$$\mathbf{H}' = \mathbf{H}_r + \mathbf{H}_{fs} + \mathbf{H}_{el}.$$

Expanding the right-hand-side terms according to Eqs. 4.9 we will get

$$\begin{aligned}
\mathbf{H}' = & \quad \text{B(r)} [(\mathbf{J}^2 - \mathbf{J}_z^2) + (\mathbf{s}^2 - \mathbf{s}_z^2) + (\mathbf{I}^2 - \mathbf{I}_z^2)] & \quad (= \mathbf{H}_1) & \quad (\text{C.15}) \\
& + \text{A(r)} \mathbf{l}_z \mathbf{s}_z & \quad (= \mathbf{H}_2) \\
& + \gamma(\text{r}) [\mathbf{J}_z \mathbf{s}_z - \mathbf{l}_z \mathbf{s}_z - \mathbf{s}^2] & \quad (= \mathbf{H}_3) \\
& - \text{B(r)} [\mathbf{J}^+ \mathbf{I} + \mathbf{J} \mathbf{I}^+] & \quad (= \mathbf{H}_4) \\
& - \text{B(r)} [\mathbf{J}^+ \mathbf{s}^- + \mathbf{J} \mathbf{s}^+] & \quad (= \mathbf{H}_5) \\
& + \frac{1}{2} \gamma(\text{r}) [\mathbf{J}^+ \mathbf{s}^- + \mathbf{J} \mathbf{s}^+] & \quad (= \mathbf{H}_6) \\
& + \text{B(r)} [\mathbf{I}^+ \mathbf{s}^- + \mathbf{I} \mathbf{s}^+] & \quad (= \mathbf{H}_7) \\
& + \frac{1}{2} \text{A(r)} [\mathbf{I}^+ \mathbf{s}^- + \mathbf{I} \mathbf{s}^+] & \quad (= \mathbf{H}_8) \\
& - \frac{1}{2} \gamma(\text{r}) [\mathbf{I}^+ \mathbf{s}^- + \mathbf{I} \mathbf{s}^+] & \quad (= \mathbf{H}_9) \\
& + \text{W}. & \quad (= \mathbf{H}_{10})
\end{aligned}$$

When we substitute Eq. C.15 into Eq. C.13 we will get many products of matrix elements, which can be schematically presented as

$$f_{ab\alpha} \langle a | \mathbf{H}_i | \alpha \rangle \langle \alpha | \mathbf{H}_j | b \rangle, \quad (\text{C.16})$$

where $i, j = 1, \dots, 10$. Thus, we can rewrite Eq. C.13 as

$$\Delta E_{ab} = \sum_{\alpha} f_{ab\alpha} \sum_{i,j} (\mathbf{H}_i)_{a\alpha} (\mathbf{H}_j)_{\alpha b}.$$

Let us assume, for example, $\mathbf{H}_i = \mathbf{H}_j = \mathbf{H}_1$ and evaluate the ΔE in the symmetrized basis set

$$\Delta_{H_1 H_1} = \sum_{\alpha} \frac{|\mathbf{H}_{a\alpha}|^2}{E_a - E_{\alpha}} = \sum_{\alpha} \frac{|\langle a | \mathbf{B}(\text{r}) | \alpha \rangle|^2}{E_a - E_{\alpha}} \left[\mathbf{J}(\mathbf{J} + 1) - \Omega^2 + \mathbf{s}(\mathbf{s} + 1) - \sigma^2 + \mathbf{l}(\mathbf{l} + 1) - \lambda^2 \right]^2.$$

The generalized sum over α can be replaced by an effective constant, $-D$,

$$D = - \sum_{\alpha} \frac{|\langle a | \mathbf{B}(\text{r}) | \alpha \rangle|^2}{E_a - E_{\alpha}}.$$

¹ Hélène Lefebvre-Brion and Robert W. Field, *Perturbations in the Spectra of Diatomic Molecules*, p. 244, Academic Press (1986).

12. Appendix D.*

12.1 Fluorescence detected OODR via the $B^2\Sigma^+$ intermediate state: transition frequencies for the ^{138}BaF molecule.

(0,0) $G^2\Sigma^+ - B^2\Sigma^+$

P_{22ff}			R_{22ff}			P_{11ee}			R_{11ee}		
3.5	16927.490	2	3.5	16931.606	-7	8.5	16928.589	3	7.5	16935.439	-11
4.5	16927.114	-4	4.5	16932.170	8	9.5	16928.651	-18	8.5	16936.407	1
21.5	16927.730	1	19.5	16945.786	-10	10.5	16928.801	4	9.5	16937.400	-8
22.5	16928.171	0	21.5	16948.377	-3	11.5	16928.971	1	10.5	16938.462	8
23.5	16928.668	8	22.5	16949.743	3	12.5	16929.176	-12	11.5	16939.539	-7
24.5	16929.190	-3	23.5	16951.153	9	13.5	16929.480	28	12.5	16940.679	-4
25.5	16929.792	20	24.5	16952.599	5	14.5	16929.770	9	13.5	16941.877	12
26.5	16930.386	-10	25.5	16954.106	17	15.5	16930.103	-12	14.5	16943.086	-6
27.5	16931.080	15	26.5	16955.629	0	16.5	16930.504	-10	15.5	16944.348	-16
28.5	16931.787	7	27.5	16957.195	-20	17.5	16930.945	-14	16.5	16945.687	6
29.5	16932.546	5	28.5	16958.851	6	18.5	16931.471	23	17.5	16947.052	9
30.5	16933.335	-11	29.5	16960.491	-30	19.5	16931.998	15	18.5	16948.434	-17
31.5	16934.183	-14	30.5	16962.241	0	20.5	16932.565	1	19.5	16949.914	11
32.5	16935.084	-10	31.5	16964.007	0	21.5	16933.188	-1	20.5	16951.417	16
33.5	16936.035	-1	32.5	16965.832	14	22.5	16933.877	17	21.5	16952.938	-6
34.5	16937.021	-3	33.5	16967.676	1	23.5	16934.575	-2	22.5	16954.533	1
35.5	16938.063	6	34.5	16969.581	5	24.5	16935.334	-5	23.5	16956.168	3
36.5	16939.128	-7	35.5	16971.514	-9	25.5	16936.153	7	24.5	16957.825	-18
37.5	16940.279	19	36.5	16973.502	-13	26.5	16936.980	-18	25.5	16959.575	8
38.5	16941.438	9	37.5	16975.552	0	27.5	16937.885	-11	26.5	16961.327	-9
39.5	16942.656	11	38.5	16977.622	-13	28.5	16938.836	-3	27.5	16963.155	6
40.5	16943.904	-2	39.5	16979.764	1	29.5	16939.824	-4	28.5	16965.033	24
41.5	16945.204	-9	40.5	16981.950	14	30.5	16940.856	-7	29.5	16966.911	-2

(1,0) $G^2\Sigma^+ - B^2\Sigma^+$

P_{22ff}			R_{22ff}			P_{11ee}			R_{11ee}		
21.5	17434.557	-9	9.5	17442.660	-17	15.5	17437.114	3	9.5	17444.491	-2
22.5	17434.976	2	9.5	17442.677	0	16.5	17437.492	8	10.5	17445.518	-2
23.5	17435.422	-4	10.5	17443.464	-13	17.5	17437.910	9	11.5	17446.580	-10
24.5	17435.934	12	10.5	17443.473	-4	18.5	17438.369	8	12.5	17447.701	-3
25.5	17436.457	-4	10.5	17443.489	12	19.5	17438.858	-7	13.5	17448.870	9
26.5	17437.035	-9	11.5	17444.300	-21	20.5	17439.399	-14	14.5	17450.074	12
26.5	17437.059	15	11.5	17444.327	6	21.5	17440.013	9	15.5	17451.309	3
27.5	17437.679	9	11.5	17444.328	7	22.5	17440.627	-12	16.5	17452.595	1
28.5	17438.341	0	11.5	17444.331	10	23.5	17441.314	-4	17.5	17453.932	7

* The 3 numbers in each column are: J'' ($B^2\Sigma^+$), Rydberg $\leftarrow B^2\Sigma^+$ transition frequency (in cm^{-1}), and observed minus calculated transition frequency (in 10^{-3}cm^{-1}).

29.5	17439.052	-4	12.5	17445.198	-10	18.5	17455.292	-8
30.5	17439.817	3	12.5	17445.223	15	19.5	17456.719	1
31.5	17440.608	-8	12.5	17445.226	18	20.5	17458.179	-1
32.5	17441.454	-8	13.5	17446.124	-15	21.5	17459.697	12
33.5	17442.357	5	13.5	17446.126	-13	22.5	17461.235	1
34.5	17443.293	7	20.5	17453.889	21	23.5	17462.823	-3
35.5	17444.261	-4	21.5	17455.172	25	24.5	17464.463	1
36.5	17445.299	12	22.5	17456.479	11	25.5	17466.136	-6
37.5	17446.331	-22	23.5	17457.812	-21	26.5	17467.862	-3
38.5	17447.463	0	23.5	17457.818	-15	27.5	17469.650	18
39.5	17448.632	14	24.5	17459.232	-10	28.5	17471.437	-6
40.5	17449.816	-1	24.5	17459.242	0	29.5	17473.287	-10
			25.5	17460.685	-9			
			25.5	17460.694	0			
			26.5	17462.185	-5			
			26.5	17462.198	8			
			27.5	17463.731	1			
			27.5	17463.740	10			
			28.5	17465.311	-2			
			28.5	17465.321	8			
			29.5	17466.930	-9			
			29.5	17466.938	-1			
			30.5	17468.619	9			
			30.5	17468.625	15			
			31.5	17470.313	-11			
			31.5	17470.328	4			
			32.5	17472.067	-14			
			33.5	17473.870	-12			
			34.5	17475.726	-2			
			35.5	17477.615	-1			
			36.5	17479.557	8			
			37.5	17481.528	3			

(2,0) $G^2\Sigma^+ - B^2\Sigma^+$

P_{22ff}			R_{22ff}			P_{11ee}			R_{11ee}		
2.5	17943.136	4	3.5	17946.794	-5	8.5	17943.671	2	7.5	17950.516	22
2.5	17943.160	28	3.5	17946.798	-1	9.5	17943.715	2	8.5	17951.433	26
3.5	17942.692	-15	4.5	17947.306	-19	10.5	17943.776	-22	9.5	17952.365	3
3.5	17942.709	2	4.5	17947.318	-7	10.5	17943.798	0	10.5	17953.362	6
4.5	17942.315	-7	5.5	17947.863	-28	11.5	17943.915	-9	11.5	17954.394	2
4.5	17942.316	-6	5.5	17947.880	-11	11.5	17943.916	-8	12.5	17955.472	4
5.5	17941.967	-11	6.5	17948.502	3	12.5	17944.086	-4	13.5	17956.583	-3
5.5	17941.971	-7	7.5	17949.146	0	12.5	17944.087	-3	14.5	17957.752	9
6.5	17941.667	-8	8.5	17949.828	-7	13.5	17944.287	-11	15.5	17958.950	8
6.5	17941.674	-1	18.5	17958.971	12	13.5	17944.305	7	16.5	17960.182	0
7.5	17941.406	-7	19.5	17960.104	9	14.5	17944.539	-7	17.5	17961.452	-10
7.5	17941.406	-7	20.5	17961.289	17	14.5	17944.548	2	18.5	17962.756	-27
8.5	17941.172	-20	21.5	17962.494	3	15.5	17944.830	-6	19.5	17964.149	4
17.5	17941.047	12	21.5	17962.497	6	15.5	17944.841	5	20.5	17965.563	15

18.5	17941.228	7	22.5	17963.749	-1	16.5	17945.179	13	21.5	17966.995	4
19.5	17941.438	-11	22.5	17963.752	2	16.5	17945.181	15	22.5	17968.477	1
20.5	17941.718	0	23.5	17965.054	4	17.5	17945.535	-2	23.5	17969.993	-8
20.5	17941.722	4	23.5	17965.070	20	17.5	17945.542	5	24.5	17971.566	-2
21.5	17942.024	-4	24.5	17966.386	-4	18.5	17945.947	-2	25.5	17973.174	-1
22.5	17942.379	1	24.5	17966.391	1	18.5	17945.953	4	26.5	17974.835	12
22.5	17942.386	8	25.5	17967.776	4	19.5	17946.393	-9	27.5	17976.510	-3
23.5	17942.780	10	25.5	17967.788	16	19.5	17946.396	-6	28.5	17978.231	-12
23.5	17942.785	15	26.5	17969.198	3	20.5	17946.889	-7	29.5	17980.016	1
24.5	17943.205	2	26.5	17969.200	5	20.5	17946.890	-6			
24.5	17943.216	13	27.5	17970.657	-2	21.5	17947.431	0			
25.5	17943.689	12	27.5	17970.669	10	21.5	17947.443	12			
25.5	17943.690	13	28.5	17972.163	0	22.5	17948.013	6			
26.5	17944.197	5	28.5	17972.174	11	22.5	17948.017	10			
26.5	17944.204	12	29.5	17973.683	-26	23.5	17948.632	8			
27.5	17944.746	-2	29.5	17973.730	21	23.5	17948.635	11			
27.5	17944.752	4	30.5	17975.287	-9	24.5	17949.276	-6			
28.5	17945.343	-3	31.5	17976.919	-4	24.5	17949.282	0			
28.5	17945.351	5	32.5	17978.567	-25	25.5	17949.985	3			
29.5	17945.984	0	32.5	17978.583	-9	26.5	17950.721	-1			
29.5	17945.993	9	33.5	17980.289	-13	27.5	17951.519	15			
30.5	17946.666	2	33.5	17980.297	-5	29.5	17953.184	-8			
30.5	17946.667	3	34.5	17982.037	-16						
31.5	17947.384	-2	34.5	17982.043	-10						
31.5	17947.398	12	35.5	17983.838	-8						
32.5	17948.144	-4	35.5	17983.845	-1						
32.5	17948.160	12	36.5	17985.673	-6						
33.5	17948.954	2	36.5	17985.674	-5						
33.5	17948.958	6	37.5	17987.557	3						
34.5	17949.782	-15	38.5	17989.458	-12						
34.5	17949.792	-5	39.5	17991.403	-25						
35.5	17950.684	0	57.5	18033.784	3						
35.5	17950.712	28	58.5	18036.541	9						
36.5	17951.614	2	59.5	18039.323	-3						
36.5	17951.614	2	60.5	18042.184	22						
37.5	17952.581	-1									
37.5	17952.582	0									
38.5	17953.573	-21									
38.5	17953.591	-3									
39.5	17954.619	-28									
39.5	17954.658	11									
40.5	17955.722	-19									
40.5	17955.727	-14									
41.5	17956.885	7									
42.5	17958.039	-17									
56.5	17978.950	-14									
57.5	17980.777	2									
58.5	17982.628	0									
59.5	17984.511	-14									

(0,0) $H^2\Sigma^+ - B^2\Sigma^+$

P_{22ff}			R_{22ff}			P_{11ee}			R_{11ee}		
2.5	17564.437	-14	3.5	17568.202	6	8.5	17565.064	-26	8.5	17572.888	-28
3.5	17564.064	18	4.5	17568.762	3	9.5	17565.182	7	9.5	17573.916	-6
4.5	17563.685	-3	5.5	17569.362	-6	10.5	17565.306	0	10.5	17574.971	-3
5.5	17563.370	-5	6.5	17570.018	-5	11.5	17565.481	-3	11.5	17576.081	8
6.5	17563.104	-5	7.5	17570.686	-38	12.5	17565.729	21	12.5	17577.247	30
20.5	17564.268	19	8.5	17571.430	-41	13.5	17565.977	-1	13.5	17578.396	-12
21.5	17564.705	27	12.5	17574.923	-1	14.5	17566.299	4	14.5	17579.631	-14
22.5	17565.202	48	19.5	17582.755	10	15.5	17566.656	-2	15.5	17580.922	-7
23.5	17565.690	14	20.5	17584.053	5	16.5	17567.082	14	16.5	17582.256	-3
24.5	17566.252	7	21.5	17585.390	-6	17.5	17567.514	-10	17.5	17583.635	0
25.5	17566.860	0	22.5	17586.785	-7	18.5	17568.025	-1	18.5	17585.042	-15
26.5	17567.519	-3	23.5	17588.236	3	19.5	17568.584	9	19.5	17586.517	-9
27.5	17568.216	-15	24.5	17589.734	13	20.5	17569.176	6	20.5	17588.056	15
28.5	17568.975	-11	25.5	17591.269	14	21.5	17569.817	5	21.5	17589.619	16
29.5	17569.791	3	26.5	17592.849	14	22.5	17570.484	-17	22.5	17591.215	4
30.5	17570.627	-9	27.5	17594.456	-6	23.5	17571.228	-8	23.5	17592.865	0
31.5	17571.516	-16	28.5	17596.144	9	24.5	17572.010	-7	24.5	17594.571	6
32.5	17572.462	-12	29.5	17597.840	-15	25.5	17572.833	-12	25.5	17596.350	38
33.5	17573.472	10	30.5	17599.625	4	26.5	17573.716	-4	26.5	17598.112	6
34.5	17574.484	-14	31.5	17601.430	-3	27.5	17574.635	-7	27.5	17599.961	15
35.5	17575.583	3	32.5	17603.276	-16	28.5	17575.608	-2	28.5	17601.845	13
36.5	17576.707	-2	33.5	17605.197	-1	29.5	17576.640	16	29.5	17603.766	1
37.5	17577.900	15	34.5	17607.144	-6	30.5	17577.685	-1	30.5	17605.738	-6
38.5	17579.106	-2	35.5	17609.160	12	31.5	17578.785	-9			
39.5	17580.364	-14	36.5	17611.200	7						
40.5	17581.711	17	37.5	17613.290	5						
41.5	17583.045	-13	38.5	17615.414	-9						
42.5	17584.461	-8	39.5	17617.612	4						
43.5	17585.915	-12	40.5	17619.854	14						
44.5	17587.433	1	41.5	17622.112	-6						
53.5	17603.088	-14	42.5	17624.464	21						
54.5	17605.087	7	43.5	17626.848	34						
55.5	17607.129	23	44.5	17629.277	44						
			45.5	17631.688	-10						
			46.5	17634.208	-2						
			47.5	17636.713	-56						
			48.5	17639.371	-3						
			49.5	17642.027	0						
			50.5	17644.712	-15						

(1,0) 32166 $^2\Sigma^+ - B^2\Sigma^+$

P_{22ff}			R_{22ff}			P_{11ee}			R_{11ee}		
2.5	18124.502	-4	3.5	18128.327	21	6.5	18125.239	0	7.5	18132.288	1
3.5	18124.113	-1	4.5	18128.902	2	7.5	18125.258	-18	8.5	18133.292	-18
4.5	18123.771	-2	5.5	18129.553	8	8.5	18125.360	-4	9.5	18134.387	1
5.5	18123.492	7	21.5	18147.075	7	9.5	18125.511	5	10.5	18135.525	10

6.5	18123.248	-2	22.5	18148.619	0	10.5	18125.709	8	11.5	18136.711	14
7.5	18123.062	-5	23.5	18150.223	-1	11.5	18125.958	10	12.5	18137.929	-3
8.5	18122.931	-6	24.5	18151.883	-1	12.5	18126.268	19	13.5	18139.216	-5
17.5	18124.140	0	25.5	18153.585	-14	13.5	18126.606	3	14.5	18140.558	-5
18.5	18124.509	-31	26.5	18155.365	-5	14.5	18127.018	8	15.5	18141.959	0
19.5	18124.979	-14				15.5	18127.471	0	16.5	18143.392	-17
20.5	18125.500	-1				16.5	18127.982	-4	18.5	18146.473	2
21.5	18126.056	-6				17.5	18128.552	-2	19.5	18148.074	-9
22.5	18126.686	9				18.5	18129.179	3	20.5	18149.763	13
23.5	18127.353	6				19.5	18129.825	-28	21.5	18151.484	12
24.5	18128.085	13				20.5	18130.597	13	22.5	18153.224	-24
25.5	18128.873	22				21.5	18131.362	-7	23.5	18155.087	7
26.5	18129.668	-18				22.5	18132.203	-6	24.5	18156.962	-6
27.5	18130.580	5				23.5	18133.106	1	25.5	18158.922	11
28.5	18131.526	5				24.5	18134.057	2	26.5	18160.922	13
29.5	18132.525	4				25.5	18135.072	11	27.5	18162.946	-19
30.5	18133.578	0				26.5	18136.119	-3			
31.5	18134.697	6				27.5	18137.232	-8			
32.5	18135.863	2				28.5	18138.428	15			
33.5	18137.093	6									
34.5	18138.376	5									
35.5	18139.719	8									
36.5	18141.101	-9									
37.5	18142.558	-8									
38.5	18144.079	-2									
39.5	18145.659	5									
40.5	18147.266	-20									
41.5	18148.992	14									

(0,0) 4.13²Π - B²Σ⁺

P _{21cc}			Q _{21fc}			R _{21cc}		
4.5	18285.925	-23	7.5	18289.885	-8	5.5	18291.570	-9
5.5	18286.079	7	7.5	18289.904	11	6.5	18292.661	-5
6.5	18286.236	-5	8.5	18290.610	1	7.5	18293.773	-25
6.5	18286.248	7	8.5	18290.622	13	9.5	18296.205	10
7.5	18286.431	-24	9.5	18291.366	-3	10.5	18297.468	7
7.5	18286.447	-8	9.5	18291.369	0	11.5	18298.751	-21
8.5	18286.690	-24	10.5	18292.167	-7	11.5	18298.773	1
8.5	18286.725	11	10.5	18292.175	1	13.5	18301.516	-11
9.5	18287.015	-2	11.5	18293.026	4	13.5	18301.517	-10
9.5	18287.020	3	11.5	18293.027	5	14.5	18302.961	-11
10.5	18287.378	13	12.5	18293.909	-7	14.5	18302.979	7
10.5	18287.392	27	12.5	18293.919	3	15.5	18304.450	-12
11.5	18287.752	-5	13.5	18294.863	10	15.5	18304.464	2
11.5	18287.763	6	13.5	18294.871	18	16.5	18305.987	-10
12.5	18288.196	1	14.5	18295.811	-24	16.5	18305.998	1
12.5	18288.199	4	14.5	18295.837	2	17.5	18307.580	3
13.5	18288.664	-13	15.5	18296.863	2	17.5	18307.600	23
13.5	18288.672	-5	15.5	18296.873	12	18.5	18309.200	-2

14.5	18289.200	-5	16.5	18297.939	8	18.5	18309.211	9
14.5	18289.221	16	16.5	18297.970	39	19.5	18310.892	20
15.5	18289.772	-5	17.5	18299.056	11	19.5	18310.894	22
15.5	18289.777	0	17.5	18299.057	12	20.5	18312.607	20
16.5	18290.388	-7	18.5	18300.196	-8	20.5	18312.611	24
16.5	18290.398	3	18.5	18300.209	5	21.5	18314.357	9
17.5	18291.050	-7	19.5	18301.406	-2	21.5	18314.367	19
18.5	18291.761	-4	19.5	18301.406	-2	22.5	18316.150	-3
18.5	18291.767	2	20.5	18302.658	3	22.5	18316.165	12
19.5	18292.510	-7	20.5	18302.661	6	23.5	18317.989	-15
19.5	18292.516	-1	21.5	18303.928	-19	24.5	18319.929	29
20.5	18293.291	-24	21.5	18303.942	-5	25.5	18321.859	17
20.5	18293.336	21	22.5	18305.275	-9	26.5	18323.818	-11
21.5	18294.153	-5	22.5	18305.283	-1	27.5	18325.853	-8
21.5	18294.160	2	23.5	18306.652	-12	28.5	18327.951	12
22.5	18295.038	-9	23.5	18306.656	-8	29.5	18330.092	29
22.5	18295.063	16	23.5	18306.679	15	30.5	18332.235	3
23.5	18295.978	-3	24.5	18308.090	1			
23.5	18295.998	17	24.5	18308.102	13			
24.5	18296.955	-5	25.5	18309.548	-11			
24.5	18296.958	-2	25.5	18309.577	18			
25.5	18297.970	-15	26.5	18311.071	-2			
25.5	18297.991	6	26.5	18311.074	1			
26.5	18299.056	1	27.5	18312.607	-25			
26.5	18299.057	2	27.5	18312.611	-21			
27.5	18300.196	25	28.5	18314.244	10			
28.5	18301.340	7	28.5	18314.247	13			
29.5	18302.551	11	29.5	18315.870	-12			
30.5	18303.750	-43	29.5	18315.880	-2			
31.5	18305.069	-23	30.5	18317.606	32			
32.5	18306.453	16						

P _{22ff}			Q _{22ef}			R _{22ff}		
2.5	18283.800	-1	2.5	18284.942	-6	2.5	18286.538	-16
3.5	18283.159	0	3.5	18284.748	-17	3.5	18286.818	-11
4.5	18282.561	0	4.5	18284.614	-13	4.5	18287.182	33
5.5	18282.009	1	5.5	18284.525	-8	5.5	18287.518	4
18.5	18278.869	11	18.5	18287.386	-4	19.5	18297.259	-6
19.5	18278.937	10	18.5	18287.398	8	20.5	18298.266	-27
20.5	18279.022	-18	19.5	18287.906	-19	20.5	18298.277	-16
20.5	18279.037	-3	19.5	18287.908	-17	21.5	18299.369	3
21.5	18279.178	-19	20.5	18288.508	4	21.5	18299.370	4
21.5	18279.202	5	20.5	18288.519	15	22.5	18300.481	-2
22.5	18279.392	-7	21.5	18289.116	-13	22.5	18300.482	-1
22.5	18279.402	3	21.5	18289.122	-7	23.5	18301.643	-2
23.5	18279.640	-6	22.5	18289.793	-7	23.5	18301.651	6
23.5	18279.650	4	22.5	18289.799	-1	24.5	18302.845	-6
24.5	18279.921	-16	23.5	18290.519	3	24.5	18302.865	14
24.5	18279.940	3	23.5	18290.521	5	25.5	18304.097	-4
25.5	18280.265	-7	24.5	18291.283	6	25.5	18304.101	0

25.5	18280.276	4	24.5	18291.284	7	26.5	18305.392	-4
26.5	18280.656	4	25.5	18292.075	-8	26.5	18305.401	5
26.5	18280.664	12	25.5	18292.096	13	27.5	18306.724	-11
27.5	18281.079	2	26.5	18292.934	-1	27.5	18306.736	1
27.5	18281.092	15	26.5	18292.944	9	28.5	18308.121	3
28.5	18281.549	2	27.5	18293.826	-7	28.5	18308.129	11
28.5	18281.561	14	27.5	18293.836	3	29.5	18309.550	4
29.5	18282.056	-5	27.5	18293.839	6	29.5	18309.550	4
29.5	18282.060	-1	28.5	18294.777	1	30.5	18311.024	5
30.5	18282.622	2	28.5	18294.785	9	31.5	18312.532	-4
30.5	18282.638	18	28.5	18294.786	10	32.5	18314.101	4
31.5	18283.234	11	29.5	18295.755	-11	33.5	18315.692	-12
31.5	18283.235	12	29.5	18295.761	-5	34.5	18317.376	21
32.5	18283.870	-1	29.5	18295.772	6	35.5	18319.060	10
32.5	18283.872	1	30.5	18296.801	1	36.5	18320.800	10
33.5	18284.573	8	30.5	18296.802	2	37.5	18322.573	-2
33.5	18284.580	15	30.5	18296.806	6	38.5	18324.401	-4
34.5	18285.308	5	31.5	18297.865	-16	39.5	18326.276	-4
34.5	18285.320	17	31.5	18297.874	-7	40.5	18328.200	1
35.5	18286.094	8	31.5	18297.885	4	41.5	18330.173	9
35.5	18286.097	11	31.5	18297.893	12	42.5	18332.161	-13
36.5	18286.903	-11	32.5	18298.995	-12	43.5	18334.213	-15
36.5	18286.916	2	32.5	18299.002	-5			
37.5	18287.784	-3	32.5	18299.021	14			
37.5	18287.785	-2	33.5	18300.176	-4			
38.5	18288.693	-12	33.5	18300.185	5			
38.5	18288.704	-1	33.5	18300.188	8			
39.5	18289.655	-13	34.5	18301.393	-5			
39.5	18289.667	-1	34.5	18301.393	-5			
40.5	18290.677	1	34.5	18301.411	13			
40.5	18290.680	4	35.5	18302.661	-1			
41.5	18291.710	-20	35.5	18302.664	2			
41.5	18291.722	-8	36.5	18303.957	-16			
42.5	18292.825	-4	36.5	18303.969	-4			
			37.5	18305.312	-18			
			37.5	18305.340	10			
			38.5	18306.724	-9			
			39.5	18308.187	5			
			40.5	18309.661	-16			
			41.5	18311.213	-6			
			42.5	18312.789	-19			

P _{11cc}			Q _{11cc}			R _{11cc}		
3.5	18229.240	-19	5.5	18231.400	32	4.5	18234.091	-18
4.5	18229.392	-9	6.5	18231.934	13	6.5	18236.339	-12
5.5	18229.588	2	7.5	18232.535	18	7.5	18237.501	-35
6.5	18229.825	11	10.5	18234.562	-6	8.5	18238.760	-4
7.5	18230.066	-19	11.5	18235.355	16	9.5	18240.039	4
8.5	18230.398	0	11.5	18235.359	20	9.5	18240.053	18
8.5	18230.400	2	12.5	18236.138	-15	10.5	18241.351	3

9.5	18230.752	-3	12.5	18236.150	-3	10.5	18241.363	15
9.5	18230.765	10	13.5	18237.017	5	11.5	18242.690	-14
10.5	18231.151	-4	13.5	18237.018	6	11.5	18242.709	5
10.5	18231.168	13	14.5	18237.905	-9	12.5	18244.090	-13
11.5	18231.600	3	14.5	18237.921	7	12.5	18244.104	1
11.5	18231.622	25	15.5	18238.836	-23	13.5	18245.533	-11
12.5	18232.064	-18	15.5	18238.855	-4	13.5	18245.538	-6
12.5	18232.083	1	16.5	18239.850	1	14.5	18247.018	-9
13.5	18232.595	-15	16.5	18239.854	5	14.5	18247.030	3
13.5	18232.629	19	17.5	18240.884	1	15.5	18248.554	0
14.5	18233.177	-3	17.5	18240.890	7	15.5	18248.556	2
14.5	18233.183	3	18.5	18241.966	5	16.5	18250.116	-6
15.5	18233.795	1	18.5	18241.970	9	16.5	18250.116	-6
15.5	18233.818	24	19.5	18243.071	-11	17.5	18251.727	-6
16.5	18234.454	4	19.5	18243.074	-8	17.5	18251.745	12
16.5	18234.465	15	20.5	18244.243	-5	18.5	18253.379	-8
17.5	18235.130	-18	20.5	18244.248	0	18.5	18253.396	9
17.5	18235.147	-1	21.5	18245.443	-15	19.5	18255.061	-22
18.5	18235.866	-24	21.5	18245.458	0	19.5	18255.112	29
18.5	18235.878	-12	22.5	18246.712	-1	20.5	18256.815	-6
19.5	18236.666	-8	22.5	18246.721	8	20.5	18256.823	2
19.5	18236.671	-3	23.5	18248.004	-7	21.5	18258.601	-1
20.5	18237.501	1	23.5	18248.008	-3	21.5	18258.606	4
20.5	18237.526	26	24.5	18249.351	-3	22.5	18260.419	-6
21.5	18238.356	-13	24.5	18249.364	10	22.5	18260.427	2
21.5	18238.358	-11	25.5	18250.732	-9	23.5	18262.289	-1
22.5	18239.302	21	25.5	18250.739	-2	23.5	18262.300	10
23.5	18240.239	4	26.5	18252.179	6	24.5	18264.192	-6
24.5	18241.225	-7	26.5	18252.192	19	24.5	18264.207	9
25.5	18242.303	32	27.5	18253.649	0	25.5	18266.138	-10
26.5	18243.352	-1	28.5	18255.143	-27	25.5	18266.156	8
27.5	18244.458	-19				26.5	18268.139	-1
28.5	18245.637	-7				26.5	18268.142	2
29.5	18246.858	5				27.5	18270.157	-17
						27.5	18270.165	-9
						28.5	18272.242	-8
						28.5	18272.250	0
						28.5	18272.251	1
						29.5	18274.354	-15
						29.5	18274.366	-3
						30.5	18276.528	-2

P _{12ff}			Q _{12ef}			R _{12ff}		
2.5	18226.873	12	19.5	18232.118	9	2.5	18229.477	5
3.5	18226.162	13	20.5	18232.724	9	3.5	18229.698	22
4.5	18225.503	23	21.5	18233.367	4	4.5	18229.946	23
12.5	18221.687	-9	21.5	18233.373	10	18.5	18237.977	22
13.5	18221.437	17	22.5	18234.038	-16	19.5	18238.882	24

20.5	18220.707	-8	22.5	18234.050	-4	20.5	18239.793	-11
21.5	18220.779	-11	23.5	18234.779	-8	21.5	18240.804	9
22.5	18220.903	-7	23.5	18234.781	-6	22.5	18241.827	-3
22.5	18220.909	-1	24.5	18235.551	-12	22.5	18241.831	1
23.5	18221.063	-12	24.5	18235.567	4	23.5	18242.905	-5
23.5	18221.077	2	25.5	18236.375	-6	23.5	18242.919	9
24.5	18221.280	-4	25.5	18236.383	2	24.5	18244.015	-18
24.5	18221.281	-3	26.5	18237.266	25	24.5	18244.031	-2
25.5	18221.518	-19	27.5	18238.149	5	25.5	18245.199	-2
25.5	18221.538	1	28.5	18239.082	-7	25.5	18245.204	3
26.5	18221.836	1	28.5	18239.091	2	26.5	18246.402	-12
26.5	18221.841	6	29.5	18240.076	-1	26.5	18246.424	10
27.5	18222.185	8	29.5	18240.082	5	27.5	18247.661	-9
27.5	18222.185	8	30.5	18241.098	-9	27.5	18247.666	-4
28.5	18222.564	0	31.5	18242.181	2	28.5	18248.966	-6
28.5	18222.567	3	31.5	18242.191	12	28.5	18248.975	3
29.5	18222.985	-11	32.5	18243.289	-5	29.5	18250.316	-2
29.5	18223.001	5	32.5	18243.292	-2	29.5	18250.318	0
30.5	18223.454	-19	33.5	18244.458	7	30.5	18251.695	-13
30.5	18223.463	-10	33.5	18244.469	18	30.5	18251.703	-5
31.5	18223.992	-3	34.5	18245.632	-19	31.5	18253.125	-19
31.5	18223.994	-1	34.5	18245.649	-2	31.5	18253.141	-3
32.5	18224.541	-20	35.5	18246.882	-11	32.5	18254.605	-19
32.5	18224.553	-8	35.5	18246.901	8	32.5	18254.625	1
33.5	18225.178	5	36.5	18248.177	0	33.5	18256.142	-7
33.5	18225.180	7	36.5	18248.185	8	33.5	18256.155	6
34.5	18225.822	-7	37.5	18249.508	4	34.5	18257.711	-8
34.5	18225.835	6	37.5	18249.516	12	34.5	18257.720	1
35.5	18226.533	2	38.5	18250.864	-9	35.5	18259.320	-13
35.5	18226.539	8	38.5	18250.865	-8	35.5	18259.329	-4
36.5	18227.266	-12	39.5	18252.269	-15	36.5	18260.991	-2
36.5	18227.291	13	39.5	18252.273	-11	36.5	18260.992	-1
37.5	18228.074	4	40.5	18253.734	-4	37.5	18262.702	4
37.5	18228.077	7	40.5	18253.734	-4	37.5	18262.703	5
38.5	18228.893	-14	41.5	18255.235	0	38.5	18264.452	5
38.5	18228.912	5	41.5	18255.240	5	38.5	18264.470	23
39.5	18229.785	-5	42.5	18256.790	16	39.5	18266.247	5
39.5	18229.802	12	42.5	18256.798	24	39.5	18266.250	8
40.5	18230.705	-13	43.5	18258.361	6	40.5	18268.080	-3
40.5	18230.729	11				40.5	18268.085	2
41.5	18231.692	0				41.5	18269.955	-13
41.5	18231.708	16				41.5	18269.970	2
42.5	18232.724	12				42.5	18271.922	23
42.5	18232.726	14				43.5	18273.875	0

(1,0) $3.95^2\Delta - B^2\Sigma^+$

	$^0P_{12ff}$	$^PQ_{12ef}+P_{22ff}$	$^QR_{12ff}+Q_{22ef}$	R_{22ff}
23.5	18199.855 -26	17.5 18208.204 -12	18.5 18217.145 -35	23.5 18232.890 11
24.5	18199.932 -16	18.5 18208.464 -9	19.5 18217.949 9	24.5 18234.333 14

25.5	18200.027	-34	19.5	18208.781	6	20.5	18218.793	47	25.5	18235.773	-31
26.5	18200.209	-10	20.5	18209.117	-5	21.5	18219.603	7	27.5	18238.882	-24
27.5	18200.427	5	21.5	18209.509	-4	22.5	18220.497	6	28.5	18240.524	0
28.5	18200.677	7	22.5	18209.936	-13	23.5	18221.437	7	30.5	18243.903	9
29.5	18200.962	0	23.5	18210.423	-6	24.5	18222.414	-1	32.5	18247.454	12
30.5	18201.289	-12	24.5	18210.946	-9	25.5	18223.463	19	33.5	18249.271	-12
31.5	18201.687	3	25.5	18211.491	-34	26.5	18224.553	35	34.5	18251.160	-8
32.5	18202.125	13	26.5	18212.120	-20	27.5	18225.654	17	36.5	18255.085	12
33.5	18202.591	5	27.5	18212.793	-7	28.5	18226.794	-7	37.5	18257.090	-2
34.5	18203.107	2	28.5	18213.491	-14	30.5	18229.267	3	38.5	18259.143	-13
35.5	18203.679	10	29.5	18214.244	-11	31.5	18230.535	-28			
36.5	18204.266	-12	30.5	18215.046	-4	32.5	18231.895	-12			
37.5	18204.926	-7	31.5	18215.846	-43	33.5	18233.279	-17			
38.5	18205.646	12	32.5	18216.755	-19	34.5	18234.710	-20			
39.5	18206.391	12	33.5	18217.695	-8	35.5	18236.183	-26			
40.5	18207.174	3	34.5	18218.681	4	36.5	18237.719	-14			
41.5	18207.993	-15	35.5	18219.696	-1	37.5	18239.284	-19			
			39.5	18224.207	-18	38.5	18240.896	-22			
			40.5	18225.460	-10	39.5	18242.545	-33			
						40.5	18244.277	-7			
						41.5	18246.002	-32			

$^O P_{11ec}$			$^P Q_{11fe} + P_{21ec}$			$^Q R_{11ec} + Q_{21fe}$			R_{21ec}		
8.5	18210.350	11	7.5	18213.523	0	6.5	18216.292	21	6.5	18219.950	6
9.5	18210.430	18	8.5	18214.012	3	7.5	18217.197	23	8.5	18222.718	7
10.5	18210.565	35	9.5	18214.545	4	8.5	18218.137	16	9.5	18224.178	16
11.5	18210.696	4	10.5	18215.114	-3	9.5	18219.124	11	10.5	18225.647	-10
12.5	18210.899	0	11.5	18215.728	-10	10.5	18220.169	20	11.5	18227.205	9
13.5	18211.143	-8	12.5	18216.418	14	11.5	18221.269	39	12.5	18228.764	-16
14.5	18211.447	0	13.5	18217.110	-4	12.5	18222.365	10	16.5	18235.555	-5
15.5	18211.787	-1	14.5	18217.878	9	13.5	18223.537	13	17.5	18237.347	-20
16.5	18212.176	2	15.5	18218.688	19	14.5	18224.750	12	21.5	18245.036	-3
17.5	18212.602	-3	16.5	18219.527	14	15.5	18226.012	16	23.5	18249.148	6
18.5	18213.078	-2	17.5	18220.424	22	16.5	18227.303	4	24.5	18251.258	-3
19.5	18213.588	-13	18.5	18221.345	9	17.5	18228.654	8	26.5	18255.666	33
20.5	18214.166	0	19.5	18222.325	10	18.5	18230.066	28	27.5	18257.894	8
21.5	18214.763	-13	20.5	18223.343	5	19.5	18231.485	11	28.5	18260.172	-12
22.5	18215.416	-14	21.5	18224.412	6	20.5	18232.975	20			
23.5	18216.157	27	22.5	18225.500	-18	21.5	18234.454	-27			
24.5	18216.883	9	23.5	18226.651	-25	22.5	18236.038	-13			
25.5	18217.670	7	24.5	18227.883	5	23.5	18237.670	5			
26.5	18218.499	2	25.5	18229.115	-10	24.5	18239.302	-22			
27.5	18219.384	8	26.5	18230.398	-20	25.5	18241.036	8			
28.5	18220.312	12	27.5	18231.750	-4	26.5	18242.769	-7			
						27.5	18244.560	-9			
						28.5	18246.396	-10			
						29.5	18248.305	17			

(1,0) 32110 $^2\Sigma^+$ - B $^2\Sigma^+$

P_{22ff}			R_{22ff}			P_{11ee}			R_{11ee}		
2.5	18068.090	-16	3.5	18071.954	8	7.5	18069.080	-6	9.5	18078.442	5
3.5	18067.726	5	4.5	18072.564	-1	8.5	18069.221	-6	10.5	18079.632	-6
4.5	18067.378	-16	5.5	18073.243	1	9.5	18069.419	-8	11.5	18080.947	50
5.5	18067.128	3	6.5	18073.974	-3	10.5	18069.673	-11	12.5	18082.241	29
6.5	18066.925	10	7.5	18074.771	2	11.5	18069.997	-3	13.5	18083.593	9
7.5	18066.768	5	8.5	18075.606	-14	12.5	18070.392	20	14.5	18085.033	20
8.5	18066.678	8	9.5	18076.522	-6	13.5	18070.831	28	15.5	18086.494	-4
17.5	18068.399	-17	10.5	18077.468	-26	14.5	18071.290	0	16.5	18088.014	-25
18.5	18068.863	-30	22.5	18093.474	11	15.5	18071.834	0	17.5	18089.634	-2
19.5	18069.430	3	23.5	18095.161	12	16.5	18072.430	-5	18.5	18091.268	-20
20.5	18070.028	12	24.5	18096.894	6	17.5	18073.099	6	19.5	18092.985	-9
21.5	18070.673	14	25.5	18098.679	0	18.5	18073.793	-13	20.5	18094.767	11
22.5	18071.381	23	26.5	18100.534	12	19.5	18074.573	-3	21.5	18096.574	2
23.5	18072.106	-4	27.5	18102.425	9	20.5	18075.405	4	22.5	18098.439	-2
24.5	18072.919	2				21.5	18076.304	23	23.5	18100.369	5
25.5	18073.817	40				22.5	18077.219	4	24.5	18102.330	-10
26.5	18074.697	7				23.5	18078.210	5			
27.5	18075.649	-6				24.5	18079.254	6			
28.5	18076.674	1				25.5	18080.336	-9			
29.5	18077.746	4				26.5	18081.462	-33			
30.5	18078.853	-10				27.5	18082.694	-3			
31.5	18080.024	-10									
32.5	18081.249	-5									
33.5	18082.532	7									
34.5	18083.828	-16									
35.5	18085.199	-12									
36.5	18086.589	-37									
37.5	18088.072	-16									
38.5	18089.599	2									
39.5	18091.138	-13									
40.5	18092.750	0									
41.5	18094.391	-2									
42.5	18096.094	14									
43.5	18097.821	11									
44.5	18099.624	42									

12.2 Fluorescence detected OODR via the B $^2\Sigma^+$ intermediate state: transition frequencies for the ^{137}BaF , ^{136}BaF , and ^{135}BaF molecules. **^{137}BaF (1, 0) G $^2\Sigma^+$ - B $^2\Sigma^+$**

P_{22ff}			R_{22ff}			P_{11ee}			R_{11ee}		
21.5	17434.760	-15	10.5	17443.685	1	17.5	17438.115	2	10.5	17445.756	24
22.5	17435.177	-7	11.5	17444.559	29	18.5	17438.565	-10	11.5	17446.811	6
23.5	17435.634	-3	21.5	17455.373	-3	19.5	17439.089	8	12.5	17447.922	1

24.5	17436.116	-18	23.5	17458.080	13	20.5	17439.623	-7	13.5	17449.100	19
25.5	17436.663	-12	26.5	17462.426	-3	21.5	17440.233	10	14.5	17450.281	-3
26.5	17437.255	-4	27.5	17463.961	-9	22.5	17440.850	-10	15.5	17451.531	0
26.5	17437.272	13	28.5	17465.562	8				16.5	17452.797	-24
27.5	17437.888	1	29.5	17467.185	3				17.5	17454.144	-11
28.5	17438.567	9	30.5	17468.855	2				18.5	17455.533	1
29.5	17439.294	21	31.5	17470.571	4				19.5	17456.960	7
30.5	17440.041	9	31.5	17470.576	9				20.5	17458.431	14
31.5	17440.834	-1	32.5	17472.333	8				21.5	17459.937	12
32.5	17441.683	2	33.5	17474.131	5				22.5	17461.467	-9
33.5	17442.566	-5	34.5	17475.957	-14				23.5	17463.070	-1
34.5	17443.484	-21	35.5	17477.860	1				24.5	17464.707	-2
35.5	17444.481	-2	36.5	17479.787	-3				25.5	17466.418	27
36.5	17445.512	8							26.5	17468.101	-15
37.5	17446.555	-14									
38.5	17447.690	13									

¹³⁶BaF (1, 0) G²Σ⁺ - B²Σ⁺

P _{22ff}			R _{22ff}			P _{11ee}			R _{11ee}		
26.5	17437.492	9	11.5	17444.800	20	21.5	17440.440	-6	14.5	17450.515	-12
27.5	17438.069	-41	23.5	17458.318	7	22.5	17441.083	2	15.5	17451.765	-8
28.5	17438.764	-17	26.5	17462.681	8				16.5	17453.057	-5
29.5	17439.503	8	27.5	17464.198	-16				17.5	17454.398	3
30.5	17440.252	-2	28.5	17465.803	5				18.5	17455.807	36
32.5	17441.905	3	30.5	17469.081	-16				19.5	17457.172	-19
33.5	17442.777	-14	31.5	17470.817	5				20.5	17458.669	15
34.5	17443.717	-8	31.5	17470.818	6				21.5	17460.153	-8
37.5	17446.780	-10	32.5	17472.570	-1				22.5	17461.698	-14
			33.5	17474.401	28				23.5	17463.319	13
			34.5	17476.221	2				24.5	17464.952	9
									25.5	17466.639	15
									26.5	17468.348	-1

¹³⁵BaF (1, 0) G²Σ⁺ - B²Σ⁺

P _{22ff}			R _{22ff}			P _{11ee}			R _{11ee}		
29.5	17439.718	13	26.5	17462.883	-18				14.5	17450.736	-11
30.5	17440.477	11	28.5	17466.050	16				15.5	17451.996	0
31.5	17441.275	3	29.5	17467.671	5				16.5	17453.282	-6
32.5	17442.141	19	30.5	17469.327	-15				17.5	17454.635	11
33.5	17442.981	-35	31.5	17471.059	-3				18.5	17456.010	7
34.5	17443.920	-34	31.5	17471.065	3				19.5	17457.427	0
35.5	17444.972	35	33.5	17474.642	8				20.5	17458.900	6
37.5	17447.050	15	34.5	17476.465	-21				21.5	17460.395	-9
									22.5	17461.959	0
									23.5	17463.575	18
									24.5	17465.176	-22
									25.5	17466.888	4

$^{137}\text{BaF}(2, 0) G^2\Sigma^+ - B^2\Sigma^+$

P_{22ff}			R_{22ff}			P_{11ee}			R_{11ee}		
24.5	17943.609	-4	20.5	17961.710	8	22.5	17948.408	-8	10.5	17953.795	7
25.5	17944.094	8	21.5	17962.917	-3	22.5	17948.415	-1	11.5	17954.833	10
27.5	17945.146	-8	22.5	17964.187	9	23.5	17949.016	-16	12.5	17955.894	-5
34.5	17950.175	-20	23.5	17965.493	15	23.5	17949.025	-7	13.5	17957.001	-15
35.5	17951.095	15	24.5	17966.821	3	24.5	17949.674	-14	15.5	17959.361	-10
37.5	17952.976	0	25.5	17968.208	9	25.5	17950.399	13	16.5	17960.608	-2
38.5	17953.983	-3	26.5	17969.622	1	26.5	17951.126	1	17.5	17961.890	0
56.5	17979.325	-12	27.5	17971.082	-2				18.5	17963.200	-10
57.5	17981.149	2	28.5	17972.593	5				19.5	17964.584	13
58.5	17983.001	1	29.5	17974.120	-13				20.5	17966.001	28
			30.5	17975.712	-7				21.5	17967.420	4
			31.5	17977.346	0				22.5	17968.890	-10
			33.5	17980.696	-28				23.5	17970.440	16
			34.5	17982.460	-14				24.5	17971.986	-4
			35.5	17984.280	14				25.5	17973.614	18
			57.5	18034.199	11				26.5	17975.251	8
			58.5	18036.983	44				27.5	17976.925	-6
			59.5	18039.727	-6				28.5	17978.668	7

 $^{137}\text{BaF}(1, 0) 32166^2\Sigma^+ - B^2\Sigma^+$

P_{22ff}			R_{22ff}			P_{11ee}			R_{11ee}		
18.5	18124.714	-9	22.5	18148.865	43	14.5	18127.219	18	10.5	18135.723	9
19.5	18125.186	9	24.5	18152.074	-15	15.5	18127.642	-20	11.5	18136.908	11
20.5	18125.677	-7	25.5	18153.792	-12	16.5	18128.189	13	12.5	18138.125	-8
21.5	18126.227	-19	26.5	18155.559	-16	17.5	18128.727	-18	13.5	18139.440	17
22.5	18126.883	22				18.5	18129.373	6	14.5	18140.765	-1
23.5	18127.534	2				19.5	18130.070	27	15.5	18142.150	-13
24.5	18128.275	19				20.5	18130.785	11	16.5	18143.596	-17
25.5	18129.031	-5				21.5	18131.544	-15	18.5	18146.672	-4
26.5	18129.840	-30				22.5	18132.398	-1	19.5	18148.295	6
28.5	18131.717	12				23.5	18133.292	-2	20.5	18149.949	-7
29.5	18132.708	2				24.5	18134.248	5	21.5	18151.686	8
30.5	18133.754	-8				25.5	18135.251	3	22.5	18153.460	5
31.5	18134.871	-4				26.5	18136.311	2	23.5	18155.271	-16
32.5	18136.054	10							25.5	18159.116	0
33.5	18137.281	11							26.5	18161.133	18
34.5	18138.576	23							27.5	18163.159	-10
35.5	18139.894	1									
36.5	18141.281	-9									
37.5	18142.748	2									
38.5	18144.259	0									
39.5	18145.816	-15									
40.5	18147.465	3									

12.3 Fluorescence detected OODR via the $C^2\Pi_{3/2}$ intermediate state: term values for the $0.88\ ^2\Sigma^+$ Rydberg series.

5.88 $^2\Sigma^+$, $v=0$

P_{22ff}			R_{22ff}			$^PQ_{12ef}$		
5.5	35585.518	17	7.5	35592.450	-3	6.5	35585.731	-4
7.5	35592.440	-13	9.5	35601.252	-6	8.5	35592.799	1
9.5	35601.259	1	11.5	35611.916	6	10.5	35601.748	1

6.88 $^2\Sigma^+$, $v=0$

P_{22ff}			R_{22ff}			$^PQ_{12ef}$		
5.5	36434.380	-4	7.5	36441.378	7	6.5	36434.239	-1
6.5	36437.643	-3	8.5	36445.553	-7	7.5	36437.482	1
7.5	36441.380	9				8.5	36441.190	3
9.5	36450.211	-2				10.5	36449.990	-4

$^OP_{12ee}$			$^OR_{12ee}$			Q_{22fe}		
13.5	36466.705	15	15.5	36480.135	-11	14.5	36480.442	11
14.5	36473.165	-20						
15.5	36480.178	32						

7.88 $^2\Sigma^+$, $v=0$

P_{22ff}			R_{22ff}			$^PQ_{12ef}$		
6.5	36989.650	10	7.5	36993.336	-26	6.5	36986.196	-7
7.5	36993.372	10	8.5	36997.537	-11	6.5	36986.216	13
8.5	36997.553	5	9.5	37002.216	20	7.5	36989.432	-5
9.5	37002.192	-4	10.5	37007.300	-8	8.5	36993.137	2
10.5	37007.311	3				9.5	36997.293	-4
						10.5	37001.916	-7
						11.5	37007.021	7

8.88 $^2\Sigma^+$, $v=0$

P_{22ff}			R_{22ff}			$^PQ_{12ef}$		
5.5	37361.024	2	7.5	37368.008	6	6.5	37360.922	5
6.5	37364.285	5	8.5	37372.187	-2	7.5	37364.170	11
7.5	37367.986	-16	9.5	37376.848	9	8.5	37367.864	-1
9.5	37376.829	-10				10.5	37376.659	-10
13.5	37400.079	-3				14.5	37399.860	13

$^OP_{12ee}$			$^OR_{12ee}$			Q_{22fe}		
			15.5	37406.783	-18	14.5	37407.044	-8
			16.5	37414.225	6	15.5	37414.486	0
			18.5	37430.445	-2	17.5	37430.758	12

9.88 $^2\Sigma^+$, $v=0$

P_{22ff}			R_{22ff}			$^PQ_{12ef}$		
5.5	37629.675	6	7.5	37636.717	9	6.5	37629.533	0

7.5	37636.699	-9	9.5	37645.619	5	8.5	37636.556	13
8.5	37640.904	-24	10.5	37650.758	-9	9.5	37640.735	-17
9.5	37645.613	-1	11.5	37656.379	-7	10.5	37645.437	7
10.5	37650.766	-1	13.5	37668.989	-33	11.5	37650.578	-1
11.5	37656.409	23				12.5	37656.193	-4
12.5	37662.511	40				13.5	37662.288	3

10.88 $^2\Sigma^+$, v=0

P_{22ff}			R_{22ff}			$^P Q_{12ef}$		
5.5	37826.551	-12	7.5	37833.544	-4	6.5	37826.441	-9
5.5	37826.566	3	8.5	37837.730	-7	6.5	37826.464	14
6.5	37829.800	-23	9.5	37842.373	-17	7.5	37829.677	-17
6.5	37829.819	-4	10.5	37847.512	5	7.5	37829.681	-13
7.5	37833.534	-14	11.5	37853.126	38	8.5	37833.397	-6
7.5	37833.550	2	12.5	37859.139	6	8.5	37833.410	7
8.5	37837.738	1	14.5	37872.634	19	9.5	37837.575	-1
9.5	37842.419	29	15.5	37880.054	2	9.5	37837.602	26
10.5	37847.513	6	16.5	37887.935	-17	10.5	37842.215	1
11.5	37853.112	24	17.5	37896.275	-41	10.5	37842.218	4
12.5	37859.141	8				11.5	37847.309	-8
14.5	37872.620	5				12.5	37852.894	10
15.5	37880.053	1				13.5	37858.923	6
						15.5	37872.382	7
						16.5	37879.804	3

$^O P_{12ee}$			$^O R_{12ee}$			Q_{22fe}		
13.5	37858.910	-7	15.5	37872.407	32	14.5	37872.658	43
14.5	37865.379	-34	16.5	37879.810	9	15.5	37880.052	0
15.5	37872.376	1	17.5	37887.677	-14	16.5	37887.948	-4
16.5	37879.807	6	18.5	37896.032	-14	17.5	37896.300	-16

11.88 $^2\Sigma^+$, v=0

P_{22ff}			R_{22ff}			$^P Q_{12ef}$		
5.5	37977.013	-24	7.5	37984.004	5	6.5	37976.878	-23
6.5	37980.286	-1	8.5	37988.183	9	7.5	37980.158	28
7.5	37984.018	19	9.5	37992.794	-18	8.5	37983.837	16
8.5	37988.195	21				9.5	37987.955	-20
9.5	37992.800	-12						

12.88 $^2\Sigma^+$, v=0

P_{22ff}			R_{22ff}			$^P Q_{12ef}$		
5.5	38093.059	-12	7.5	38100.045	-14	6.5	38092.962	-2
6.5	38096.334	1	8.5	38104.250	0	7.5	38096.218	6
7.5	38100.068	9	9.5	38108.918	13	8.5	38099.918	-7
8.5	38104.267	17	10.5	38114.008	-16	9.5	38104.116	12
9.5	38108.908	3				10.5	38108.739	-10
10.5	38114.021	-3				11.5	38113.860	1

13.88 ${}^2\Sigma^+$, v=0

P_{22ff}			R_{22ff}			${}^P Q_{12ef}$		
5.5	38185.310	-7	7.5	38192.304	-3	6.5	38185.221	7
6.5	38188.577	-2	8.5	38196.495	-5	7.5	38188.463	1
7.5	38192.318	11				8.5	38192.168	-6
8.5	38196.505	5				9.5	38196.350	-1

4.88 ${}^2\Sigma^+$, v=1

P_{22ff}			R_{22ff}			${}^P Q_{12ef}$		
5.5	34698.780	-86	7.5	34705.760	-50	6.5	34698.600	2
5.5	34698.820	-46	7.5	34705.800	-10	6.5	34698.650	52
7.5	34705.840	30	7.5	34705.812	2	8.5	34705.510	50
8.5	34709.920	-52	7.5	34705.840	30	9.5	34709.570	-11
10.5	34719.710	33	9.5	34714.600	5	11.5	34719.250	46
			9.5	34714.610	15			
			10.5	34719.690	13			
			12.5	34731.260	38			

${}^U P_{12ee}$			${}^U R_{12ee}$			Q_{22fe}		
13.5	34730.620	-46	15.5	34744.000	32	14.5	34744.530	-76
15.5	34743.960	-8	17.5	34759.190	80	16.5	34759.770	-60

4.88 ${}^4\Sigma^+$, v=3

P_{22ff}			R_{22ff}			${}^P Q_{12ef}$		
5.5	35746.077	-3	9.5	35761.763	-10	6.5	35745.745	-13
6.5	35749.311	-4				7.5	35748.959	15
7.5	35753.019	10				8.5	35752.563	-26
9.5	35761.771	-2				10.5	35761.254	1
10.5	35766.840	-3				11.5	35766.288	14
11.5	35772.389	18				12.5	35771.766	14
14.5	35791.706	1				15.5	35790.943	5

${}^U P_{12ee}$			${}^U R_{12ee}$			Q_{22fe}		
13.5	35777.641	-48	15.5	35790.951	13	14.5	35791.710	5
14.5	35784.077	-8	16.5	35798.241	-9	15.5	35799.072	5
15.5	35790.937	-1	17.5	35806.009	-12	16.5	35806.889	3
16.5	35798.244	-6	18.5	35814.260	11	17.5	35815.148	-16

6.88 ${}^2\Sigma^+$, v=2

P_{22ff}			R_{22ff}			${}^P Q_{12ef}$		
5.5	37498.120	-46	7.5	37505.160	5	8.5	37504.800	-36
7.5	37505.210	55						

${}^U P_{12ee}$			${}^U R_{12ee}$			Q_{22fe}		
13.5	37530.250	19	15.5	37543.620	-11	14.5	37544.210	-3

7.88 $^2\Sigma^+$, v=1

P_{22ff}			R_{22ff}			$^P Q_{12ef}$		
5.5	37520.640	30	9.5	37536.830	3	6.5	37520.290	-4
7.5	37527.710	-60				8.5	37527.360	3

5.76 $^2\Sigma^+$, v=0

P_{22ff}			R_{22ff}			$^P Q_{12ef}$		
5.5	35450.913	-4	7.5	35457.825	-12	6.5	35451.002	4
6.5	35454.145	-1	8.5	35461.988	-3	7.5	35454.245	6
7.5	35457.841	4				8.5	35457.941	-2
9.5	35466.619	13				10.5	35466.735	-1
11.5	35477.222	0				12.5	35477.378	0
13.5	35489.676	-11				14.5	35489.877	10
15.5	35504.008	10				16.5	35504.192	-11

6.76 $^2\Sigma^+$, v=0

P_{22ff}			R_{22ff}			$^P Q_{12ef}$		
5.5	36357.226	-1	9.5	36372.940	14	6.5	36357.298	-9
7.5	36364.153	1	10.5	36377.988	-19	8.5	36364.256	0
8.5	36368.315	7				9.5	36368.426	1
9.5	36372.926	0				10.5	36373.060	5

4.76 $^2\Sigma^+$, v=1

P_{22ff}			R_{22ff}			$^P Q_{12ef}$		
7.5	34451.060	13	9.5	34459.950	4	8.5	34451.160	11
8.5	34455.230	-32	11.5	34470.730	10	9.5	34455.380	4
9.5	34459.950	4				10.5	34460.060	-11
						13.5	34476.970	-1

6.76 $^2\Sigma^+$, v=2

P_{22ff}			R_{22ff}			$^P Q_{12ef}$		
7.5	37428.221	20				6.5	37421.550	-14
8.5	37432.313	-1				8.5	37428.480	0
9.5	37436.872	-15				9.5	37432.639	12
						10.5	37437.245	13
						11.5	37442.287	-9
						14.5	37460.261	21
$^O P_{12ee}$			$^O R_{12ee}$			Q_{22fe}		
13.5	37453.774	-26						
14.5	37460.241	1						

8.76 $^2\Sigma^+$, v=1

P_{22ff}			R_{22ff}			$^P Q_{12ef}$		
6.5	37865.202	-21				6.5	37862.024	-97
7.5	37868.906	-5				7.5	37865.351	-15
8.5	37873.076	15				8.5	37869.066	-8
9.5	37877.711	38				9.5	37873.259	16
10.5	37882.757	9				11.5	37883.022	54
11.5	37888.276	-8				12.5	37888.527	3
12.5	37894.257	-25				13.5	37894.537	-4
$^O P_{12ee}$			$^O R_{12ee}$			Q_{22fe}		
13.5	37894.545	4						
14.5	37901.021	0						
15.5	37907.904	-58						

5.08 $^2\Sigma^+$, v=0

P_{22ff}			R_{22ff}			$^P Q_{12ef}$		
7.5	34504.048	-19	7.5	34504.059	-8	6.5	34497.041	4
9.5	34513.342	11				8.5	34504.466	18
11.5	34524.531	9				10.5	34513.799	-3
						12.5	34525.071	-11

6.08 $^2\Sigma^+$, v=0

P_{22ff}			R_{22ff}			$^P Q_{12ef}$		
5.5	35785.327	2	7.5	35792.931	-1	6.5	35785.660	-5
6.5	35788.880	4	8.5	35797.499	9	7.5	35789.274	5
7.5	35792.928	-4				8.5	35793.372	-5
8.5	35797.488	-2				9.5	35797.984	-3
9.5	35802.539	-7				10.5	35803.103	7

7.08 $^2\Sigma^+$, v=0

P_{22ff}			R_{22ff}			$^P Q_{12ef}$		
5.5	36568.298	-31				6.5	36568.587	-6
6.5	36571.961	-47				7.5	36572.361	31
7.5	36576.206	1				8.5	36576.605	12
8.5	36580.871	-44				9.5	36581.401	24
9.5	36586.182	48				10.5	36586.733	53
10.5	36591.906	49				11.5	36592.469	-28
11.5	36598.108	29				12.5	36598.801	-24
12.5	36604.813	19				13.5	36605.599	-59
14.5	36619.633	-46				15.5	36620.797	-24
						16.5	36629.141	2
						17.5	36637.980	40

6.08 $^2\Sigma^+$, v=1

P_{22ff}			R_{22ff}			$^PQ_{12ef}$		
5.5	36320.554	4	7.5	36328.127	1	6.5	36320.931	-4
7.5	36328.121	-5	9.5	36337.689	0	8.5	36328.632	3

7.08 $^2\Sigma^+$, v=1

P_{22ff}			R_{22ff}			$^PQ_{12ef}$		
5.5	37105.719	-3	7.5	37113.605	5	6.5	37105.924	-8
6.5	37109.415	11				7.5	37109.665	5
7.5	37113.598	-2				8.5	37113.914	6
8.5	37118.284	-20				9.5	37118.668	-2
9.5	37123.518	10				10.5	37123.939	-2

5.24 $^2\Sigma^+$, v=0

P_{22ff}			R_{22ff}			$^PQ_{12ef}$		
5.5	34758.234	-9	7.5	34765.421	6	6.5	34757.066	9
6.5	34761.596	-2				7.5	34760.229	-8
7.5	34765.414	-1				8.5	34763.894	12
8.5	34769.712	17				9.5	34767.972	-21
9.5	34774.428	-7				10.5	34772.576	7
10.5	34779.626	-9				11.5	34777.611	2
11.5	34785.298	4				12.5	34783.111	0

6.24 $^2\Sigma^+$, v=0

P_{22ff}			R_{22ff}			$^PQ_{12ef}$		
5.5	35934.405	-3	7.5	35941.696	-4	6.5	35933.086	6
5.5	35934.416	8	7.5	35941.712	12	6.5	35933.088	8
6.5	35937.816	-2	8.5	35946.046	-9	7.5	35936.284	1
6.5	35937.816	-2	9.5	35950.926	42	7.5	35936.296	13
7.5	35941.686	-14	10.5	35956.246	61	8.5	35939.957	0
7.5	35941.702	2	11.5	35962.036	77	8.5	35939.976	19
8.5	35946.006	-49	12.5	35968.286	79	9.5	35944.106	3
9.5	35950.786	-98	13.5	35974.966	39	10.5	35948.724	4
9.5	35950.877	-7	14.5	35982.176	55	10.5	35948.736	16
10.5	35956.196	11	15.5	35989.836	48	11.5	35953.806	-2
11.5	35961.936	-23	16.5	35997.996	68	12.5	35959.386	19
12.5	35968.136	-71	17.5	36006.626	85	13.5	35965.376	-22
12.5	35968.198	-9	18.5	36015.666	39	13.5	35965.380	-18
13.5	35974.866	-61	19.5	36025.196	10	14.5	35971.896	-3
14.5	35982.046	-75				15.5	35978.846	-25
15.5	35989.746	-42				16.5	35986.296	-18
						17.5	35994.156	-71
						18.5	36002.556	-55
						19.5	36011.426	-38
						20.5	36020.796	8

${}^0P_{12ee}$			${}^0R_{12ee}$			Q_{22fe}		
13.5	35965.426	28	15.5	35978.806	-65	14.5	35982.176	55
14.5	35971.926	27	16.5	35986.306	-8	15.5	35989.856	68
15.5	35978.926	55	17.5	35994.166	-61	16.5	35997.956	28
16.5	35986.356	42	18.5	36002.576	-35	17.5	36006.556	15
17.5	35994.306	79	19.5	36011.466	2	18.5	36015.656	29
18.5	36002.686	75	20.5	36020.796	8	19.5	36025.226	40
19.5	36011.566	102	21.5	36030.716	135	20.5	36035.296	77

8.24 ${}^2\Sigma^+$, $v=0$

P_{22ff}			R_{22ff}			${}^PQ_{12ef}$		
8.5	37153.184	12	8.5	37153.181	9	6.5	37139.690	-19
9.5	37158.107	-9	9.5	37158.112	-4	7.5	37143.016	20
10.5	37163.530	-9	10.5	37163.532	-7	8.5	37146.781	11
			12.5	37175.832	9	9.5	37151.026	-8
						10.5	37155.772	-14
						11.5	37161.038	9

9.24 ${}^2\Sigma^+$, $v=0$

P_{22ff}			R_{22ff}			${}^PQ_{12ef}$		
5.5	37470.166	-2	7.5	37477.329	12	6.5	37469.560	-3
6.5	37473.508	-4	8.5	37481.586	4	7.5	37472.882	2
7.5	37477.316	-1				8.5	37476.690	4
8.5	37481.572	-10				9.5	37480.982	-3

7.24 ${}^2\Sigma^+$, $v=2$

P_{22ff}			R_{22ff}			${}^PQ_{12ef}$		
5.5	37731.211	4	7.5	37738.507	-8	6.5	37729.901	-3
6.5	37734.641	17	8.5	37742.884	2	7.5	37733.107	-5
7.5	37738.506	-9	9.5	37747.713	-11	8.5	37736.801	9
8.5	37742.876	-6	10.5	37753.055	13	9.5	37740.942	-2

5.45 ${}^2\Pi$, $v=1$

P_{22ff}			R_{22ff}			Q_{22ef}		
5.5	35594.910	-2	7.5	35601.476	10	6.5	35597.940	-15
7.5	35601.477	11	9.5	35609.896	5	8.5	35605.440	-4
9.5	35609.888	-3	11.5	35620.176	-8	10.5	35614.809	6

5.45 ${}^2\Pi$, $v=3$

P_{22ff}			R_{22ff}			Q_{22ef}		
5.5	36655.156	21	7.5	36661.744	-15	6.5	36658.194	-12
6.5	36658.214	3	8.5	36665.783	3	7.5	36661.731	-21
7.5	36661.761	2				8.5	36665.779	9
8.5	36665.783	3				9.5	36670.273	13

9.5	36670.270	-4	10.5	36675.218	-3
10.5	36675.241	1			

6.45 $^2\Pi$, v=1

P_{22ff}			R_{22ff}			Q_{22ef}		
5.5	36653.312	-29	7.5	36660.222	46	6.5	36656.438	-71
6.5	36656.499	-16	8.5	36664.342	18	7.5	36660.197	29
7.5	36660.203	27	9.5	36668.976	20	8.5	36664.334	23
8.5	36664.343	19	10.5	36674.039	-35	9.5	36668.930	-10
9.5	36668.974	18						
10.5	36674.036	-38						

6.45 $^2\Pi$, v=3

P_{22ff}			R_{22ff}			Q_{22ef}		
5.5	37716.115	-2	7.5	37722.694	3	6.5	37719.162	-8
6.5	37719.171	1	8.5	37726.683	4	7.5	37722.704	13
7.5	37722.683	-8	9.5	37731.135	0	8.5	37726.679	0
8.5	37726.682	3	10.5	37736.055	-2	9.5	37731.129	-5

5.23 $^2\Delta$, v=0

P_{22ff}			R_{22ff}			Q_{22ef}		
5.5	34738.638	12	7.5	34745.273	14	6.5	34741.725	19
7.5	34745.221	-38	9.5	34753.758	-24	8.5	34749.222	-62
8.5	34749.307	23	10.5	34758.795	44	9.5	34753.793	11
9.5	34753.787	5				10.5	34758.778	27
11.5	34764.165	-27				12.5	34770.101	-3

P_{12ff}			R_{12ff}			Q_{12ef}		
			7.5	34732.677	51	6.5	34729.233	16
			9.5	34740.769	-41	8.5	34736.432	-58
			10.5	34745.566	-19	9.5	34740.840	30
			11.5	34750.786	-31	10.5	34745.604	19
			13.5	34762.678	27	12.5	34756.511	6

6.23 $^2\Delta$, v=0

P_{22ff}			R_{22ff}			Q_{22ef}		
5.5	35930.322	-29	7.5	35937.020	-47	6.5	35933.527	53
5.5	35930.380	29	7.5	35937.057	-10	6.5	35933.540	66
6.5	35933.456	-15	8.5	35941.100	-38	7.5	35937.120	47
6.5	35933.470	-1	8.5	35941.128	-10	7.5	35937.123	50
7.5	35937.050	-17	9.5	35945.630	-53	8.5	35941.170	21
7.5	35937.130	63	9.5	35945.646	-37	8.5	35941.195	46
8.5	35941.180	42	10.5	35950.620	-80	9.5	35945.740	39
9.5	35945.647	-36	11.5	35956.120	-68	10.5	35950.680	-48
9.5	35945.700	17	12.5	35962.090	-56	10.5	35950.773	45
10.5	35950.700	0	13.5	35968.510	-63	11.5	35956.200	-30

11.5	35956.170	-18	14.5	35975.420	-46	12.5	35962.230	23
12.5	35962.093	-53	15.5	35982.830	4	13.5	35968.640	-17
12.5	35962.120	-26	16.5	35990.680	28	13.5	35968.678	21
13.5	35968.550	-23	17.5	35998.990	49	14.5	35975.570	-11
14.5	35975.420	-46	18.5	36007.710	17	15.5	35983.000	21
15.5	35982.800	-26	19.5	36016.970	62	16.5	35990.840	-11
16.5	35990.580	-72	20.5	36026.670	87	17.5	35999.090	-106
17.5	35998.910	-31	21.5	36036.830	112	18.5	36007.900	-115
18.5	36007.680	-13				19.5	36017.220	-88
19.5	36016.920	12				20.5	36026.970	-105

P _{12ff}			R _{12ff}			Q _{12ef}		
8.5	35933.300	100	7.5	35929.330	-44	7.5	35929.350	-48
9.5	35937.490	10	7.5	35929.373	-1	8.5	35933.250	18
10.5	35942.260	45	8.5	35933.204	4	9.5	35937.580	59
11.5	35947.420	14	8.5	35933.210	10	10.5	35942.230	-35
12.5	35953.090	35	9.5	35937.489	9	11.5	35947.460	-6
13.5	35959.210	48	9.5	35937.510	30	12.5	35953.070	-55
14.5	35965.730	1	10.5	35942.210	-5	13.5	35959.200	-40
15.5	35972.790	35	11.5	35947.380	-26	14.5	35965.820	6
16.5	35980.260	18	11.5	35947.390	-16	15.5	35972.830	-15
17.5	35988.180	-11	12.5	35953.080	25	16.5	35980.330	-5
18.5	35996.640	37	13.5	35959.120	-42	17.5	35988.230	-53
19.5	36005.500	23	14.5	35965.716	-13	18.5	35996.660	-28
			14.5	35965.780	51	19.5	36005.570	18
			15.5	35972.750	-5	20.5	36014.920	47
			16.5	35980.230	-12			
			17.5	35988.170	-21			
			18.5	35996.510	-93			
			19.5	36005.410	-67			
			20.5	36014.780	-35			
			21.5	36024.540	-78			

P _{22ee}			R _{22ee}			Q _{22fe}		
13.5	35968.760	103	15.5	35983.050	71	14.5	35975.420	-46
14.5	35975.650	69	16.5	35990.930	79	15.5	35982.770	-56
15.5	35983.030	51	17.5	35999.270	74	16.5	35990.590	-62
16.5	35990.860	9	18.5	36008.100	85	17.5	35998.880	-61
17.5	35999.260	64	19.5	36017.360	52	18.5	36007.660	-33
18.5	36008.040	25	20.5	36027.080	5	19.5	36016.870	-38
19.5	36017.310	2	21.5	36037.340	23	20.5	36026.620	37

P _{12ee}			R _{12ee}			Q _{12fe}		
13.5	35959.240	0	15.5	35972.820	-25	14.5	35965.830	101
14.5	35965.770	-44	16.5	35980.250	-85	15.5	35972.830	75
15.5	35972.850	5	17.5	35988.200	-83	16.5	35980.280	38
16.5	35980.350	15	18.5	35996.660	-28	17.5	35988.240	49
17.5	35988.310	27	19.5	36005.510	-42	18.5	35996.650	47
18.5	35996.730	42	20.5	36014.900	27	19.5	36005.520	43
19.5	36005.640	88	21.5	36024.680	28	20.5	36014.860	45

8.23 $^2\Delta, v=0$

P_{22ff}			R_{22ff}			Q_{22ef}		
5.5	37137.445	2	8.5	37148.526	-7	6.5	37140.794	91
6.5	37140.691	22	9.5	37153.147	-18	7.5	37144.489	62
7.5	37144.367	0	10.5	37158.243	-16	8.5	37148.731	99
8.5	37148.523	-10	12.5	37169.843	17	9.5	37153.381	63
9.5	37153.150	-15				10.5	37158.509	25
10.5	37158.268	9				11.5	37164.123	-10
P_{12ff}			R_{12ff}			Q_{12ef}		
5.5	37133.871	4	7.5	37140.041	23	6.5	37136.746	-1
6.5	37136.716	3	8.5	37143.803	17	7.5	37140.044	-17
7.5	37140.017	-1	9.5	37148.017	-2	8.5	37143.803	-32
8.5	37143.782	-4	10.5	37152.723	4	9.5	37148.077	8
9.5	37148.017	-2	11.5	37157.869	-18	10.5	37152.769	4
			12.5	37163.530	4	11.5	37157.930	9

9.23 $^2\Delta, v=0$

P_{22ff}			R_{22ff}			Q_{22ef}		
6.5	37472.726	2	7.5	37476.335	-39	7.5	37475.948	38
7.5	37476.374	0	8.5	37480.503	-19	8.5	37479.725	-30
8.5	37480.566	44				9.5	37483.990	4
P_{12ff}			R_{12ff}			Q_{12ef}		
						6.5	37469.347	-22
						7.5	37472.628	17
						8.5	37476.374	28
						9.5	37480.566	-22

7.23 $^2\Delta, v=2$

P_{22ff}			R_{22ff}			Q_{22ef}		
5.5	37727.956	-16	7.5	37734.721	-3	6.5	37731.176	37
6.5	37731.101	-12	8.5	37738.811	10	7.5	37734.791	20
7.5	37734.711	-13	9.5	37743.334	-6	8.5	37738.869	-13
8.5	37738.790	-11	10.5	37748.346	7	9.5	37743.468	-2
P_{12ff}			R_{12ff}			Q_{12ef}		
6.5	37726.074	11	7.5	37729.358	-2	6.5	37726.070	-16
7.5	37729.370	10	8.5	37733.107	-3	7.5	37729.380	-6
8.5	37733.119	9	9.5	37737.314	-2	8.5	37733.127	-6
			10.5	37741.974	-7	9.5	37737.342	12

4.94 $^2\Delta, v=0$

P_{22ff}			R_{22ff}			Q_{22ef}		
			7.5	34270.717	-120	6.5	34267.213	46
						7.5	34270.890	53
						8.5	34274.972	10

P _{12ff}			R _{12ff}			Q _{12ef}		
5.5	34261.302	-43				6.5	34264.042	-39
6.5	34264.094	13				7.5	34267.327	49
7.5	34267.356	78				8.5	34270.885	-49

5.94 ²Δ, v=0

P _{22ff}			R _{22ff}			Q _{22ef}		
5.5	35643.371	5	7.5	35650.249	-2	6.5	35646.587	3
6.5	35646.578	-2	8.5	35654.382	1	7.5	35650.260	3
7.5	35650.251	0	9.5	35658.957	-12	8.5	35654.392	3
9.5	35658.974	5	10.5	35664.010	-5	9.5	35658.978	-2
14.5	35688.785	6	11.5	35669.508	-11	10.5	35664.031	1

P _{12ff}			R _{12ff}			Q _{12ef}		
5.5	35640.634	-17				6.5	35643.408	4
6.5	35643.410	9				7.5	35646.619	5
7.5	35646.606	-4				8.5	35650.271	-13
8.5	35650.281	3				9.5	35654.414	1
9.5	35654.420	15				10.5	35659.008	6
						15.5	35688.827	-2

6.94 ²Δ, v=0

P _{22ff}			R _{22ff}			Q _{22ef}		
5.5	36475.453	1	7.5	36482.311	3	6.5	36478.674	18
6.5	36478.646	-7	8.5	36486.417	1	7.5	36482.327	14
7.5	36482.313	5	9.5	36490.989	9	8.5	36486.423	-2
8.5	36486.403	-13	11.5	36501.479	9	9.5	36490.986	-8
9.5	36490.971	-9	13.5	36513.774	-5	10.5	36496.013	-5
10.5	36495.942	-56	16.5	36535.653	4	11.5	36501.499	0
11.5	36501.453	-17				12.5	36507.432	-6
14.5	36520.620	5				15.5	36528.004	6

P _{12ff}			R _{12ff}			Q _{12ef}		
5.5	36472.905	5	7.5	36478.838	10	6.5	36475.629	-2
6.5	36475.633	-1	8.5	36482.482	1	7.5	36478.829	6
7.5	36478.838	10	9.5	36486.595	3	8.5	36482.478	6
			10.5	36491.156	-5	9.5	36486.567	-11
			11.5	36496.194	6	10.5	36491.148	8
			12.5	36501.658	-15	11.5	36496.128	-30
			13.5	36507.606	-10	12.5	36501.617	-15
			16.5	36528.207	11	15.5	36520.805	21

8.94 ²Δ, v=0

P _{22ff}			R _{22ff}			Q _{22ef}		
			8.5	37391.023	3	6.5	37383.448	-5
			9.5	37395.470	-15	7.5	37387.066	7
						8.5	37391.146	27

10.5 37400.591 -19
 11.5 37406.040 -4

P_{12ff}			R_{12ff}			Q_{12ef}		
5.5	37377.622	-1				6.5	37380.298	3
6.5	37380.326	3				7.5	37383.410	-16
7.5	37383.460	-16				8.5	37387.002	1
9.5	37391.147	0				10.5	37395.497	19
10.5	37395.684	17				11.5	37400.371	-4

9.94 $^2\Delta$, $v=0$

P_{22ff}			R_{22ff}			Q_{22ef}		
			7.5	37649.659	16	6.5	37646.253	7
			9.5	37657.953	26	8.5	37653.816	-26
			10.5	37662.668	-33	9.5	37658.333	6
P_{12ff}			R_{12ff}			Q_{12ef}		
7.5	37646.238	1				6.5	37643.041	-35
8.5	37649.814	11				8.5	37649.668	12
						9.5	37653.606	15

10.94 $^2\Delta$, $v=0$

P_{22ff}			R_{22ff}			Q_{22ef}		
			7.5	37843.579	-1	6.5	37840.402	12
						7.5	37843.931	-12
						8.5	37847.966	3
P_{12ff}			R_{12ff}			Q_{12ef}		
5.5	37834.642	-10				6.5	37837.168	-6
6.5	37837.294	2				7.5	37840.172	0
7.5	37840.397	13				8.5	37843.584	2
8.5	37843.944	8						
9.5	37847.942	-11						

11.94 $^2\Delta$, $v=0$

P_{22ff}			R_{22ff}			Q_{22ef}		
						6.5	37987.763	21
						7.5	37991.261	-12
P_{12ff}			R_{12ff}			Q_{12ef}		
						6.5	37984.476	3
						7.5	37987.352	-26
						8.5	37990.676	15

6.94 $^2\Delta$, $v=1$

P_{22ff}			R_{22ff}			Q_{22ef}		
			7.5	37017.357	-16	6.5	37013.787	34
			8.5	37021.419	-38	7.5	37017.394	1

16.5 37070.371 3 8.5 37021.503 16
 9.5 37026.034 -3
 15.5 37062.928 -2

P_{12ff}			R_{12ff}			Q_{12ef}		
5.5	37007.896	28				6.5	37010.589	-1
6.5	37010.585	-8				7.5	37013.772	5
7.5	37013.762	-10				8.5	37017.401	4
8.5	37017.410	3				9.5	37021.493	12
						15.5	37055.475	-6

9.86 $^2\Phi$, $v=0$

Q_{22fe}			Q_{22ef}		
15.5	37671.562	-18	15.5	37671.638	58
16.5	37678.851	-76	16.5	37678.943	16
			17.5	37686.711	5
			18.5	37694.930	13
			19.5	37703.545	-15

10.86 $^2\Phi$, $v=0$

P_{12ff}			Q_{22ef}		
5.5	37818.255	6	6.5	37823.731	-3
7.5	37823.741	7	7.5	37827.122	12
8.5	37827.103	-7	8.5	37830.889	-18
9.5	37830.903	-4	9.5	37835.133	6
10.5	37835.126	-1	10.5	37839.784	17
11.5	37839.752	-15	11.5	37844.836	6
12.5	37844.831	1	12.5	37850.288	-26
13.5	37850.314	0	13.5	37856.232	12
14.5	37856.229	9	14.5	37862.577	29
			15.5	37869.250	-47
			16.5	37876.487	19

11.86 $^2\Phi$, $v=0$

Q_{22ef}		
7.5	37977.597	-6
8.5	37981.295	-6
9.5	37985.409	-1
10.5	37989.949	19
11.5	37994.867	7
12.5	38000.189	-12
13.5	38005.986	34
14.5	38012.070	-44

12.86 $^2\Phi$, $\nu=0$

			Q_{22ef}
6.5	38090.998	16	
7.5	38094.181	-7	
8.5	38097.784	-12	
9.5	38101.790	-14	
10.5	38106.229	17	

13. Appendix E: List of program and data files.

b138_all.dat	- ^{138}BaF fluorescence detected OODR via $\text{B}^2\Sigma^+$ intermediate: fit input
b138_all.out	- ^{138}BaF fluorescence detected OODR via $\text{B}^2\Sigma^+$ intermediate: fit output
b_lines.xls	- list of lines (OODR via $\text{B}^2\Sigma^+$): Excel 5.0 file
b_g1-bi1.out	- ^{137}BaF (1, 0) $\text{G}^2\Sigma^+ - \text{B}^2\Sigma^+$: fit output
b_g1-bi1.dat	- ^{137}BaF (1, 0) $\text{G}^2\Sigma^+ - \text{B}^2\Sigma^+$: fit input
b_g1-bi2.dat	- ^{136}BaF (1, 0) $\text{G}^2\Sigma^+ - \text{B}^2\Sigma^+$: fit input
b_g1-bi2.out	- ^{136}BaF (1, 0) $\text{G}^2\Sigma^+ - \text{B}^2\Sigma^+$: fit output
b_g1-bi3.dat	- ^{135}BaF (1, 0) $\text{G}^2\Sigma^+ - \text{B}^2\Sigma^+$: fit input
b_g1-bi3.out	- ^{135}BaF (1, 0) $\text{G}^2\Sigma^+ - \text{B}^2\Sigma^+$: fit output
b_g2-bi1.dat	- ^{137}BaF (2, 0) $\text{G}^2\Sigma^+ - \text{B}^2\Sigma^+$: fit input
b_g2-bi1.out	- ^{137}BaF (2, 0) $\text{G}^2\Sigma^+ - \text{B}^2\Sigma^+$: fit output
b_1-bi1.dat	- ^{137}BaF (1, 0) 32166 $^2\Sigma^+ - \text{B}^2\Sigma^+$: fit input
b_1-bi1.out	- ^{137}BaF (1, 0) 32166 $^2\Sigma^+ - \text{B}^2\Sigma^+$: fit output
si_588.dat	- 5.88 $^2\Sigma^+$, v=0 - input file
si_588.out	- 5.88 $^2\Sigma^+$, v=0 - output file
si_688.dat	- 6.88 $^2\Sigma^+$, v=0 - input file
si_688.out	- 6.88 $^2\Sigma^+$, v=0 - output file
si_788.dat	- 7.88 $^2\Sigma^+$, v=0 - input file
si_788.out	- 7.88 $^2\Sigma^+$, v=0 - output file
si_888.dat	- 8.88 $^2\Sigma^+$, v=0 - input file
si_888.out	- 8.88 $^2\Sigma^+$, v=0 - output file
si_988.dat	- 9.88 $^2\Sigma^+$, v=0 - input file
si_988.out	- 9.88 $^2\Sigma^+$, v=0 - output file
si_1088.dat	- 10.88 $^2\Sigma^+$, v=0 - input file
si_1088.out	- 10.88 $^2\Sigma^+$, v=0 - output file
si_1188.dat	- 11.88 $^2\Sigma^+$, v=0 - input file
si_1188.out	- 11.88 $^2\Sigma^+$, v=0 - output file
si_1288.dat	- 12.88 $^2\Sigma^+$, v=0 - input file

si_1288.out - 12.88 $^2\Sigma^+$, v=0 - output file
 si_1388.dat - 13.88 $^2\Sigma^+$, v=0 - input file
 si_1388.out - 13.88 $^2\Sigma^+$, v=0 - output file
 si_488v1.dat - 4.88 $^2\Sigma^+$, v=1 - input file
 si_488v1.out - 4.88 $^2\Sigma^+$, v=1 - output file
 si_488v3.dat - 4.88 $^2\Sigma^+$, v=3 - input file
 si_488v3.out - 4.88 $^2\Sigma^+$, v=3 - output file
 si_688v2.dat - 6.88 $^2\Sigma^+$, v=2 - input file
 si_688v2.out - 6.88 $^2\Sigma^+$, v=2 - output file
 si_788v1.dat - 7.88 $^2\Sigma^+$, v=1 - input file
 si_788v1.out - 7.88 $^2\Sigma^+$, v=1 - output file
 si_576.dat - 5.76 $^2\Sigma^+$, v=0 - input file
 si_576.out - 5.76 $^2\Sigma^+$, v=0 - output file
 si_676.dat - 6.76 $^2\Sigma^+$, v=0 - input file
 si_676.out - 6.76 $^2\Sigma^+$, v=0 - output file
 si_476v1.dat - 4.76 $^2\Sigma^+$, v=1 - input file
 si_476v1.out - 4.76 $^2\Sigma^+$, v=1 - output file
 si_676v2.dat - 6.76 $^2\Sigma^+$, v=2 - input file
 si_676v2.out - 6.76 $^2\Sigma^+$, v=2 - output file
 si_876v1.dat - 8.76 $^2\Sigma^+$, v=1 - input file
 si_876v1.out - 8.76 $^2\Sigma^+$, v=1 - output file
 si_508.dat - 5.08 $^2\Sigma^+$, v=0 - input file
 si_508.out - 5.08 $^2\Sigma^+$, v=0 - output file
 si_608.dat - 6.08 $^2\Sigma^+$, v=0 - input file
 si_608.out - 6.08 $^2\Sigma^+$, v=0 - output file
 si_708.dat - 7.08 $^2\Sigma^+$, v=0 - input file
 si_708.out - 7.08 $^2\Sigma^+$, v=0 - output file
 si_608v1.dat - 6.08 $^2\Sigma^+$, v=1 - input file
 si_608v1.out - 6.08 $^2\Sigma^+$, v=1 - output file

si_708v1.dat - 7.08 $^2\Sigma^+$, v=1 - input file
 si_708v1.out - 7.08 $^2\Sigma^+$, v=1 - output file
 si_524.dat - 5.24 $^2\Sigma^+$, v=0 - input file
 si_524.out - 5.24 $^2\Sigma^+$, v=0 - output file
 si_624.dat - 6.24 $^2\Sigma^+$, v=0 - input file
 si_624.out - 6.24 $^2\Sigma^+$, v=0 - output file
 si_824.dat - 8.24 $^2\Sigma^+$, v=0 - input file
 si_824.out - 8.24 $^2\Sigma^+$, v=0 - output file
 si_924.dat - 9.24 $^2\Sigma^+$, v=0 - input file
 si_924.out - 9.24 $^2\Sigma^+$, v=0 - output file
 si_724v2.dat - 7.24 $^2\Sigma^+$, v=2 - input file
 si_724v2.out - 7.24 $^2\Sigma^+$, v=2 - output file
 pi_545v1.dat - 5.45 $^2\Pi$, v=1 - input file
 pi_545v1.out - 5.45 $^2\Pi$, v=1 - output file
 pi_545v3.dat - 5.45 $^2\Pi$, v=3 - input file
 pi_545v3.out - 5.45 $^2\Pi$, v=3 - output file
 pi_645v1.dat - 6.45 $^2\Pi$, v=1 - input file
 pi_645v1.out - 6.45 $^2\Pi$, v=1 - output file
 pi_645v3.dat - 6.45 $^2\Pi$, v=3 - input file
 pi_645v3.out - 6.45 $^2\Pi$, v=3 - output file
 de_523.dat - 5.23 $^2\Delta$, v=0 - input file
 de_523.out - 5.23 $^2\Delta$, v=0 - output file
 de_623.dat - 6.23 $^2\Delta$, v=0 - input file
 de_623.out - 6.23 $^2\Delta$, v=0 - output file
 de_823.dat - 8.23 $^2\Delta$, v=0 - input file
 de_823.out - 8.23 $^2\Delta$, v=0 - output file
 de_923.dat - 9.23 $^2\Delta$, v=0 - input file
 de_923.out - 9.23 $^2\Delta$, v=0 - output file
 de_723v2.dat - 7.23 $^2\Delta$, v=2 - input file

de_723v2.out - 7.23 $^2\Delta$, v=2 - output file
de_494.dat - 4.94 $^2\Delta$, v=0 - input file
de_494.out - 4.94 $^2\Delta$, v=0 - output file
de_594.dat - 5.94 $^2\Delta$, v=0 - input file
de_594.out - 5.94 $^2\Delta$, v=0 - output file
de_694.dat - 6.94 $^2\Delta$, v=0 - input file
de_694.out - 6.94 $^2\Delta$, v=0 - output file
de_894.dat - 8.94 $^2\Delta$, v=0 - input file
de_894.out - 8.94 $^2\Delta$, v=0 - output file
de_994.dat - 9.94 $^2\Delta$, v=0 - input file
de_994.out - 9.94 $^2\Delta$, v=0 - output file
de_1094.dat - 10.94 $^2\Delta$, v=0 - input file
de_1094.out - 10.94 $^2\Delta$, v=0 - output file
de_1194.dat - 11.94 $^2\Delta$, v=0 - input file
de_1194.out - 11.94 $^2\Delta$, v=0 - output file
de_694v1.dat - 6.94 $^2\Delta$, v=1 - input file
de_694v1.out - 6.94 $^2\Delta$, v=1 - output file
fi_986.dat - 9.86 $^2\Phi$, v=0 - input file
fi_986.out - 9.86 $^2\Phi$, v=0 - output file
fi_1086.dat - 10.86 $^2\Phi$, v=0 - input file
fi_1086.out - 10.86 $^2\Phi$, v=0 - output file
fi_1186.dat - 11.86 $^2\Phi$, v=0 - input file
fi_1186.out - 11.86 $^2\Phi$, v=0 - output file
fi_1286.dat - 12.86 $^2\Phi$, v=0 - input file
fi_1286.out - 12.86 $^2\Phi$, v=0 - output file
tocenter.for - fortran source code for TOCENTER program
tocenter.exe - MS DOS executable code for TOCENTER program
b_lines.xls - Excel 5 file with data shown in Appendix D, Sections 12.1 and 12.2
c_lines.xls - Excel 5 file with data shown in Appendix D, Section 12.3

baf10.xls	- Excel 5 file with $n \approx 10$ supercomplex data and graphs
baf11.xls	- Excel 5 file with $n \approx 11$ supercomplex data and graphs
baf12.xls	- Excel 5 file with $n \approx 12$ supercomplex data and graphs
baf13.xls	- Excel 5 file with $n \approx 13$ supercomplex data and graphs
baf14.xls	- Excel 5 file with $n \approx 14$ supercomplex data and graphs
china14.xls	- Excel 5 file with $n \approx 14, v=1$ supercomplex data and graphs
china15.xls	- Excel 5 file with $n \approx 15, v=1$ supercomplex data and graphs
china16.xls	- Excel 5 file with $n \approx 16, v=1$ supercomplex data and graphs
radial.for	- fortran source code for the RADIAL program
radial.exe	- MS DOS executable code for the Radial program
bafspec.for	- fortran source code for the BAFSPEC program
bafspec.exe	- MS DOS executable code for the BAFSPEC program
lsq.for	- fortran source code for the least-squares fitter
thesis.doc	- this document in MS Word 6.1 format
thesis.prn	- this document printed into file, HP 4 printer